DESIGN AND FABRICATION OF MULTI-FINGERED LINES AND ANTENNA

YU YU KYI

NATIONAL UNIVERSITY OF SINGAPORE

2003

DESIGN AND FABRICATION OF MULTI-FINGERED LINES AND ANTENNA

BY

YU YU KYI
B.E (Electronics) Yangon Technological University

A THESIS SUBMITTED

FOR THE DEGREE OF MASTER OF ENGINEERING

DEPARTMENT OF ELECTRICAL AND COMPUTER ENGINEERING

NATIONAL UNIVERSITY OF SINGAPORE

2003

ABSTRACT

The trend of any maturing electrical technology is toward miniaturizing, lighter weight, lower cost and increased complexity with several functions in a single chip. Microwave integrated circuits (MICs) fulfill this requirement. Microwave integrated circuit can be divided into two types: hybrid MICs and monolithic MICs (MMICs). In MIC and MMIC design, the dimensions of the circuit are always a concern due to circuit miniaturization and material cost reduction. To achieve a remarkable circuit area reduction, it is needed to use artificial transmission lines which have similar behavior to transmission line but with reduced physical dimensions by incorporating with lumped elements.

Successful antenna design with proximity feed a novel Π-shaped proximity feed U-slot rectangular patch antenna which is fabricated with a Duroid substrate of $\varepsilon_r = 2.35$ and thickness of 62 mils based on differing stub lengths is presented. Antenna characteristics like impedance bandwidth, resonant frequencies and radiation properties are investigated. The objectives of the design are broadband, compact, easy to fabricate and good radiation pattern across antenna bandwidth.

In this project, two types of microstrip structures are described, namely the microstrip dipole with the conventional microstrip feedline and the other with the photonic bandgap (PBG) structure feedline. The design of tri-band microstrip dipole antenna was next investigated using the feeding method of electromagnetically coupling (EMC) between the feed line and the dipole in transverse configuration in this project. The design of single dipole antenna was first investigated using IE3D simulation software in this project. Based upon the single dipole antenna, the tri-band dipole antennas are further improved to get better bandwidth. They are versatile in terms of resonant frequency, polarization, pattern and impedance depending on the patch shape. All the dimensions and the patterns are directly influenced on the design of bandwidth, efficiency, return loss and the center frequency of the microstrip dipole. The height of the substrate is the important element in controlling the efficiency and bandwidth of the dipole antenna. The PBG structure microstrip feedline is not only remarkable reduced in physical dimension also the better bandwidth than the conventional microstrip feedline.

ACKNOWLEDGEMENT

I respectfully wish to express my gratitude to my supervisor, Professor Leong Mook Seng, Head of Microwave & RF group, who gives me invaluable guidance and aids. I also state to thank Dr. Ooi Ban Leong, Assistant Professor, my advisor and supervisor, giving instructions, guidance, patience and advices how to learn and study in research-work in all respects and help in the completion of my project. I also thank my former supervisor, Dr. Kimberly Wallace Eccleston, Senior Lecturer, who instructs me research interests well. At the same time, I also thank the staff from Microwave laboratory, namely Mr Wu Bin who is a professional lab officer, Mr Neo Hong Keem who is a laboratory officer from Antenna scattering laboratory compact range, Mr. Sing Cheng Hiong, Mr. Jalil Bin Din and Mdm Lee Siew Choo, who give great services and helps in their respective laborites and Mr. Chan Leong Hin of electrical workshop. I never forget to thank the writers of multifarious materials as well as thinkers in the course of my research-work. Lastly I would like to thank all my colleagues from Microwave lab for their help whenever I need anytime.

CONTENTS

LIST OF FIGURES

LIST OF TABLES

LIST OF SYMBOLS

Z_0	Characteristic impedance of transmission line
Z_{0ATL}	Characteristic impedance of artificial transmission line
ATL	Artificial transmission line
TL	Transmission line
L	Inductance per unit length of transmission line
C	Capacitance per unit length of transmission line
C_p	Capacitance value of loaded capacitor
d	Unit length of artificial transmission line
W_{stub}	Width of microstrip open stub
l_{stub}	Length of microstrip open stub
c	Speed of light in free space (3×10^8 m/s)
v_p	Phase velocity
μ_0	Permeability of free space ($4\pi\times10^{-7}$ H/m)
ε_0	Permittivity of free space (8.854×10^{-12} F/m)
β	Propagation constant
λ_g	Guided wavelength
ω	Angular frequency
f	Operating frequency
ε_r	Relative dielectric constant
ε_e	Effective dielectic constant
$\tan\delta$	Dielectric loss tangent
σ	Conductivity of material
ρ	Resitivity of material
R_{RF}	Skin effect coefficient
δ	Skin depth of conductor
W	Width of microstrip line
h	Distance between the microstrip line and the ground plane
W_d	Width of the dipole antenna

W_f	Width of the microstrip feedline
L_d	Physical length of the dipole antenna
L_f	Physical length of the microstrip feedline
L_y	Distance from the feedline port
d_x	Transverse from dipole
f_0	Resonant frequency of EMC dipole
EMC	Electromagnetically coupled
PBG	Photonic Bandgap

CHAPTER I
INTRODUCTION

1.1 Background

Miniaturization and integration are the current trend in microwave technology. The most commonly used microwave integrated circuit (MIC) transmission line is the microstrip line which has many advantages such as low cost, small size, absence of critical matching and cutoff frequency, ease of active device integration, use of photolithographic method for circuit production, and compatibility with monolithic circuits. It is an essential component in modern wireless systems. The key difference between the circuit analysis and transmission line theory is that the physical dimensions of a network are much smaller than the electrical wavelength but for the transmission lines, it may be a considerable fractional of a wavelength or many wavelength in size. In transmission line the voltage and currents are varied along the length of the line thus it is looked like a distributed parameter network.

In the design of electronic systems such as satellite communications, phase-array radar systems and other applications, circuit size and weight are the critical factors and this requirement is fulfilled by microwave integrated circuits (MICs). Monolithic microwave integrated circuits (MMIC) use microstrip lines as matching networks and the active and passive circuit elements are fabricated on the same chip with the use of the transmission line. In order to have a smaller area occupying on the circuit, it is attempted to design the artificial transmission lines which have similar behavior to transmission lines but with reduced physical dimensions by incorporating with lumped elements.

The simplest form of a microstrip device consists of a sandwich of two parallel conducting layers separated by a thin dielectric substrate. The lower layer is functioned as a ground plane and the upper conductor is dependent on its application. If the upper conductor is a long narrow strip, it is performed as a microstrip transmission line and if it is a fraction of a wavelength size patch, then it is become a microstrip antenna. The electromagnetic wave propagation constant in the microstrip substrate must be exactly known in order to predict the resonant frequency, resonant resistance and other antenna

quantities. The dielectric constant of the substrate material is the most sensitive parameter in microstrip antenna performance consideration.

The antenna is a component that radiates and receives RF or microwave signal and hence the antenna serve as bidirectional device that is a receiving or transmitting device. The function of an antenna is that it converts the guided electromagnetic wave on a transmission line to a plane wave propagation in free space. Because of this, one side of an antenna serves as an electrical circuit element while the other side provides an interface with a propagation plane wave. The guided electromagnetic waves are confined to the boundaries of a transmission line to transport signals from one point to another but the free-space waves radiate unbounded [3].

In general, microstrip antennas have a conducting patch printed on a grounded microwave substrate. The attractive features of the microstrip antennas are low profile, light weight, easy fabrication, conformable to planar and non-planar surfaces, simple and inexpensive to manufacture using modern printed-circuit technology, mechanically robust when mounted on rigid surfaces, compatible with MMIC designs and also conformability to mounting hosts. Thus they are found wide applications in high performance such as aircraft, satellite and missile applications where size, weight, cost, performance, ease of installation and aerodynamic profile are constraint and the low profile antennas are required [1]. The present-day mobile communication systems are demanded smaller antenna size in order to meet the miniaturization requirement of mobile units. Microstrip antennas can satisfy all these requirements, and various types of microstrip antennas have been developed for use in mobile communication systems. However, the most serious limitation of the micorstrip antenna elements is the narrow bandwidth and the bandwidth enhancement is the main for the practical applications.

Microstrip antennas have been exploited to many forms of geometric shapes to achieve certain specifications including rectangular and circular microstrip patches. Microstrip dipole antennas and conformal printed circuited antennas are another type of antennas that have been accepting more attentions in research area. Antennas are categorized by the way they are feed and excited, some categories include the normal transmission line feed; coaxial line feed and electromagnetically coupled (EMC) feed. In this project it is concentrated on the bandwidth improvement of a tri-band EMC microstrip dipole antenna.

Electromagnetically coupled (EMC) microstrip dipole is a new class of printed circuit radiator where there is no direct contact between the feed line and the radiation

element. This type of feeding technique is provided to match easily with the radiator. Generally there are numerous configuration of EMC microstrip dipole antenna but it can be grouped into two main configurations namely longitudinal and transversal configuration. The advantages of EMC microstrip dipole antennas include greater bandwidth and efficiency which can be obtained by increasing radiator-ground plane spacing. At the same time microstrip feed line closer to the ground plane than the dipole reduces feed line radiation due to discontinuities. Such radiation has been shown to be reduced when the circuit-ground plane spacing is decreased. Another advantage of the EMC dipole antenna is that the dipole can be matched to its microstrip feedline. This is due to the field-coupling nature of this geometry in addition to the involvement of both magnetic and electric field, which allows a perfect match to be found in most cases.

The good electrical performances of conformable structure, relatively low cost, compact size and light in weight, the microstrip antennas are very attractive in cellular phone wireless local loop networks, and wireless data transmission systems. At present days, the cellular phone systems is widely used around the world, the development of the multiband resonant frequency of different countries was depend on using the different frequencies band where tri-band cellular system suggests that there is a need for tri-band antenna with the multi-band of resonant frequency of 0.9GHz, 1.8GHz and 2.4GHz was interested in this project.

The photonic bandgap (PBG) structure, also called electromagnetic crystals is a periodic structure in which the propagation of the electromagnetic waves within a certain frequency band is prohibited. The microstrip feedline incorporating a photonic bandgap (PBG) structure has shown great potential application in antennas, filters and other microwave devices. These structures have slow wave and bandstop characteristic and can forbid certain band of frequencies and reduce the physical dimension of the microstrip structure. In this project, one dimensional (1-D) microstrip photonic bandgap (PBG) cells are investigated. In the study of microstrip transmission line over a periodically perforated ground plane, it is found that the propagation constant is strongly depend on the orientation and location of the transmission line with respect to the two principle axes of the periodic perforations suspended so that the circuit cannot be fixed on a metal base for mechanic robustness. Perforation on transmission line itself of this one dimensional PBG structure is a potential solution to these problems.

1.2 Objective

The objective of this project is to improve the bandwidth of a family of Π-shaped proximity fed patch, to develop the application of artificial transmission line concept in a tri-band EMC microstrip dipole antenna by microstrip technology in transverse configuration. The investigation was based first on the conventional microstrip feed line and then on the compact one dimensional (1-D) photonic bandgap (PBG) structure feedline. The study was based on the three frequencies of 0.9GHz, 1.8GHz and 2.4GHz with varying the dipole length, width, and position longitudinally and transversally. The final design has improved bandwidth over the EMC dipole with the tapered shape and the bandwidth improvement is obtained 0.3%.

1.3 Scope

The background study of the artificial transmission based on the microstrip transmission line was first explained in Chapter 2. The design consideration for the compact size is concentrated on the artificial concept and the simulation results. The novel Π-shaped proximity coupled U-slot patch antennas with the simulations results and the measurement results are presented in Chapter 3, the EMC microstrip dipole antenna in transverse configuration has been stated in Chapter 4. The EMC dipole antenna with the compact PBG feedline investigation is also explained in Chapter 4. This structure is displayed that a considerable improvement in antenna performance of increase power radiated, bandwidth and efficiency can be accomplished. The design of single band and tri-band antennas consideration based on the electromagnetically coupled dipole was expressed in Chapter 5. The further analysis of bandwidth improvement techniques with the taper-shaped on the dipole antenna was investigated in Chapter 5 using the simulation software IE3D. A final tri-band dipole antenna with the taper dipole antenna designs, fabrications and measurement data results are presented in Chapter 5. The final chapter concludes the project and provides suggestions for future work.

List of Contribution

As a result of my usual work, the following paper was accepted for publication:
"Novel Multi-fingered Antenna", paper accepted for publication in the proceeding of 2003 IEEE Topical Conference on Wireless Communication Technology, Hawaii.

CHAPTER II
ARTIFICIAL TRANSMISSION LINE THEORY

2.1 Microstrip Transmission Line

The microstrip transmission line is one of the widespread planar transmission lines. The general structure of the microstrip transmission line is shown in Figure 2.1. It is a simple device with a conducting strip (microstrip line) with a width *W* and a thickness *t* is on the top of a dielectric substrate which has a relative dielectric constant ε_r and a thickness *h*, and the bottom of the substrate is a ground (conducting) plane. The most important parameters in microstrip circuit design are *W*, *h*, and ε_r. The effect of strip thickness *t* and the conductivity σ are secondary. The development of solid-state microwave devices become popular use of parallel-plate transmission line called microstrip lines which can be fabricated by photolithographic process and it is easily integrated with other active and passive circuit components.

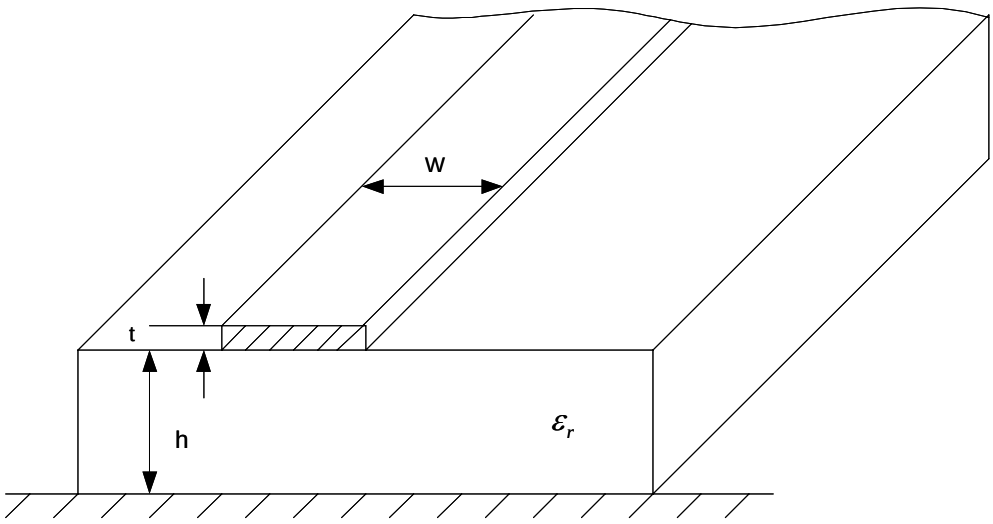

Figure 2.1: The geometry of the microstrip transmission line

The fields in the microstrip are contained within two media, air above and dielectric below that is some of the fields is concentrated in the dielectric region and the others are in the air region which is inhomogeneous nature. Due to this inhomogeneous nature, the microstrip cannot support a pure TEM wave. This is called the quasi-TEM approximation which has only transverse components. Thus the waves

in a microstrip line have electric and magnetic fields with the presence of the two guided-wave media (the dielectric substrate and the air) and the propagation velocities is dependent not only on the material properties, the permittivity, ε and the permeability, μ but also on the physical dimensions of the microstrip line. In the quasi-TEM approximation, a homogeneous dielectric material with an effective dielectric permittivity replaces the inhomogeneous dielectric– air media of microstrip.

The phase velocity and propagation constant in the dielectric region can be expressed as

$$v_p = \frac{c}{\sqrt{\varepsilon_e}} \tag{2.1}$$

$$\beta = \frac{\omega}{c}\sqrt{\varepsilon_e} \tag{2.2}$$

where, ε_e is the effective dielectric constant of the microstrip line and this effective dielectric constant is satisfied the relation

$$1 < \varepsilon_e < \varepsilon_r$$

and is dependent on the substrate thickness, *h*, and the conductor width, *W*. The design formulas for effective dielectric constant and characteristic impedance of the microstrip line can be presented as follows by Pozar [pp162].

The effective dielectric constant of a microstrip line is given approximately by

$$\varepsilon_e = \frac{\varepsilon_r + 1}{2} + \frac{\varepsilon_r - 1}{2}\frac{1}{\sqrt{1 + 12\,h/W}} \tag{2.3}$$

If the dimension of the microstrip line can be known, the characteristic impedance can be calculated as

$$Z_0 = \begin{cases} \dfrac{60}{\sqrt{\varepsilon_e}}\ln\left(\dfrac{8h}{W} + \dfrac{W}{4h}\right) \; for \; \dfrac{W}{h} \le 1 \\ \dfrac{120\pi}{\sqrt{\varepsilon_e}\left[\dfrac{W}{h} + 1.393 + 0.667\ln\left(\dfrac{W}{h} + 1.444\right)\right]} \; for \; \dfrac{W}{h} \ge 1 \end{cases} \tag{2.4}$$

For a given characteristic impedance Z_0 and dielectric constant ε_r, the $\dfrac{W}{h}$ ratio can be found as

$$\frac{W}{h}=\begin{cases}\dfrac{8e^{A}}{e^{2A}-2} \; for \; \dfrac{W}{h}<2 \\ \dfrac{2}{\pi}\left[B-1-\ln(2B-1)+\dfrac{\varepsilon_r-1}{2\varepsilon_r}\left\{\ln(B-1)+0.39-\dfrac{0.61}{\varepsilon_r}\right\}\right] for \; \dfrac{W}{h}>2\end{cases} \tag{2.5}$$

where $A=\dfrac{Z_0}{60}\sqrt{\dfrac{\varepsilon_r+1}{2}}+\dfrac{\varepsilon_r-1}{\varepsilon_r+1}\left[0.23+\dfrac{0.11}{\varepsilon_r}\right]$

$$B=\frac{377\pi}{2Z_0\sqrt{\varepsilon_r}}$$

Once the effective dielectric constant of a microstrip is determined, the guided wavelength of the quasi-TEM mode of microstrip is given by

$$\lambda_g=\frac{\lambda_0}{\sqrt{\varepsilon_e}} \tag{2.6a}$$

where, λ_0 is the free space wavelength at operation frequency *f*. More conveniently, where the frequency is given in gigahertz (GHz), the guided wavelength can be evaluated in millimeters as follows:

$$\lambda_g=\frac{300}{f(GHz)\sqrt{\varepsilon_e}} \tag{2.6b}$$

2.1.1 Losses in Microstrip Lines

A microstrip has higher losses than a rectangular waveguide and the loss components of a microstrip line consist of conductor loss, dielectric loss, radiation loss, surface-wave propagation and the magnetic loss which is only for magnetic substrates such as ferrite. The conductor loss and the dielectric loss are due to dissipative effects while the radiation loss and surface–wave propagation are due to the parasitic effects. Conductor loss is caused due to the current flow between the conductor and the ground plane it is dominates at microwave frequencies. The dielectric loss is small for most substrate materials while the radiation loss is due to discontinuities on the microatrip line. The radiation loss is negligible for MMIC and MIC substrate thickness i.e., $h/\lambda_0 \ll 0.01$. But the discontinuities due to radiation loss excite higher-order mode and radiates energy. According to Hammerstad and Bekkadal, the conductor loss can be calculated

$$\alpha_c = 0.072 \frac{\sqrt{f}}{\omega Z_0} \lambda_g \, dB/\text{guided wavelength} \tag{2.7}$$

where, f is in gigahertz and Z_0 is in ohms.

The attention due to the dielectric loss is related to the loss tangent of the substrate and it can be known as:

$$\alpha_d = 27.3 \frac{\varepsilon_r(\varepsilon_e - 1)\tan\delta}{\varepsilon_e(\varepsilon_r - 1)} dB/\text{guided wavelength} \tag{2.8}$$

where $\tan\delta$ denotes the loss tangent of the dielectric substrate.

2.1.2 Effect of Dispersion

In quasistatic case, the characteristic impedance of the transmission line, Z_0, and the effective dielectric constant , ε_e, are independent of frequency. If these two parameters are not constant but depends on functions of frequency especially true fro high frequencies, then there is a dispersion in microstrips. This dispersion effect increases as the frequency, f ,or the substrate thickness, h ,or the dielectric constant, ε_r, is increased. The results calculated including dispersion effect is markedly different from those static-TEM calculations at higher frequencies. The frequency variation of $\varepsilon_e(f)$ and $Z_0(f)$ can be calculated as the following equations:

$$\varepsilon_e(f) = \left(\frac{\sqrt{\varepsilon_r} - \sqrt{\varepsilon_e(0)}}{1 + 4F^{-1.5}} + \sqrt{\varepsilon_e(0)} \right)^2 \tag{2.9}$$

where,
$$F = \frac{4hf\sqrt{\varepsilon_r - 1}}{c} \left\{ 0.5 + \left[1 + 2\log\left(1 + \frac{W}{h} \right) \right]^2 \right\},$$

$$Z_0(f) = Z_0(0) \frac{\varepsilon_e(f) - 1}{\varepsilon_e(0) - 1} \sqrt{\frac{\varepsilon_e(0)}{\varepsilon_e(f)}} \tag{2.10}$$

where, $\varepsilon_e(0)$ and $Z_0(0)$ are quasistatic results assuming at $f = 0$.

According to Owens, the dynamic problem of the frequency dependence of the microstrip characteristic impedance can also be considered with the effective microstrip width concept. Developed from Owens, the frequency dependence of the microstrip characteristic impedance can be calculated as follows:

$$Z_0(f) = \frac{h\eta}{W_{eff}(f)\sqrt{\varepsilon_e(f)}} \tag{2.11}$$

where $W_{eff}(f)$ is the effective microstrip width and can be written as

$$W_{eff}(f) = W + \frac{W_{eff}(f) - W}{1 + (f / f_p)^2} \tag{2.12}$$

where, the characteristic impedance in free space, $\eta = \sqrt{\mu_0 / \varepsilon_0}$ (2.13)

$$f_p = \frac{c}{2W_{eff}\sqrt{\varepsilon_e}} \tag{2.14}$$

$$W_{eff} = \frac{h\eta}{Z_0\sqrt{\varepsilon_e}} \tag{2.15}$$

2.2 Coupled Microstrip lines

The cross section of a coupled microstrip lines with the two microstrip lines of width W are in parallel- or edge-coupled configuration with a separation S is shown in Figure 2.2. The properties of coupled microstrip lines are determined by the self and mutual inductances and capacitances between the lines and these structures support two quais-TEM modes of the even mode and the odd mode as shown in Figure 2.3.

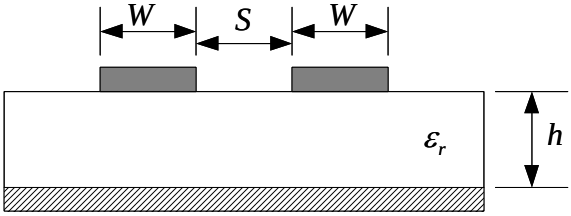

Figure 2.2: The cross section of coupled microstrip lines

Under the quasi-TEM approximation, the self-inductance can be expressed in terms of self-capacitance, and hence, only capacitance parameters are evaluated for coupled microstrip lines. In an even mode excitation, the two parallel microstrip lines have the same voltage potential of carry the same positive sign charges resulting in a magnetic wall while in an odd mode excitation, the two parallel microstrip lines have the opposite voltage potential or carry the opposite charge resulting in an electric wall.

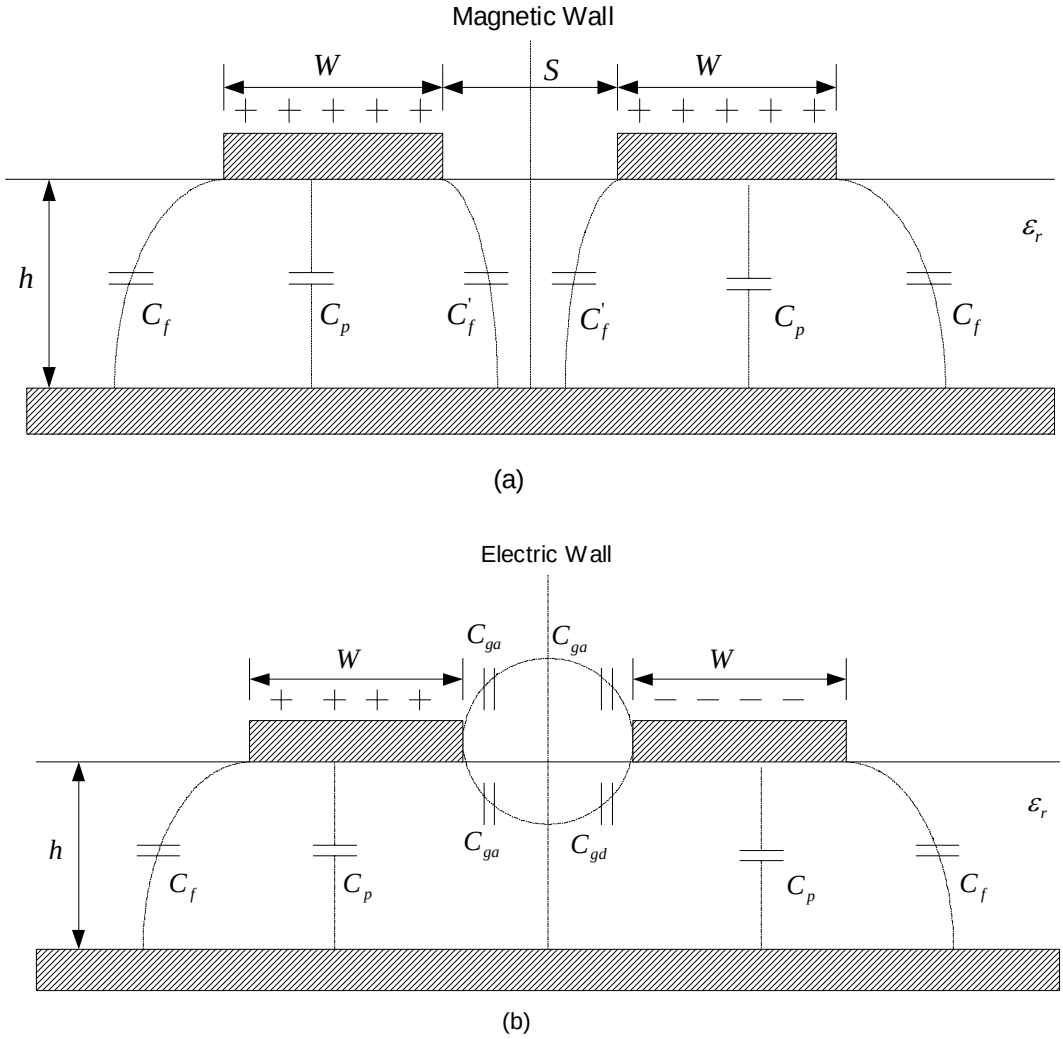

Figure 2.3: Decompositon of total capacitance of coupled microstrip lines in (a) even mode capacitances and (b) odd mode capacitances

The separation distance between the adjacent microstrip lines (S) should be much smaller than the thickness of the substrate to have significant coupling between them. If the distance apart (S) is comparable to the substrate thickness (h), then the microstrip lines are treated as normal single transmission line with small amount of coupling. Both the even and the odd mode excitation are occurred at the same time but they propagate with different phase velocities as they are not pure TEM modes. Hence, the coupled microstrip lines are characterized by the characteristic impedances as well as the effective dielectric constants for the two modes.

The total even and odd mode capacitances can be written as

$$C_e = C_p + C_f + C_f' \tag{2.16}$$

$$C_0 = C_p + C_f + C_{ga} + C_{gd} \tag{2.17}$$

Parallel plate capacitance, $$C_p = \varepsilon_0 \varepsilon_r \frac{W}{h} \tag{2.18}$$

The rest of the capacitances such as $C_f, C_f^{'}, C_{ga}$ and C_{gd} represent various fringing capacitances which is given by

$$C_f = \frac{1}{2}\left(\frac{\sqrt{\varepsilon_e}}{cZ_0} - C_p \right) \tag{2.19}$$

The expression for $C_f^{'}$ is obtained as

$$C_f^{'} = \frac{C_f}{1 + A(h/S)\tanh(8S/h)} \sqrt{\frac{\varepsilon_r}{\varepsilon_e}} \tag{2.20}$$

where $$A = \exp[-0.1\exp(2.33 - 2.53W/h)]$$

C_{ga} is the capacitance term in odd mode for fringing field across the gap of distance, S, in the air region. It is derived from an equivalent geometry of coplanar strips which is given by

$$C_{ga} = \varepsilon_0 \frac{K(k^{'})}{K(k)} \tag{2.21}$$

where $$k = \frac{S/h}{S/h + 2W/h} \tag{2.22}$$

$$k^{'} = \sqrt{1 - k^2} \tag{2.23}$$

where the ratio of the complete elliptic function $K(k)$ and its complementary $K(k^{'})$ is derived to be

$$\frac{K(k)}{K^{'}(k)} = \begin{cases} \left[\frac{1}{\pi} \ln\left(2\frac{1+\sqrt{k^{'}}}{1-\sqrt{k^{'}}} \right) \right]^{-1}, & for\, 0 < k < 0.7 \\ \frac{1}{\pi} \ln\left[2\frac{1+\sqrt{k}}{1-\sqrt{k}} \right], & for\, 0.7 < k < 1 \end{cases} \tag{2.24}$$

C_{gd} is the capacitance in odd mode for fringing field across the gap of distance, S, in the dielectric region, which is obtained as follows:

$$C_{gd} = \frac{\varepsilon_0 \varepsilon_r}{\pi} \ln\left\{ \coth\left(\frac{\pi S}{4h} \right) \right\} + 0.654 C_f \left[\frac{0.02}{S/h} \sqrt{\varepsilon_r} + 1 - \varepsilon_r^{-2} \right] \tag{2.25}$$

The characteristic impedance and the effective microstrip permittivities for the two modes, namely, even mode and odd mode, can be obtained from the capacitance value using the relations below:

$$Z_{0m} = \left[c\sqrt{C_m C_m^a} \right]^{-1} \tag{2.26}$$

$$\varepsilon_{e,m} = C_m / C_{ma} \tag{2.27}$$

where, m denotes for even or odd mode, while C^a denotes the capacitance with air as dielectric $(\varepsilon_r = 1)$. However, the accuracy of calculated impedance values of the coupled line shows an arrangement better than 3 percent for $0.2 \le W/h \le 2$, $0.05 \le S/h \le 2$ and $\varepsilon_r \ge 1$.

When two parallel microstrips are placed to each other, separated by a distance, S, presence of coupling effect between them can affect the characteristic behavior of the artificial transmission line structure.

The coupling effect between two parallel microstrip lines is given as,

Coupling per unit length= $\frac{C_{ga} + C_{gd}}{2}$

Coupling= (Coupling per unit length) x (length of the microstrip)

2.3 Microstrip components

The artificial transmission line can be realized incorporating lumped elements like passive lumped capacitors and inductors. The size of lumped-circuit element is very smaller than the operating wavelength, and hence exhibits negligible phase shift. Lumped circuit elements with lower Q than the distributed circuits have the advantages of smaller size, lower cost, and wide-band characteristic. These are especially suitable for monolithic MICs and for broad-band hybrid MICs.

At low frequencies, lumped elements have the advantages of smaller size and wider bandwidth as compared to distributive elements (stubs, line sections, etc.). At high frequencies, however, distributed circuits are used because of lower loss (or higher Q), and the size advantage of the lumped element is no longer a significant factor. Lumped element components normally exhibit undesirable effects such as spurious resonances, fringing fields, parasitic capacitance and inductance, parasitic resistance and loss and various perturbations.

2.3.1 Design of Capacitors

There are a variety of planar capacitors suitable for monolithic circuits. Some are with a single metallization technology scheme such as broadside coupled, end coupled lines, open-circuit microstrip line and interdigital capacitor, and others are utilizing a two-level metallization technology in conjuction with dielectric films like metal-insulator-metal (MIM) capacitor. Generally, there are three types of passive capacitors generally used in microwave circuits: microstrip patch, interdigital, and metal-insulator-metal (MIM). Microstrip patch capacitors are comprised of a conductor patch on a dielectric substrate having the ground plane on the other side. These capacitors are only be used for low capacitance values (<0.2pF) due to practical considerations such as capacitance per unit area. The interdigital structures are used in order to have a large value of capacitance per unit area as well as to decrease the distance between the two conductors (top and bottom) of the transmission-line section. The choice between the interdigital and MIM capacitors depends on the capacitance value to be realized and the processing technology. Normally for the values less than 1pF, interdigital capacitors can be used, while for values greater than 1pF, MIM techniques are generally used to minimize the overall size.

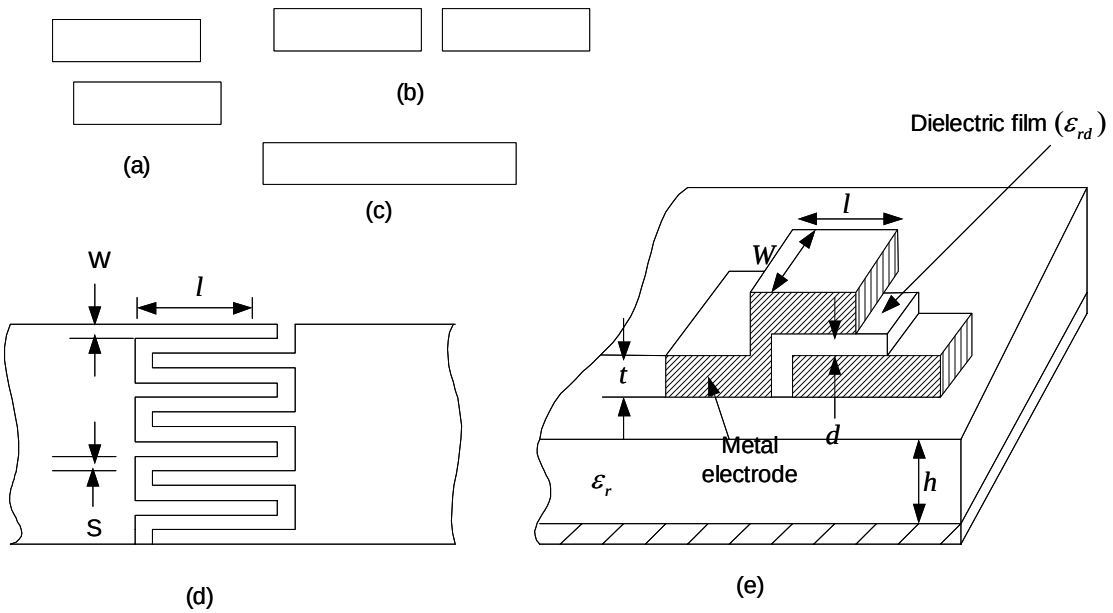

Figure 2.4 : Some Planar Capacitors. (a) Broadside coupled. (b) End Coupled (c) Open circuit line (d) Interdigital Capacitor (e) MIM Capacitor

2.3.1.1 Open Circuit microstrip

A loaded capacitance in the artificial transmission line structure is shown in Figure 2.5 and it can be realized as a small length of an open-circuit stub of a transmission line ($Z_L = \infty$) as shown below.

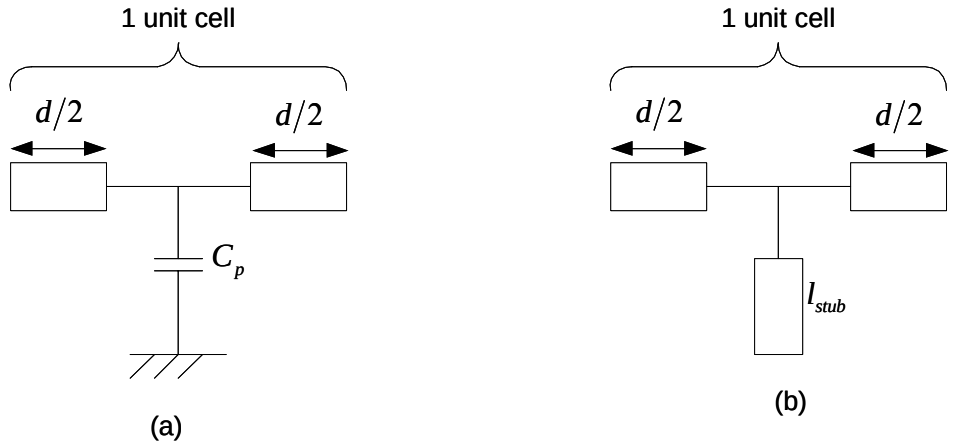

Figure 2.5: One unit cell structure (a) with loaded capacitor (b) with open-circuit line

An open-circuited line has input impedance as follows:

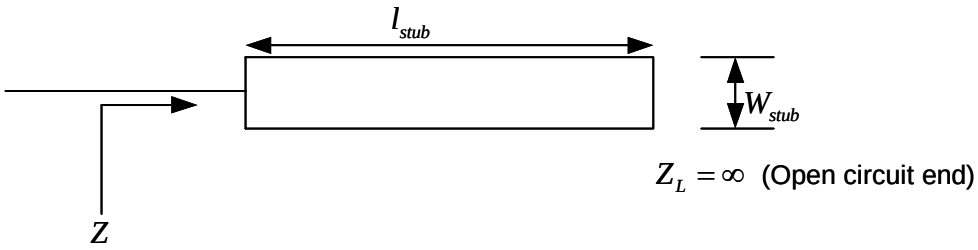

Figure 2.6: Open circuit stub transmission line

An expression for input impedance of a length, l , of transmission line with an arbitiary load impedance, Z , is given by Pozar [pp. 68]

$$Z = Z_0 \frac{Z_{L+} jZ_0 \tan(\beta l_{stub})}{Z_0 + jZ_L \tan(\beta l_{stub})}$$

For open circuit, $Z_L = \infty$, thus the input impedance of an open circuit line is

$$Z = -jZ_0 \cot(\beta l_{stub}) \tag{2.28}$$

From equation (2.28), the input impedance will always remain negative imaginary of capacitive value if and only if the length of the open-circuited line is less than $\lambda/4$ ($l < \lambda/4$).

2.3.1.2 Interdigital Capacitor

Alternatively, in MMIC, design, interdigital capacitor and MIM capacitor can be realized. The expression for an interdigital capacitor is given as shown in Figure 2.7.

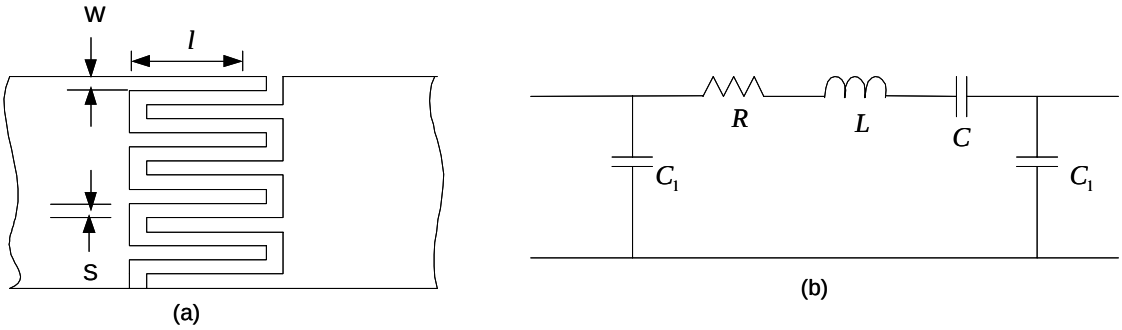

Figure 2.7: Interdigital Capacitor (a) and its equivalent circuit (b)

The capacitance value derived from the interdigital capacitor is given by

$$C(pF) = \frac{\varepsilon_{eff} 10^{-3} K(k)}{18\pi K^{'}(k)}(N-1)l \tag{2.29}$$

where ,

$$k = \tan^2\left(\frac{a\pi}{4b}\right),$$

$$a = W/2$$

$$b = (W+S)/2$$

and,

$$\frac{K(k)}{K^{'}(k)} = \begin{cases} \left[\frac{1}{\pi}\ln\left(2\frac{1+\sqrt{k^{'}}}{1-\sqrt{k^{'}}}\right)\right]^{-1}, & for\, 0 < k < 0.7 \\ \frac{1}{\pi}\ln\left[2\frac{1+\sqrt{k}}{1-\sqrt{k}}\right], & for\, 0.7 < k < 1 \end{cases} \tag{2.30}$$

$$k^{'} = \sqrt{1-k^2}$$

$$R(\Omega) = \frac{4R_s l}{3WN} \tag{2.31}$$

$$C(pF) = \frac{10^{-3}\varepsilon_{rd} Wl}{36\pi d} \tag{2.32}$$

All the dimensions are in micrometers. Since the interdigital capacitor is used as a shunt capacitor, one of the adjacent plates of the capacitor is shorted to the ground. By ignoring the parasitic components, a simplified circuit model to represent a shunt interdigital capacitor is given by

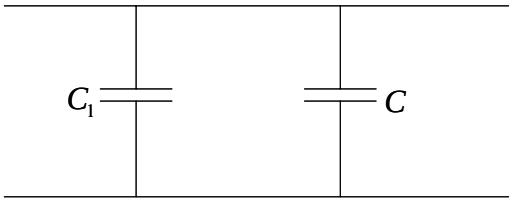

Figure 2.8: The equivalent circuit model for the simplified interdigital capacitor

$$C_{effective} = C_1 + C_2 \tag{2.33}$$

2.3.1.3 MIM Capacitor

The expression for a MIM capacitor is given as shown below.

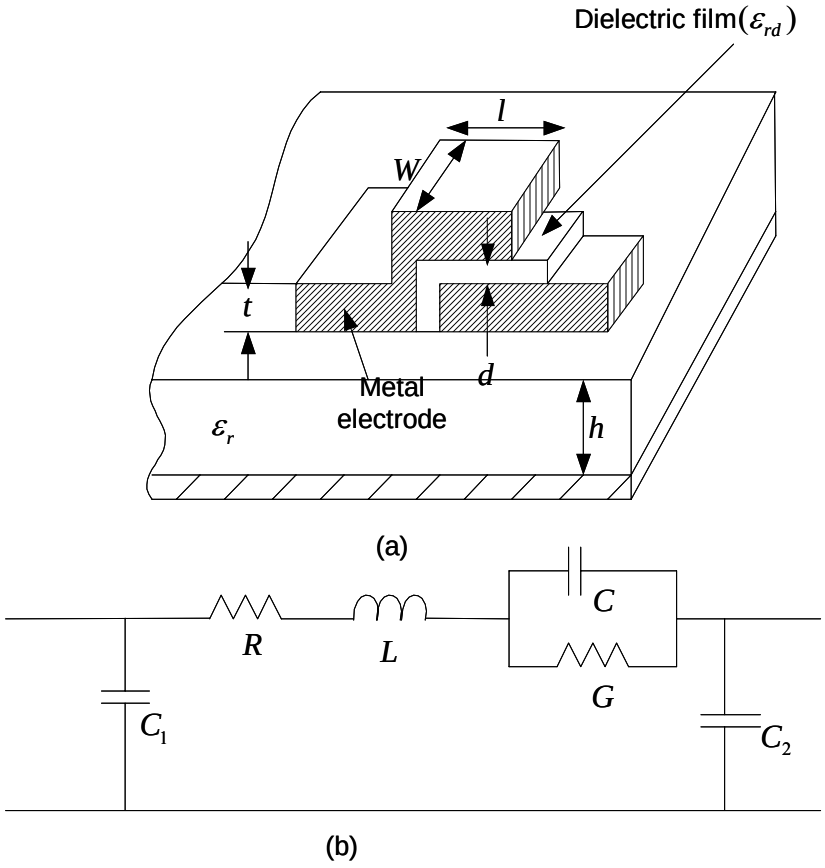

Figure 2.9: MIM Capacitor (a) and itsequivalent circuit (b)

The component values derived from the circuit structure of MIM capacitor are given by

$$C(pF) = \frac{10^{-3}\varepsilon_{rd} W l}{36\pi d} \tag{2.34}$$

$$R(\Omega) = \frac{K R_s l}{W + t} \tag{2.35}$$

$$G(\mho) = \omega C \tan\delta \tag{2.36}$$

$$C_1 = C_2(pF) = 10^{-2}\left[\frac{\sqrt{\varepsilon_{eff}}}{Z_0(W,h,\varepsilon_r)} - \frac{\varepsilon_r W}{360\pi h}\right] l \tag{2.37}$$

Since MIM capacitor is used as a shunt capacitor, one of the capacitor plate is shorted to the ground. By ignoring the parasitic components, a simplified circuit model to represent a shunt MIM capacitor is given by

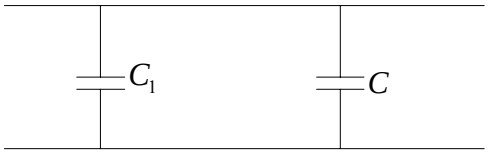

Figure 2.10: The equivalent circuit model for the simplified MIM capacitor

$$C_{effective} = C_1 + C_2$$

2.4 Design Equation

In general, two-conductor uniform transmission lines that consist of parallel plate, two-wire, and coaxial lines have loss due to finite conductivity and/or lossy dielectric, but these losses are usually small. The short piece of length Δz of a transmission line can be modeled as a lumped network circuit consisting of inductances, capacitances and resistances as shown in Figure 2.11.

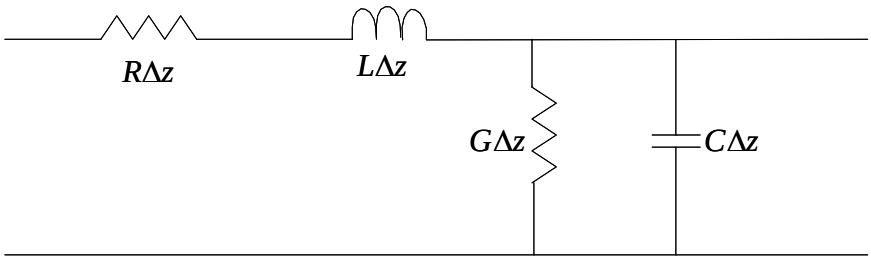

Figure 2.11: Equivalent circuit for a very short length (infinitesimally short)

where, R = series resistance per unit length, in Ω/m

L = series inductance per unit length, in H/m

G = shunt conductance per unit length, in S/m

C = shunt capacitance per unit length, in F/m

The general expression for the propagation constant, γ, and the characteristic impedance, Z_0, of a transmission line with lumped elements are given by

$$\gamma = \sqrt{(R + j\omega L)(G + j\omega C)} = \alpha + j\beta$$

$$Z_0 = \sqrt{\frac{R + j\omega L}{G + j\omega C}}$$

In practice, the short length of transmission line is equivalent to when losses are assumed negligible.

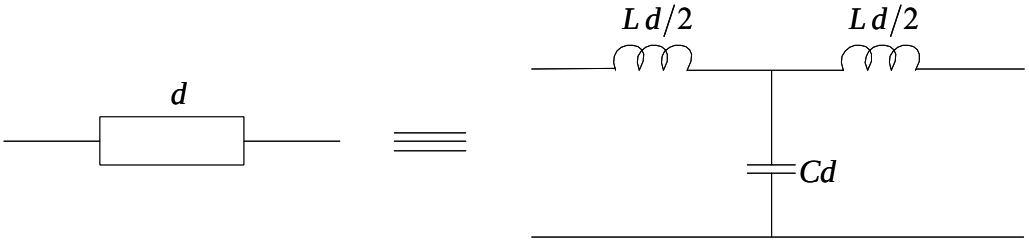

Figure 2.12: The equivalent circuit of short length transmission line

Setting R and $G \to 0$, and the propagation constant and the characteristic of a transmission line becomes

$$\gamma = \alpha + j\beta = j\omega\sqrt{LC}$$

$$\beta = \omega\sqrt{LC} \tag{2.38}$$

$$Z_0 = \sqrt{\frac{L}{C}} \tag{2.39}$$

The wavelength is $$\lambda = \frac{2\pi}{\beta} = \frac{2\pi}{\omega\sqrt{LC}} \tag{2.40}$$

and the phase velocity is $$v_p = \frac{\omega}{\beta} = \frac{1}{\sqrt{LC}} \tag{2.41}$$

At microwave frequencies, the inductors can be realized with a high impedance transmission line. A short length of artificial transmission line can be represented by a tee (T) or a pi (π) network and this can be compared by the ABCD matrices of a transmission line.

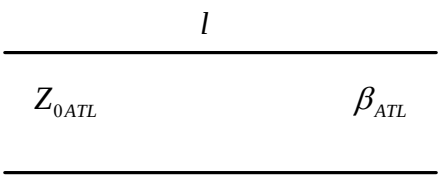

(a)

$$A = \cos\beta_{ATL} \tag{1}$$

$$B = jZ_{0ATL}\sin\beta_{ATL}l \tag{2}$$

$$C = j\frac{1}{Z_{0ATL}}\sin\beta_{ATL}l \tag{3}$$

$$D = \cos\beta_{ATL}l \tag{4}$$

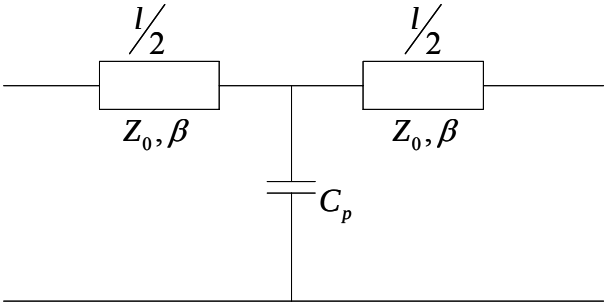

(b)

Figure 2.13: ABCD parameters of some useful two-port circuit (a) and (b)

$$ABCD = \begin{pmatrix} \cos\frac{\beta l}{2} & jZ_0\sin\frac{\beta l}{2} \\ j\frac{1}{Z_0}\sin\frac{\beta l}{2} & \cos\frac{\beta l}{2} \end{pmatrix}\begin{pmatrix} 1 & 0 \\ j\omega C_p & 1 \end{pmatrix}\begin{pmatrix} \cos\frac{\beta l}{2} & jZ_0\sin\frac{\beta l}{2} \\ j\frac{1}{Z_0}\sin\frac{\beta l}{2} & \cos\frac{\beta l}{2} \end{pmatrix}$$

$$= \begin{pmatrix} \cos\frac{\beta l}{2} - \omega C_p Z_0\sin\frac{\beta l}{2} & jZ_0\sin\frac{\beta l}{2} \\ j\frac{1}{Z_0}\sin\frac{\beta l}{2} + j\omega C_p\cos\frac{\beta l}{2} & \cos\frac{\beta l}{2} \end{pmatrix}\begin{pmatrix} \cos\frac{\beta l}{2} & jZ_0\sin\frac{\beta l}{2} \\ j\frac{1}{Z_0}\sin\frac{\beta l}{2} & \cos\frac{\beta l}{2} \end{pmatrix}$$

$$A = D = \cos^2\frac{\beta l}{2} - \omega C_p Z_0\sin\frac{\beta l}{2}\cos\frac{\beta l}{2} - \sin^2\frac{\beta l}{2}$$

$$B = j2Z_0\sin\frac{\beta l}{2}\cos\frac{\beta l}{2} - jZ_0^2\omega C_p\sin^2\frac{\beta l}{2}$$

$$C = j\frac{2}{Z_0}\sin\frac{\beta l}{2}\cos\frac{\beta l}{2} + j\omega C_p\cos^2\frac{\beta l}{2}$$

$$A = D = \cos^2\frac{\beta l}{2} - \sin^2\frac{\beta l}{2} - \omega C_p Z_0\sin\frac{\beta l}{2}\cos\frac{\beta l}{2} \tag{5A}$$

$$= \cos^2\frac{\beta l}{2} - \sin^2\frac{\beta l}{2} - \frac{\omega C_p Z_0}{2}\left[\sin(\frac{\beta l}{2} + \frac{\beta l}{2}) + \sin(\frac{\beta l}{2} - \frac{\beta l}{2})\right]$$

$$= \cos^2\frac{\beta l}{2} - \sin^2\frac{\beta l}{2} - \frac{\omega C_p Z_0}{2}\sin\beta l$$

$$= \cos\beta l - \frac{\omega C_p Z_0}{2}\sin\beta l$$

If the periodic structure is supporting a propagation wave, the voltage and current at (n+1) terminal to be equal to voltage and current at n^{th} terminal with phase delay.

$$V_{n+1} = e^{\gamma d} V_n$$

$I_{n+1} = e^{-\gamma d} I_n$ where $\gamma = \alpha + j\beta$, is the propagation constant for periodic structure. The voltage and the current on either side of n^{th} unit cell using ABCD matrix

$$\begin{pmatrix} V_n \\ I_n \end{pmatrix} = \begin{pmatrix} A & B \\ C & D \end{pmatrix} \begin{pmatrix} V_{n+1} \\ I_{n+1} \end{pmatrix}$$

where A,B,C,D are matrix parameters for a cascade of a transmission line section of length $\frac{l}{2}$.

$$\begin{pmatrix} V_n \\ I_n \end{pmatrix} = \begin{pmatrix} A & B \\ C & D \end{pmatrix} \begin{pmatrix} V_{n+1} \\ I_{n+1} \end{pmatrix} = e^{\gamma l} \begin{pmatrix} V_{n+1} \\ I_{n+1} \end{pmatrix}$$

$$\left(\begin{pmatrix} A & B \\ C & D \end{pmatrix} - \begin{pmatrix} e^{\gamma l} & 0 \\ 0 & e^{\gamma l} \end{pmatrix} \right) \begin{pmatrix} V_{n+1} \\ I_{n+1} \end{pmatrix} = 0$$

For a nontrivial solution, the determinant of the above matrix must vanish.

$$AD + e^{2\gamma l} - Ae^{\gamma l} - De^{\gamma l} - BC = 0$$

Since, $AD - BC = 1$

$$1 + e^{2\gamma l} - (A+D)e^{\gamma l} = 0$$

$$1 + e^{\gamma l} = (A+D)e^{\gamma l}$$

$$e^{\gamma l} + e^{-\gamma l} = A + D$$

$$\cosh\gamma l = \frac{A+D}{2} = \cos\beta l - \frac{\omega C_p Z_0}{2}\sin\beta l$$

Assuming, $\cos\beta_{ATL} l \approx \cos\beta l - \frac{\omega C_p Z_0}{2}\sin\beta l$

When, $l \ll \lambda_g \Rightarrow \beta l = k_0 l$ is small and replace $\cos\beta l$ by $1 - \frac{\beta^2 l^2}{2}$ and $\sin\beta l$ by βl.

(1) = (5A) $\Rightarrow$ $1 - \frac{\beta_{ATL}^2 l^2}{2} = 1 - \frac{k_0^2 l^2}{2} - \frac{\omega C_p Z_0}{2} k_0 l$, where $k_0^2 = \omega^2 LC = \beta^2$

$$\beta_{ATL}^2 l^2 = \omega^2 LCl^2 + \omega C_p \sqrt{\frac{L}{C}}\omega\sqrt{LC} \times l$$

$$\beta_{ATL} = \omega^2 LC + \omega^2 l \frac{C_p}{l}$$

$$\beta_{ATL} = \omega\sqrt{L(C + \frac{C_p}{d})} \tag{2.42}$$

For component B,

$$jZ_{0ATL} \sin \beta_{ATL} l = jZ_0 \sin \frac{\beta l}{2} \cos \frac{\beta l}{2} - jZ_0^2 \omega C_p \sin^2 \frac{\beta l}{2} + jZ_0 \sin \frac{\beta l}{2} \cos \frac{\beta l}{2}$$

(6) = (2) $\Rightarrow$ $\quad Z_{0ATL}(\beta_{ATL} l) = Z_0 \sin \beta l - Z_0^2 \omega C_p \sin^2 \frac{\beta l}{2}$

$$Z_{0ATL}(\beta_{ATL} l) = Z_0 \beta l - Z_0^2 \omega C_p \sin^2 \frac{\beta l}{2}$$

$$Z_{0ATL} = \sqrt{\frac{L}{C}} \frac{\omega\sqrt{LC} \times l}{\omega\sqrt{(C + \frac{C_p}{d})L} \times l}$$

$$Z_{0ATL} = \sqrt{\frac{L}{C + \frac{C_p}{d}}} \tag{2.43}$$

For component C,

$$j \frac{1}{Z_{0ATL}} (\beta_{ATL} l) = j \frac{2}{Z_0} \sin \frac{\beta l}{2} \cos \frac{\beta l}{2} + j\omega C_p \cos^2 \frac{\beta l}{2}$$

$$\frac{1}{Z_{0ATL}} (\beta_{ATL} l) = \frac{1}{Z_0} \sin \beta l + \omega C_p \left[1 - \frac{\beta^2 l^2}{4} \right]$$

$$\frac{\beta_{ATL} l}{Z_{0ATL}} \approx \frac{\beta l}{Z_0} + \omega C_p$$

$$Z_{0ATL} = \frac{\beta_{ATL} l}{\frac{\beta l}{Z_0} + \omega C_p} = \frac{\beta_{ATL} d}{\frac{\beta d}{Z_0} + \omega C_p}$$

$$Z_{0ATL} = \frac{d\omega\sqrt{L(C + \frac{C_p}{d})}}{\frac{d\omega\sqrt{LC}\sqrt{C}}{\sqrt{L}} + \omega C_p}$$

$$Z_{0ATL} = \frac{d\sqrt{L(C + \frac{C_p}{d})}}{dC + C_p} = \frac{\sqrt{L(C + \frac{C_p}{d})}}{C + \frac{C_p}{d}}$$

$$Z_{0ATL} = \sqrt{\frac{L}{C + \frac{C_p}{d}}}$$

From transmission line theory, the characteristic impedance and the phase velocity are known as,

$$Z_0 = \sqrt{\frac{L}{C}}$$

$$v_p = \frac{c}{\sqrt{\varepsilon_e}} = \frac{1}{\sqrt{LC}}$$

From that, the inductance and the capacitance per unit length are such that

$$L = C \times Z_0 \times Z_0$$

$$C = \frac{1}{v_p \times v_p \times L} = \frac{1}{v_p Z_0} = \frac{\sqrt{\varepsilon_e}}{cZ_0}$$

$$L = \frac{Z_0}{v_p} = \frac{\sqrt{\varepsilon_e}}{c} Z_0$$

From ATL design equations, it can be known that,

$$Z_{0ATL}(Z_0, \varepsilon_e, C_p, d) = \sqrt{\frac{L}{C + \frac{C_p}{d}}} = \sqrt{\frac{Z_0 \frac{\sqrt{\varepsilon_e}}{3\times10^8}}{\left(\frac{\sqrt{\varepsilon_e}}{Z_0 \times 3\times10^8}\right) + \frac{C_p}{d}}}$$

$$\phi_{ATL}(Z_0, \varepsilon_e, C_p, d, \omega) = \omega N d \sqrt{L\left(C + \frac{C_p}{d}\right)} = \omega N d \sqrt{\left(Z_0 . \frac{\sqrt{\varepsilon_e}}{3\times10^8}\right) . \left[\left(\frac{\sqrt{\varepsilon_e}}{Z_0 . 3\times10^8}\right) + \frac{C_p}{d}\right]}$$

Thus, the design equation for one unit length and the loading capacitance are as follows:

$$d(Z_0, \varepsilon_e, \phi, Z_{0ATL}, \omega) = \frac{\phi . Z_{0ATL}}{\omega\left(Z_0 \frac{\sqrt{\varepsilon_e}}{3\times10^8}\right)} \tag{2.44}$$

$$C_p(Z_0, \varepsilon_e, \phi, Z_{0ATL}, \omega) = \frac{\phi}{\omega\left(Z_0 . \frac{\sqrt{\varepsilon_e}}{3\times10^8}\right)} \left[\frac{Z_0 \frac{\sqrt{\varepsilon_e}}{3\times10^8}}{Z_{0ATL}} - \frac{\sqrt{\varepsilon_e}}{Z_0 . 3\times10^8} . Z_{0ATL}\right] \tag{2.45}$$

The design equation for the parallel stub length is,

$$l_{stub}(Z_{0stub},\varepsilon_e,C_p,\omega)=\frac{3\times10^8}{\sqrt{\varepsilon_e}}.\frac{1}{\omega}.a\tan\left(\frac{\omega C_p.Z_{0stub}}{N}\right) \quad (2.46)$$

where, N= number of stubs.

The derivation for equation (2.40) is illustrated in section 3.3.

2.5 Microwave Integrated Circuit

Miniaturization of passive components plays an important role in the progress of low-cost passive and active circuits. This can be done by using lumped components on microwave integrated circuit which consists of different circuit functions assembled together formed by strip or microstrip transmission lines and it can be integrated with planar semiconductor devices and passive distributed or lumped circuit elements. At lower frequencies MICs and MMICs are used lumped circuit elements of magnitude smaller size than the circuits of distributed elements such as microstrip lines or coplanar waveguide [3]. MICs have the advantages of higher reliability, reproducibility, better performance, smaller size and lower cost than other microwave circuits. There are two distinct types of microwave integrated circuits.

Hybrid MICs can be divided into two parts: hybrid MICs and miniature hybrid MICs. In hybrid MICs, the distributed elements that are fabricated on a substrate with a single layer metallization while the discrete circuit elements such as inductors, capacitors, resistors and solid-state devices are wire bonded to the substrate [3]. In miniature hybrid MICs, the components such as inductors, capacitors, resistors and distributed circuit elements with the metal patterns are deposited on the substrate and the solid-state devices in the form of chips and packaged are attached to the substrate using multilevel metallization techniques. Generally, the distributed circuit elements such as microstrip line or coplanar waveguide are fabricated using single-layer metallization and the lumped elements such as capacitors, resistors and inductors may be fabricated using multilevel metallization techniques or attached to the substrate in a chip form.

Monolithic integrated circuits (MMICs) are a more recent development, where all active and passive elements are grown onto the substrate of a semi-insulating substrate by some deposition scheme such as epitaxy, ion implantation, sputtering, evaporation, diffusion, or a combination of these processes. The substrate is a

semiconductor material and several layers of metal, dielectric, and resistive films are used. Three general types of circuit components can be utilized for MICs: distributed transmission line (microstrip, coplanar, and strip line, etc.), lumped elements (resistors, inductors, and capacitors) and solid state devices (field-effect transistors, schottky-barrier diode, etc.). Most MMICs can be operated in the frequency range from 0.5~30GHz microwave region and can also be covered in millimeter-wave spectrum from 30~200GHz.

Generally the substrate material is of primary importance for any type of MIC; characteristics such as electrical conductivity, dielectric constant, loss tangent, thermal transfer, mechanical strength, and manufacturing compatibility must be evaluated. Since the prominent feature of low cost, small size, low weight, circuit design flexibility, elimination of circuit tweaking, high-volume manufacturing capability, package simplification, improved reliability, multifunction performance on a single chip and broadband performance, MMICs have some particular advantages over other types of circuits. Since it is very easy to fabricate additional FETs in an MMIC design, circuit performance can often be enhanced with little additional cost. Because of monolithic integrated devices have much less parasitic reactance than discrete packaged devices, MMIC circuits can often be made with broader bandwidth than hybrid circuits.

The general materials for fabricating MICs are divided into four categories:

(1) Substrate materials

(2) Conductor materials

(3) Dielectric films

(4) Resistive films

2.6 ATL Design steps

To overcome the physical size of the large circuit design, artificial transmission line can be used. In this chapter, a series of evolution in design is required before realizing the final ATL design using the equations described in above sections.

2.6.1 Realizing the dimension of transmission line

The first step is to find out the width and the length of transmission lines that has characteristics impedances from 20Ω to 8Ω with phase $\beta l = 90^{\circ}$ at 1.8GHz for Duroid substrate design, using the equation from (2.1) to (2.6).

2.6.2 ATL design with loaded capacitor

A reduction in physical dimension of a transmission line which can be obtained by incorporating artificial transmission line with lumped capacitor (capacitive loading), C_p, to the transmission line structure to give rise to ATL but still having the same characteristics impedance and phase $\beta l = 90^{\circ}$ at the desired frequency. The required parameters such as the length of one unit cell, *lunit*, and the value of loaded capacitor, C_p used in ATL design are obtained by running the Matlab program [Appendix A] or by utilizing equations below,

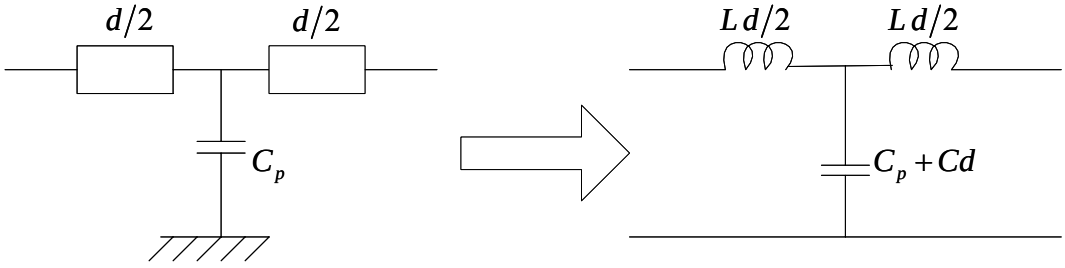

Figure 2.14: One unit cell structure of ATL with loaded capacitor

The equivalent circuit of ATL design structure becomes,

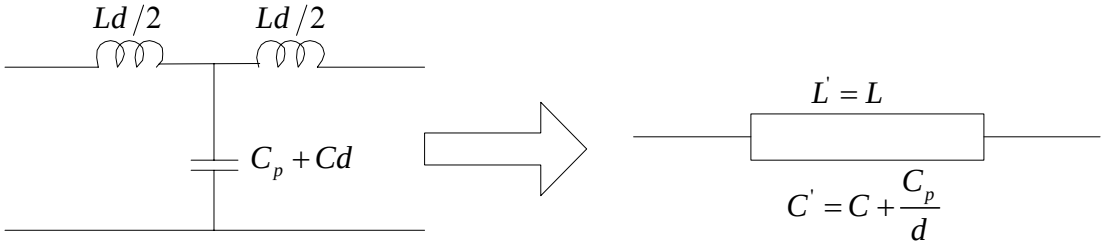

Figure 2.15: The equivalent circuit of ATL design

$$Z_{0ATL} = \sqrt{\frac{L'}{C'}} = \sqrt{\frac{L}{C + \frac{C_p}{d}}}$$

$$\beta_{ATL} = \omega\sqrt{L'C'} = \omega\sqrt{L\left(C + \frac{C_p}{d}\right)}$$

when assuming $d \ll \lambda_g$.

To get wider bandwidth with low characteristic impedance in this design, it is considered as more than or 12 sections cell cascaded in series with the overall phase of 90°.

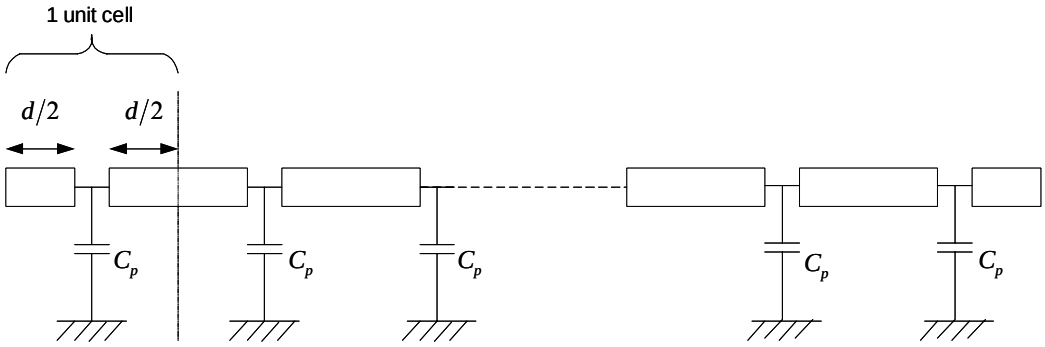

Fiure 2.16: Structure of Artificial Transmission Lines with loaded capacitor

The d is defined as the small length of transmission line per unit cell. The loading capacitance can be realized wit an open-circuit stub of a transmission lines as shown below.

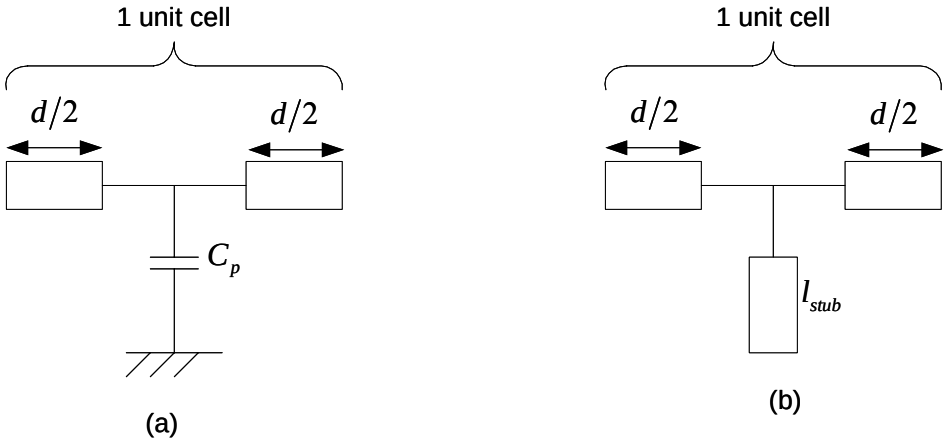

Figure 2.17: One unit cell structure (a) with loaded capacitor (b) with open-circuit line

The input impedance of an open-circuited transmission line with length, l, can be calculated as follows:

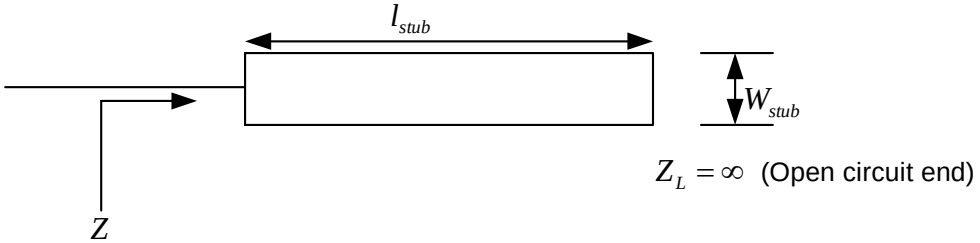

Figure 2.18: Open circuit stub transmission line

$$Z = -jZ_{0stub}\cot(\beta l)$$

The susceptance of the loading capacitance is $Y = j\omega C_p$ (2.47)

And the susceptance of the open stub is, $Y = j\frac{1}{Z_{0stub}}\tan(\beta l)$ (2.48)

It can be made $\omega C_p = \frac{1}{Z_{0stub}}\tan(\beta l)$ at a particular frequency.

If it is wanted to be $\omega C_p = \frac{1}{Z_{0stub}}\tan(\beta l)$ over a wide frequency range.

where, Z_{0stub} = characteristic impedance of an open-circuited transmission line, providing with the length of the stub, $l \ll \lambda$.

The length of the open-circuited stub can be known as follows:

$$l_{stub} = \frac{1}{\beta} a\tan(\omega C_p Z_{0stub}) \quad (2.49)$$

If the length of an open-circuited stub is lengthy, the line can be bent so it can be reduced by increasing the width of the stub. But in this project, instead of the single open stub it is needed to consider with the parallel open stubs. It is because two parallel stubs can provide the double susceptance of the single stub.

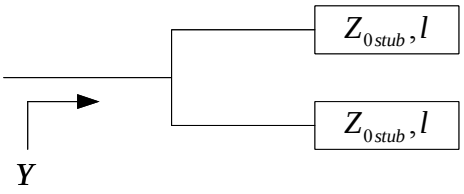

Figure 2.19: Structure of parallel open stubs

The susceptance of the parallel open stub is, $Y = \frac{2}{Z_{0stub}}\tan(\beta l)$

As known the susceptance of the parallel stub is, $Y = j\omega C_p$

And then for a wide range, $\omega C_p = \frac{2}{Z_{0stub}}\tan(\beta l)$

The structure of the parallel open stub for two unit cells is shown in Figure 2.19 and the length of the parallel open stub is,

$$l_{stub} = \frac{1}{\beta} a\tan\left(\frac{\omega C_p Z_{0stub}}{2}\right) \quad (2.50)$$

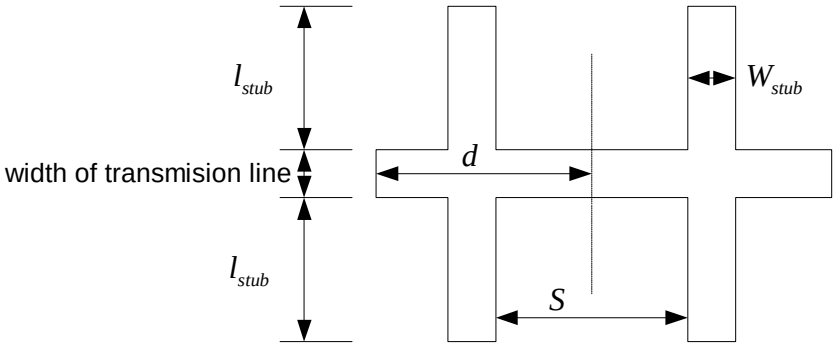

Figure 2.20: Two unit cells of ATL design

2.7 Choice of substrate for Hybrid MIC

There are some considerations, which are important to design hybrid MIC circuits. First it is needed to know that a high dielectric constant substrate is used in smaller-sized circuit designs, but the trade off for smaller size is the performance of the circuit. Secondly, the thinner substrates are used in lower frequency circuit applications. Finally it is noted that the integration of circuit components into small package, that means the individual components are placed in close proximity to each another which consequencets in coupling between two adjacent circuit components that it should be kept to the minimal (les than 30dB).

A duroid substrate (Taconic), with dielectric constant, $\varepsilon_r = 2.2$ and the substrate thickness, 0.254mm is used for hybrid MIC in this project. The substrate has copper (Cu) metallization of $1/2$ oz. per square foot. The thickness of copper should be considered as follows:

The skin depth of copper is defined by

Skin depth $\delta = \sqrt{\dfrac{\rho}{\pi \mu f}}$

The conductivity of copper is, $\sigma = 5.813 \times 10^7$ S/m

The resistivity is defined by, $\rho = \dfrac{1}{\sigma}$

Thus the skin depth of copper is, $\delta = 1.556 \mu m$

The thickness of copper metallization is determined as follows:

$$1 sq.foot = 9.29 \times 10^{-2} m^2$$
$$1 ounce = 2.835 \times 10^{-2} kg$$

From that the density of copper, $\rho_{Cu} = 8910 kg/m^3$

The volume of copper per sq.foot is that

$$\text{volume per sq foot} = 1.591 \times 10^{-6} m^3 / sq.foot$$

Therefore the thickness of copper, $t = 17.125 \mu m$

2.8 Software used

A number of software used in obtaining the simulation analysis of the artificial transmission line design, namely, Ansoft Serenade and Sonnet Lite.

2.8.1 Ansoft Serenade

Serenade Student Version (SV) provides powerful capabilities for academic study and fundamental circuit designs. It is a general purpose CAD package for performing high frequency circuit and system simulation. It is a limited version of the commercial Serenade 8.5 Design Environment, which is intended for electrical engineering students studying topics in high-frequency circuit design and communications. It is a powerful tool for synthesizing, analyzing and tuning systems and circuits ranging from audio to microwave frequencies. Serenade 8.5 SV has two types of simulators such as Harmonica for high frequency circuit simulation and Symphony for communication system simulation. In this project, Harmonica SV is used as it contains linear S-parameter analysis, tuning and optimization. A large number of circuit models for lumped, ideal distributed, microstrip, stripline, coax a set of vendor S-parameter and nonlinear diodes and transistors are found in the device library. Serenade 8.5 Student version (SV) is available for download at this website, http://www.ansoft.com.

2.8.2 Sonnet Lite

Sonnet software provides commercial EDA software solutions for high-frequency electromagnetic (EM) analysis. The electromagnetic simulation software are used for design and analysis of high-frequency circuits, distributed filters, transistors,

LTTC and multi-layer RF packages, waveguides and antennas. The Sonnet software product is wide application in the fields of microwave and millimeter wave design, EMC and EMI analysis. The purpose of Sonnet's suites of high-frequency electromagnetic (EM) software are at today's demanding design challenges involving predominantly planar (3D planar) circuits and antennas. Predominantly planar circuits are microstrip, stripline, coplanar waveguide, PCB (single and multiple layers) and combinations with vias, vertical metal sheets and number of layers of metal traces which are embedded in stratified dielectric material. Since Sonnet Lite is a free download software, it is a feature-limited version of the Sonnet Professional Suit and there is a number of restrictions in this free version like the analysis memory is allowed for 16 Megabytes for registered version and 1 Megabyte for unregistered version, two metal layers available instead of unlimited number of layers in Sonnet Professional Suite and the circuit ports of 4 is the maximum instead of unlimited number in Sonnet Professional Suite. The reason for using the Sonnet rather than Ansoft serenade is that Sonnet accounts for coupling effect between independent components which are close to each other while Ansoft Serenade analysis does not account for coupling effect between the two components. Therefore, Sonnet simulation analysis is more useful in planar circuit like microstrip transmission line which accounts the coupling effect and Sonnet Lite software can be free-downloaded at the website of http://www.sonnetusa.com.

2.9 Design Results

First the microstrip transmission line of characteristic impedance range from 20Ω to 8Ω simulation results are expressed and then the artificial transmission lines, which have similar behavior to transmission lines but with reduced physical dimensions by incorporating lumped elements, are described.

2.9.1 Transmisssion Line

The substrate used in the ATL design and the dimensions of the width and the length of transmission lines, that has characteristics impedances from 20Ω to 8Ω with phase $\beta l = 90^{\circ}$ at 1.8GHz for Duroid substrate design, using the equation from (2.1) to (2.6) , are as follows:

Substrate height, h	0.254mm
Thickness of copper metallization, t	17.1um
Phase in degree (βl)	90°
Operation frequency , f	1.8GHz

Table 2.1: The dimension of Duroid substrate in ATL design

Ideal Z_0	20Ω	15Ω	10Ω	8Ω
Width, W (mm)	2.6	3.7	5.8	7.3
Length, l (mm)	29.4	29.2	28.9	28.7
Effective Dielectric, ε_e	2.0075	2.0429	2.0851	2.1044
Phase velocity, v_p (m/s)	2.1174×10^8	2.09879×10^8	2.0776×10^8	2.068×10^8

Table 2.2: The dimension of ideal transmission line at 1.8 GHz

An example of 20Ω transmission line (width, W = 2.6mm and length, l = 29.4mm) simulated on Ansoft Serenade software is shown below. This is then followed by its simulation analysis for transmission line of characteristic impedance, Z_0 = 20Ω, 15Ω, 10Ω, 8Ω , with phase, $\beta l = 90^{\circ}$ at 1.8GHz with reference impedance of 20Ω, 15Ω, 10Ω, 8Ω respectively.

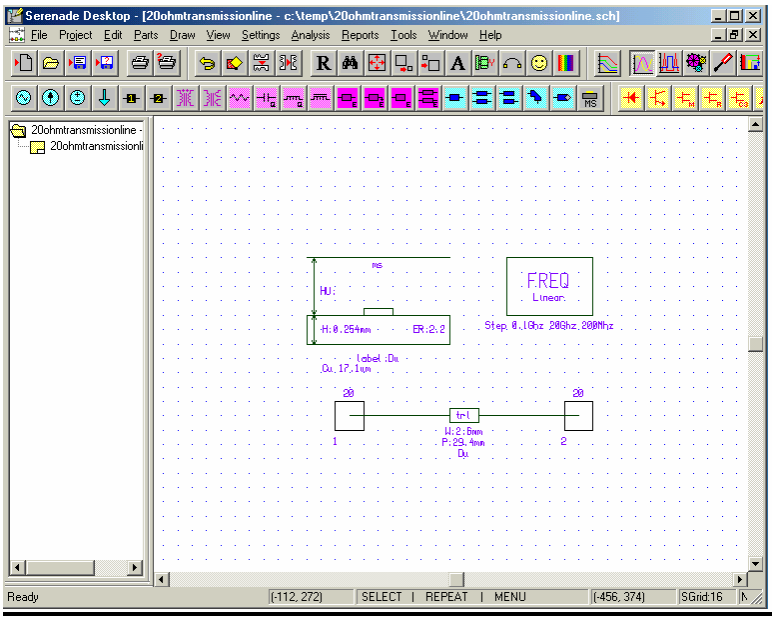

Figure 2.21: Schematic diagram of 20Ω transmission line in Ansoft Serenade

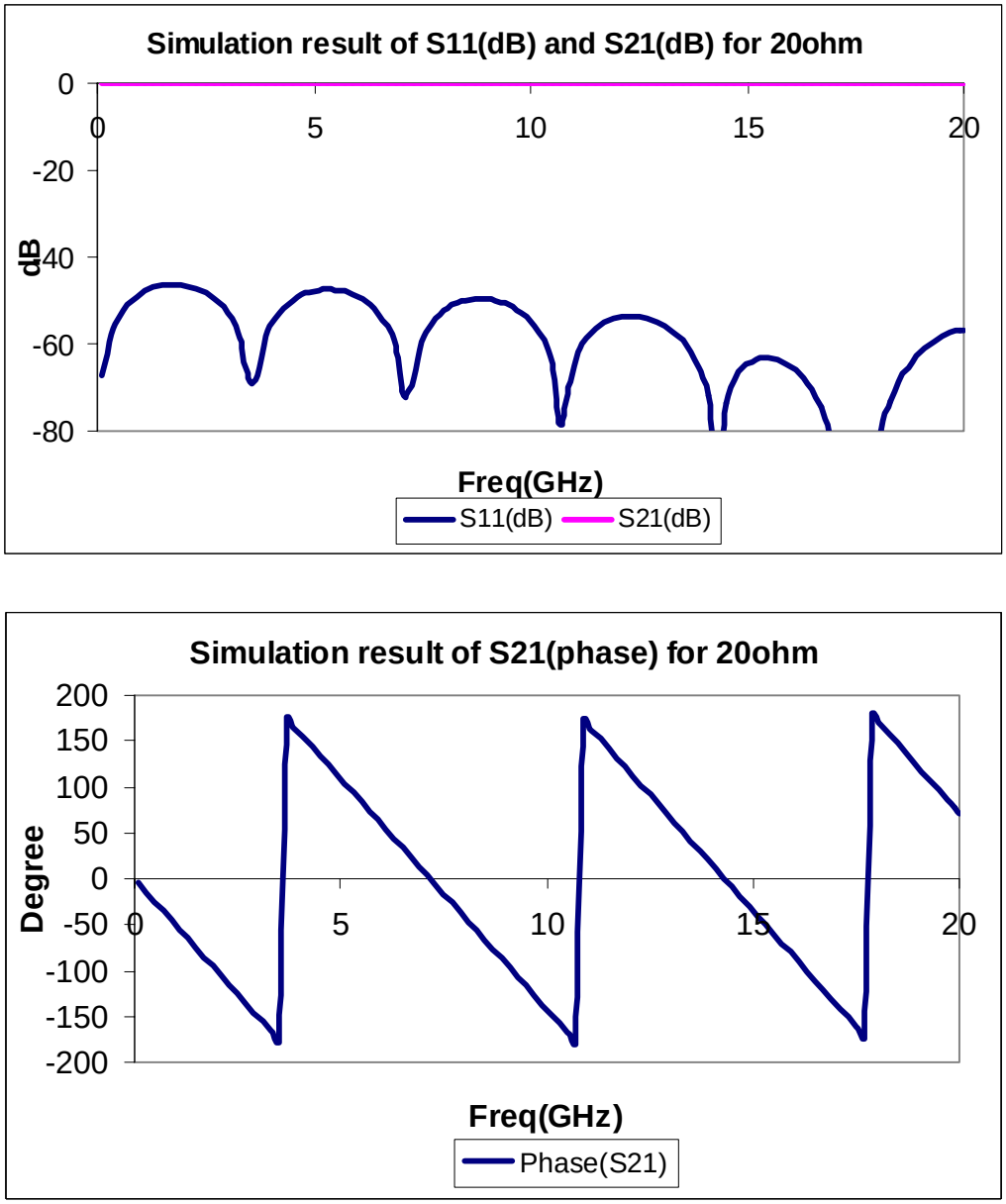

Figure 2.22: Simulation results of transmission line with characteristic impedance of 20Ω

The simulation result shows that the transmission coefficient, S_{21}, approximately 0dB throughout with a phase of 90° at 1.8GHz, while the reflection coefficient, S_{11}, falls approach to -45dB at 1.8GHz. The phase, S_{21}, verges to 90° at f_0=1.8GHz which indicates that a transmission line has the effective guided wavelength of a quarter of the guided wavelength at the operating frequency. Because of the reflection coefficient of S_{11} with -40 dB or less can be neglected in practical case, it can be taken that the transmission signal will pass through the transmission line without attenuation at the operating frequency.

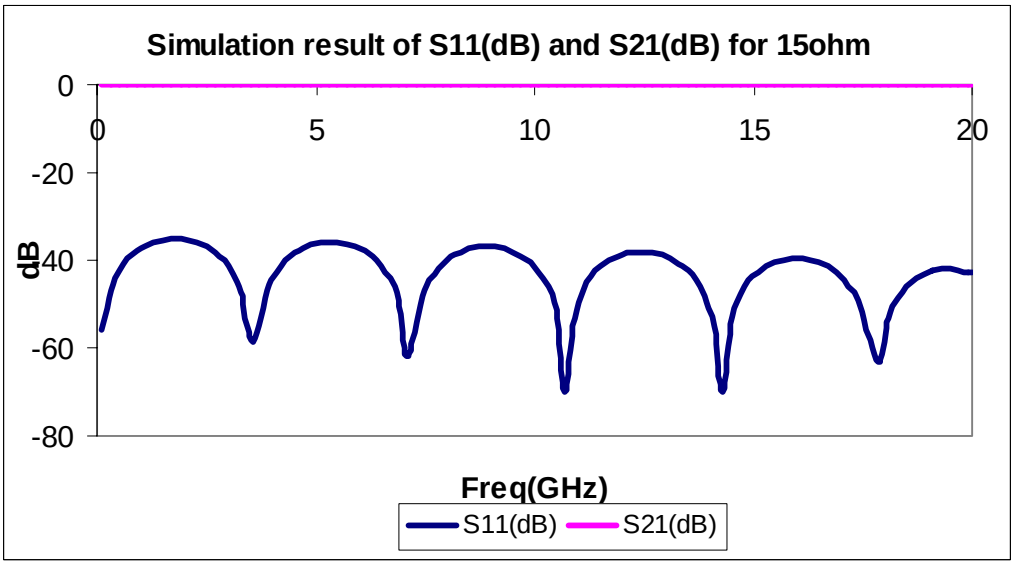

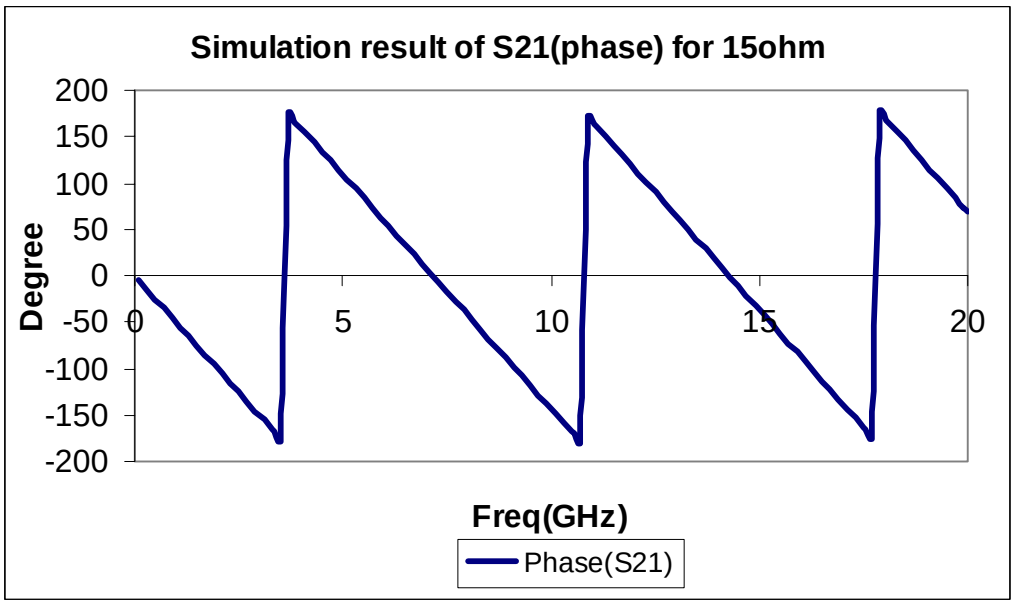

Figure 2.23: Simulation results of transmission line with characteristic impedance of 15Ω

The simulation result of 15Ω, which is doing the same procedure as 20Ω, shows that the transmission coefficient, S_{21}, approximately 0dB throughout with a phase of 90° at 1.8GHz, while the reflection coefficient, S_{11}, falls approach to -35dB at 1.8GHz. The phase, S_{21}, converges to 90° at f_0=1.8GHz which also shows that a transmission line has the effective guided wavelength of a quarter of the guided wavelength at the operating frequency. Because of the reflection coefficient of S_{11} with -40 dB or less can be neglected in practical case, it can be taken that the transmission signal will pass through the transmission line without attenuation at the operating frequency.

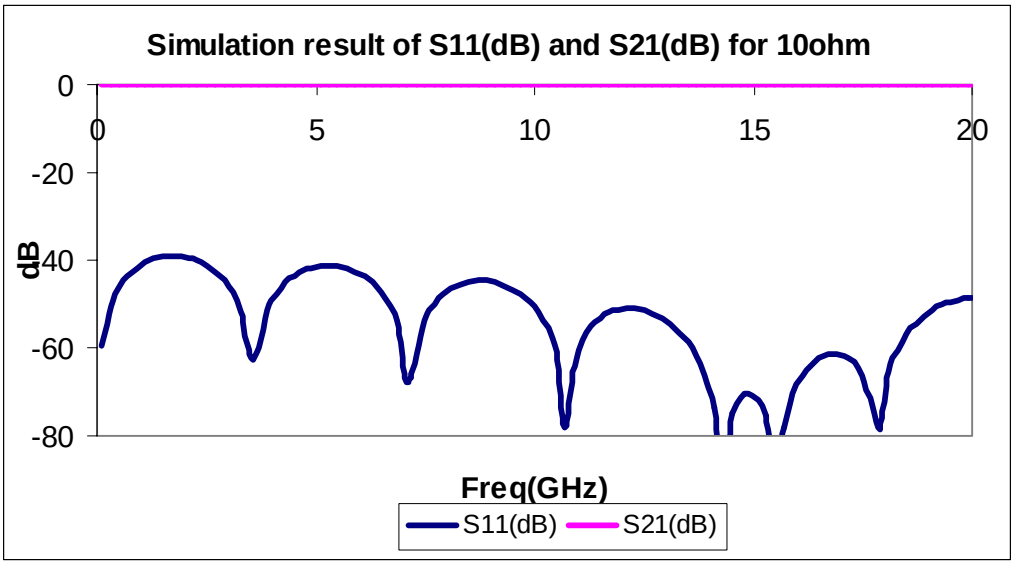

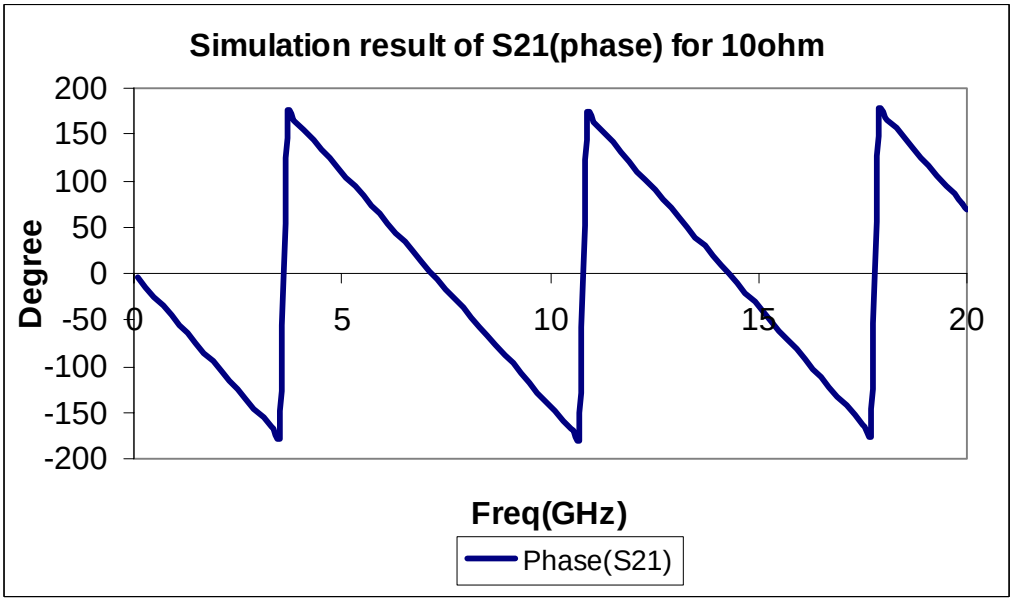

Figure 2.24: Simulation results of transmission line with characteristic impedance of 10Ω

The simulation result of 10Ω, which is doing the same procedure as 20Ω and 15Ω, shows that the transmission coefficient, S_{21}, nearly 0dB throughout with a phase of 90° at 1.8GHz, while the reflection coefficient, S_{11}, drops approach to -40dB at 1.8GHz. The phase, S_{21}, converges to 90° at f_0=1.8GHz which also covers that a transmission line has the effective guided wavelength of a quarter of the guided wavelength at the operating frequency. Because of the reflection coefficient of S_{11} with -40 dB or less can be neglected in practical case, it can be taken that the transmission signal will pass through the transmission line without attenuation at the operating frequency.

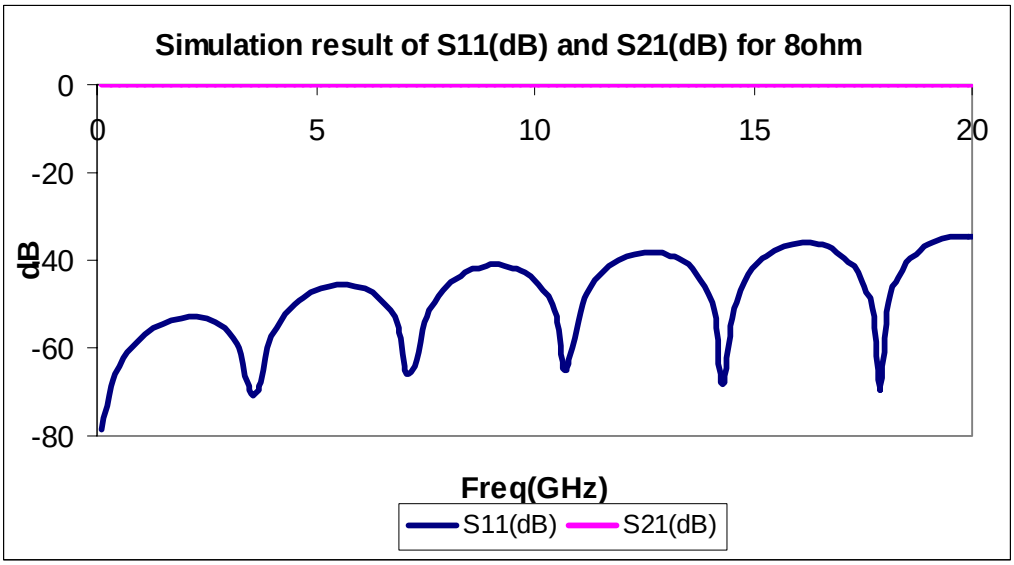

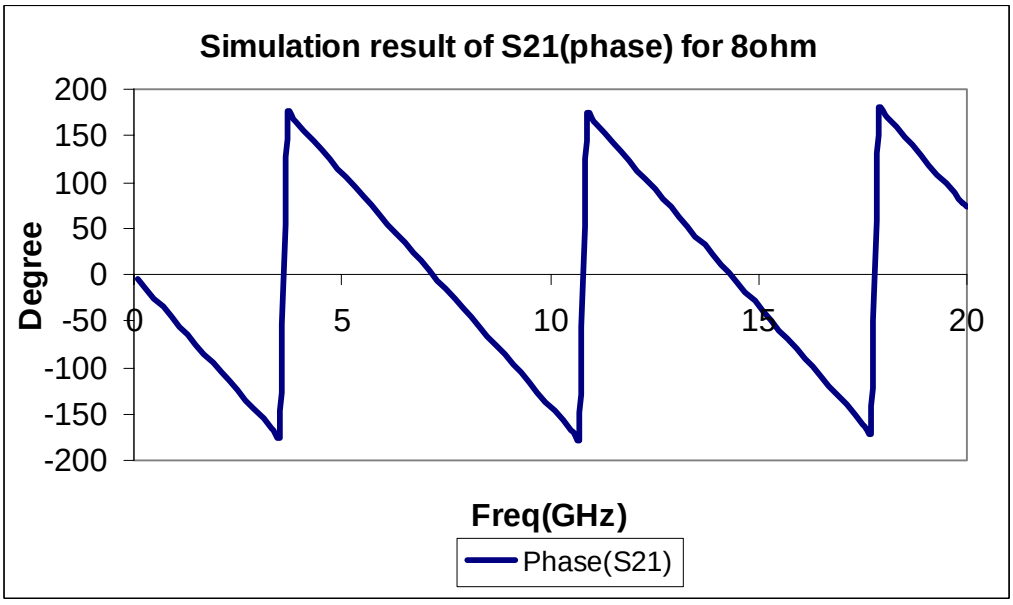

Figure 2.25: Simulation results of transmission line with characteristic impedance of 8Ω

Doing the same procedure as 20Ω, 15Ω and 10Ω, the simulation result of 8Ω shows that the transmission coefficient, S_{21}, nearly 0dB throughout with a phase of 90° at 1.8GHz, while the reflection coefficient, S_{11}, drops approach to -50dB at 1.8GHz. The phase, S_{21}, converges to 90° at f_0=1.8GHz which also covers that a transmission line has the effective guided wavelength of a quarter of the guided wavelength at the operating frequency. Because of the reflection coefficient of S_{11} with -40 dB or less can be neglected in practical case, it can be taken that the transmission signal will pass through the transmission line without attenuation at the operating frequency.

2.9.2 ATL design with lumped capacitor

The next stage is to incorporate the lumped capacitor to reduce the physical length of transmission line and still having the characteristic impedance of 20Ω, 15Ω, 10Ω and 8Ω with phase of 90°. By running the Matlab program [Appendix A], it generates out the possible combination of parameters such as the length of one unit cell, d, and the values of loaded capacitor, C_p, that satisfy the conditions mentioned above. After known the loading capacitance value, it can be realized with the parallel open stub in order to provide the double susceptance of the single stub with a known width of a transmission line. All these parameters can be determined using equation (2.44) to (2.46).

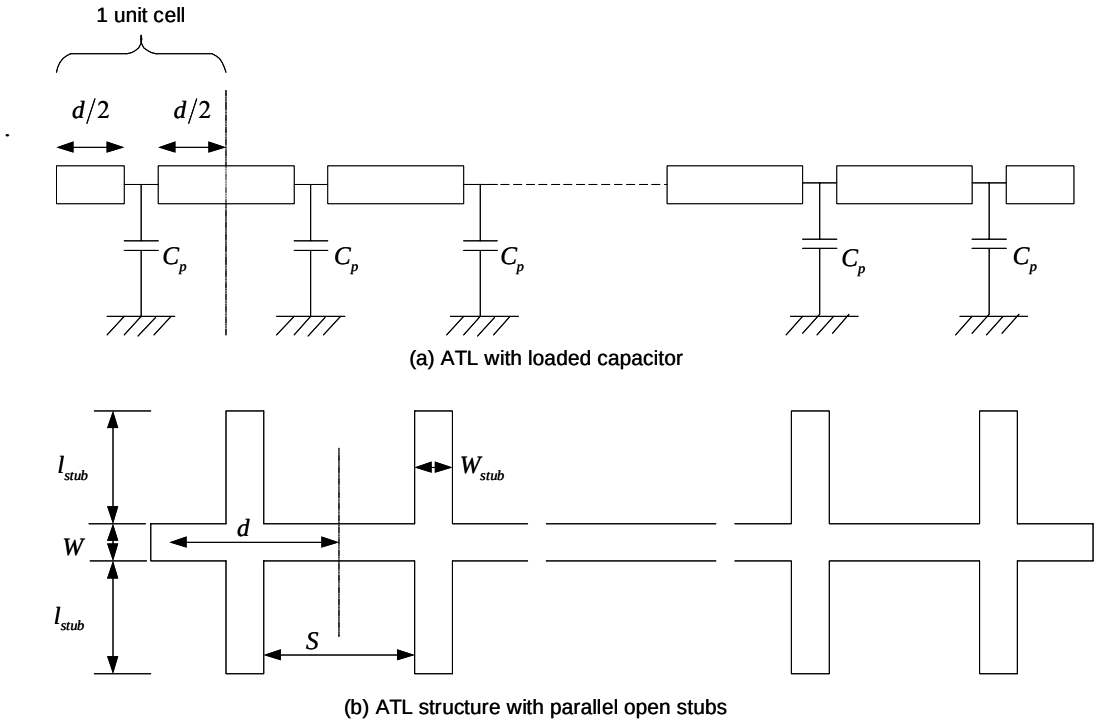

(a) ATL with loaded capacitor

(b) ATL structure with parallel open stubs

Fiure 2.26: Structure of Artificial Transmission Lines with (a) loaded capacitor and (b)its equivalent structure with parallel open stubs

2.9.3 Calculation the maximum width of microstrip line

In designing microwave circuits, the component values are limited according to parasitic effects which show its parasitic behavior when increasing the frequency while these component values are infinite in theory. When the frequency is increased, the range of component values is deviated from the expected values. The planar transmission microstrip line maximum width is also limited by the transverse resonances. This transverse resonant mode can exist which can also couple strongly to

the quasi-TEM microstrip mode for a sufficiently wide microstrip line. At the cutoff frequency, this transverse resonant mode the equivalent circuit is a resonant transmission line of length ($W + 2d$) where $d = 0.2h$.

The cut off half-wavelength can be calculated as follow:

$$\frac{\lambda_{CT}}{2} = W + 2d = W + 0.4h$$

$$\frac{c}{2 f_{CT} \sqrt{\varepsilon_r}} = W + 0.4h$$

$$f_{CT} = \frac{c}{\sqrt{\varepsilon_r}} \frac{1}{(2W + 0.8h)}$$

For Duroid substrate,

$h = 0.254mm$

$f = 1.8GHz$

$\varepsilon_r = 2.2$

$c = 3 \times 10^8 m/s$

Let cut-off frequency= 18GHz

$$2W + 0.8h = \frac{c}{\sqrt{\varepsilon_r} f_{CT}}$$

$$W = 5.5mm \Rightarrow Z_0 = 10\Omega$$

From the above result, it can be taken the maximum width of the microstrip line up to 5.5mm which is equivalent to the characteristic impedance of 10Ω for duroid substrate with the substrate height 0.254mm.

2.10 Simulation Results

2.10.1 20Ω ATL design with 25Ω microstrip transmission line

Using a Duroid substrate with dielectric constant, $\varepsilon_r = 2.2$, the substrate thickness, $h = 0.254mm$, the ATL design of 20Ω with 25Ω transmission line with overall phase 90° can be calculated at the operating frequency 1.8GHz by running the Matlab program [Appendix A] and the simulation results are calculated as follows:

Width of TL, W	2mm
Characteristic impedance of TL, Z_0	25Ω
Effective dielectric constant, ε_e	1.977
Length of TL per unit cell, d	2mm
Inductance per unit cell, L	117.17nH/m
Capacitance per unit cell, C	187.5pF/m
Loaded capacitor, C_p	0.21pF
Stub length, l_{stub}	1.2mm
Stub width, W_{stub}	0.73mm
Total dimension of structure	24mm by 4.4mm

Table 2.3: The calculation result of ATL 20Ω structure incorporating with 25Ω microstrip transmission line

The artificial transmission line of 20Ω is represented with the microstrip transmission line of 25Ω because the work on this artificial transmission project is intended to reduce the physical dimension of a transmission line incorporating with lumped capacitor to give rise to ATL but still having the same characteristics impedance with phase $\beta l = 90^\circ$ at the operating frequency. This project is purposed only on wide-bandwidth low characteristic impedance planar artificial transmission line based on microstrip transmission line. As the unit cells are more cascaded, the artificial transmission line is resembled to the ideal transmission line. In this project both Ansoft serenade and Sonnet are using for simulation and compare the results. Sonnet analysis is more accurate for planar circuit like microstrip transmission line because it accounts for coupling effect between the individual components while Ansoft serenade does not account.

The following are the examples schematic diagrams of 20Ω for analysis in Ansoft serenade and Sonnet software.

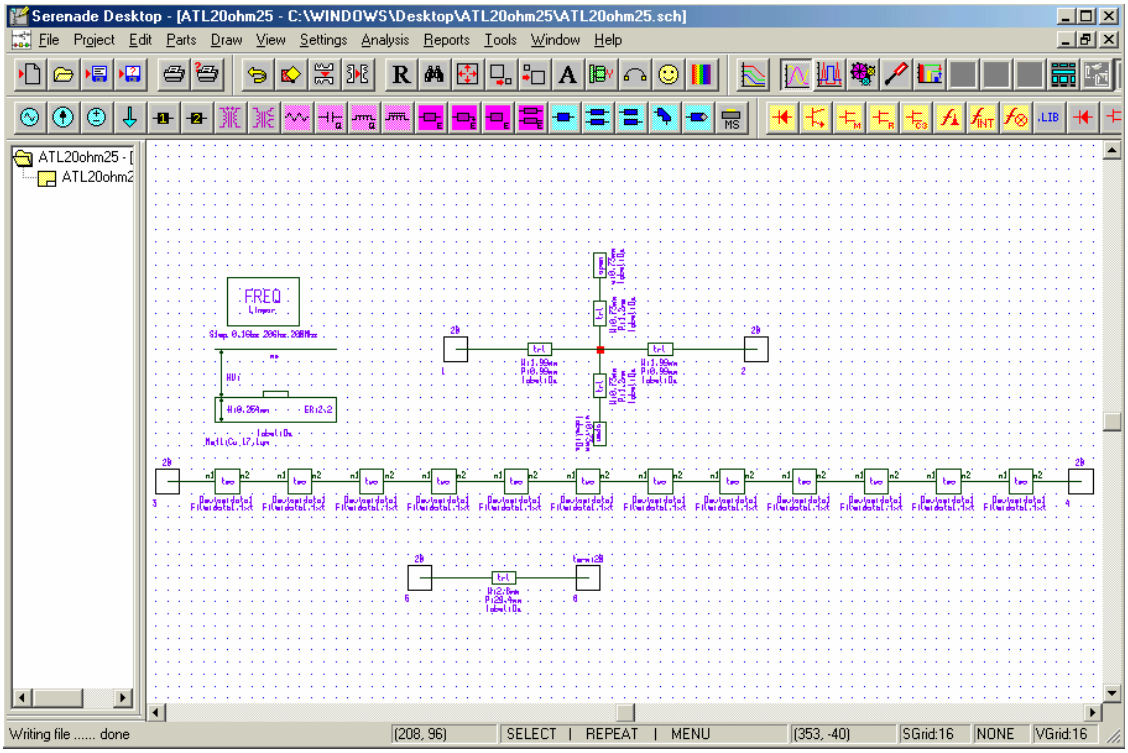

(a) Schematic diagram in Ansoft Serenade

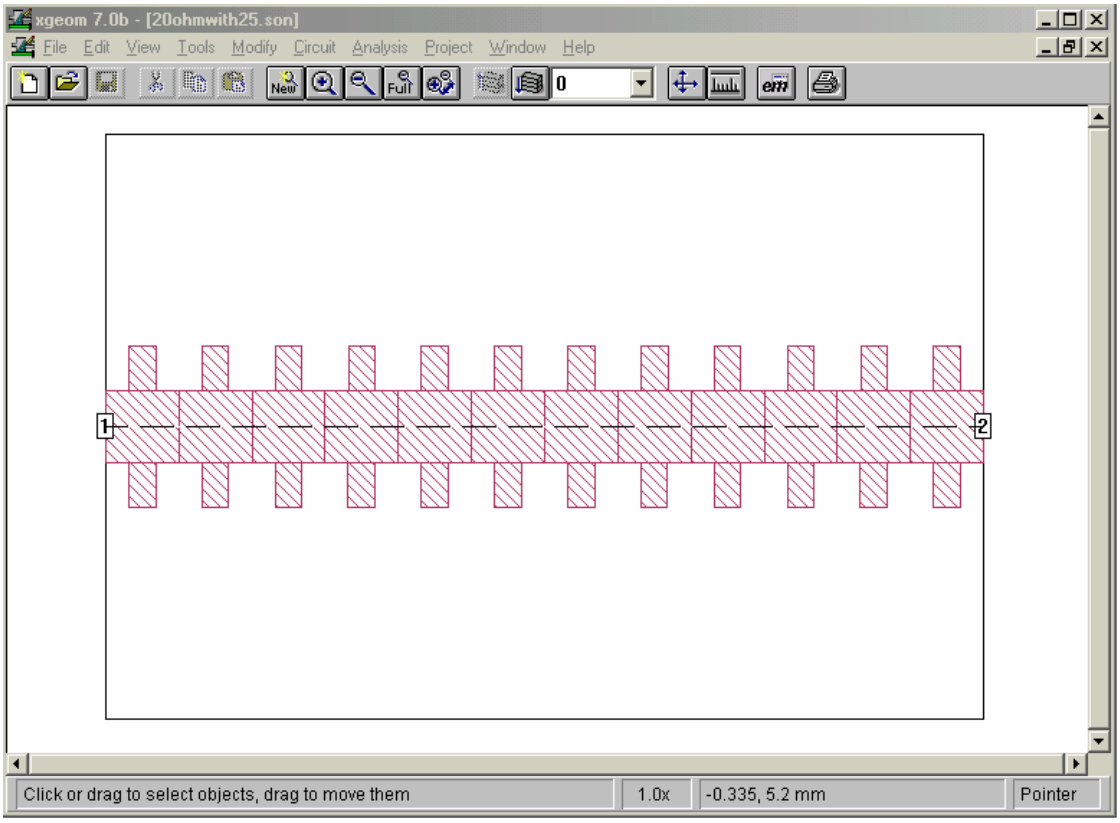

(b) Schematic diagram in Sonnet Lite

Figure 2.27: Schematic diagram for artificial transmission line analysis in (a) Ansoft Serenade (b) Sonnet Lite

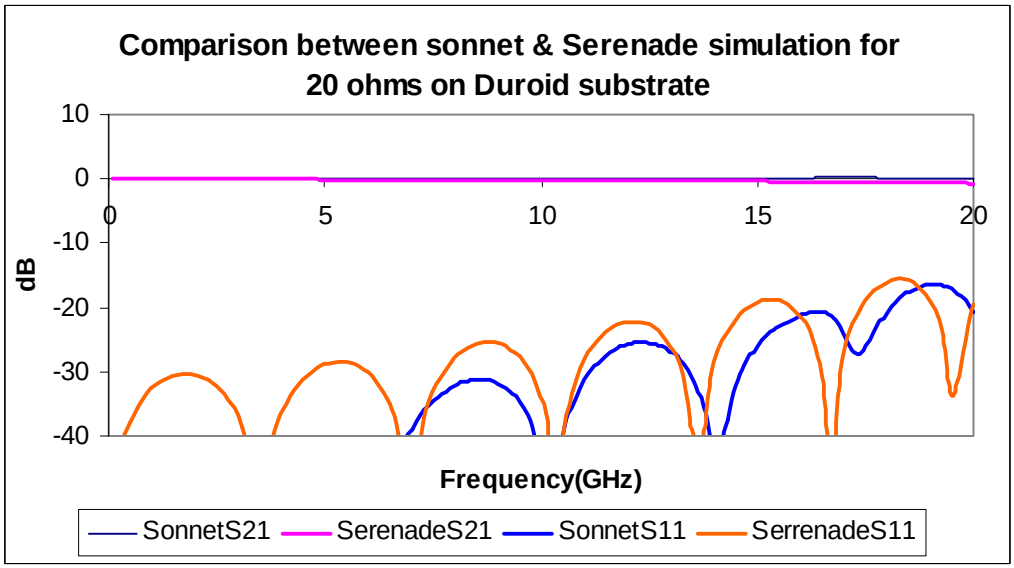

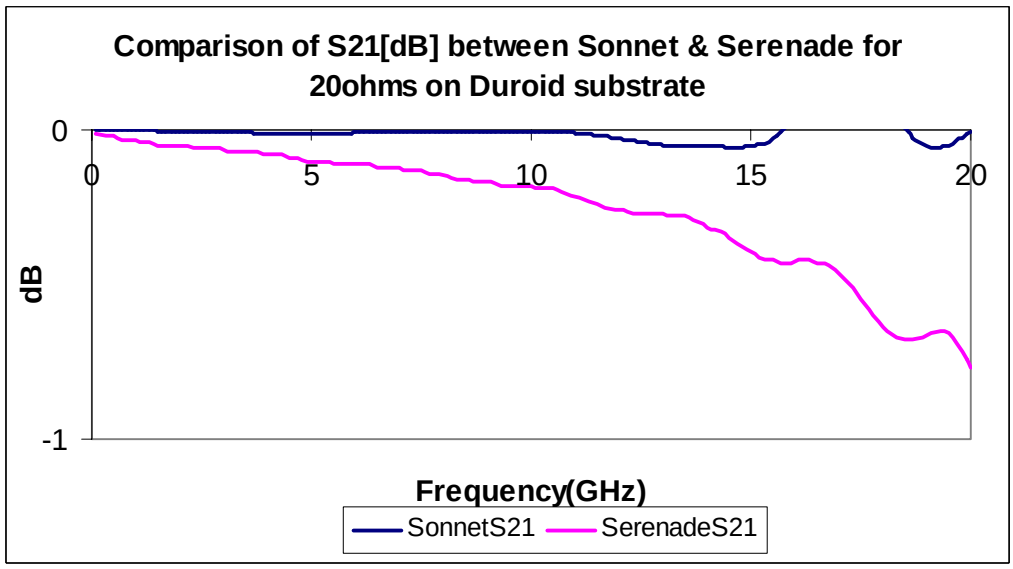

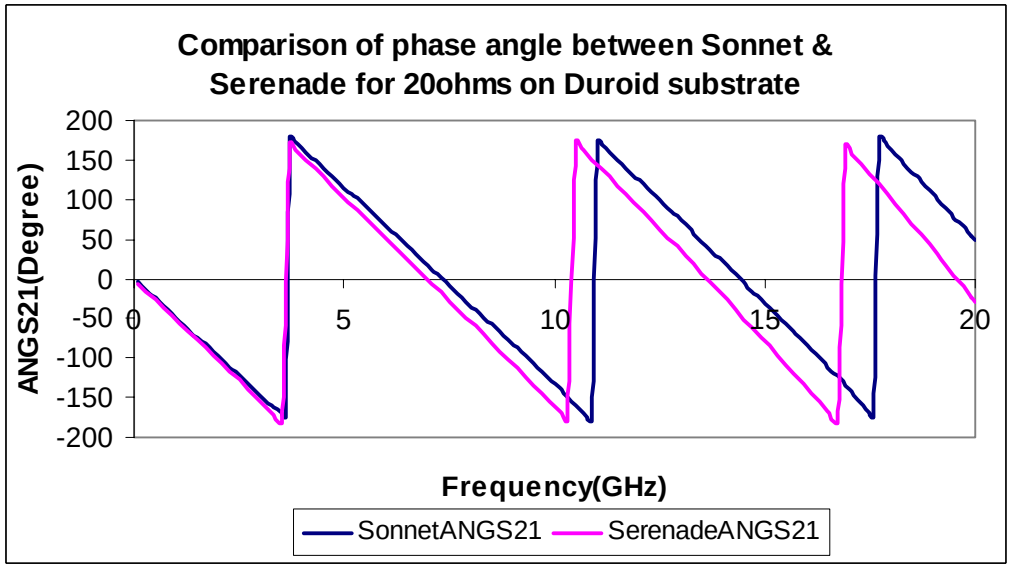

Figure 2.28: The compared results of ATL 20Ω structure with 25Ω microstrip transmission line using Ansoft Serenade and Sonnet software

The physical length of 12 cascaded unit cells ATL design is 24mm which is 18.4% length reduction then the ideal transmission line 20Ω whose length is 29.4mm. In Figure 2.28: the first figure shows the compared response of transmission coefficient, $S_{11}(dB)$, response for Sonnet and Serenade software. The transmission coefficient, S_{11}, is displayed a dip of -35dB for Sonnet and below -40dB for Serenade at 1.8GHz. This result can be adopted as the ATL design behaves as 20Ω transmission line up to 20GHz because the magnitude of input reflection coefficient, $S_{11}(dB)$, can be accepted up to -10dB or less in generally. The second figure result shows that the transmit signal of the ATL designed is passed through with a little bit loss up to 15GHz. The phase response of the last figure represents the phase of the reflection coefficient, S_{21}, is close to 90° at 1.8GHz.

2.10.2 15Ω ATL design with 25Ω microstrip transmission line

Similar to 20Ω ATL deign, the ATL design of 15Ω with 25Ω transmission line with overall phase 90° can be calculated at the operating frequency 1.8GHz by running the Matlab program [Appendix A] and the simulation results are calculated as follows:

Width of TL, W	2mm
Characteristic impedance of TL, Z_0	25Ω
Effective dielectric constant, ε_e	1.977
Length of TL per unit cell, d	1.5mm
Inductance per unit cell, L	117.17nH/m
Capacitance per unit cell, C	187.5pF/m
Loaded capacitor, C_p	0.5pF
Stub length, l_{stub}	2.1mm
Stub width, W_{stub}	1.1mm
Total dimension of structure	18mm by 6.2mm

Table 2.4: The calculation result of ATL 15Ω structure incorporating with 25Ω microstrip transmission line

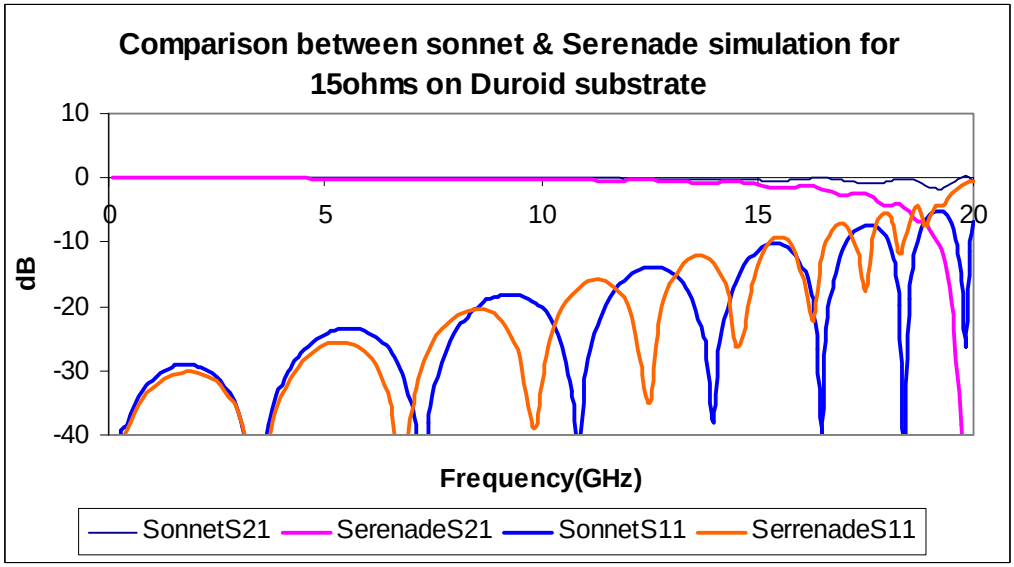

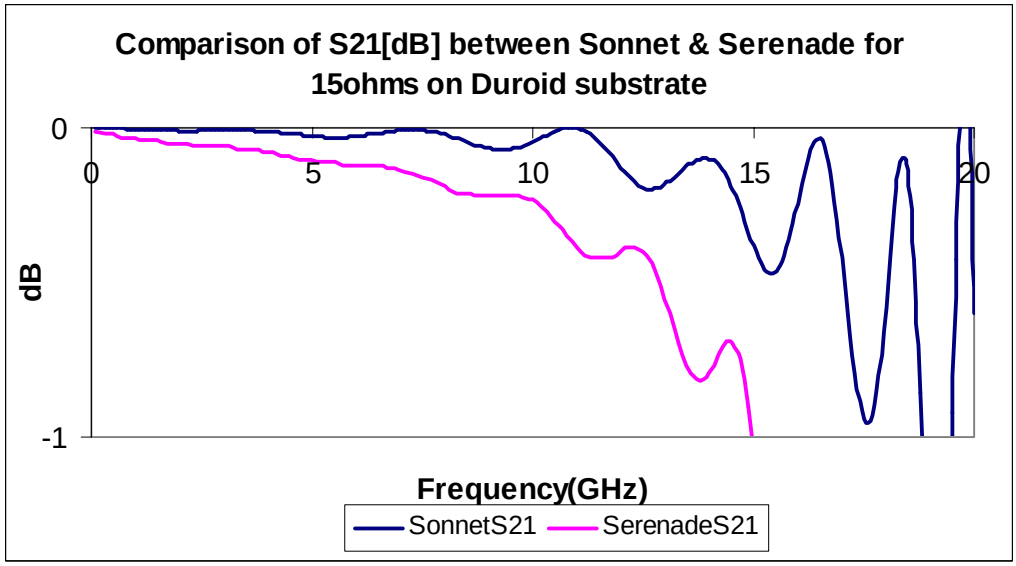

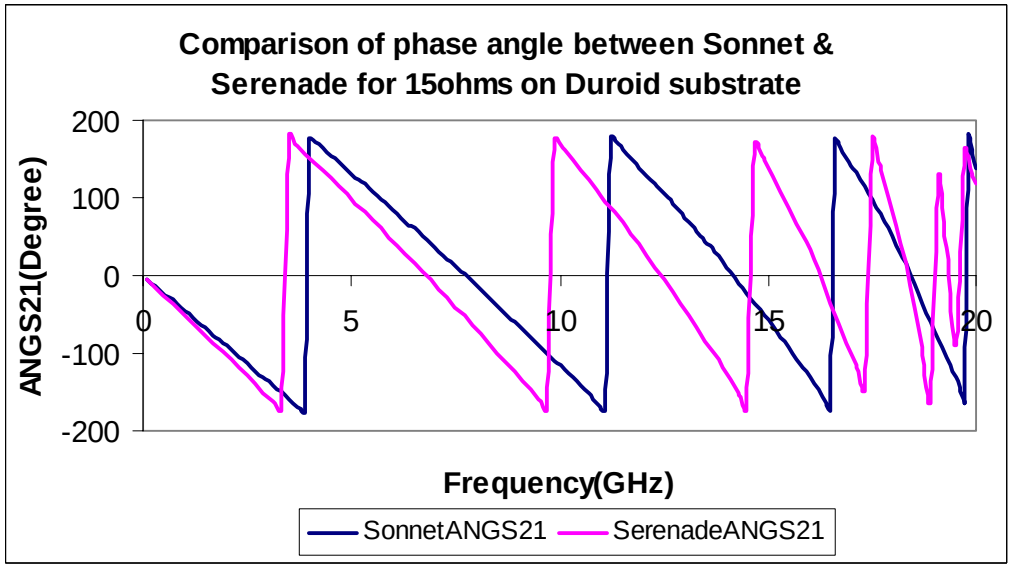

Figure 2.29: The compared results of ATL 15Ω structure with 25Ω microstrip transmission line using Ansoft Serenade and Sonnet software

The physical length of 12 cascaded unit cells ATL design is 24mm which is 25.6% length reduction then the ideal transmission line 20Ω whose length is 29.15mm. In Figure 2.29: the first figure shows the compared response of transmission coefficient, $S_{11}(dB)$, response for Sonnet and Serenade software. The transmission coefficient, S_{11}, is displayed a dip of -30dB for both Sonnet and Serenade at 1.8GHz. This result can be adopted as the ATL design behaves as 15Ω transmission line up to 20GHz because the magnitude of input reflection coefficient, $S_{11}(dB)$, can be accepted up to -10dB or less in generally. The second figure result shows that the transmit signal of the ATL designed is passed through with a little bit loss up to 15GHz. The phase response of the last figure represents the phase of the reflection coefficient, S_{21}, is close to 90° at 1.8GHz.

2.10.3 15Ω ATL design with 20Ω microstrip transmission line

Similar to 20Ω ATL deign, the ATL design of 15Ω with 20Ω transmission line with overall phase 90° can be calculated at the operating frequency 1.8GHz by running the Matlab program [Appendix A] and the simulation results are calculated as follows:

Width of TL, W	2.6mm
Characteristic impedance of TL, Z_0	20Ω
Effective dielectric constant, ε_e	2.008
Length of TL per unit cell, d	1.8mm
Inductance per unit cell, L	94.46nH/m
Capacitance per unit cell, C	236.14pF/m
Loaded capacitor, C_p	0.34pF
Stub length, l_{stub}	1.2mm
Stub width, W_{stub}	1.4mm
Total dimension of structure	21.6mm by 5mm

Table 2.5: The calculation result of ATL 15Ω structure incorporating with 20Ω microstrip transmission line

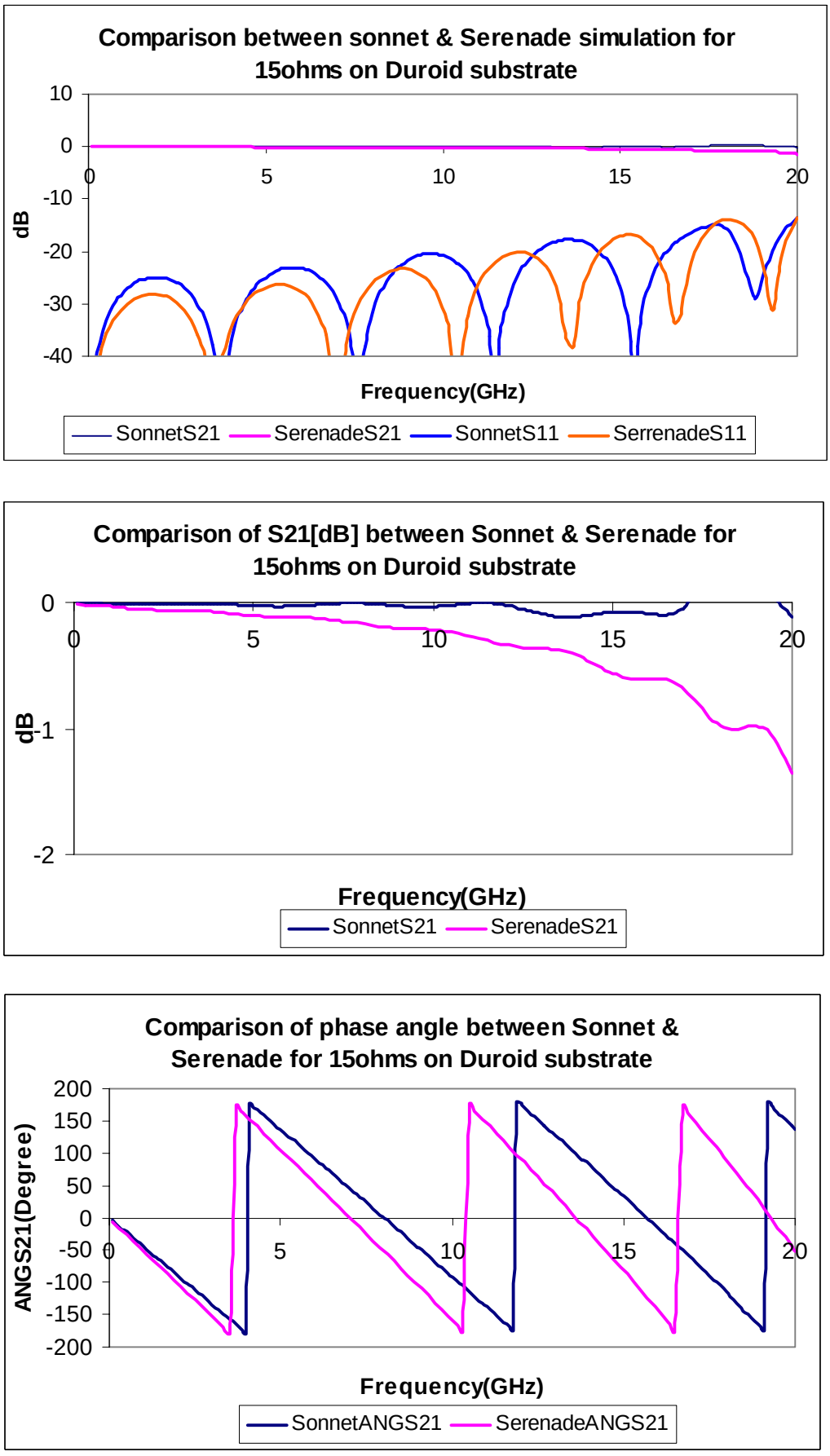

Figure 2.30: The compared results of ATL 15Ω structure with 20Ω microstrip transmission line using Ansoft Serenade and Sonnet software

The physical length of 12 cascaded unit cells ATL design is 24mm which is 25.6% length reduction then the ideal transmission line 20Ω whose length is 29.15mm. In Figure 2.30: the first figure shows the compared response of transmission coefficient, $S_{11}(dB)$, response for Sonnet and Serenade software. The transmission coefficient, S_{11}, is displayed a dip of -25dB for Sonnet and below -30dB for Serenade at 1.8GHz. This result can be adopted as the ATL design behaves as 15Ω transmission line up to 20GHz because the magnitude of input reflection coefficient, $S_{11}(dB)$, can be accepted up to -10dB or less in generally. The second figure result shows that the transmit signal of the ATL designed is passed through with a little bit loss up to 15GHz. The phase response of the last figure represents the phase of the reflection coefficient, S_{21}, is close to 90° at 1.8GHz. The 15Ω ATL design with 20Ω microstrip transmission line is more wider bandwidth than with 25Ω microstrip transmission line. The result for 15Ω ATL design with 20Ω microstrip transmission line is more correspond to the purpose of wide bandwidth of this project.

2.10.4 10Ω ATL design with 15Ω microstrip transmission line

Similar to 20Ω and 15Ω ATL deign, the ATL design of 10Ω with 15Ω transmission line with overall phase 90° can be calculated at the operating frequency 1.8GHz by running the Matlab program [Appendix A] and the simulation results are calculated as follows:

Width of TL, W	3.7mm
Characteristic impedance of TL, Z_0	15Ω
Effective dielectric constant, ε_e	2.043
Length of TL per unit cell, d	1.6mm
Inductance per unit cell, L	71.47nH/m
Capacitance per unit cell, C	317.63pF/m
Loaded capacitor, C_p	0.64pF
Stub length, l_{stub}	2.5mm
Stub width, W_{stub}	1.2mm
Total dimension of structure	19.2mm by 8.7mm

Table 2.6: The calculation result of ATL 10Ω structure incorporating with 15Ω microstrip transmission line

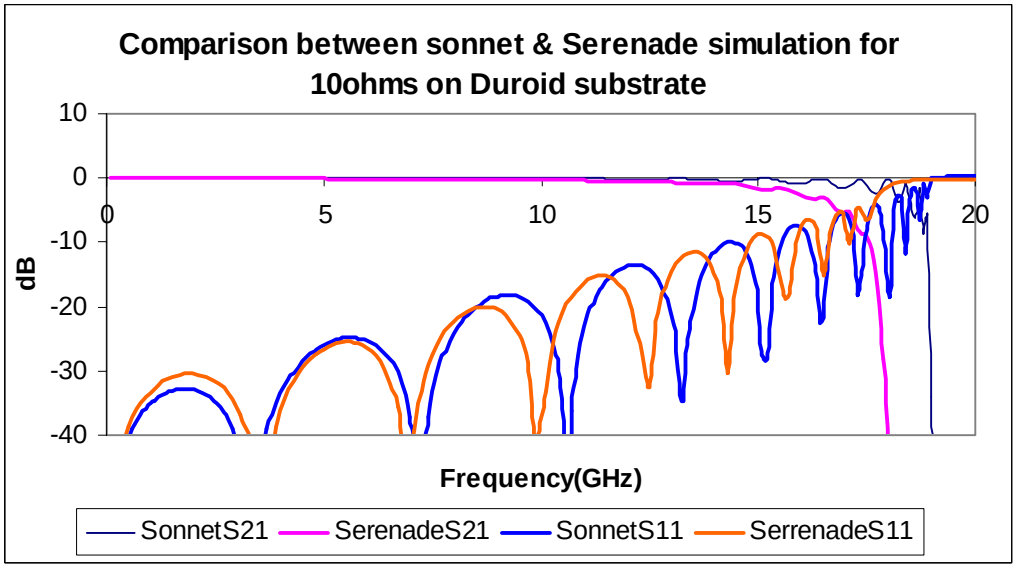

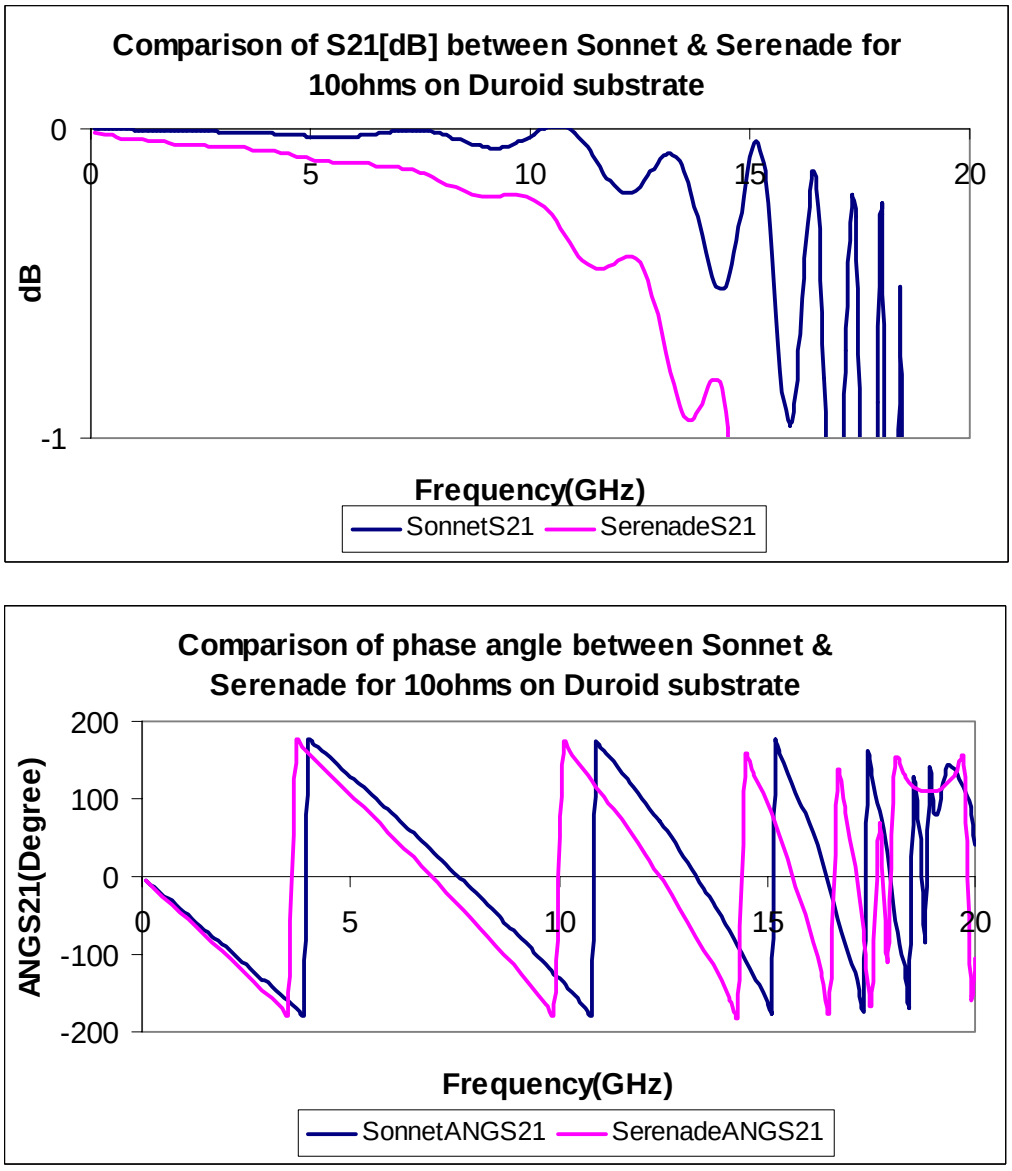

Figure 2.31: The compared results of ATL 10Ω structure with 15Ω microstrip transmission line using Ansoft Serenade and Sonnet software

The physical length of 12 cascaded unit cells ATL design is 24mm which is 33.6% length reduction then the ideal transmission line 20Ω whose length is 28.9mm. In Figure 2.31: the first figure shows the compared response of transmission coefficient, $S_{11}(dB)$, response for Sonnet and Serenade software. The transmission coefficient, S_{11}, is displayed a dip of -30dB for Sonnet and below -35dB for Serenade at 1.8GHz. This result can be adopted as the ATL design behaves as 10Ω transmission line up to 15GHz because the magnitude of input reflection coefficient, $S_{11}(dB)$, can be accepted up to -10dB or less in generally. The second figure result shows that the

transmit signal of the ATL designed is passed through with a little bit loss up to 15GHz. The phase response of the last figure represents the phase of the reflection coefficient, S_{21}, is close to 90° at 1.8GHz.

2.10.5 8Ω ATL design with 13Ω microstrip transmission line

Similar to 20Ω, 15Ω and 10Ω ATL deign, the ATL design of 8Ω with 13Ω transmission line with overall phase 90° can be calculated at the operating frequency 1.8GHz by running the Matlab program [Appendix A] and the simulation results are calculated as follows:

Width of TL, W	4.3mm
Characteristic impedance of TL, Z_0	13Ω
Effective dielectric constant, ε_e	2.059
Length of TL per unit cell, d	1.5mm
Inductance per unit cell, L	62.18nH/m
Capacitance per unit cell, C	367.92pF/m
Loaded capacitor, C_p	0.9pF
Stub length, l_{stub}	2.8mm
Stub width, W_{stub}	1.1mm
Totl dimension of structure	18mm by 9.9mm

Table 2.7: The calculation result of ATL 8Ω structure incorporating with 13Ω microstrip transmission line

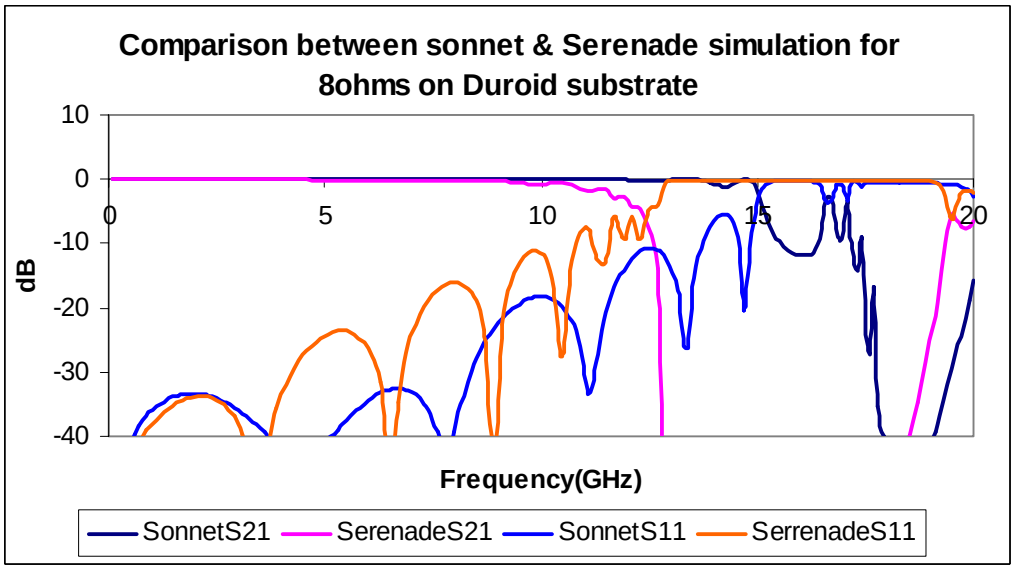

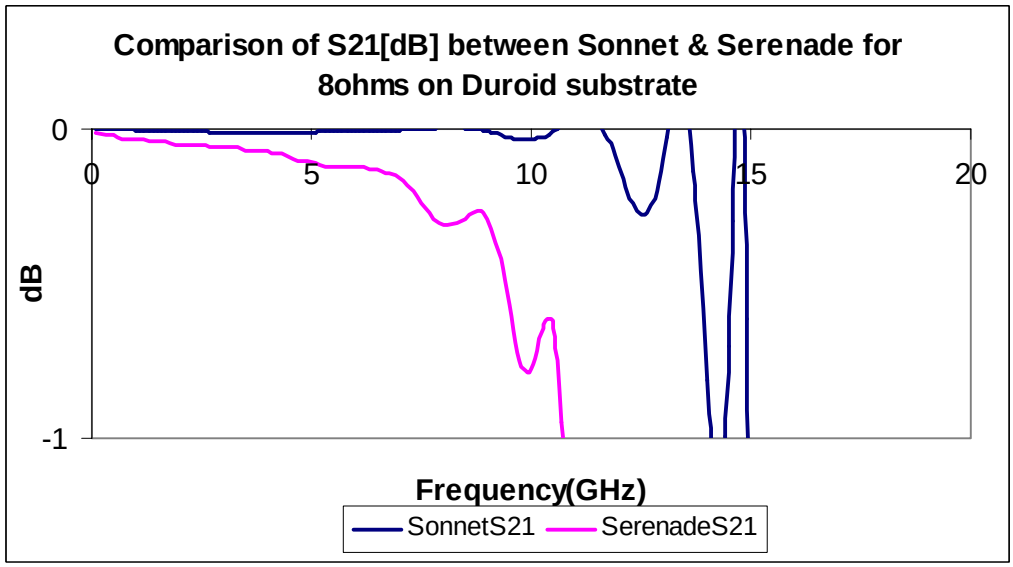

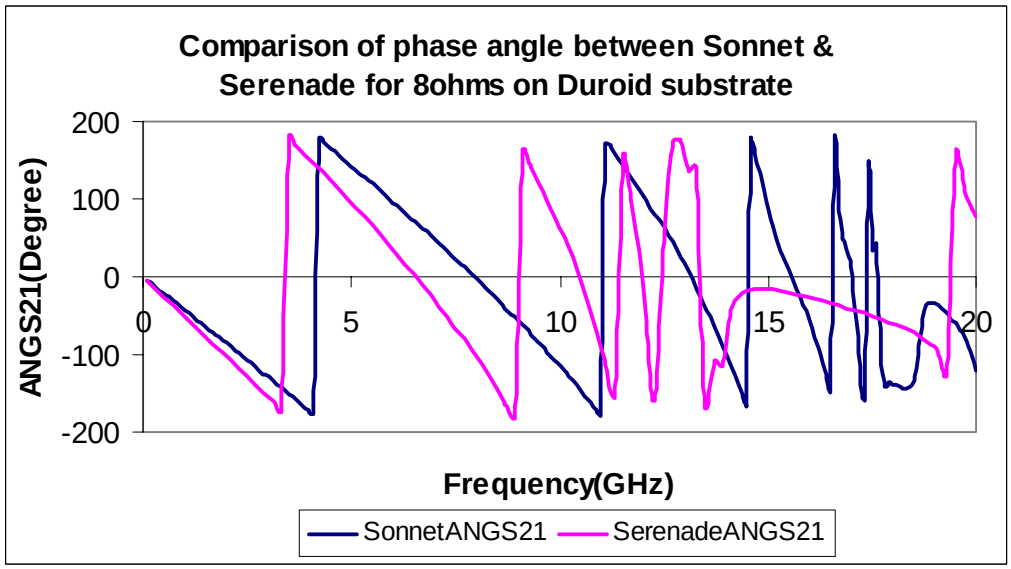

Figure 2.32: The compared results of ATL 8Ω structure with 13Ω microstrip transmission line using Ansoft Serenade and Sonnet software

The physical length of 12 cascaded unit cells ATL design is 24mm which is 34.4% length reduction then the ideal transmission line 20Ω whose length is 27.45mm. In Figure 2.32: the first figure shows the compared response of transmission coefficient, $S_{11}(dB)$, response for Sonnet and Serenade software. The transmission coefficient, S_{11}, is displayed a dip of -35dB for both Sonnet and Serenade at 1.8GHz. This result can be adopted as the ATL design behaves as 8Ω transmission line up to 10GHz because the magnitude of input reflection coefficient, $S_{11}(dB)$, can be accepted up to -10dB or less in generally. The second figure result shows that the transmit signal of the ATL designed is passed through with a little bit loss up to 10GHz. The phase response of the last figure represents the phase of the reflection coefficient, S_{21}, is close to 90° at 1.8GHz.

2.11 The study from ATL design work

In ATL design, the one unit cell length, d, and the capacitive loading value, C_p, are inversely proportional to each other which mean the one unit cell length value becomes smaller as Z_{0ATL} value smaller while the capacitive loading value becomes larger as Z_{0ATL} value smaller. Generally the length of open-circuit stub, l_{stub}, can be reduced by increasing the width of the stub, W_{stub}. Although the length of the parallel open stubs can be further reduced by increasing the width of the stubs, the choice of the open stub width is based on the one unit cell length, d. The separation distance between the two parallel open stubs cannot be reduced more than 0.4mm in this project which is bounded to choose the width of the open stub. The largest dimension choose of the artificial transmission line structure of the open stub width, W_{stub} is dependent not only the one unit cell length also on the separation distance between the two parallel open stubs according to stronger coupling effect between them when these two parallel open stubs are too close to each other.

The relation between the open stub length, l_{stub}, and the open stub width, W_{stub}, can also be known from the equation (2.49) where l_{stub} is directly proportionally to the characteristic impedance the open stub, Z_{stub}, which means l_{stub} is inversely

proportional to the width of the stub, W_{stub}. The relations of Z_{0ATL} to the one unit cell length, d and the capacitive loading value, C_p can be studied from the following figures.

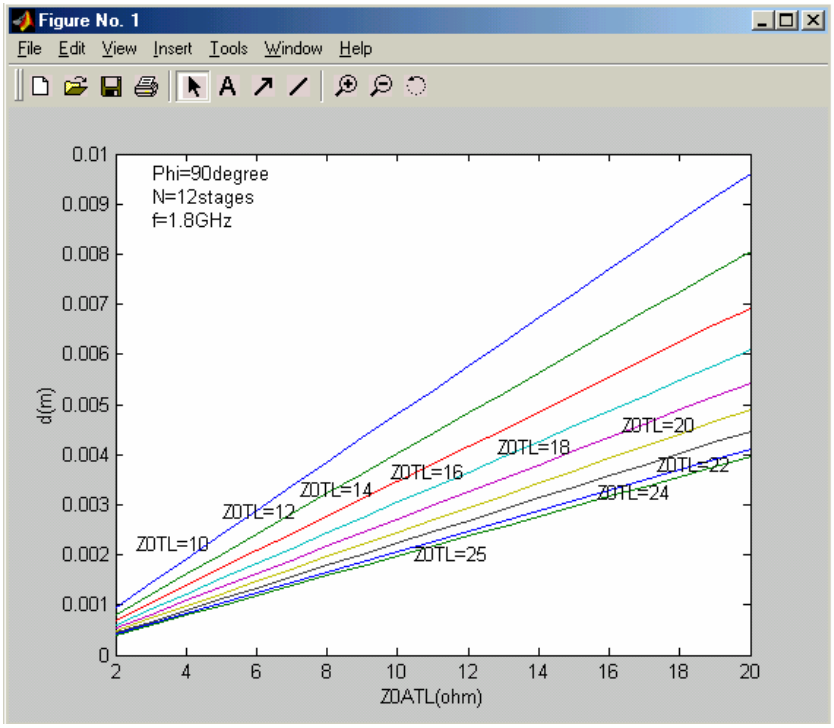

(a)

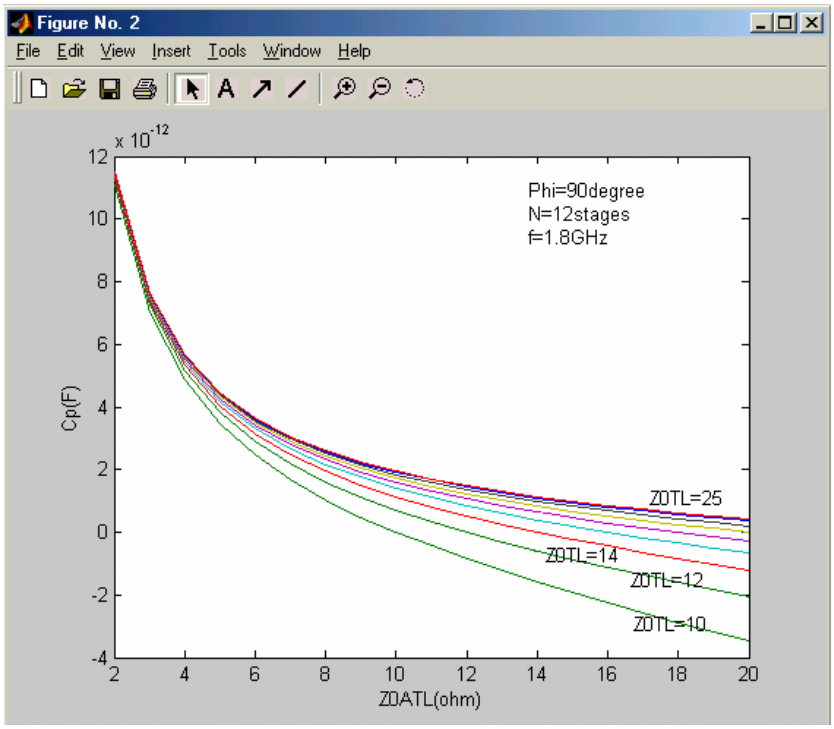

(b)

Figure 2.33: The relations of Z_{0ATL} (a) with the one unit cell length, d
(b) with the capacitive loading, C_p

CHAPTER III
COMPACT WIDEBAND MICROSTRIP ANTENNA

3.1 Background

The concept of microstrip radiator was first proposed by Deschamps [1] as early as 1953. However twenty years passed before practical antennas were fabricated, as better the theoretical models and photo-etch techniques for copper or gold-clad dielectric substrate with a wide range of dielectric constants, attractive thermal and mechanical properties and of low loss tangent were developed. The first practical antennas were developed in the early 1970's by Howell [2] and Munson [3]. Various types of flat profile printed antennas have been developed- the microstrip antenna, the stripline slot antenna, the cavity backed printed antenna and the printed dipole antenna.

A microstrip antenna in its simplest configuration consists of a radiating patch on one side of a dielectric substrate ($\varepsilon_r \ll 10$) which has a grounded plane on the other side, as shown in Figure 3.1 [4]. The patch conductors, normally of copper and gold, can assume virtually any shape, but conventional shapes are generally used to simplify analysis and performance prediction [4]. Ideally, the dielectric constant, ε_r, of the substrate should be low ($\varepsilon_r \approx 2.5$) so as to enhance the fringe fields which account for the radiation [4]. However, other performance requirements may dictate the use of substrate materials whose dielectric constants may be greater than, say, 5 [4].

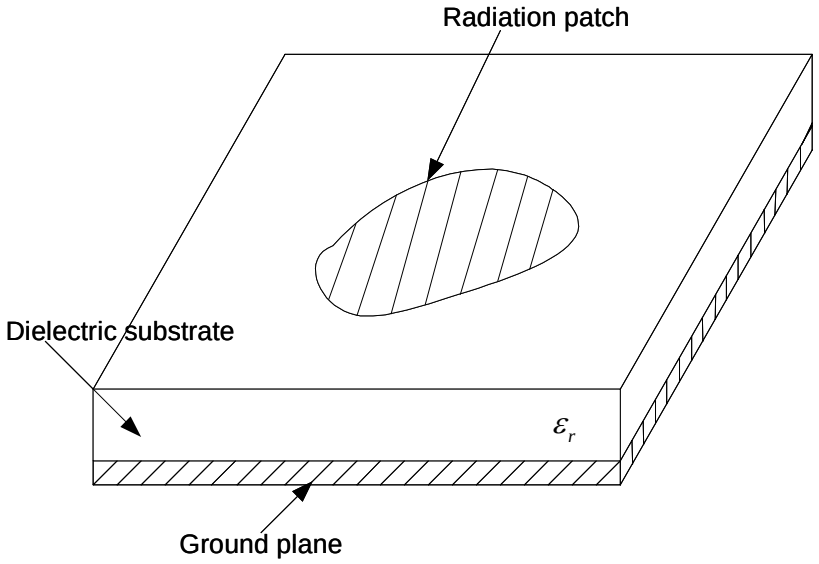

Figure 3.1: Microstrip Antenna Configuration

3.1.1 Advantages and Limitation

Microstrip antennas have several advantages compared to conventional microwave antennas and therefore many applications over the broad frequency range from ~100MHz to ~50GHz [4]. Some of the principle advantages of microstrip antennas compared to conventional microwave antennas are: light weight, low volume, thin profile planar configurations which can be made conformal; low fabrication cost; readily amenable to mass production; the antennas may be easily mounted on missile, rockets and satellite without major alterations; linear and circular polarizations are possible with simple feed; dual frequency and dual polarization antennas can be easily made; no cavity backing required; microstrip antennas can be easily integrated with microwave integrated circuits; feedline and matching networks can be fabricated simultaneously with the antenna structure.

However microstrip antennas also have some limitations compared to conventional microwave antennas: narrow bandwidth and associated tolerance problems; somewhat lower gain; most microstrip antennas radiate into an half-space; polarization purity is difficult to achieve; extraneous radiation from feeds and junctions; low power handling capability; reduced gain and efficiency as well as unacceptably high levels of cross-polarization; microstrip antennas fabricated on a substrate with a high dielectric constant are strongly preferred for easy integration with MMIC RF front-end circuitry; poor isolation between the feed and the radiation elements, possibility of excitation of surface waves; and lower power handling capability [4].

Radiation from a microstrip line, a structure similar to a microstrip antenna, occurs from the fringing fields between the edge of the conductor and the ground plane and can be lessened considerably if the substrate used is thin and has a higher relative dielectric constant. On the other hand, the radiation from a microstrip antenna is developed for better radiation efficiency where this radiation can be determined from the field distribution between the patch metallization and ground plane. Radiation from discontinuities in microstrip was examined on the currents flowing in the conductors and the effect of radiation on the quality factor Q of microstrip resonators was calculated on the fields in the aperature formed by the open end of the microstrip and the ground plane, first introduced by Lewin. From this analysis, the effect of radiation on the overall Q-factor was expressed as a function of resonator dimensions, operating

frequency, relative dielectric constant and thickness of the substrate. The radiation loss is much larger than conductor and dielectric losses at high frequency can be known from the theoretical and experimental results. The open-circuited microstrip line radiate more power when fabricated on thick low dielectric constant substrate.

3.1.2 Properties of Microstrip Antenna

The basic microstrip element has the narrow impedance bandwidth due to its electrically thin ground-plane dielectric substrate, which leads to a high Q resonance behavior. Bandwidth increases with the substrate thickness, but the problem with using a substrate thicker than 0.01λ or 0.02λ is that the impedance locus of the element becomes increasingly inductive, making impedance matching increasingly difficult. Furthermore, a thick substrate can not be used to the coplanar microstrip lines for feedline purposes, because spurious radiation from microstrip line bends and other discontinuities is unacceptably high for substrate thicker than a few hundred of wavelength.

Bandwidth decreases with increase in substrate dielectric constant and can be known by the effect that element size decrease in dielectric constant, which raises the Q of the resonator. Another disadvantages of thick high-dielectric constant substrate is that surface wave excitation will be higher, which will lower efficiency, and may lead to spurious radiation and pattern degradation. Therefore the thick substrate with low dielectric constant is preferred for good bandwidth.

3.2 Microstrip Antenna Configurations

Microstrip antennas are characterized by a large number of physical parameters than are conventional microwave antennas and they may be of any geometrical shape and any dimension. All microstrip antennas can be divided into four basic categories: microstrip patch antennas, microstrip dipoles, printed slot antennas, and microstrip strip traveling-wave antennas [12].

3.2.1 Microstrip Patch Antennas

Some microstrip patch antennas are shown in Figure 3.2. It consists of a conducting patch of arbitrary planar geometry on one side of a dielectric substrate on the top of the ground plane. Although there are numerous patch patterns for which radiation characteristic may be calculated, the rectangular, the circular, the equitriangular and the annular ring are the common shapes in practical case.

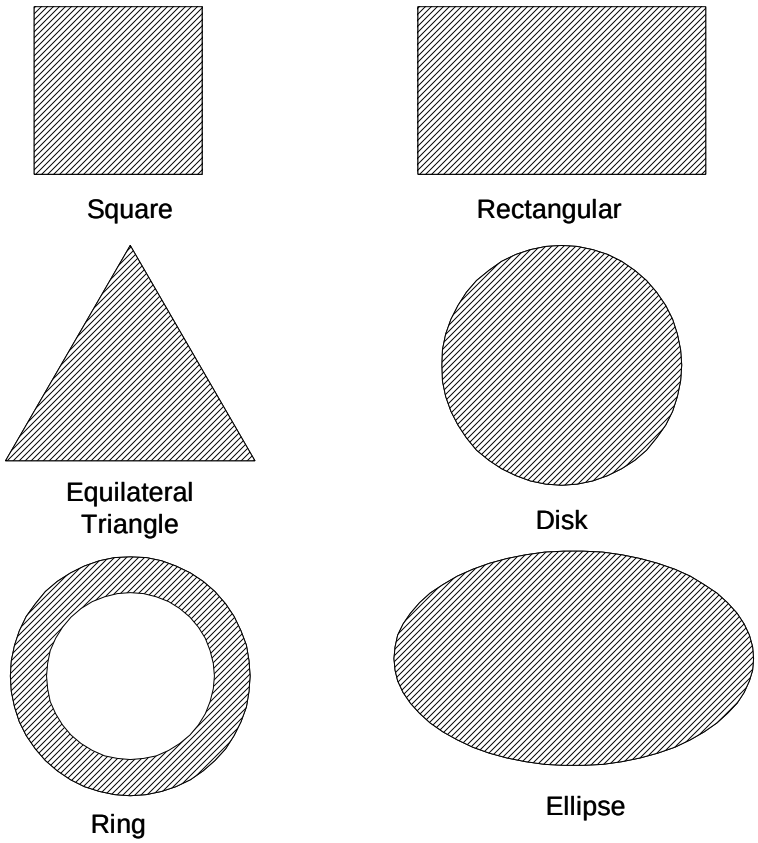

Figure 3.2: The practical used microstrip antenna configuration

3.2.2 Microstrip or Printed Dipole Antennas

Microstrip or printed dipoles differ geometrically from rectangular patch antennas in their length-to-width ratio. The width of a dipole is typically less than $0.05\lambda_0$ [12]. The radiation patterns of the dipole and patch are similar owing to similar longitudinal current distributions [12]. However, the radiation resistance, bandwidth, and cross-polar radiation differ widely [12]. Microstrip dipoles are attractive elements owing to their desirable properties such as small size and linear polarization [12]. The dipoles are well suited for higher frequencies for which the substrate can be electrically thick, and therefore can attain significant bandwidth [12]. The choice of feed

mechanism is very important in the microstrip dipoles and should be included in the analysis [12].

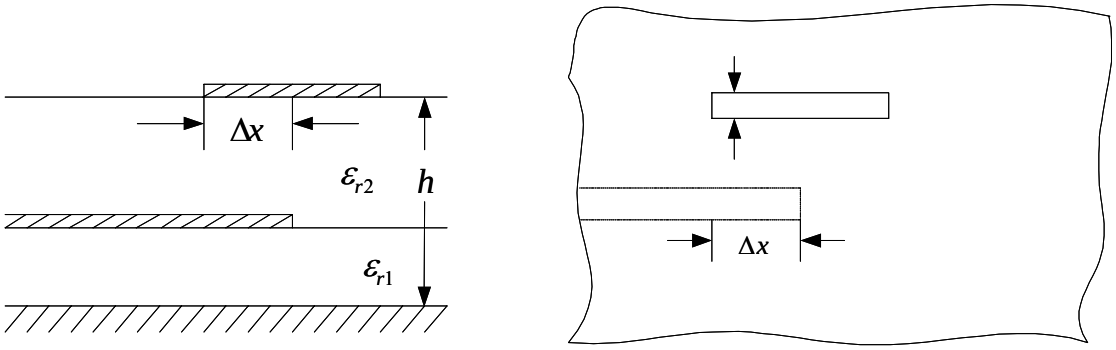

Figure 3.3: Configuration of proximity-coupled strip dipole antenna

3.2.3 Microstrip Printed Slot Antennas

Microstrip slot antennas consist of a slot in the ground plane fed by microstrip line and the slot may be in any shape like a rectangle (narrow or wide), a circle or an annulus [4]. Some microstrip slot antenna configurations are as shown in Figure 3.4.

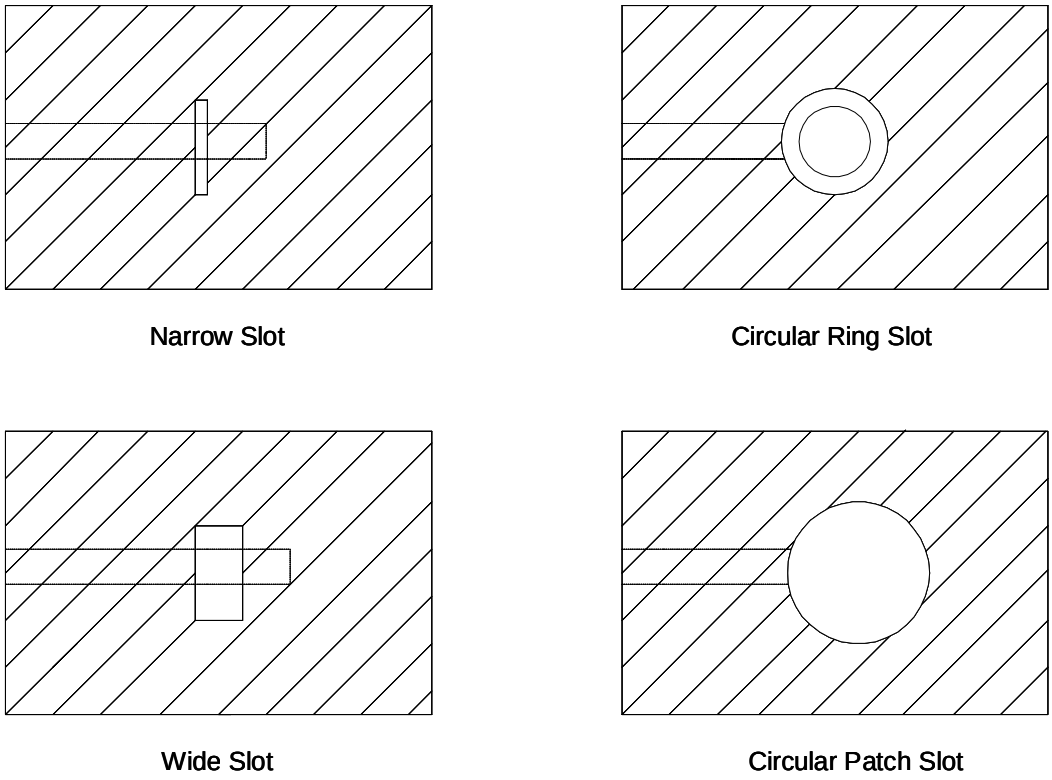

Figure3.4: Microstrip Slot Antennas

3.2.4 Microwave Traveling –Wave Antennas

Microstrip traveling-wave antennas consist of chain-shaped periodic conductors or an ordinary long TEM line which also support TE mode, on a substrate backed by a ground plane. The open end of the TEM line is terminated in a matched resistive load. As antenna support traveling waves, their structures may be designed so that the main beam lies in any direction from broadside to endfire. Various configurations for MTA are shown in Figure 3.5.

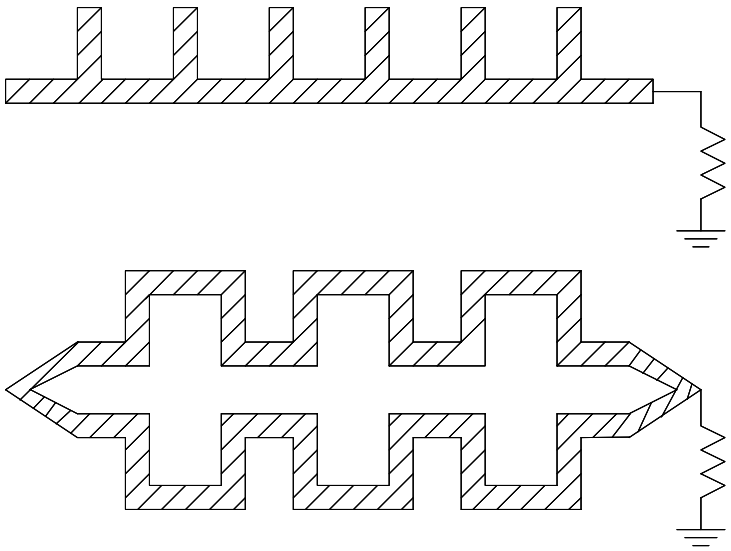

Figure 3.5:Some of microstrip traveling-wave antenna conffiguration

3.3 Feeding Techniques

Microstrip antennas have radiating elements on one side of a dielectric substrate, and thus early microstrip antennas were fed either by a microstrip line or a coaxial probe through the ground plane [12]. Since then a number of new feeding techniques have been developed [12]. Prominent among these are coaxial feed, microstrip (coplanar) feed, proximity-coupled microstrip feed, aperture-coupled microstrip feed, and coplanar waveguide feed [12]. The most important consideration is the efficient transfer of power between the radiation structure and feed structure, that is, impedance matching between the two [12]. Associated with impedance matching are stepped impedance transformers, bends, stubs, junctions, transitions, and so on, which introduce discontinuities leading to spurious radiation and surface wave loss

[12]. The undesired radiation may increase the side lobe level and the cross-polar amplitude of the radiation pattern [12]. Minimization of spurious radiation and its effect on the radiation pattern is one of the important factors for the evaluation of the feed [12].

3.3.1 Coaxial Feed/Probe Coupling

Coupling of power through a probe is one of the basic mechanisms for the transfer of microwave power. The probe can be an inner conductor of a coaxial line in the case of coaxial line feeding or it can be used to transfer power from a triplate line (strip line) to a microstrip antenna through a slot in the common ground plane. A typical microstrip antenna using a type N coaxial connector is shown in Figure 3.6. The coaxial connector is attached to the back side of the printed circuit board, and the coaxial conductor after passing through the substrate is soldered to the patch metallization. The location of the feed point is determined for the given mode so that the best impedance match is achieved.

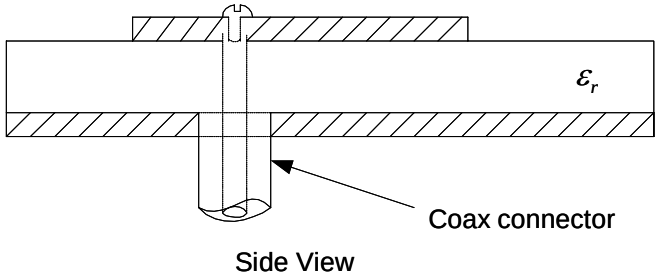

Figure 3.6: Side view of coasial probe feeding of a microstrip antenna

3.3.2 Microstrip (Coplanar) Feeds

Excitation of the microstrip antenna by a microstrip line on the same substrate appears to be a natural choice because the patch can be considered an extension of the microstrip line, and both can be fabricated simultaneously. But this technique has some limitations. The coupling between the micrstrip line and the patch could be in the form of edge/butt-in coupling as shown in Figure 3.7(a), or through a gap between them, as shown in Figure 3.7(b).

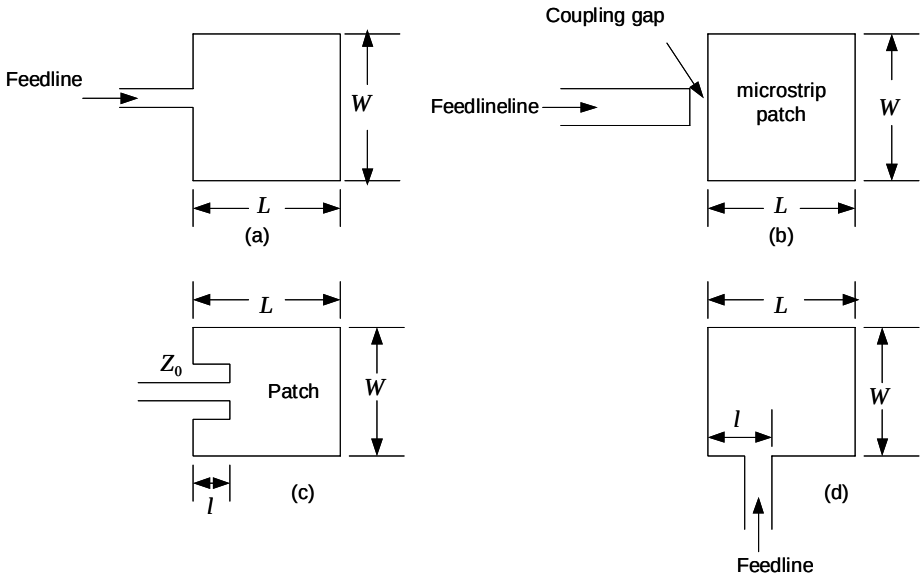

Figure 3.7: Various type of microstrip feed. (a) Micrsostrip feed at the radiating edge, (b) gap-coupled microstrip feed, (c) microstrip inset feed at the radiating edge, (d) microstrip feed at the nonradiating edge

An improvement of the coplanar feed that overcomes some of the short-coming mentioned is shown in Figure 3.7(c). Here the microstrip line is inset into the patch. The feed position is 50Ω. In another configuration for the direct microstrip feed, the feed point is selected on the nonradiation edge of the patch as in Figure 3.7(d). The cross-polarized radiation is high in this case, but can be minimized by optimizing ahe aspect ratio W/L.

3.3.3 Proximity (Electromagnetically) Coupled Microstrip Feed

Proximity coupled microstrip feed is a noncontacting noncoplanar microstrip feed which uses a two-layer substrate with the microstrip line on the lower substrate layer and the patch antenna on the upper one. The feed line that terminates in an open end is in a stub structure and this can be used to increase the bandwidth. Coupling between the patch and the microstrip is capacitive in nature and this coupling is known as an electromagnetically coupled microstrip feed as shown in Figure 3.8 (a). The detailed of electromagnetically coupled microstrip feed is explained in next section. This feeding technique is given the bandwidth order of 13%. Fabrication of this feed is slightly more difficult because of the requirement for accurate alignment between the patch and the feed line but soldering is eliminated [17].

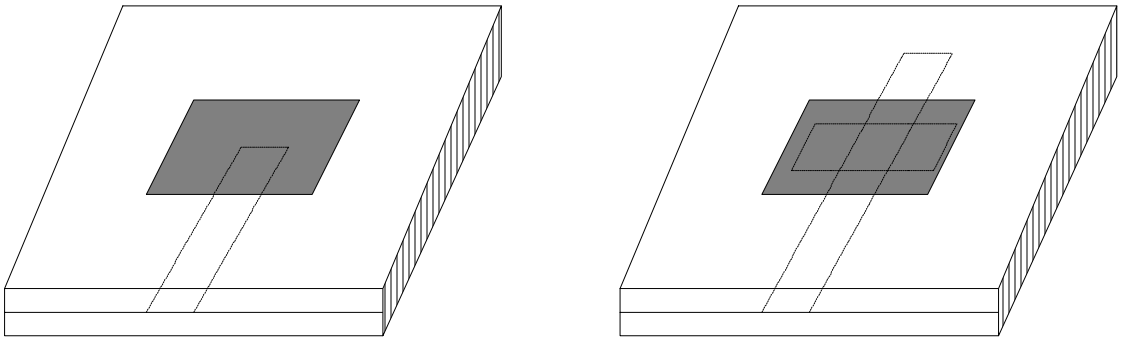

Figure 3.8: The microstrip antenna feed (a) proximity coupled microstrip feed (b) aperture coupled microstrip feed

3.3.4 Aperture-Coupled Microstrip Feed

The distinguished features of the aperture feed configuration are wider bandwidth and the shielding of the radiating patch from the radiation emanating from the feed structure [17]. It uses two substrate separated by a common ground plane as shown in Figure 3.8(b). The cross section and the planar view of the aperture-coupled microstrip feed is shown in Figure 3.9. A microstrip feedline on the lower substrate is electromagnetically coupled to the patch through a slot aperture in the common ground plane [17]. The slot in the ground plane is fed by a microstrip line and this slot can be of any shape or size and these parameters can be used to improve the bandwidth [17]. The substrate parameters for the two layers are chosen in a manner to optimize the feed a radiation functions independently [17]. The radiation from the open end of the feed line does not interfere with the radiation pattern of the patch because of the shielding effect of the ground plane [17]. This feature also improves the polarization purity.

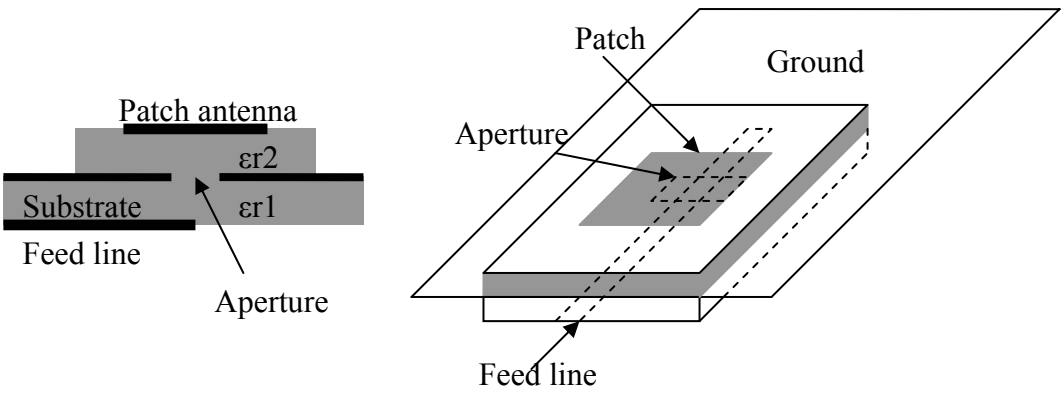

Figure 3.9: The cross section and planar view of the aperture-coupled feed

3.3.5 Coplanar Waveguide Feed

A coplanar waveguide (CPW) is the preferred transmission line for microwave monolithic integrated circuits (MMICs). This type of feeding technique is shown in Figure 3.10. The CPW is etched in the ground plane of the microstrip antenna and coupling is accomplished via a slot [17]. There are three possibilities excitation: in Figure 3.10(a) the center conductor of the CPW divides the coupling slot in two and the coupling between the patch and CPW is inductive; in Figure 3.10 (b) the CPW is transformed into a slot of length L_s and the coupling between the patch and CPW is capacitive [17]. The advantage of a CPW feed is that the radiation from the feed structure is negligible because the coplanar waveguide is excited in the odd mode of the coupled slot line [17]. This feature of a CPW feed is useful in the design of antenna arrays since mutual coupling between adjacent lines is minimized [17].

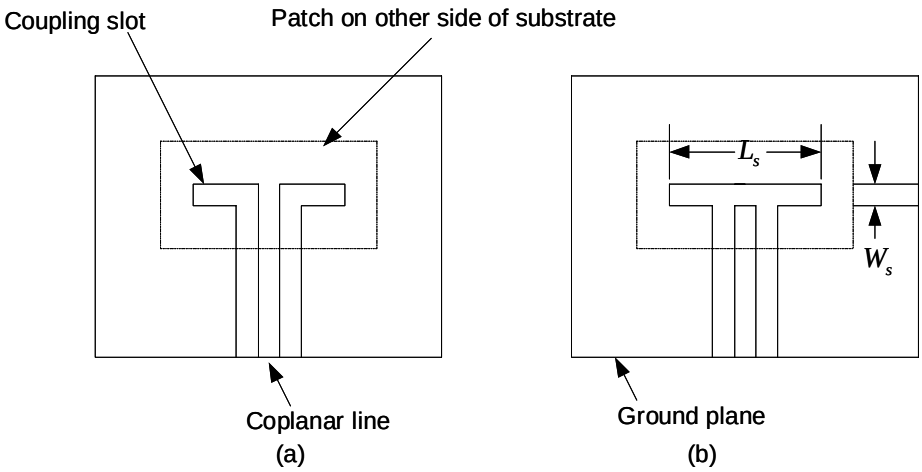

Figure 3.10: Coplanar waveguide of the microstrip patch antenna (a) Inductive coupling (b) Capacitive coupling

3.4 Methods Consideration to Enhance Impedance Bandwidth of U-slot patch antenna with Π shaped feed

The major drawback of patch antennas is the narrow frequency band. The technique commonly used to widen the bandwidth of resonant circuits is to couple several resonators with very closely spaced resonances. This approach has been used to widen the frequency width of microstrip patches by exciting several resonant modes of a single patch, or use several radiating structures closely coupled to each other but

resonating at slightly different frequencies. The elements can be either all be placed on the same level or on top of each other.

The method developed by Dubost is that it is incorporating several closely spaced modes of resonance in a single structure such as a dipole is folded at both ends and then combined with another mirror image dipole to yield a symmetrical structure. Alternately, the structure is considered as a rectangular patch with an H-shaped slot and it is fed by a buried stripline that extends below the metal. The use of this geometry increased the frequency bandwidth of a thin structure to 16% for a VSWR of 2:1.

The recent developed on U-slot patches with various feeding techniques exhibits broadband characteristics. The simplest feed into a U-slot patch is by coaxial probe [30] [31] [32]. Other methods include using an L-probe proximity feed [34] or using an array of 4 novel Π-shaped stub proximity fed U-shape slotted patches, arranged asymmetrically [35]. Although coaxial and L-probe proximity feed have superior bandwidth performances, they are hard to fabricate and have small tolerances to errors. An array of novel Π-shaped stub feed antennas, which are simplest to fabricate, requires an estate area of more than 6 times of single element patch and have inferior impedance bandwidth performance.

A novel Π-shaped proximity feed U-slot patch method utilized by this proximity fed patch is multimode operations with several virtue characteristics: unlike other feeding techniques, the fabrication technique is simple, both the patches, at the top and bottom substrates, can be separately fabricated and placed together at the final stage of fabrication. But there is minimal spurious radiation because the feed is sandwiched between the radiating patch and ground plane.

This chapter is investigated the Π-shaped proximity feed U-slot antenna and compared the simulated and reported result from the paper, varies the feed and patch dimensions, and analyses the resonant modes of the patch. The antenna described in is proximity feed patch antenna and the feeding structure is a novel Π-shaped stub, which is claimed to have broadband property. The patch structure is a U-slot rectangular patch spaced out on top of the feeding structure by air.

The patch antenna's details can be seen in the Figure 3.11 below.

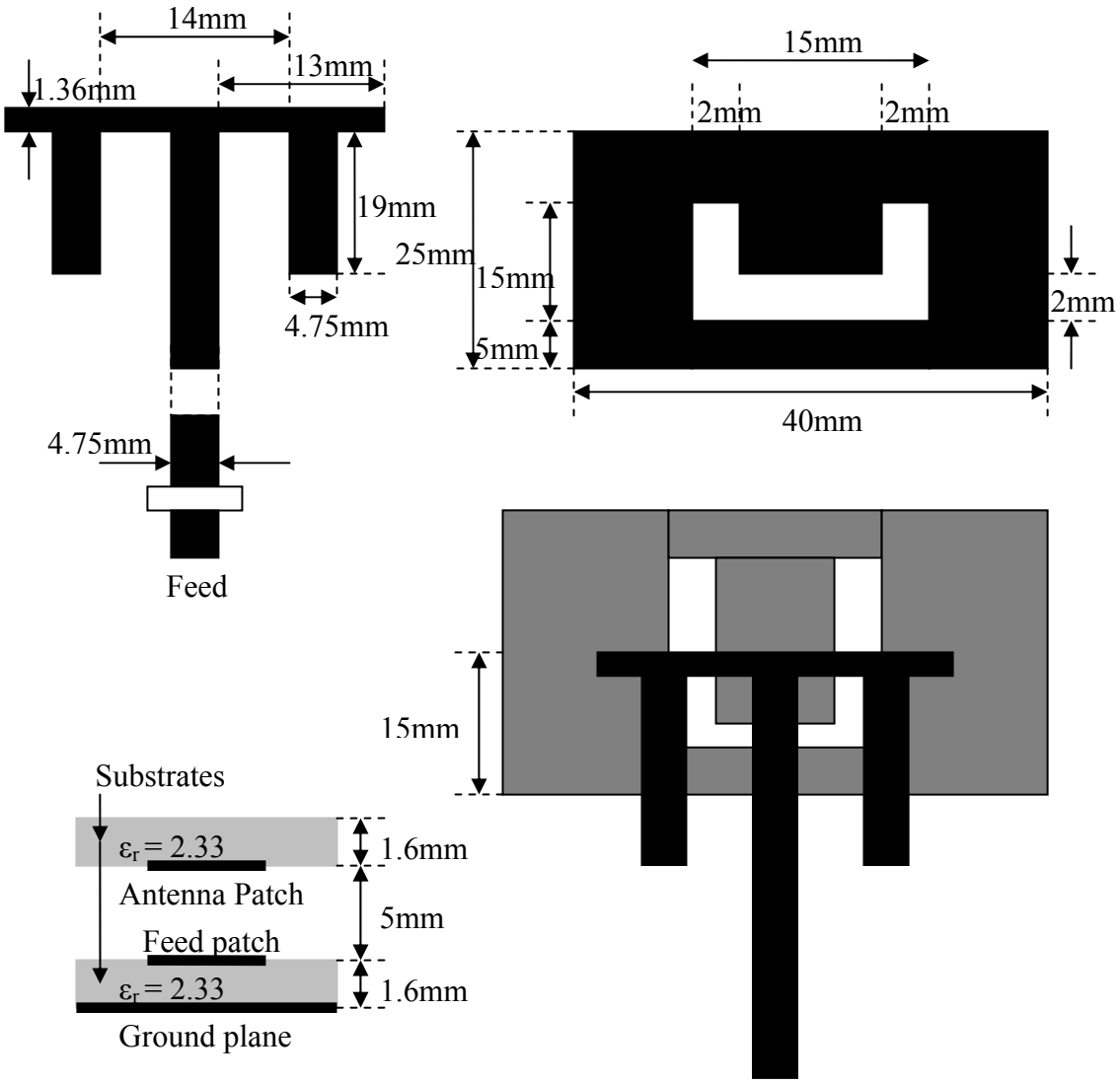

Figure 3.11: The configuration and physical dimensions of patch antenna

This patch structure is drawn in IE3D and simulated from 3 GHz to 5 GHz and the simulation is given the results of impedance bandwidth, the smith chart and VSWR graph showing the impedance bandwidth of novel Π-shaped feed U-slot patch.

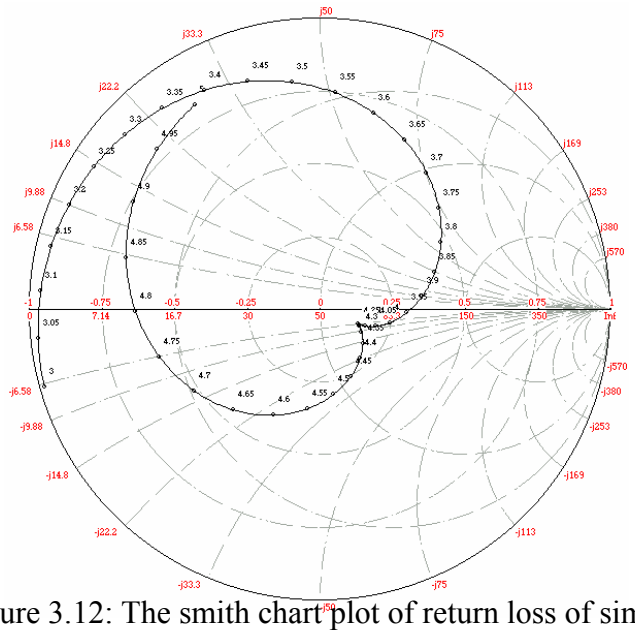

Figure 3.12: The smith chart plot of return loss of simulated results for patch antenna

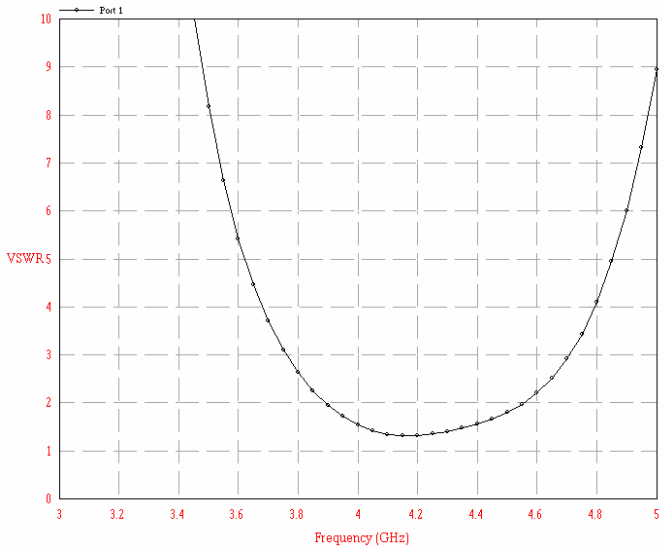

Figure 3.13: Plot for VSWR simulated results

The frequency range at which the antenna VSWR is less than 2 is 3.9 to 4.54 GHz with the simulated impedance bandwidth of about 15.2 %. The resonance frequency, according to the smith chart, is at 3.93 GHz and 4.8 GHz.

3.4.1 Analysis of Patch Antenna

A Π-shaped proximity feed U-slot rectangular patch is constructed from a simple proximity coupled rectangular patch with the same patch dimensions.

3.4.1.1 Single Microstrip Line Proximity Feed

Figure 3.14 below is a schematic of the patch that is simulated.

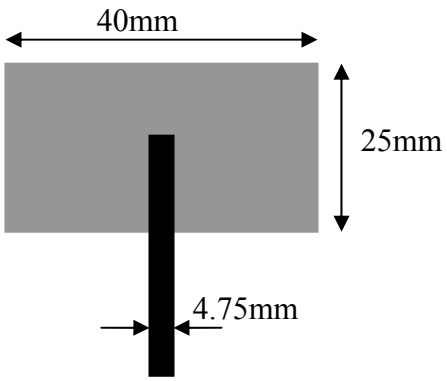

Figure 3.14: Schematic of single line feed

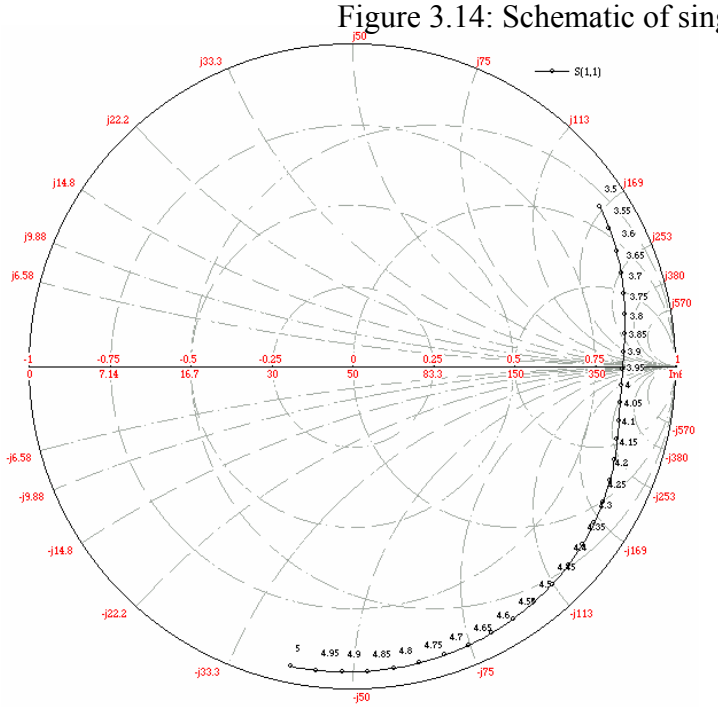

Figure 3.15: Simulated return loss for patch antenna of figure 3.14

Figure 3.15 shows the simulated results of this simple rectangular patch with proximity feed. The resonant frequency is about 3.93 GHz at TM_{10} mode, but feed is not matched as return loss is high.

3.4.1.2 T-shaped Proximity Feed Rectangular Patch

Connecting a T-junction beneath the patch with a horizontal stub of 100Ω line terminated at open circuit would change the resonant frequency by shifting the response clockwise. This configuration is shown in Figure 3.16 below.

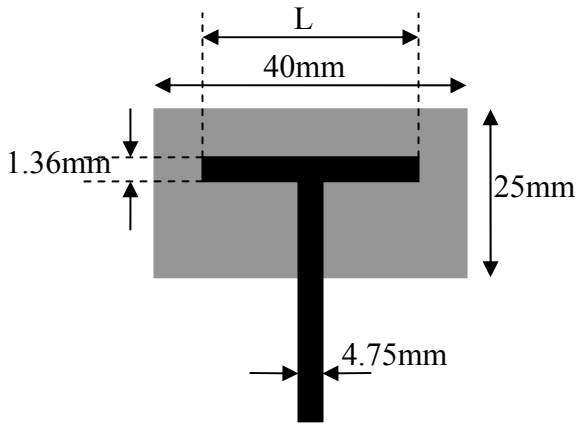

Figure 3.16: Schematic of T-shaped feed

When L = 25.75 mm, both the resonant frequencies decreases to 3 GHz, and 4.55 GHz. A clockwise shift of the response means that the interaction between the feed and patch is now more capacitive. Additional stubs increases the surface area of the capacitive interaction between the feed and the patch. Antenna is still either unmatched or the coupling from the feed to patch is not good.

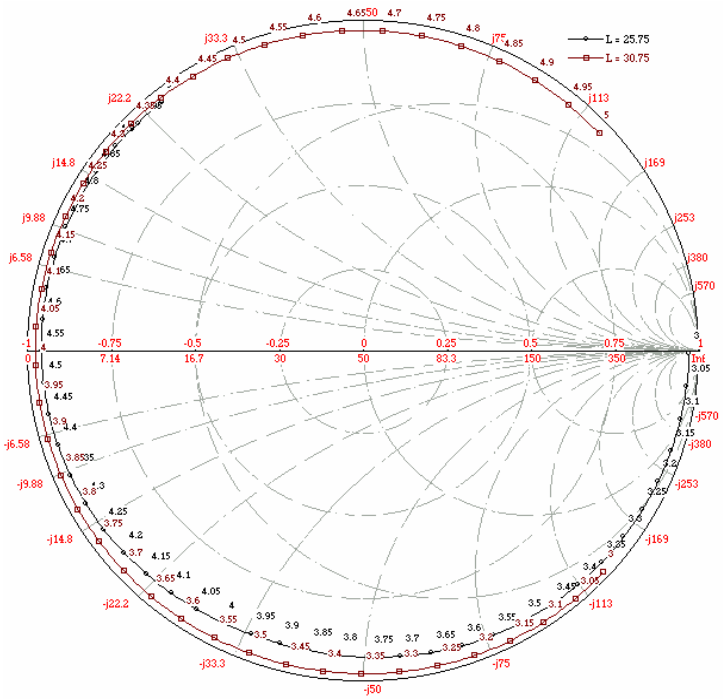

Figure 3.17: Simulated return loss for patch antenna of figure 3.16

3.4.1.3 Π-shaped Proximity Feed Rectangular Patch

Adding 2 vertical 50 Ω stubs from the middle of 100 Ω lines terminated as open circuit shifts the response clockwise further. It increases the capacitive interaction between the feed and patch. As L increases, the feed and patch gradually becomes match with each other.

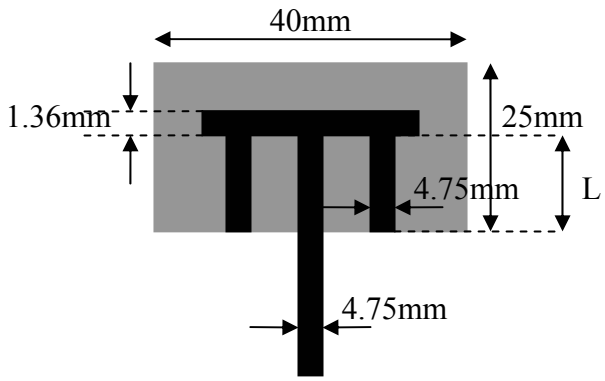

Figure 3.18: Schematic of Π -shaped feed

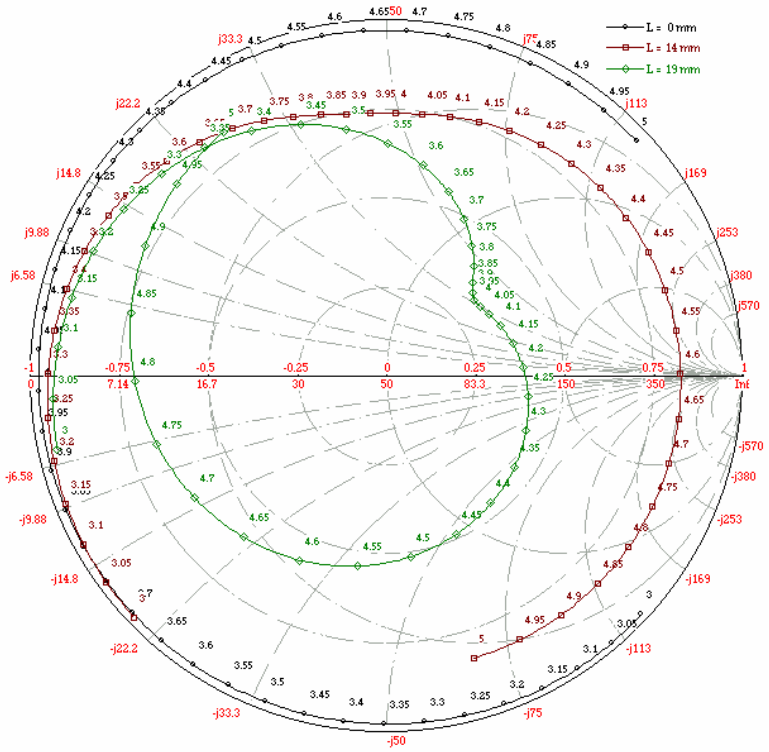

Figure 3.19: Simulated return loss for patch antenna of figure 3.18

The coupling from the feeding structure and the matching improves tremendously with the introduction of side stubs. It is observed that the side stubs are solely responsible for matching and coupling of energy from feed to patch.

3.4.1.4 Π-shaped Proximity I I-Slotted Rectangular Patch

Fixing the feed structure as Π-shaped, we introduce two vertical slots symmetrical about the y-axis of the patch, as shown in Figure 3.20 below.

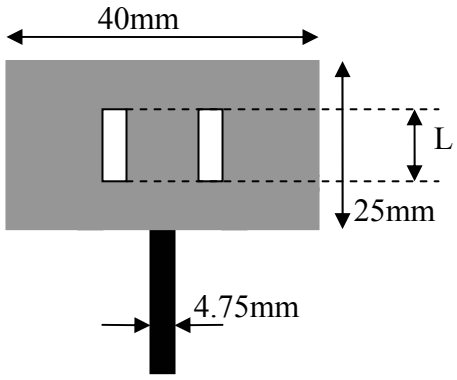

Figure 3.20: Schematic of Π -shaped proximity I I-slotted rectangular antenna

Introduction of vertical, symmetrical slots on patch do match the antenna further. However, there is a slight anticlockwise movement of the response – the response is getting inductive as L is increased. It is observed that adding vertical slots would make the antenna more inductive.

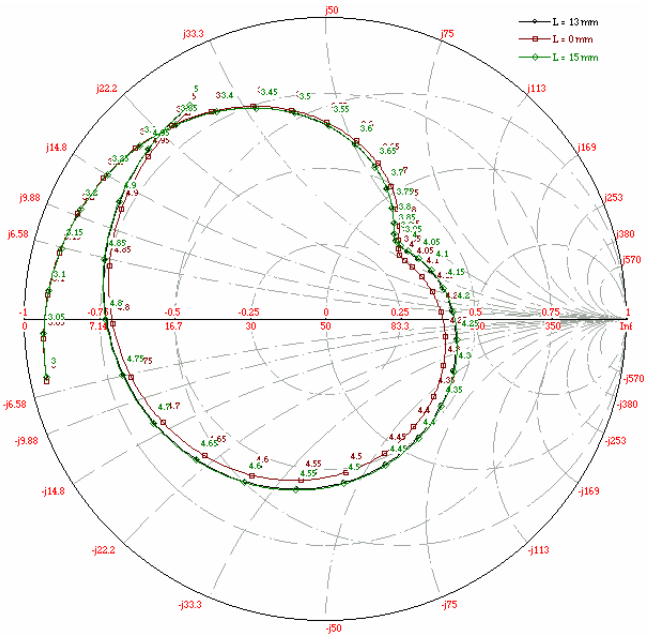

Figure 3.21: Simulated return loss for patch antenna of figure 3.20

3.4.1.5 Π-shaped Proximity Feed Line-slotted Patch

A horizontal slot is introduced on the patch. Figure 3.22 shows the schematics diagram of the simulation.

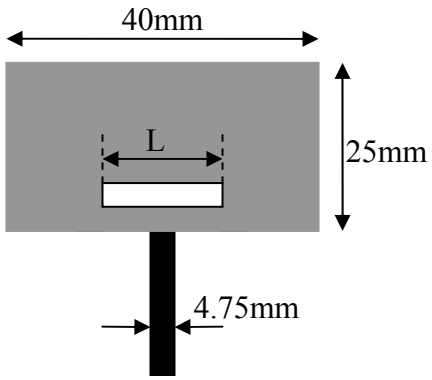

Figure 3.22: Schematic of Π -shaped proximity feed line slotted patch

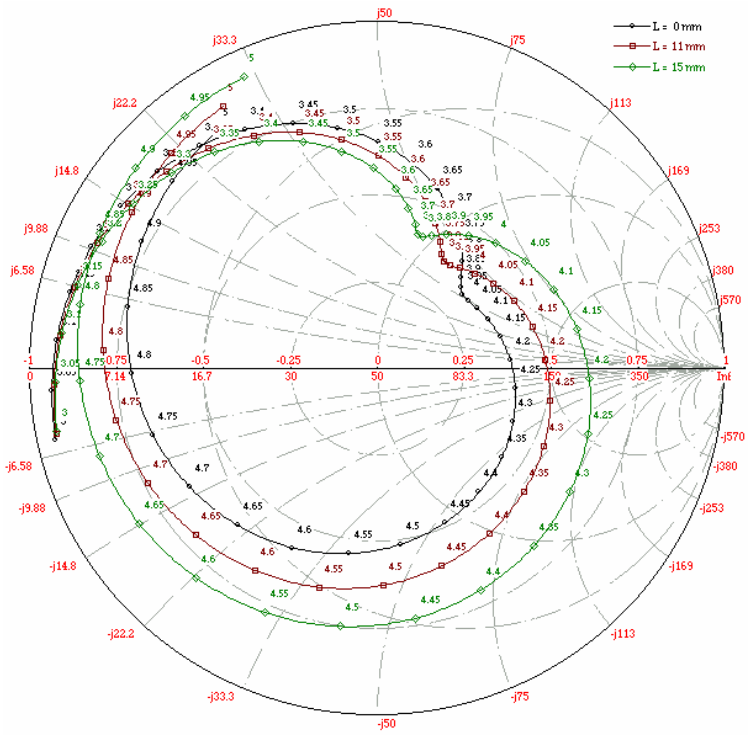

Figure 3.23: Simulated return loss for patch antenna of figure 3.22

Increase in L shifts response anticlockwise and reduces the resonant frequency. Slot adds inductance to the antenna patch, since resonant frequency is inversely proportional to the square root of L and C.

3.4.1.6 Π-shaped Proximity Feed U-slotted Patch

Both sides of the U-slot lengths are varied. Figure 3.24 below shows the schematics of the variations while Figure 3.24 below shows the simulated results.

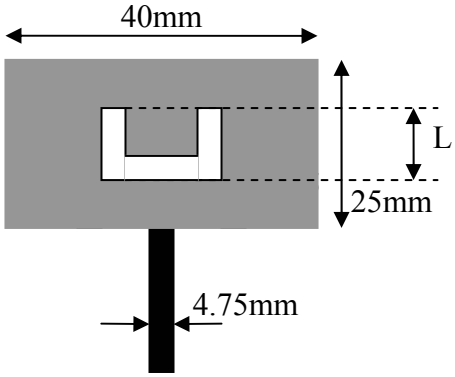

Figure 3.24: Schematic of Π -shaped proximity U-slotted patch

Adding side stubs length, L shifts response anticlockwise. Initial increment of L makes the patch more inductive, but the general trend is to shift the response to the negative half z-plane of the smith chart, making the antenna capacitive. Increase in L increases the overall matching of the patch.

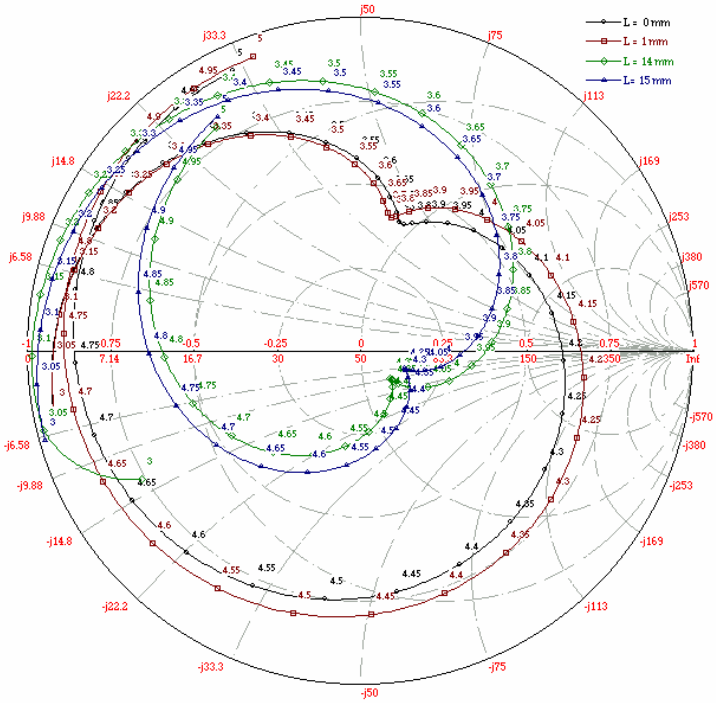

Figure 3.25: Simulated return loss for patch antenna of figure 3.24

3.5 The Compact Wideband Four-Stub Feed Design

The design of four-stub feed comes by considering like stub widening vs. tapering, and solving the problem of having unequal length stubs while maintaining antenna's symmetry. The only way to do is to have two stubs at each side of the central feed line with different stub lengths with this configuration will not affect the symmetry of the antenna structure since the other side of the feed line can be the mirror image of this side.

The first step of design is to see the difference in matching between a 2-stub and a 4-stub feed. Figure 3.26 below shows the schematics of the comparison. Figure 3.27 shows the simulated S_{11}. A magnitude comparison is done between these two feed configurations. It is found that addition of two more stubs significantly increased the matching.

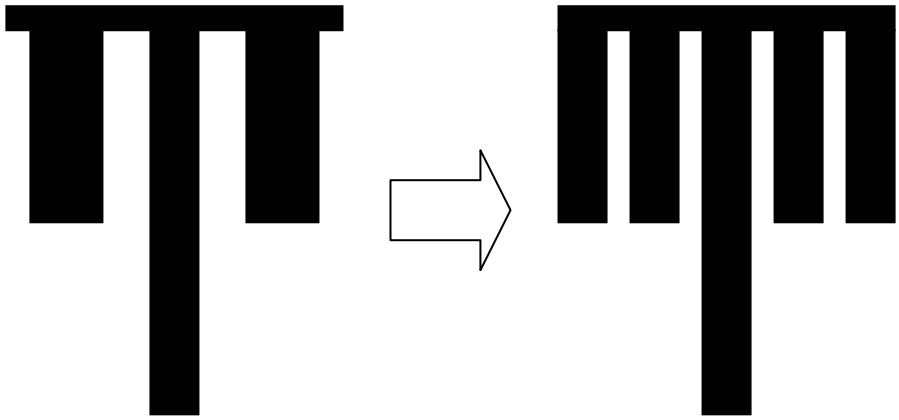

Figure 3.26: Comparison between 2-stubs and 4-stubs feed

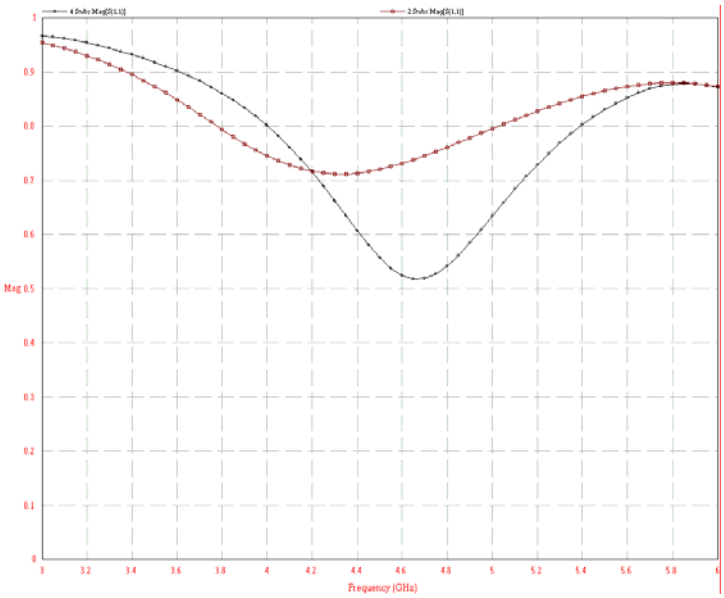

Figure 3.27: Magnitude response for return loss of 2-stubs and 4-stubs feed

3.6 The Final Physical Dimensions of Patch Antenna

The geometry and detailed dimensions of the four-stub feed U-slot rectangular patch are shown in Figure 3.28. All units stated are in millimeters. Figure 3.28(c) illustrates the relative lateral position between the top patch and bottom feed. Figure 3.28(d) shows a vertical cross-section of the antenna.

The top and bottom dielectric layers are of the same material, with ε_r=2.35 and thickness of 1.5748mm. The middle is an air gap of ~ 6mm (0.087λ). The U-slot patch is located at the lower side of the top dielectric layer. The four stubs and feed line are printed on the upper side of the bottom dielectric layer. This configuration provides protection for both the patch and the feed from wear and tear. The U-slot patch is electromagnetically coupled by this feed line and 4 stubs.

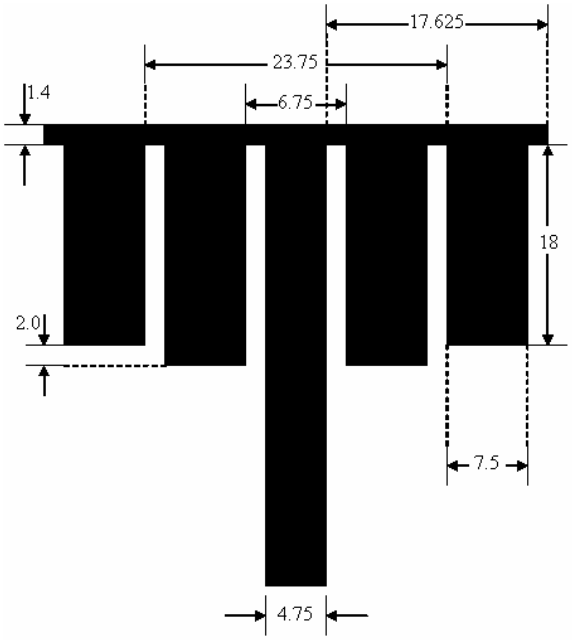

All the dimensions are in (mm)

(a) 4-stubs feed line

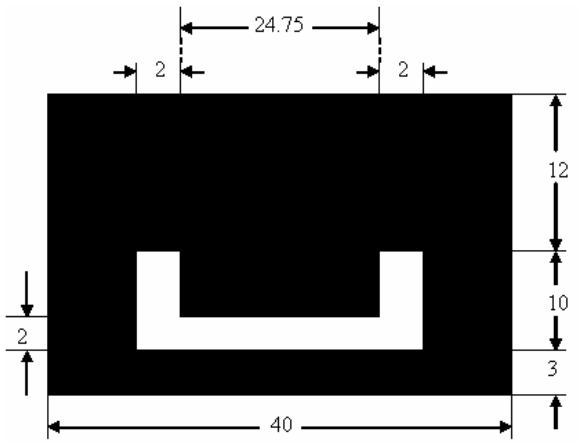

All the dimensions are in (mm)

(b) rectangular patch

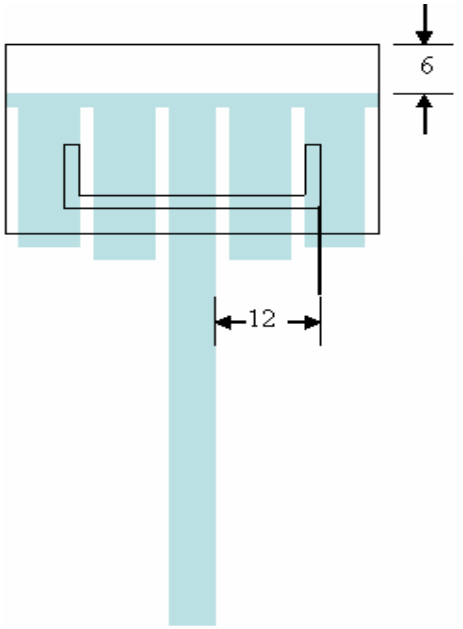

All the dimensions are in (mm)

(c) final design

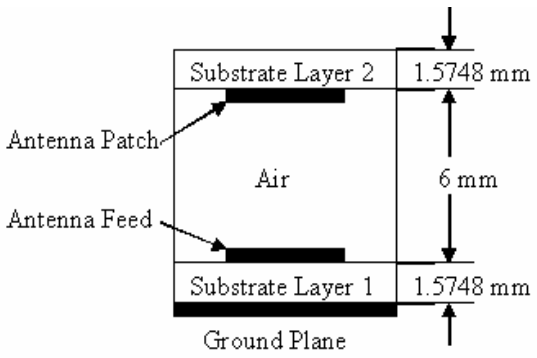

(d) side view of final design

Figure 3.28: The geometry of final design

The antenna is fabricated with all the parameters stated as above. Its impedance bandwidth is then measured with an HP8510 Vector Analyzer. The S_{11} of the antenna, both simulated and measured, can be found in Figure 3.29. Figure 3.29(a) shows the simulated and fabricated results in dB (S_{11}) and Figure 3.29 (b) and (c) show the polar plots of simulated and measured S_{11} respectively.

For the simulated results, the pass band is 3.862-4.997 GHz, which corresponds to ~26% in impedance bandwidth. For measured results, the pass band is 3.885-4.845 GHz, which corresponds to ~22% in impedance bandwidth.

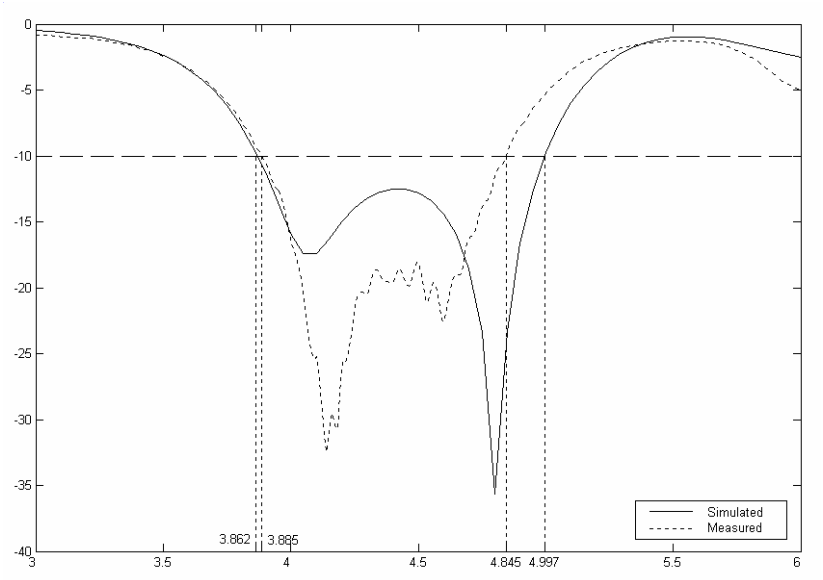

Figure 3.29(a)

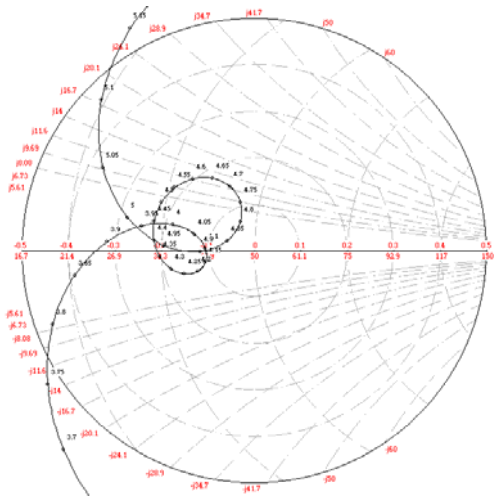

Figure 3.29(b)

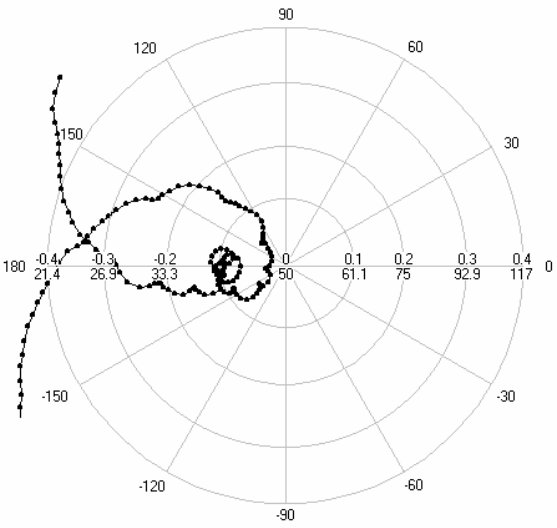

Figure 3.29(c)

Figure 3.29: Impedance bandwidth of antenna

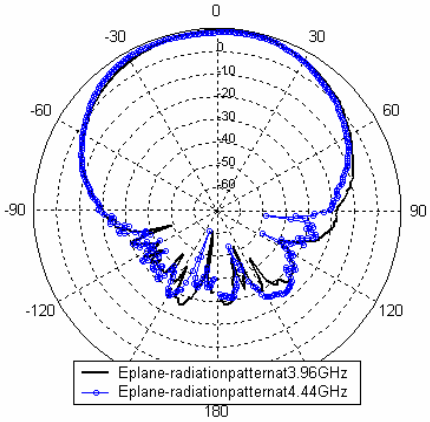

Figure 3.30: The measurement radiation E-plane pattern for the final design

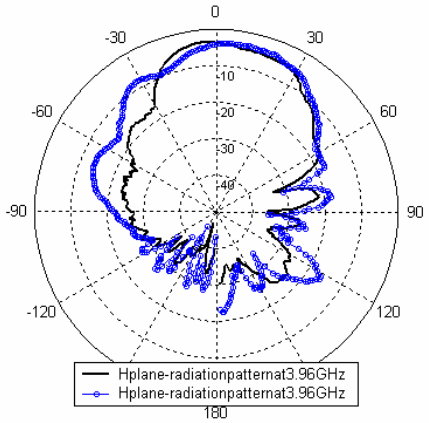

Figure 3.31: The measurement radiation H-plane pattern for the final design

CHAPTER IV
ATL IN MICROSTRIP ANTENNA APPLICATIONS

4.1 Electomagnetically Coupled Microstrip Dipoles

The new class of printed circuit radiator consisting of a microstrip dipole electromagnetically coupled to a microstrip feedline in transverse configuration have been investigated and found as single antenna elements or for arrays applications and is shown in Figure 4.1. According to first introduced by Oltman and Huebner, the EMC dipole has the radiator imbedded within the dielectric substrate at higher level, feedline at lower level and the ground plane at the bottom level of the substrate. This coupling feed has several advantages over the direct edge feed and probe feed techniques. The radiating element is covered with the dielectric substrate thickness $2t_{sub}$. Electromagnetic coupling (EMC) in which no physical connection is made between the feed line which is placed on the lower substrate and terminated in an open-end at a point below the radiating element and the radiating element. EMC dipole configuration has the advantages of greater bandwidth and efficiency, followed directly from the increase in radiation conductance associated with a growth in radiator-ground plane spacing when the dipole is placed further from the ground plane than the feedline [10]. The possibility of placing the feed network closer to the ground plane than the dipole results in reduction of feed line radiation from bends, junctions and various transmission line discontinuities [10]. Selecting an appropriate line-dipole overlap is the match of the dipole to the feedline. Thus the dipole can be placed farther from the ground plane to enhance its desired radiation while the feed is simultaneously located to close to the ground plane to reduce its parasitic radiation [10]. It is also known that EMC dipole can be simply matched to its microstrip feed line.

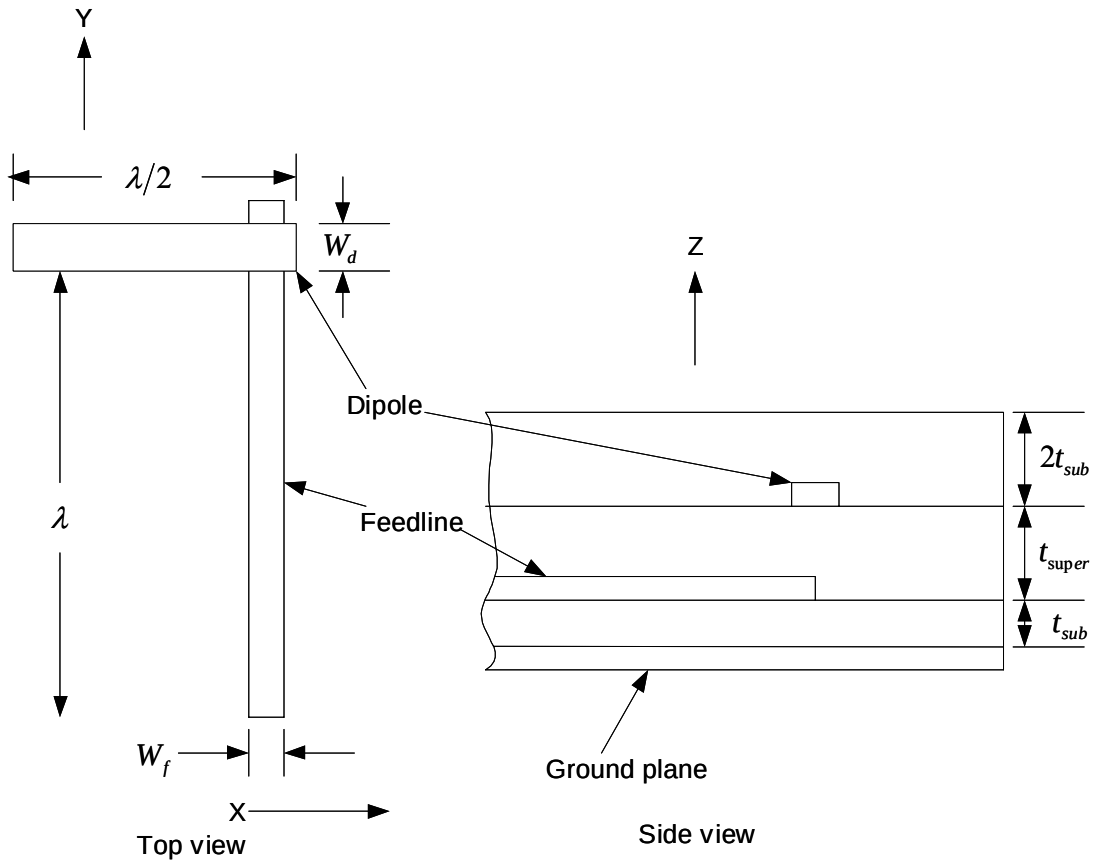

Figure 4.1 The basic structure of electromagnetically dipole antenns

The loci of dipole center position results a near ellipsoidal surface over which the dipole is matched to the microstrip line. This is because it is field-coupled and involves both electric and magnetic fields. As the dipole-feed spacing is increased, the ellipse is reduced in size until it is a single point [10]. For any spacing larger than its critical value, the coupling is too weak to match the dipole to the feed line; for any spacing less than this critical value, it is always possible to readily achieve a match by simply sliding the dipole strip over the feed terminal until a match is observed [10]. The resonant frequency of the EMC dipole is primarily determined by its length but it can be significantly perturbed by the coupling [10].

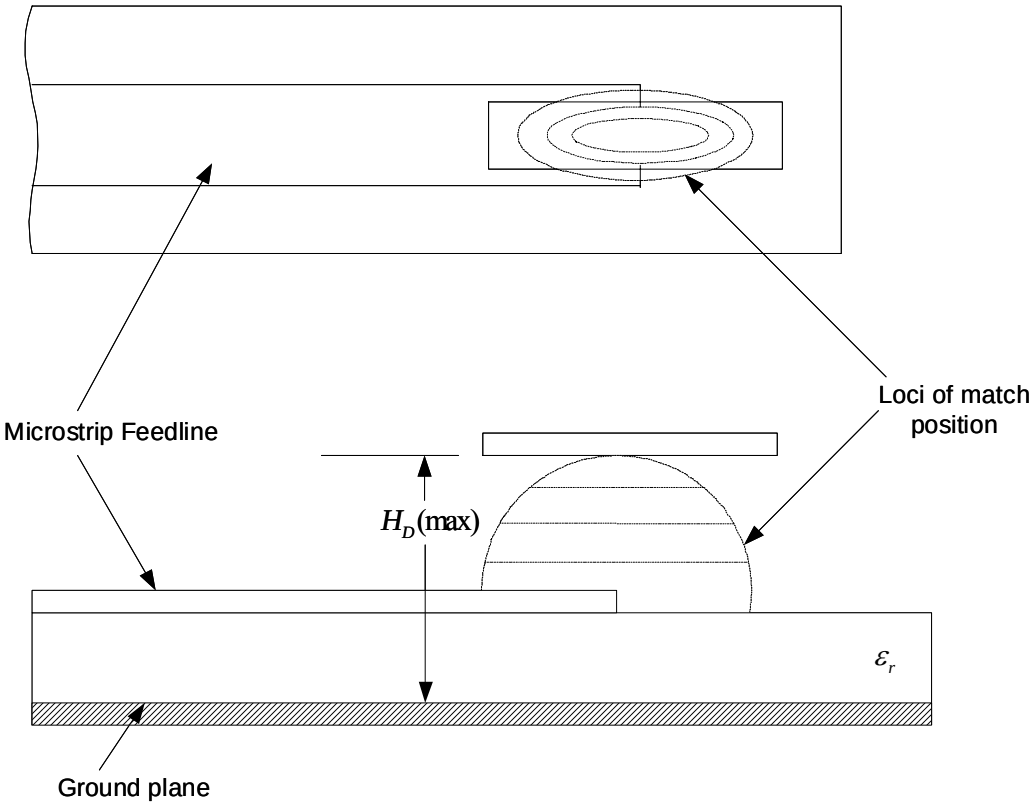

Figure 4.2:Loci of dipole positions for which dipole is matched to microstrip line

The main advantages of the EMC dipole when compared to classically fed printed antennas (coaxial connector; microstrip line with contact) are not only greater bandwidth and efficiency, but also the simplicity with which the EMC dipole can be matched to its microostrip feed line in numerous configurations that can be grouped into two main configurations: longitudinal and transversal. According to Lepeltier, Floc'h and Citerne, the transverse dipole was chosen over the longitudinal dipole as the longitudinal dipole reveals a major drawback as it is necessary to have an individual feedline for each dipole which leads to very cumbersome in power dividers for an antenna array. In transverse configuration, many dipoles can be easily fed in series from the same line, providing substantial simplification in the feeding network architecture.

In a microstrip antenna, the resonant frequency of a particular mode is determined by the shape and the size of conducting patch, the relative permittivity of the substrate and, the thickness of the substrate. Thus the dimension of the dipole determines the frequency of the antenna and its performance. The length of the dipole directly affects the frequency of the resonant frequency while the width determines its characteristics impedance.

The dimensions of the dipole are found using the following formulas:

$$\varepsilon_e = \frac{\varepsilon_r + 1}{2} + \frac{\varepsilon_r - 1}{2} \frac{1}{\sqrt{1 + 12 h/W}} \tag{4.1}$$

$$Z_0 = \frac{120\pi}{\sqrt{\varepsilon_e \left[\frac{W}{h} + 1.393 + 0.667 \ln(\frac{W}{h} + 1.444) \right]}} \tag{4.2}$$

where Z_0 = the characteristic impedance of the microstrip line

W = the width of the microstrip line

h = the distance between the microstrip line and the ground plane

ε_e = the effective permittivity of the substrate

ε_r = the relative permittivity of substrate

For $Z_0 = 50\Omega, \varepsilon_e = 4.4, \frac{W}{h} = 1.485$,

the width of the feedline, $W_f = 2.3mm$

the width of the dipole, $W_d = 4.6mm$

The length of the feedline can be found by the following equation:

$$L_f = \frac{c}{f\sqrt{\varepsilon_e}} \tag{4.3}$$

where f = the frequency is taken to be 0.9GHz , the lowest frequency

L_f = the length of the feed line

c = the speed of light, $3 \times 10^8 m/s$

The length of the dipole can also be found by the following equation:

$$\lambda = \frac{c}{f\sqrt{\varepsilon_e}} \tag{4.4}$$

$$L_d = \frac{\lambda}{2} \tag{4.5}$$

where λ = the physical wavelength of the dipole

L_d = the physical length of the dipole

4.1.1 Loci of the EMC Microstrip Dipole

Studied on the loci of the EMC dipole, for which the dipole is matched to the feed line, the loci is formed as a nearly ellipsoidal surface, centered on the feedline end and the configuration of the loci of dipole are shown in Figure 4.2. To investigate more on how the loci impact, the return loss and the bandwidth of the EMC dipole was further analyzed against with the dipole longitude and transverse positions on the feedline and the height of the substrate using IE3D software. Generally the EMC microstrip dipole resonant frequency is predominantly examined by its length, it is considerably disturbed by coupling effect. Accordingly to the dependence of resonance on the coupling where the electric and magnetic energies are incorporated, the perturbation is varied.

4.1.1.1 Effects of dipole shifting in X-Y plane

The half-wavelength dipole, with the length of $\lambda = 158.9mm$ at 0.9GHz, was placed at the end of the feedline. The return loss and the bandwidth of the dipole were first investigated by sliding the dipole transversally to the feedline and then varying the longitude position of the dipole on the feedline with the dipole dimension of $W_d = 4.6mm, L_d = 78.4mm$ and the feedline dimension of $W_f = 2.3mm, L_f = 158.9mm$ at the frequency of 900MHz. It is possible to find a match point for any y-coordinate, as well as the corresponding X-coordinate producing the high return loss. The optimum position of X-Y plane, X-offset of 0.69mm and Y-offset of 65.6mm, are given the high return loss which is meant that there is a good match between the dipole and the feedline and the results are shown in Figure 4.3 (a) and (b).

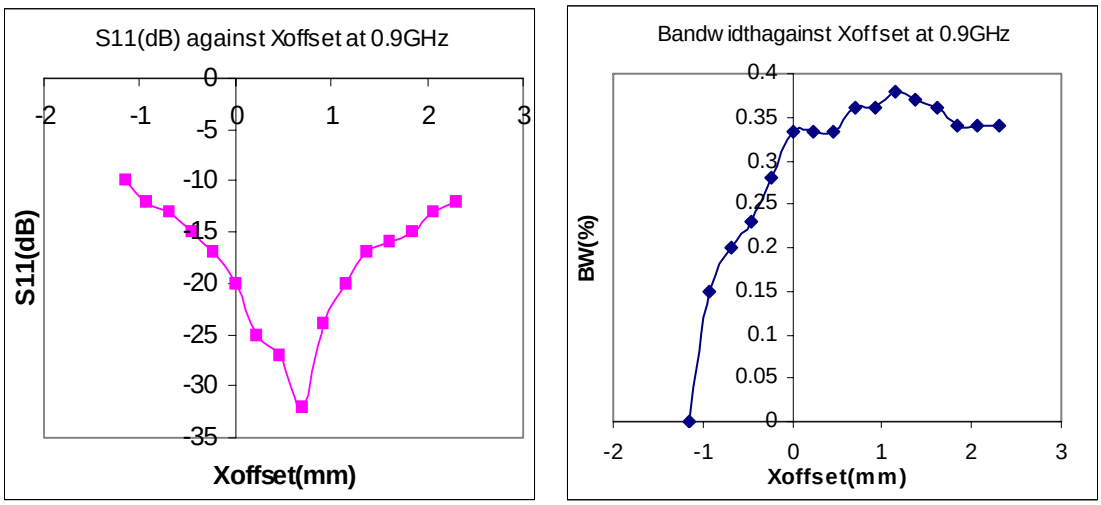

(a)

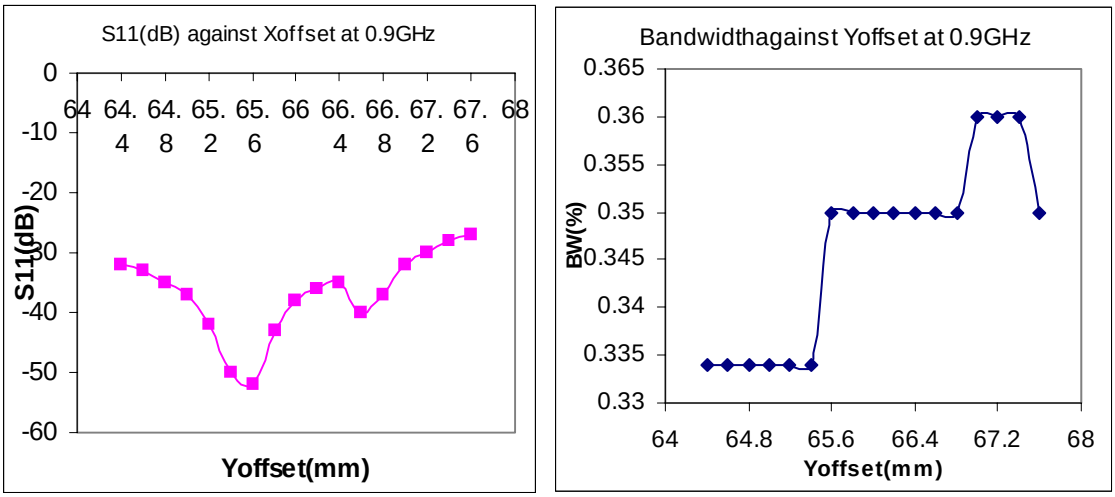

(b)

Figure 4.3: Bandwidth and return loss against frequency for single dipole at 0.9GHz
(a) changed the dipole position transversally and (b) changed the dipole position longitudinall

4.1.1.2 Effects of dipole shifting in Z-axis

The effect of dipole shifting in Z-coordinate was studied with the difference substrate height of the feedline to the ground plane. But the thickness of FR4 substrate which is available in the Microwave Laboratory in NUS, the relative permittivity of $\varepsilon_r = 1.57mm$, one layer above the ground plane. Because of this constraint, the dipoles can be placed at the multiple of the substrate thickness z =3.14mm, z =4.71mm or z =6.28mm and so on. From the simulation results it is obvious that there is only placed the dipole at either at z =3.14mm or z =5.71mm,the maximum height of the ellipsoidal loci of the dipole , and placing the dipole at z =6.28mm is designate that the dipole is not electromagnetically coupled to feedline which means the coupling is too weak to match the dipole to the feedline.

4.1.1.3 Effects of substrate and superstrate

The effect of varying the values of substrate and superstrate was studied which is useful for the final tri-band design. From the above explanations, it can be known that the greater the distance between the dipole and the ground plane, the larger the impedance bandwidth and the efficiency. It is noted that the efficiency is decrease for the increased substrate thickness but is lower for higher the substrate permittivity [15]. Theoretically it is possible to improve bandwidth by increasing the substrate height, however, due to the coupling effect, the spacing can not be greater than the above the maximum dipole-ground plane spacing, $H_D(\max)$. Due to the limitation of the used

ubstrate thickness in this project, it is not possible to vary the substrate height for other height instead of using multiple layers. The other limitation for a thin substrate is that although the efficiency is high for thin substrate, the radiation power become very low and the bandwidth is very small [15].

A typical microstrip line configuration is that the dipole is layered above a superstrate layer and the air. The feed line is placed between the superstrate and the substrate which in turn placed above the ground plane. However, in this project, the superstrate (cover) layer on top of the microstrip dipole is significantly influence the radiation properties of the microstrip dipole [15]. The benefit of the microstrip line covered by the two dielectric layers is that it can be eliminated fringing field effect that would exist according to the superstrate and also act as a protection layer for the whole structure.

4.2 Basic Properties of Photonic Bandgap

The photonic bandgap (PBG) structures, also called electromagnetic crystals, which can provide effective and flexible control of the propagation of electromagnetic waves whether they are guided waves, surface waves or radiation waves within a particular frequency, is periodic structures inspired by the geometry of both natural crystals and the artificial crystals. These artificially created periodic structures are built in metals or substrates in order to influence the electromagnetic properties of materials. The lack of electromagnetic propagating modes is referred to as a PBG within these structures. It is first invented for radio and microwaves as well as for optical wavelengths but PBG structures are increasingly scaleable and applicable to a wide range of frequencies, including microwaves and millimeter waves. It is characterized by frequency bands where waves propagate freely in certain directions in the structure as passbands where waves propagate in the same direction are highly attenuated as stopbands.

The microstrip lines incorporating a photonic bandgap (PBG) structure have have been used to improve radiation pattern of microstrip antennas, increase the output power and efficiency of power amplifier, resonant cavities, filters, design of reflectors, broadband absorbers and frequency selective surfaces and other devices in the microwave region. In the study of microstrip technology, PBG structure is obtained by

drilling an appropriate periodic pattern in the substrate or etching the holes in the ground plane. The PBG structures can be achieved by using metallic, dielectric, ferromagnetic or ferroelectric implants [26].

4.2.1 Applications in Microwave and Millimeter Wave Circuit

Periodic structures, also known as photonic bandgap (PBG) crystals, which are used in controlling the behavior of electromagnetic waves in modern microwave and millimeter wave circuits and antenna, have been included: (1) Dielectric-based PBG microstrip lines; PBG ground plane for microstrip lines; (2) PBG-based high Q image guide resonator; (3) Compact 2D PBG lattice for surface wave suppression in microstrip patch antenna and (4) Uniplanar compact PBG (UC-PBG) structure.

The microstrip circuits are developed with the dielectric-based PBG substrate which requires to form a periodic pattern through the substrate of microstrip in order to possess distinct stopbands for TEM wave propagation in microstrip lines. There are four types of such PBG structures: square lattice with square hole; triangular lattice with square hole, and honeycomb lattice with circular or square hole, which show distinct stopbands for quasi-TEM wave propagation in microstrip lines. A 50Ω microstrip line fabricated on honeycomb lattice of circular holes drilled through the dielectric substrate structure is one of the applications which has been used for harmonic tuning in a class AB amplifier.

A two-dimensional (2-D) photonic bandgap (PBG) structures consisting of circles which is etched in the ground plane of microstrip line was proposed by YongxiQian, Vesna Radisic and Tatsuo was used the PBG ground plane effect. This type of PBG structure are possessed more deeper and wider stopbands compatible with monolithic technology than the drilling holes on the dielectric PBG structure substrate [27]. The fabrication process is simplified as there is not required to drill through the substrate. A broadband second harmonic tuning of a high efficiency class AB power amplifier is one of the application to use this PBG ground plane structure.

Design with high-Q components technique provide increased signal losses at higher microwave and millimeter-wave frequencies for non-metallic structure such as dielectric waveguide and image guide .

The square lattice of small metal pads with grounding vias in the center of each pad structure is offered a band gap for the TM surface wave mode over a certain frequency range. These PBG 2D structures are forbidden the propagation and/or radiation of EM waves along a certain range or all angles instead of one single direction instead of the previous 1D PBG structures. An improvement bandwidth Ku-band imcrostip antenna, due to proper suppression of the surface wave in the dielectric substrate, has been employed this 2D PBG lattice [27].

The last periodic UC-PBG structure has the smallest electrical size among all PBG structures which consists of a square metal pad with four connecting branches in each element. There are many characteristics of UC-PBG structure such as wide stopband, slow-wave effect with low insertion loss, the possibility of realizing a perfect magnetic conductor (PMC) impedance surface and a deep and very broad stopband.

4.3 The Design PBG structure

The one dimensional (1-D) microstrip PBG cell designed at the place of feed line in this project is shown in Figure 4.4. These structures have slow wave and bandstop characteristic and can forbid certain band of frequencies and reduce the physical dimension of the microstrip structure. The cells are primarily a section of microstrip line with some metallic parts removed. In the study of microstrip transmission line over a periodically perforated ground plane, it is found that the propagation constant strongly depends on the orientation and location of the transmission line with respect to the two principle axes of the periodic perforations. As ground plane is perforated the substrate must be suspended so that the circuit cannot be fixed on a metal base where these problems can be solved by the special perforation pattern of etching on the line itself of the one dimensional PBG structure.

From the transmission line of theory, the propagation constant and the phase velocity of a line without loss is $\beta = \omega\sqrt{LC}$ and $v_p = 1/\sqrt{LC}$ where ω is the angular frequency, C and L are the distributed shunt capacitance and series inductance per unit length along the transmission line. Generally, it can be known that the slow wave (large propagation constant) can be achieved by increasing C and L values in the transmission line [19]. It can be accomplished by drilling the holes in the substrate

itself or etching the patterns in the microstrip ground plane where they are created periodic variations of the propagation. If the values of C and L are not increased continuously but periodically, the transmission line is possible to form PBG structure [19]. The narrow branch is used to create the inductive effect which affects to increase the series inductance values and the gap across the widths of the line increases the shunt capacitance which is combined with the inductive effect to increase the propagation constant as well as to determine the propagation constant and the characteristic impedance of the slow wave structure. Since the propagation is increased, the cutoff frequency is increased without increasing the lattice period.

According to James Sor, Yongxi Qian and Tatsuo Itoh [18], the unit cell length which is equal to one-half the guided wavelength in the periodic transmission line get the broad stopband effect and the required unit cell length at the operating frequency, f , can be known by

$$l = \frac{c}{2f\sqrt{\varepsilon_e}} \tag{4.6}$$

where ε_e is the effective dielectric constant of the transmission line.

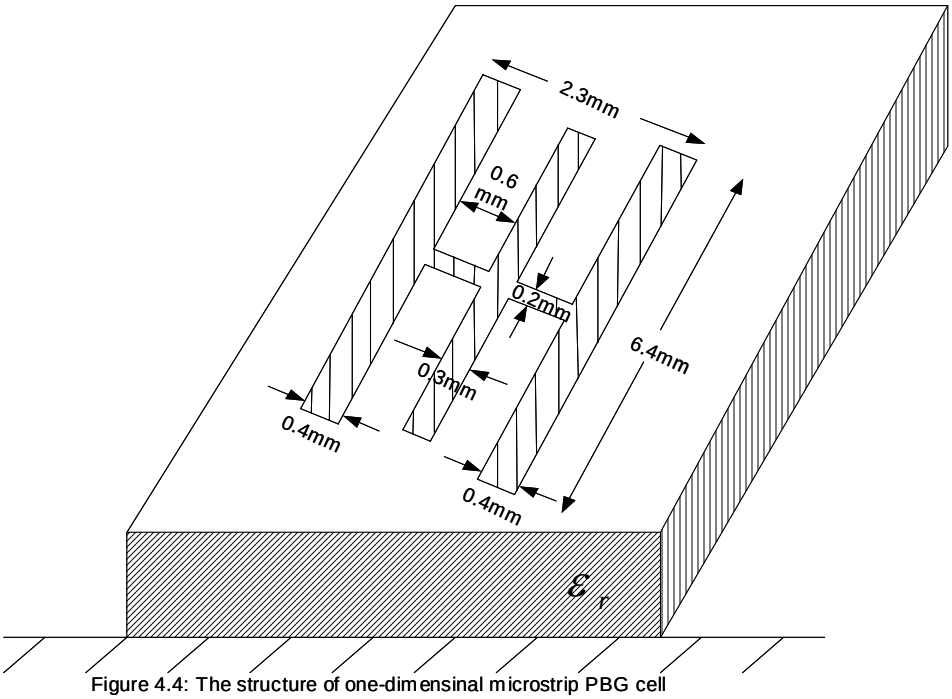

Figure 4.4: The structure of one-dimensinal microstrip PBG cell

The width of the one-dimensional microstrip PBG cell is 2.3mm corresponding to 50Ω microstrip line. It is then cascaded twelve unit cells properly which give the deep attenuation levels and the increased insertion loss for the feedline structure as well as the reduced physical dimension then the conventional feedline structure.

4.4 Bandwidth Enhancement Techniques

The most serious limitation of the basic microstrip antenna element is its narrow impedance bandwidth, so it is attempted to enhance the bandwidth with various techniques. Although the operating range of the typical microstrip patch element on a thin substrate is limited by a narrow impedance bandwidth of around 1%, the completing antenna elements such as dipoles, slots and waveguide horns have operating bandwidth of 15-50%. Generally there are several bandwidth definitions such as impedance bandwidth, pattern bandwidth and gain bandwidth but the fundamental enhancement to improve the bandwidth of the microstrip antenna element is the impedance bandwidth and it is defined as the impedance variation with the frequency of the antenna element result in a limitation of the frequency range over which the element can be matched to its feedline [8]. In general, the impedance bandwidth is determined with a return loss or maximum SWR (typically less than 2.0 or 1.5) over a frequency range.

There has been dozen of different element design and variations proposed for bandwidth improvement but the bandwidth enhancement methods are categorized into three basic types: impedance matching in which the element can be viewed as a high-Q circuit element and matched over the desired operating band with using a matching network, the use of multiple resonances in which one or more resonant elements, that are tuned to slightly different frequencies, can be applied and the use of lossy materials [8]. The basic microstrip element has narrow impedance bandwidth according to a consequence of its electrically thin ground-plane dielectric substrate, which results a high-Q resonance behavior.

Bandwidth improves as the substrate thickness is increased or as the dielectric constant is reduced but the problem with using substrate thicker than (0.01λ to 0.02λ thick) range is that the impedance locus of the element becomes inductive which in turn increasingly difficult to match [8]. The spurious radiation from microstrip line bends and other discontinuities is high for substrates thicker than a few hundredths of a wavelength. The bandwidth can also improve with the high dielectric constant but the element size decreases with an increase in dielectric constant, which raises the Q of the resonator and thick high-dielectric constant substrate can cause the surface wave excitation will be higher which will lower efficiency, and lead to spurious radiation and pattern degradation [8].

4.4.1 Impedance Matching

The increased in bandwidth by increasing the substrate thickness or by reducing the dielectric constant is limited by an inductive impedance offset that increases with thickness and therefore a logical approach is to use a thick substrate with some type of additional impedance matching to cancel this inductance [8].

The impedance bandwidth improved of a microstrip antenna without altering the antenna element itself is to attach a separate lossless matching network where the element can be matched over the desired band. This can be done by in microstrip form using a coplanar matching network or with an off-board network in which if the network is mounted as close as possible to the radiating element, it gives the better bandwidth and efficiency [8]. Pues and Van de Capelle [36] improved that the improved bandwidth of the microstrip antenna is obtained bandwidth of 10-12% by using a passive coplanar matching network. The input impedance of a probe- or microstrip-fed microstrip antenna becomes increasingly inductive as the substrate thickness increases, so the bandwidth improvement is to tune out this inductance with a series capacitor.

Since the matching network is coplanar with the antenna element, it is needed to consider for spurious radiation from the matching network. The design of a broad-band matching network is a difficult network synthesis problem in generally. It is a lengthy trial-and-error tuning procedure, which is done by computer simulation and optimization.

A related method is to use a two-layer proximity-coupled design and the advantages of the proximity (electromagnetically coupled) feed are explained in section 3.3.3 already. In proximity coupled design, a micorstrip feed line is placed on the lower substrate, and terminated in an open-end at a point approximately below the midpoint of the patch element, which is fabricated on a superstrate layer. This type of coupling is resulted in tight capacitive coupling to the patch and the equivalent circuit is a capacitor in series with the parallel RLC resonator and the further improved bandwidth of 13% can be performed by including a small tuning stub on the feedline.

4.4.2 Introduction of Multiple Resonances

A bandwidth broadening technique with introduction of multiple resonances is to stagger-tune or more resonators to cover the frequency range of interest and this

type of bandwidth improvement technique has been applied to several types of antennas. The basic idea is to introduce additional resonant patches to provide two or more closely spaced resonances. The impedance locus of multiply tuned antennas has the characteristic feature of two or more loops enclosing the center of the Smith chart, while a single microstrip resonator has one loop enclosing the center of the chart, in the vicinity of its operating range [8].

One of the most practical ways of implementing a doubly tuned microstrip element is to use the stacked patch configuration. The stacked patched design is attractive for several reasons because it does not increase the surface area occupied by the element, and a stacked patch can also be used in array configurations without the need for increased element spacing. In stack configuration, the bottom patch may be fed by coaxial probe or microstrip feed line or by aperture coupling. The two patches where the shape can be square, rectangular or circular, are usually very close in size with the top element being slightly larger than the bottom element. If the patches are not very close in size, two distinct resonances will result which may be useful for dual band performance [8].

4.4.3 Introduction of Losses

It is always possible to increase impedance bandwidth by introducing loss into the antenna system. One of the methods is to add an attenuator in series with a microstrip antenna but reduced in antenna gain [8]. Besides adding loss external to the antenna element, there are several ways of fabricating a microstrip antenna with integral loss such as lossy substrate materials can be used, or lossy films can be added underneath, or on top of, the conducting patch element. The other way to improve bandwidth by introducing losses is to connect discrete chip resistors or similar loads to the patch element, or its feedlines [8].

4.4.4 Introduction of Air Gap

Another bandwidth improvement technique is introducing of an air gap which can be realized by adding a layer of foam between the dielectric layers of by separating the layers using spacers and it is benefited to improve the impedance bandwidth of the microstrip antenna. The introducing of air gap is made partly due to the increase of the effective height of the dielectric medium than a single layer structure of the substrate

thickness, simply because the effective permittivity is smaller than the single layer one. The air gap also has the advantage of being to provide a simple method for tuning the resonant frequencies according to Lee and Dahele investigation. But according to Oltman and Huebner, the air gap spacing is limited depend on the impedance matched between the radiating element and the feedline is limited by the ellipse centered over the end of the microstrip line. If the spacing is larger than this critical value, then the coupling is too weak to match the dipole to the feedline.

4.4.5 Tapered-dipole Design

A tapered transition that varies characteristic impedance continuously in a smooth way from the impedance of microstrip line with width W_1 to that of a microstrip line with a width W_2 is shown in Figure 4.5. Although a taper shape is easy to design and has a characteristic of broad bandwidth, there is the disadvantage which requires a long transition section. In general, the tapered transitions are used in antennas such as a horn antenna and the notch antenna. The longer the taper section are used, it gets the better the matching and the lower the VSWR [3].

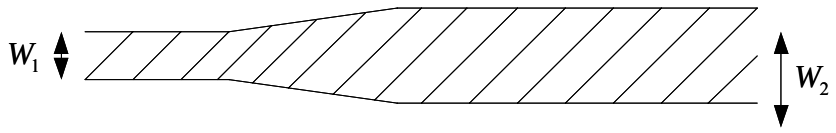

Figure 4.5: The taper transition structure

4.5 EMC Microstrip Dipole Design

The microstrip dipole electromagnetically coupled to the microstrip feedline is expressed in above. The compact microstrip feedline using PBG cell design is also explained in section 4.3. In this section, it will discuss how to consider the EMC dipole antenna design in single band and tri-band and how to improve the bandwidth using photonic bandgap (PBG) effect. The final design of better bandwidth enhancement with the taper dipole effect will explain in the last section. Using the IE3D software the resonant frequencies of 0.9GHz, 1.8GHz and 2.4GHz tri-band antenna design simulation and measurement results will be discussed.

4.6 Choice of substrate for EMC microstrip dipoles

FR4 with the relative permittivity of 4.4 and with a thickness of 62mil or 1.57mm is used as the substrate in this project. In practically, it is possible to vary the substrate height for design considerations by using multiple layers, the substrate thickness is restricted. Thus the design is restricted to the multiple height of 1.57mm. A superstrate layer which is the double thickness of the FR4 substrate is added on top of the dipoles as a protection layer with the advantage of reducing the dimension of the structure with effective permittivity, ε_e, equal to the FR4 relative permittivity, ε_r and can also eliminate the fringing effect which likely exists due to insufficient thickness of the superstrate (cover).

4.7 Zeland Software

Zeland software has been recognized as high-frequency electromagnetic simulation and design tools for microwave, semiconductor, wireless, and telecom industries government laboratories, and universities around the world. Zeland's product is the moment-method based EM simulation and optimization package IE3D has become a standard tool in the design of MMICs, RFICs, LTTC circuits, IC interconnects and packages, HTS circuits, microstrip antennas, wire antennas and other RF/wireless antennas. The other product includes FDTD package FIDELITY for modeling true 3D structures, MDSPICE for mixed frequency- and time-domain S-parameter SPICE simulations, COCAFIL for analysis and synthesis of waveguide filters, FILTERSYN fir planar filter synthesis, and LINEGUAGE for transmission design.

IE3D is a full-wave, method-of-moments based electromagnetic simulator solving the current distribution on 3D and multilayer structures of general shape and has been widely used in the design of MMICs, RFICs, LTTC circuits, microwave, millimeter-wave circuits, IC interconnects and packages, HTS circuits, patch antennas, wire antennas, and other RF/wireless antennas. IE3D is most suitable for the antenna designer who is looking for accurate, efficient and tool.

4.8 EMC Microstrip Dipole Design Process

Before considering the tri-band EMC microstrip dipole, the design of single band EMC microstrip dipole is first considered.

4.8.1 Single Band Design

The single band 0.9GHZ microstrip dipole was first started to investigate with the feedline length of 158.9mm which is fixed for all design frequencies, the feedline width of 2.3mm using the equation form (4.1) to (4.3). The dimensions of single band 0.9GHz dipole can also be determined with the equations from (4.1) to (4.5). The design structure of the single band 0.9GHz dipole is shown in Figure 4.6.

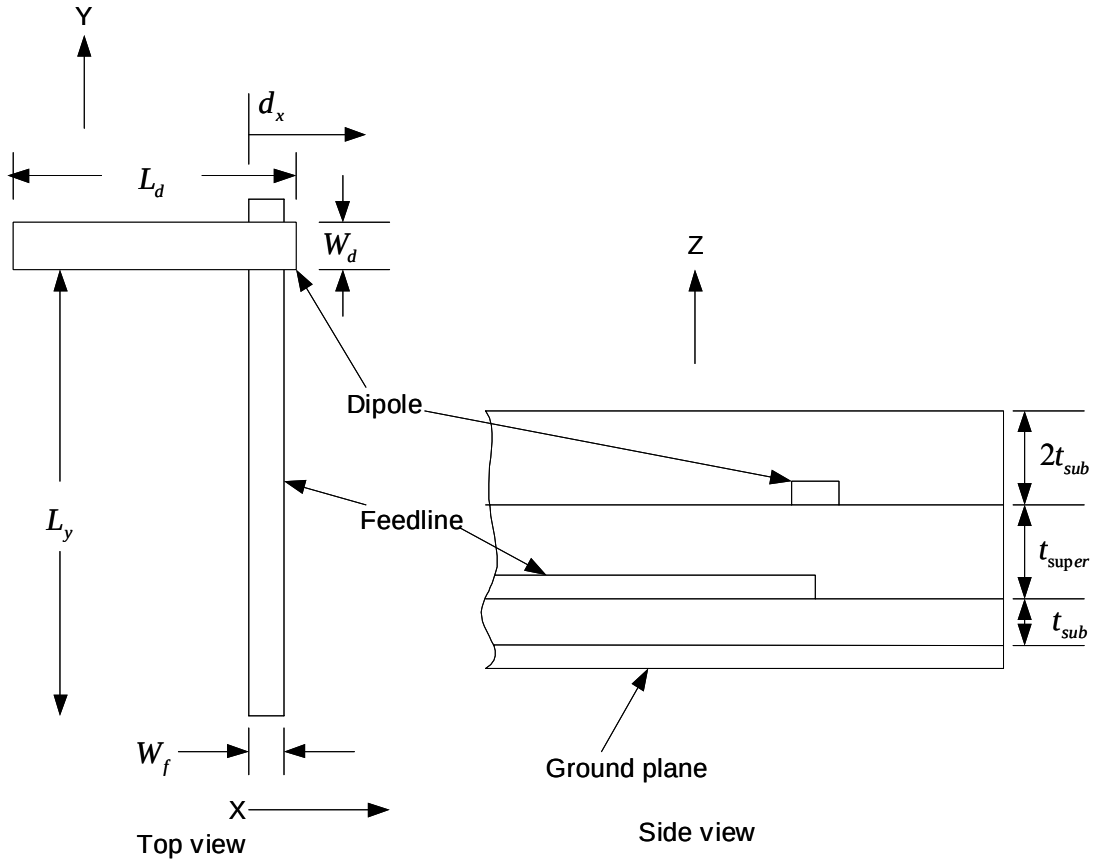

Figure 4.6: The single band design of electromagnetically coupled dipole antennas

The EMC microstrip dipole configuration has the radiator imbedded within the dielectric substrate at higher level and the feedline at lower level and the ground plane at the bottom level of the substrate. The dipole is covered with a layer of dielectric of thickness $2t_{sub}$. Using the IE3D software, the initially half wavelength dipole length is

put near the center of the feedline and the dipole is sliding transversally (Xoffset) to the feedline with X-plane direction and then sliding longitudinally (Yoffset) to the feedline with Y-plane direction for each frequency range. The dipole width is also changed in order to get the optimum result for each frequency range. The 0.9GHz dipole is positioned at the halfway of the length of the feedline is found that gives the better return loss and also allows the other dipoles to put far away from the feelline port in the later stage of the design. The single band design of 1.8GHz and 2.4GHz EMC dipole are also simulated with changing the dipole transversally and longitudinally to the feedline and the width of the dipole at 1.8GHz and 2.4GHz are also investigated. The following results are the single band design at each frequency and taking the best result based on the bandwidth and the return loss.

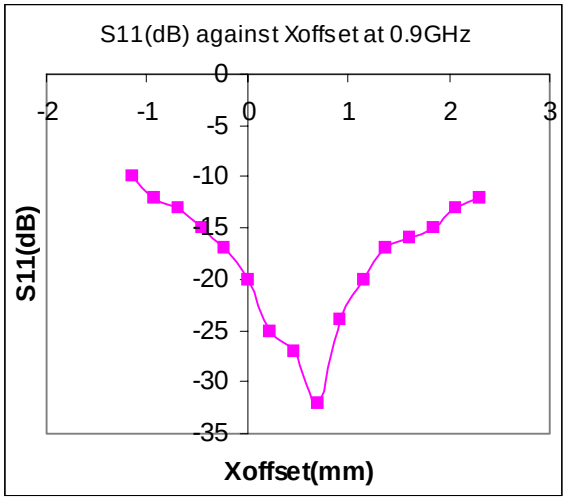

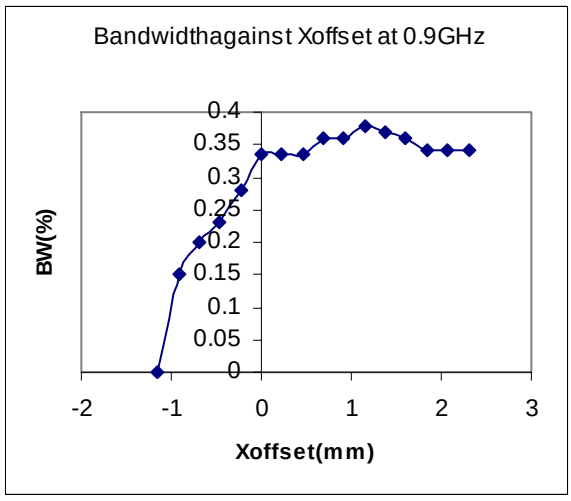

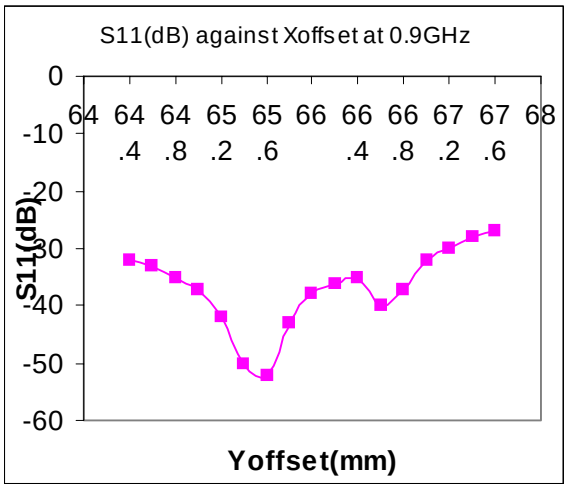

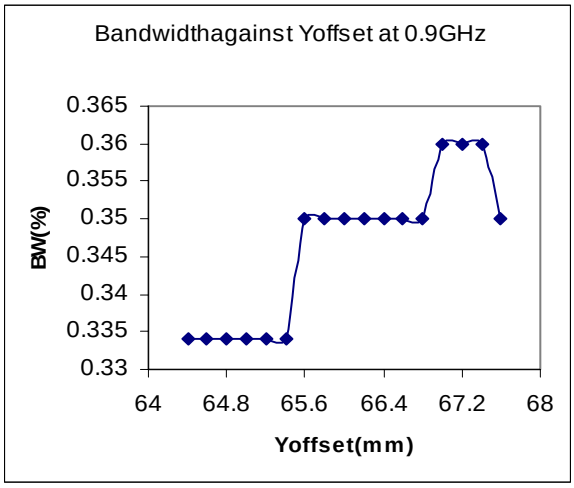

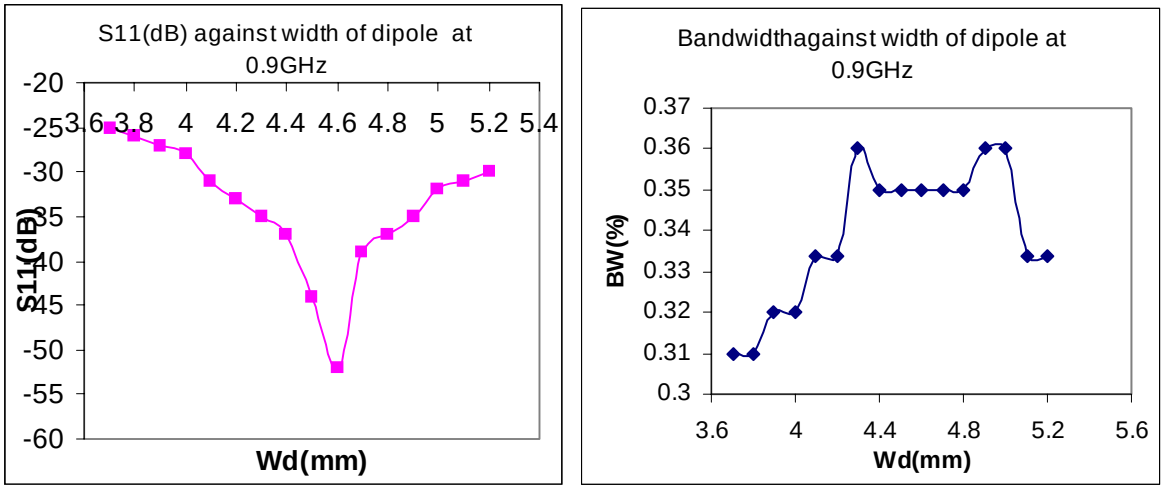

Figure 4.7: The bandwidth and return loss against frequency of single dipole at 0.9GHz

The optimum dimension of the single band 0.9GHz dipole from the IE3D simulation is tabulated in Table 4.1.

Length of feedline (L_f)	158.9mm
Width of feedline (W_f)	2.3mm
Length of dipole (L_d)	78.4mm
Width of dipole (W_d)	4.6mm
Distance from the feedline port (L_y)	65.6mm
Transverse distance from dipole (d_x)	0.69mm
Resonant frequency (f_0)	0.8975GHz
Bandwidth (BW)	0.35%
Return loss (S_{11})	-50dB

Table 4.1:The dimensions for the single band EMC dipole at 0.9GHz

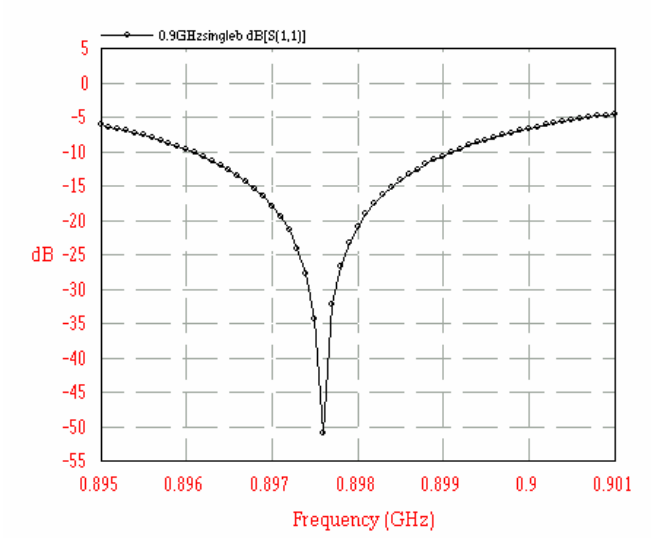

Figure 4.8: Plot of return loss against frequency for the range at 0.9GHz single band dipole antenna

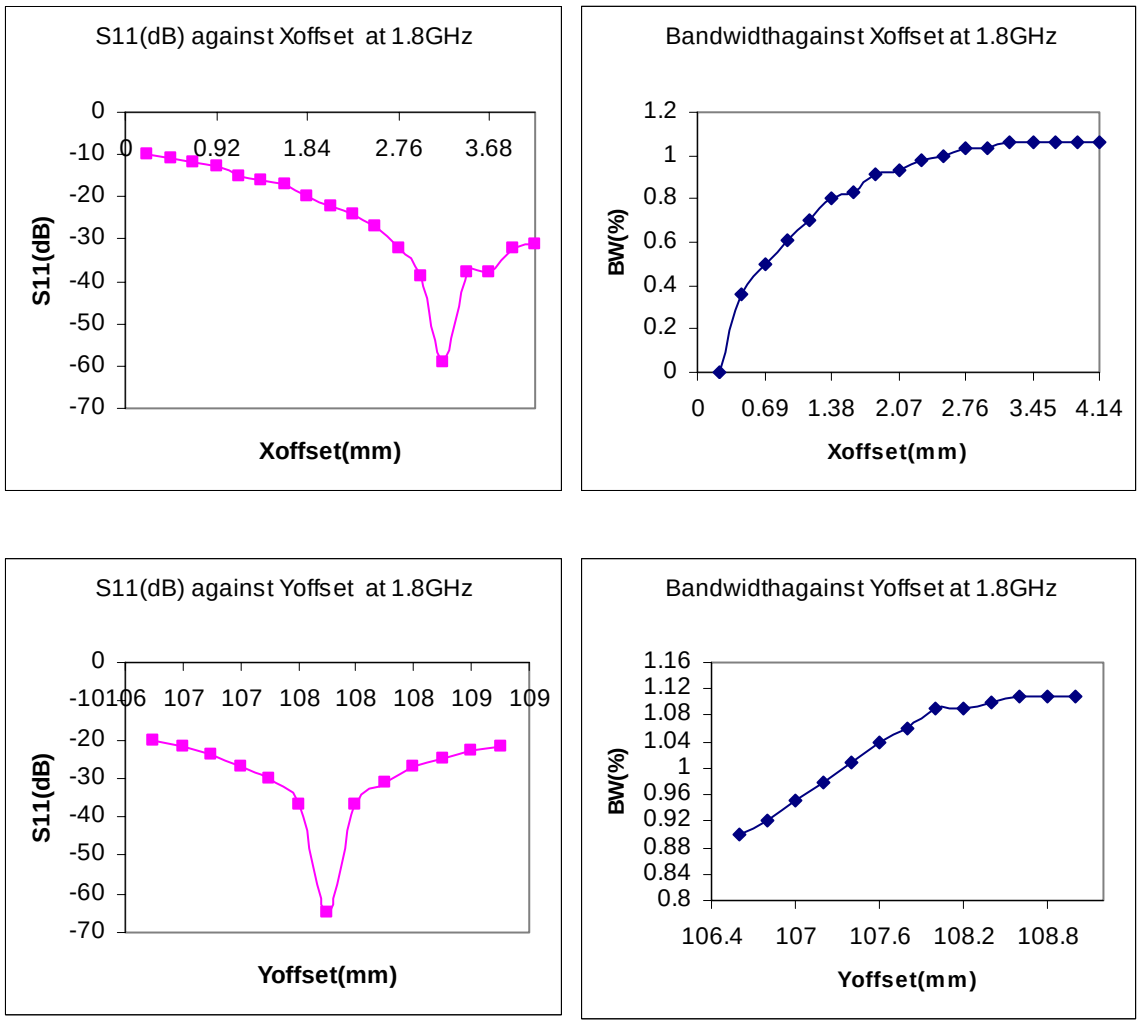

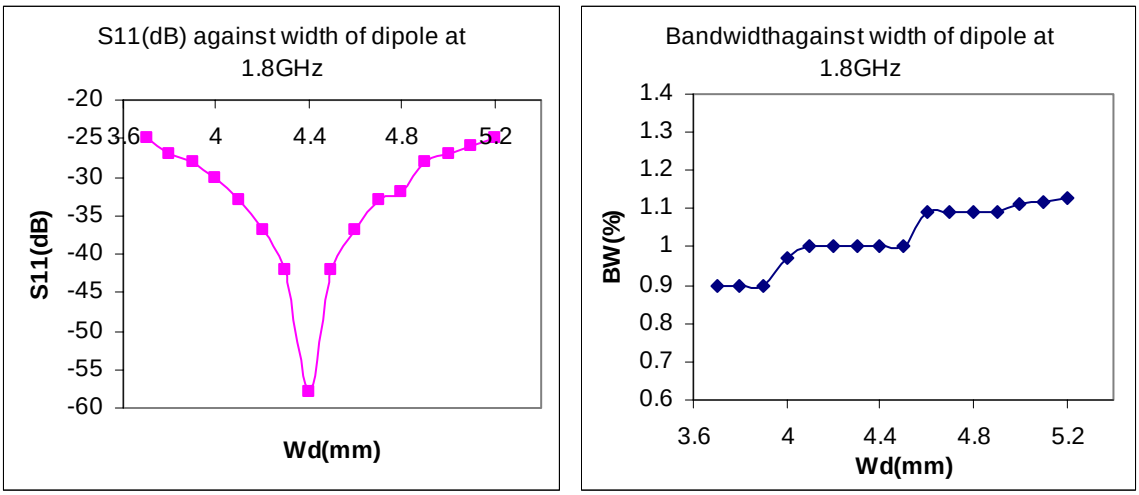

Figure 4.9: The bandwidth and return loss against frequency of single dipole at 1.8GHz

The optimum dimension of the single band 1.8GHz dipole from the IE3D simulation is listed in Table 4.2.

Length of feedline (L_f)	158.9mm
Width of feedline (W_f)	2.3mm
Length of dipole (L_d)	36.54mm
Width of dipole (W_d)	4.6mm
Distance from the feedline port (L_y)	107.8mm
Transverse distance from dipole (d_x)	3.22mm
Resonant frequency (f_0)	1.798GHz
Bandwidth (BW)	1.09%
Return loss (S_{11})	-60dB

Table 4.2:The dimensions for the single band EMC dipole at 1.8GHz

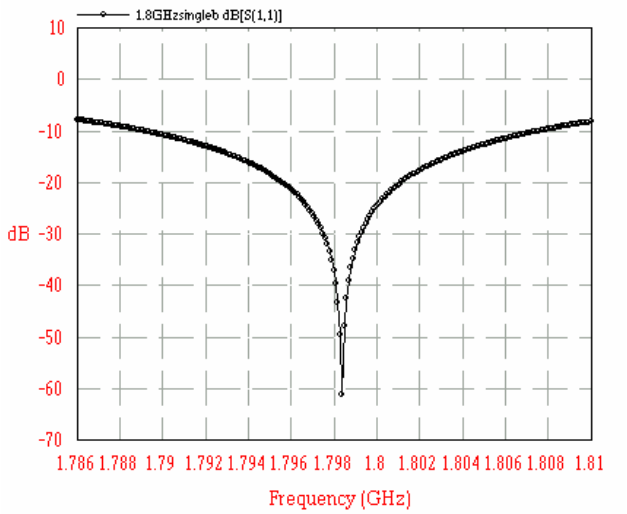

Figure 4.10: Plot of return loss against frequency for the range at 1.8GHz single band dipole antenna

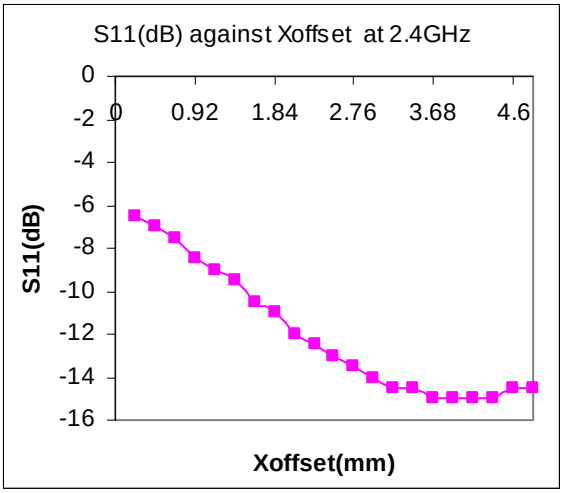

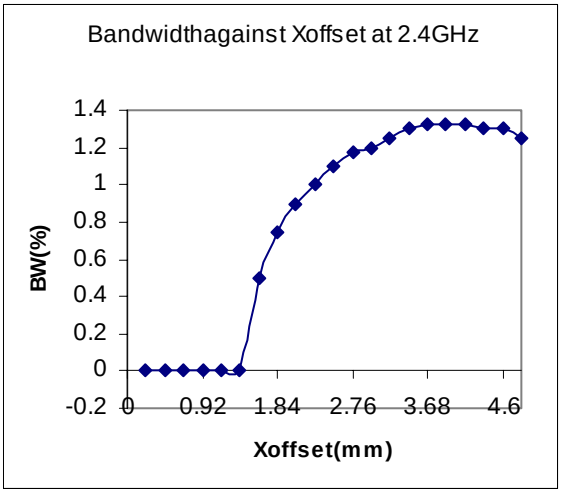

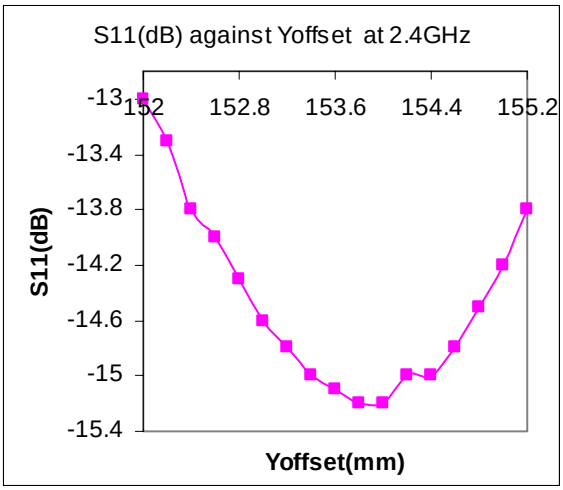

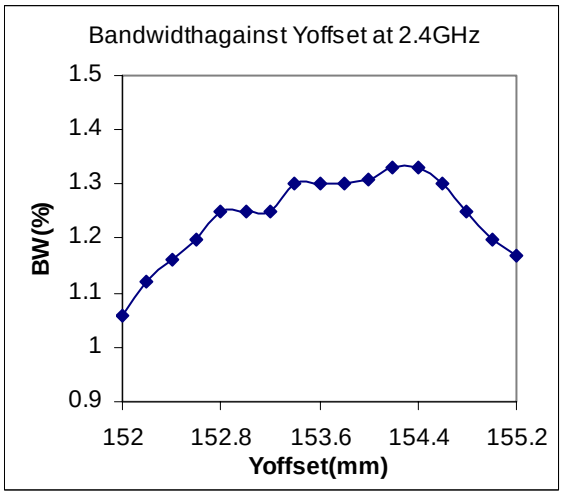

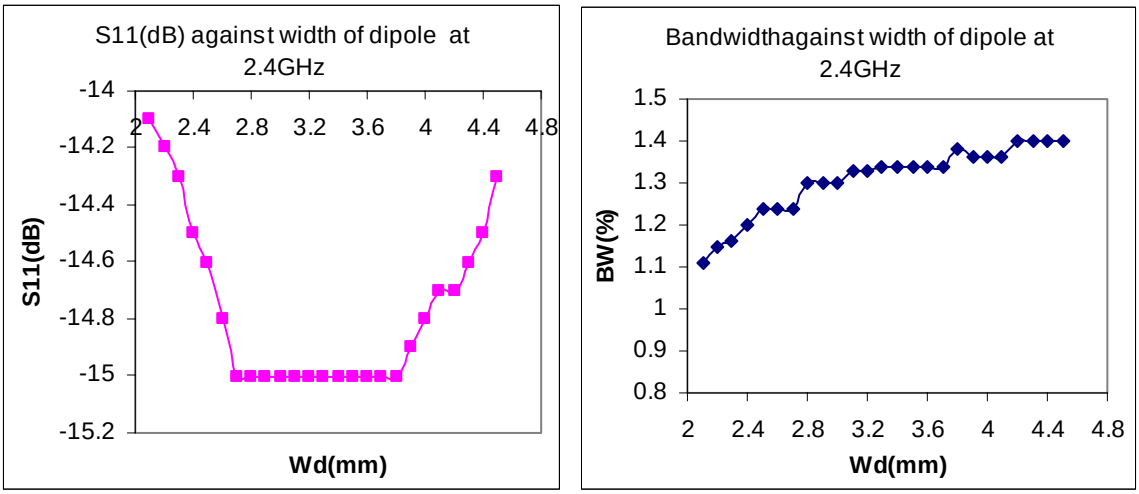

Figure 4.11: The bandwidth and return loss against frequency of single dipole at 2.4GHz

The optimum dimension of the single band 2.4GHz dipole from the IE3D simulation is also tabulated in Table 4.3.

Length of feedline (L_f)	158.9mm
Width of feedline (W_f)	2.3mm
Length of dipole (L_d)	26.95mm
Width of dipole (W_d)	3.1mm
Distance from the feedline port (L_y)	154.4mm
Transverse distance from dipole (d_x)	3.91mm
Resonant frequency (f_0)	2.4GHz
Bandwidth (BW)	1.33%
Return loss (S_{11})	-15dB

Table 4.3:The dimensions for the single band EMC dipole at 2.4GHz

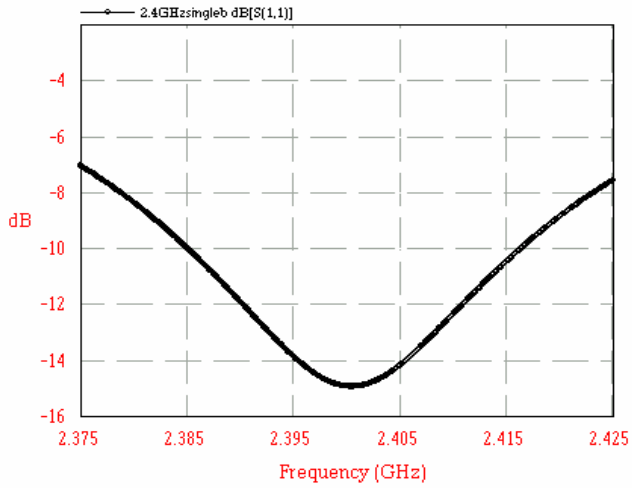

Figure 4.12: Plot of return loss against frequency for the range at 2.4GHz single band dipole antenna

4.8.2 Tri-Band Design

The structure of electromagnetically coupled (EMC) tri-band microstrip dipole antenna in transverse configuration is shown in Figure 4.13. For the tri-band process, it is also taken the feedline length of 158.9mm which is fixed for all design frequencies and the feedline width of 2.3mm, which is the same dimension as the single band design, using the equation form (4.1) to (4.3). The tri-band EMC dipole with the conventional feed line is started to base upon the single band design dimensions vary and tried to further improve the bandwidth.

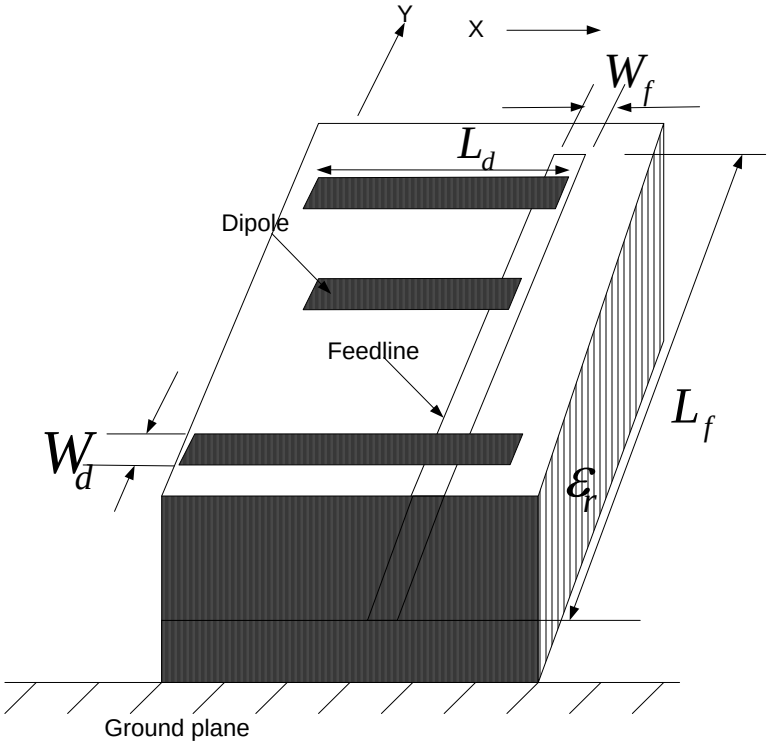

Figure 4.13: The structure of the tri-band electromagnetically coupled microstrip dipole antennas

When all the three dipoles are placed together electromagnetically coupled to the feedline, it is needed to consider changed first the dipole longitudinal position especially for 1.8GHz dipole because it is the second resonance of 0.9GHz dipole. Hence 1.8GHz dipole should be placed further from 0.9GHz dipole to avoid the resonance effect. Using the IE3D software, it is started to vary the longitudinal position of 1.8GHz dipole first while the other two dipole parameters are constant at this time.

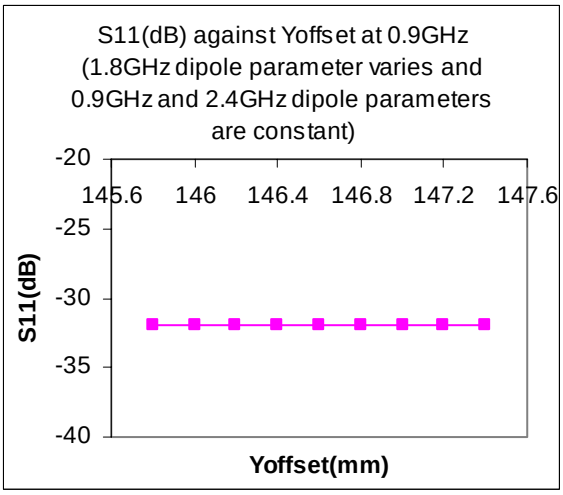

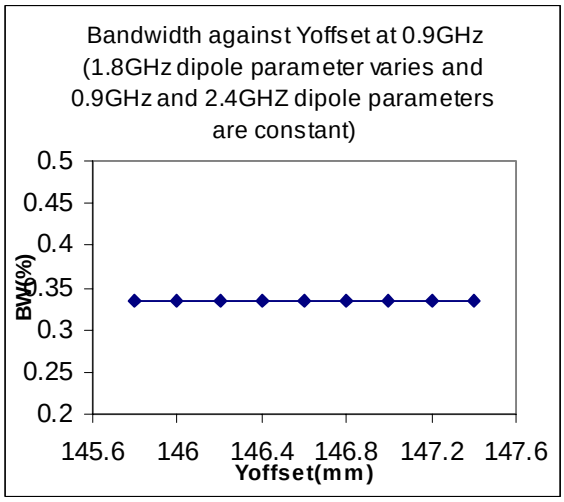

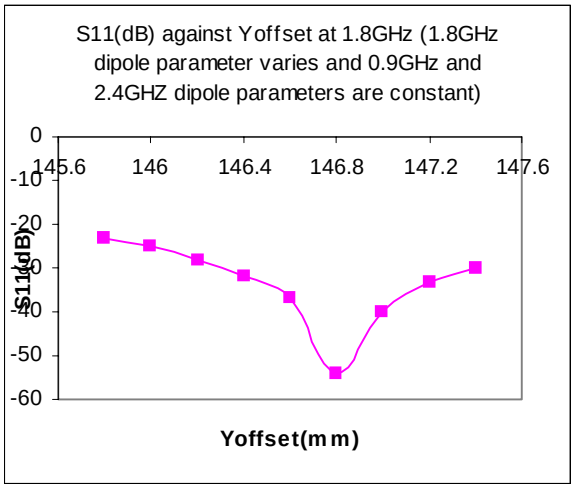

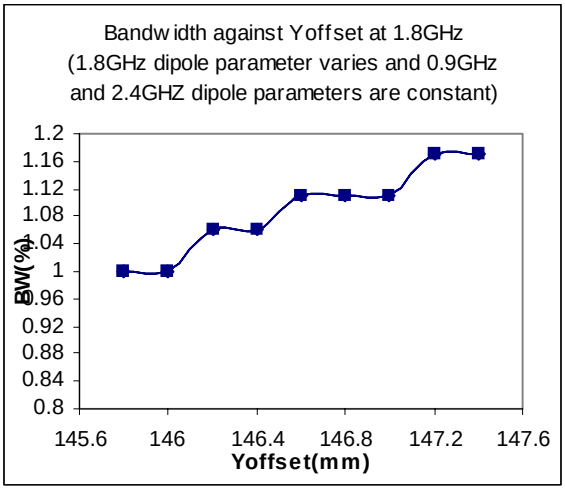

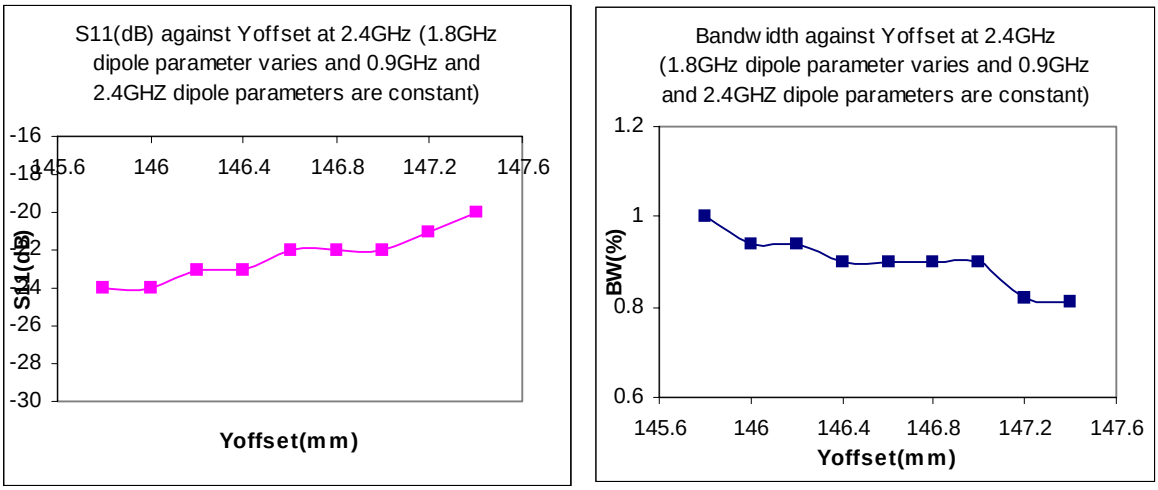

Figure 4.14: Bandwidth and return loss against frequency for tri-band structure with 1.8GHz dipole parameter varies longitudinally

From the above 1.8GHz dipole longitudinal parameter varies where the 1.8GHz dipole parameter placed at 146.8mm from the feedline port gives the optimum bandwidth and return loss.

Band	0.9GHz	1.8GHz	2.4GHz
Bandwidth (BW)	0.334%	1.11%	0.9%
Return loss (S_{11})	-32dB	-54dB	-22dB

Table 4.4: The simulation result of tri-band with 1.8GHz dipole parameter varies longitudinally

Taking the longitudinal position of 146.8mm for 1.8GHz, it is then tried to vary 1.8GHz dipole transversely and the simulation results are as follows:

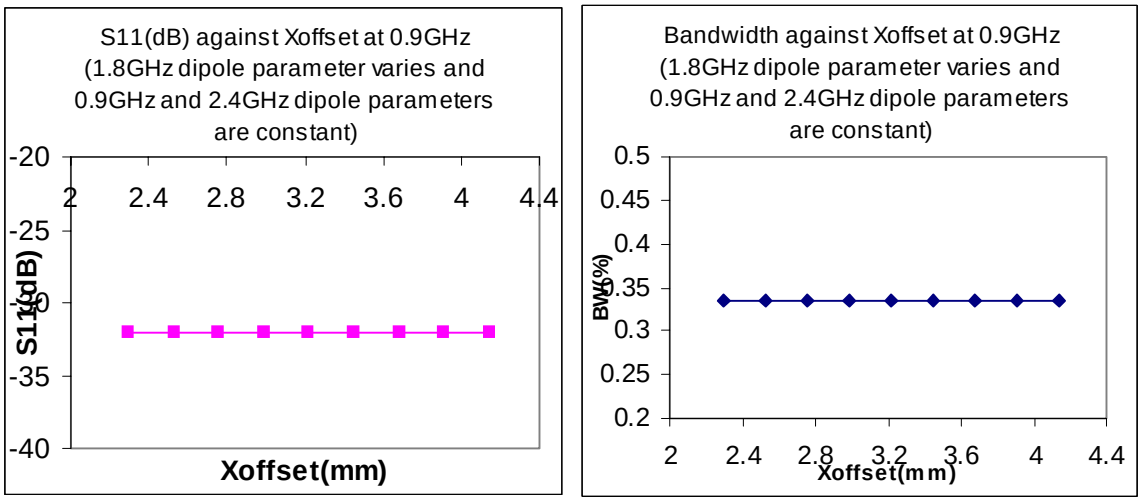

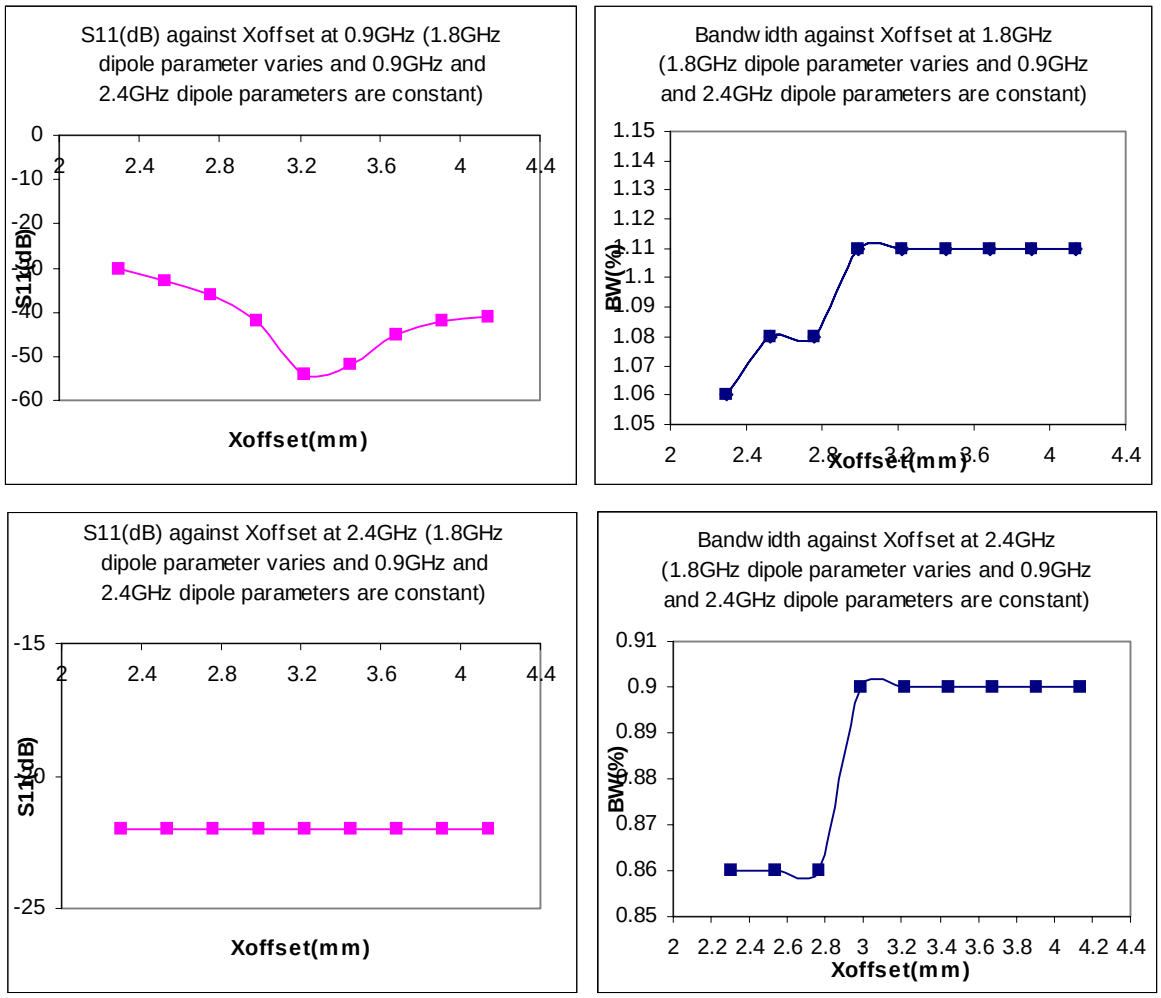

Figure 4.15: Bandwidth and return loss against frequency for tri-band structure with 1.8GHz dipole parameter varies transversely

Although the 1.8GHz dipole parameter vary horizontally as shown in Figure 4.15, the 1.8GHz dipole position placed at 3.22mm, which is the same as the horizontal single band position, gives the optimum bandwidth and return loss and is tabulated as Table 4.5.

Band	0.9GHz	1.8GHz	2.4GHz
Bandwidth (BW)	0.334%	1.11%	0.9%
Return loss (S_{11})	-32dB	-54dB	-22dB

Table 4.5: The simulation result of tri-band with 1.8GHz dipole parameter varies transversely

After getting the proper position for 1.8GHz dipole, it is tried to slide the 2.4GHz dipole position with the other left two dipole positions are at constant. The 2.4GHz

dipole length, L_d , first start to vary in order to get resonance at 2.4GHz range and the simulation results are as follows:

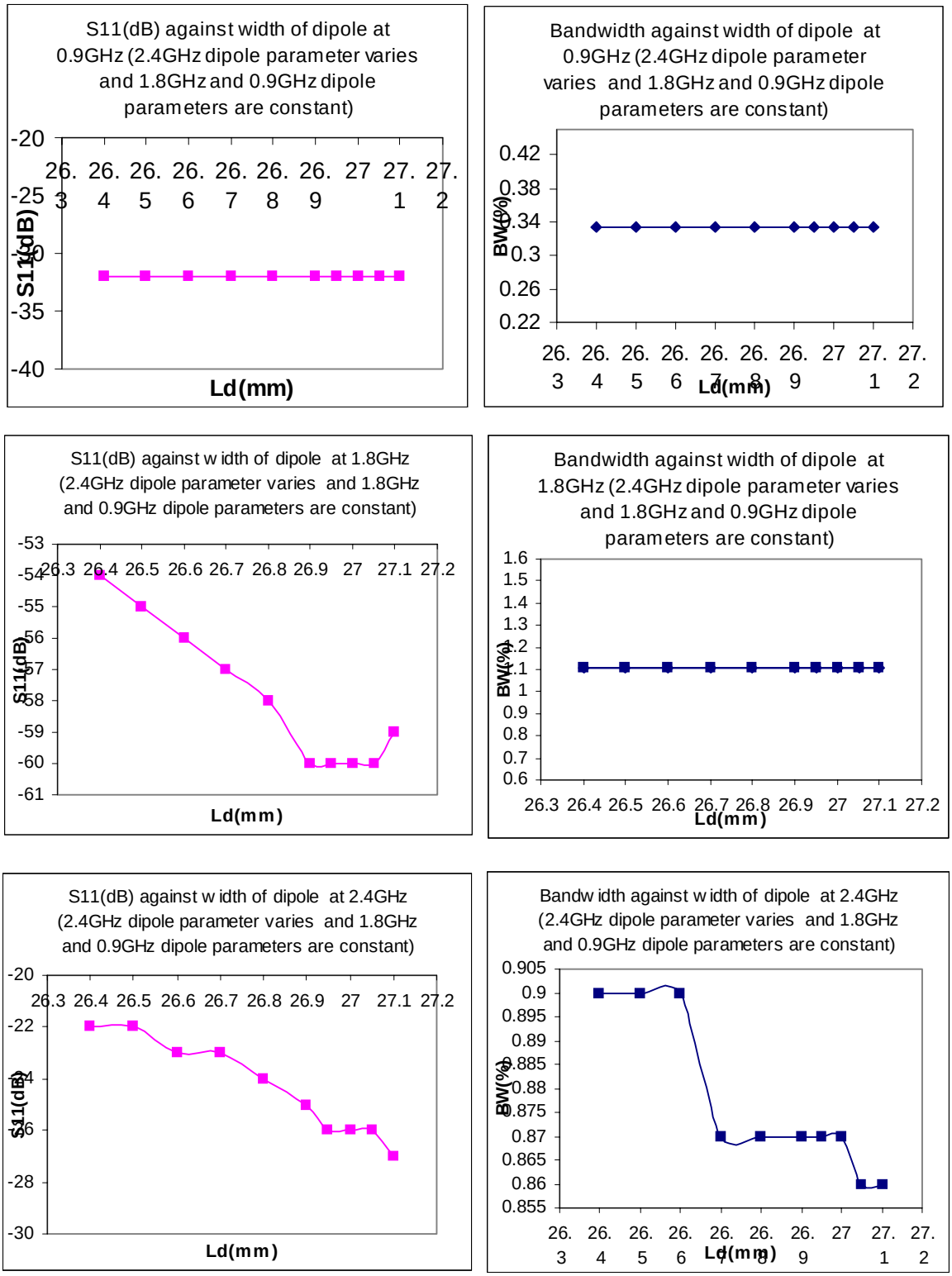

Figure 4.16: Bandwidth and return loss against frequency for tri-band structure with 2.4GHz dipole length parameter varies

From the above 2.4GHz dipole length parameter varies, where the 2.4GHz dipole parameter placed at 154.4mm from the feedline port, and it is resonance at 2.4GHz frequency range with the optimum bandwidth and return loss and is tabulated as Table 4.6.

Band	0.9GHz	1.8GHz	2.4GHz
Bandwidth (BW)	0.334%	1.11%	0.87%
Return loss (S_{11})	-32dB	-60dB	-26dB

Table 4.6: The simulation result of tri-band with 2.4GHz dipole length parameter varies

Taking the 2.4GHz dipole length parameter result and the other two dipole parameters are constant, the 2.4GHz dipole position is varied longitudinally again. The results compared are obtained as follows:

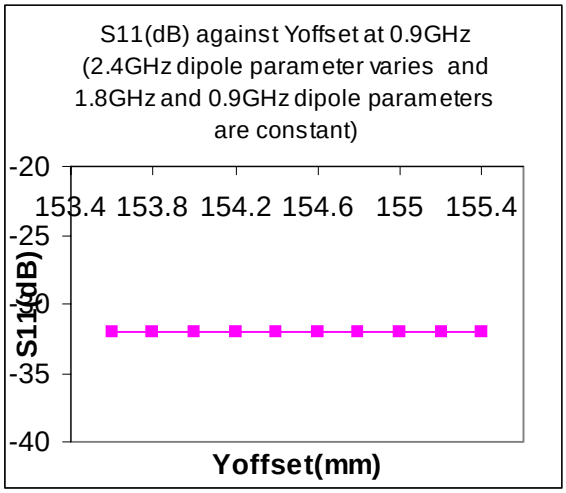

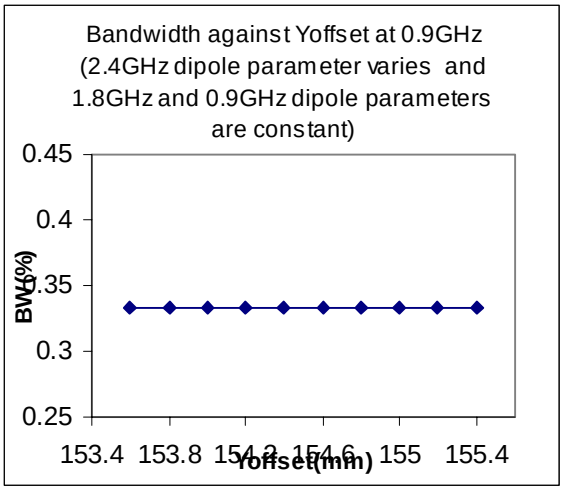

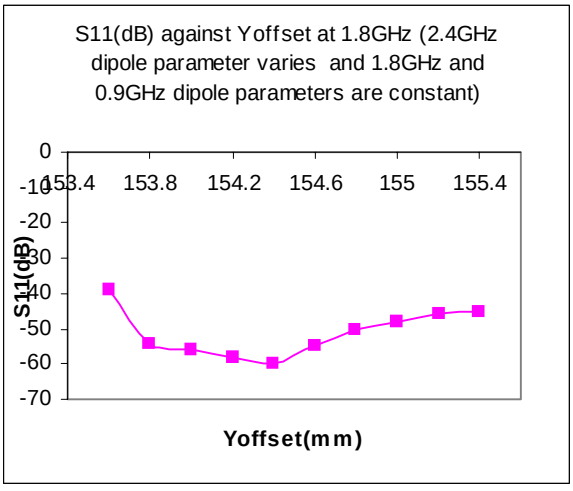

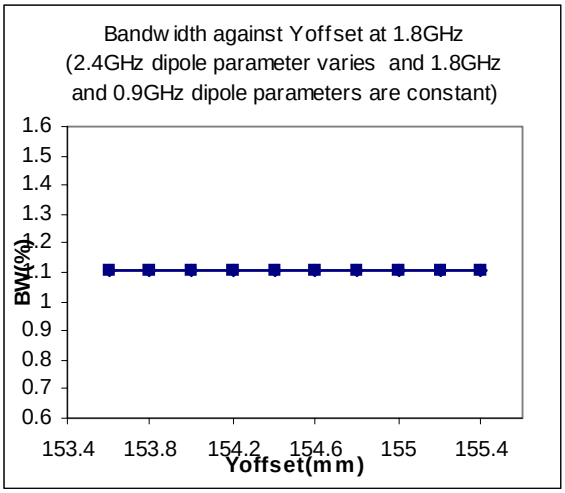

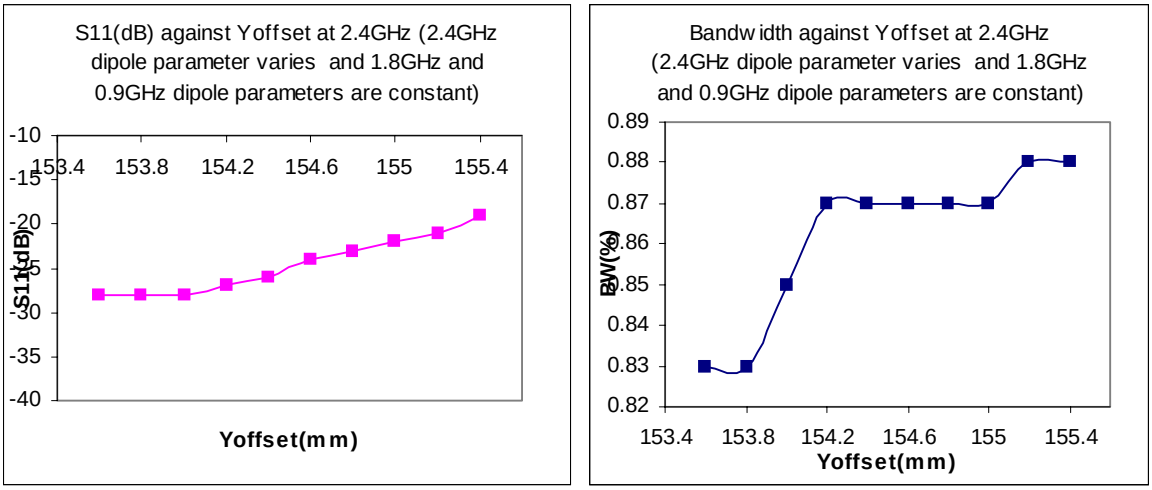

Figure 4.17: Bandwidth and return loss against frequency for tri-band structure with 2.4GHz dipole parameter varies longitudinally

From the above 2.4GHz dipole longitudinal parameter varies where the 2.4GHz dipole parameter placed at 154.6mm from the feedline port gives the optimum bandwidth and return loss and is tabulated as Table 4.7.

Band	0.9GHz	1.8GHz	2.4GHz
Bandwidth (BW)	0.334%	1.11%	0.87%
Return loss (S_{11})	-32dB	-55dB	-24dB

Table 4.7: The simulation result of tri-band with 2.4GHz dipole parameter varies longitudinally

The two dipoles of 1.8GHz dipole and 2.4GHz dipole parameters are varied ready to get the optimum result. Taking the two dipole parameter results, the left one 0.9 GHz dipole parameter are varied longitudinally and the compared result are as follows:

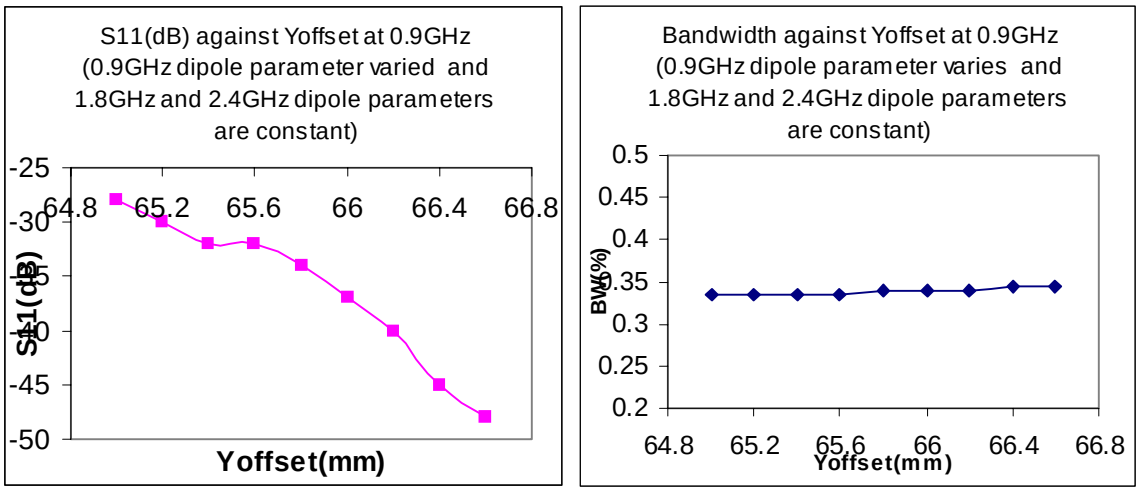

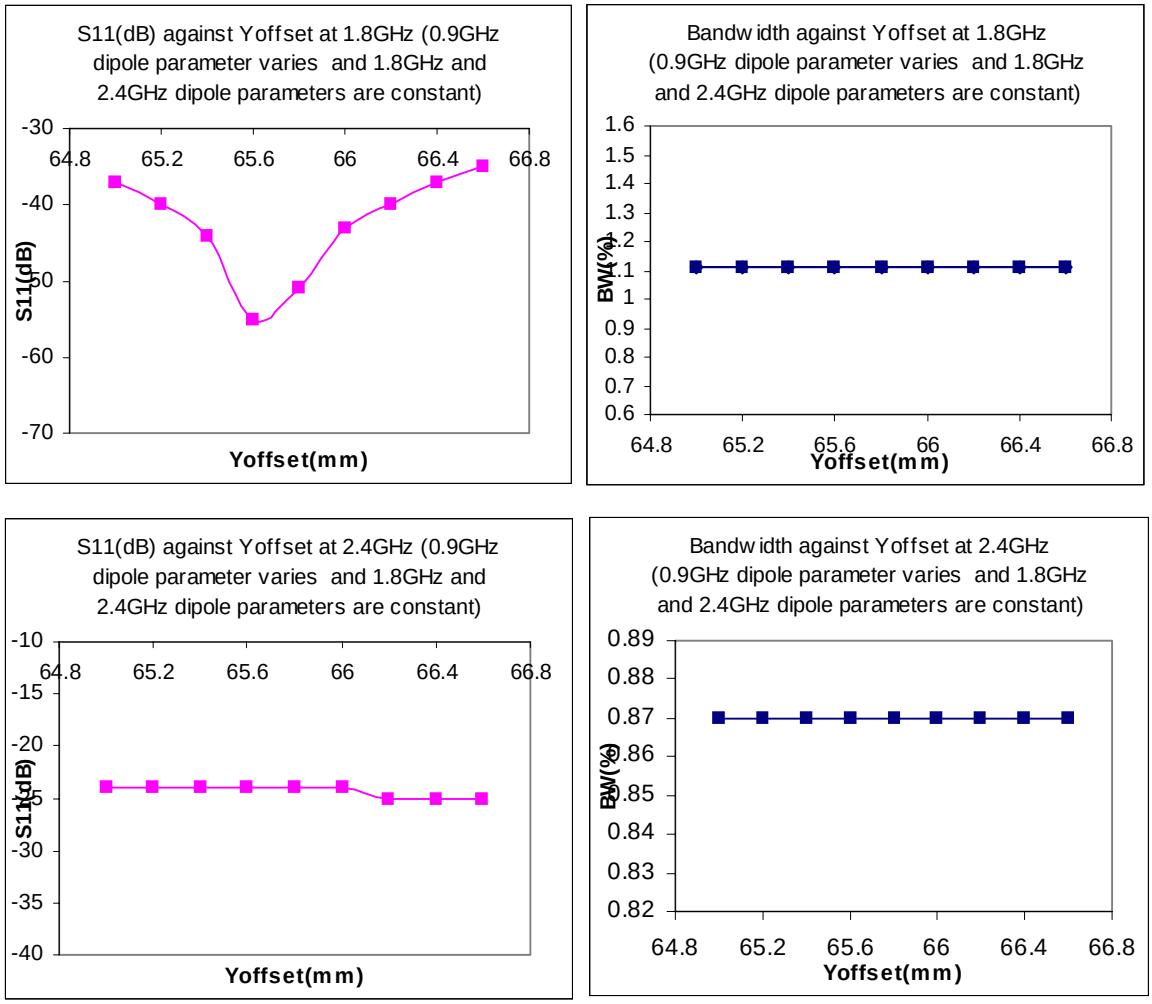

Figure 4.18: Bandwidth and return loss against frequency for tri-band structure with 0.9GHz dipole parameter varies longitudinally

Although the 0.9GHz dipole longitudinal parameter varies, the 0.9GHz dipole parameter placed at 65.6mm from the feedline port gives the optimum bandwidth and return loss and is tabulated as Table 4.8.

Band	0.9GHz	1.8GHz	2.4GHz
Bandwidth (BW)	0.334%	1.11%	0.87%
Return loss (S_{11})	-32dB	-55dB	-24dB

Table 4.8: The simulation result of tri-band with 0.9GHz dipole parameter varies longitudinally

Taking the 0.9GHz dipole parameter longitudinal varies result and the other two dipole parameters are constant, the 0.9GHz dipole position is varied horizontally again. The results compared are obtained as follows:

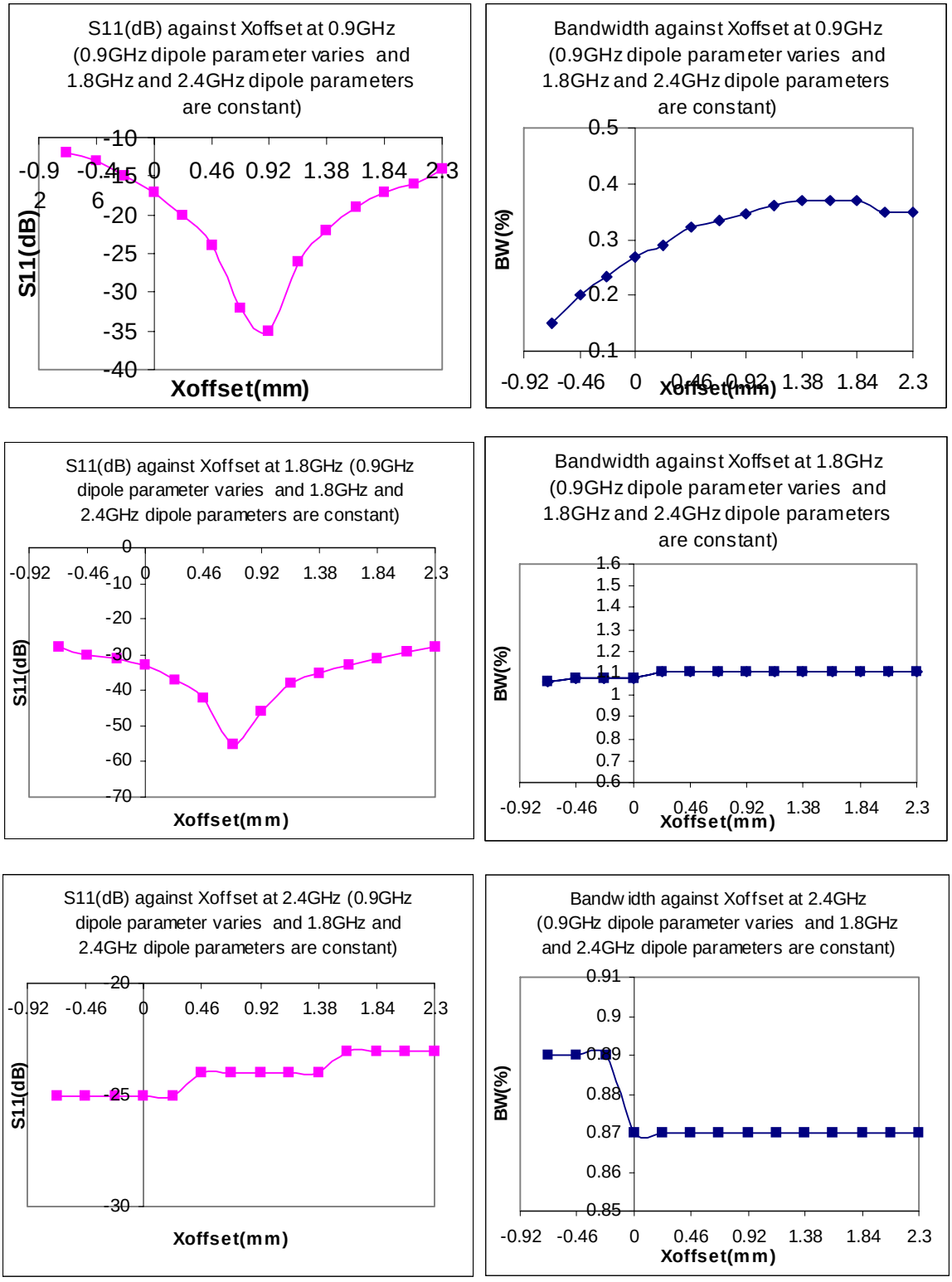

Figure 4.19: Bandwidth and return loss against frequency for tri-band structure with 0.9GHz dipole parameter varies transversely

Although the 0.9GHz dipole transverse parameter varies, the 0.9GHz dipole parameter placed at 0.69mm from the feedline port horizontal position gives the optimum bandwidth and return loss and is tabulated as Table 4.9.

Band	0.9GHz	1.8GHz	2.4GHz
Bandwidth (BW)	0.334%	1.11%	0.87%
Return loss (S_{11})	-32dB	-55dB	-24dB

Table 4.9: The simulation result of tri-band with 0.9GHz dipole parameter varies transversely

After varying each dipole parameters transversally (Xoffset), longitudinally (Yoffset), the dipole length in order to resonance for the required frequency and the dipole width in order to match properly with the feedline, the first investigation of final tri-band antenna dimensions are tabulated in Table 4.10.

Band	0.9GHz	1.8GHz	2.4GHz
Width of dipole (W_d)	4.6mm	4.6mm	4.6mm
Length of dipole (L_d)	78.4mm	36.55mm	26.95mm
Distance from the feedline port (L_y)	65.6mm	146.8mm	154.6mm
Transverse distance from dipole (d_x)	0.69mm	3.22mm	3.91mm
Resonant frequency (f_0)	0.8977GHz	1.8GHz	2.4GHz
Bandwidth (BW)	0.334%	1.1%	0.87%
Return loss (S_{11})	-32dB	-55dB	-24dB

Table 4.10: The dimensions of first investigation of tri-band antenna design

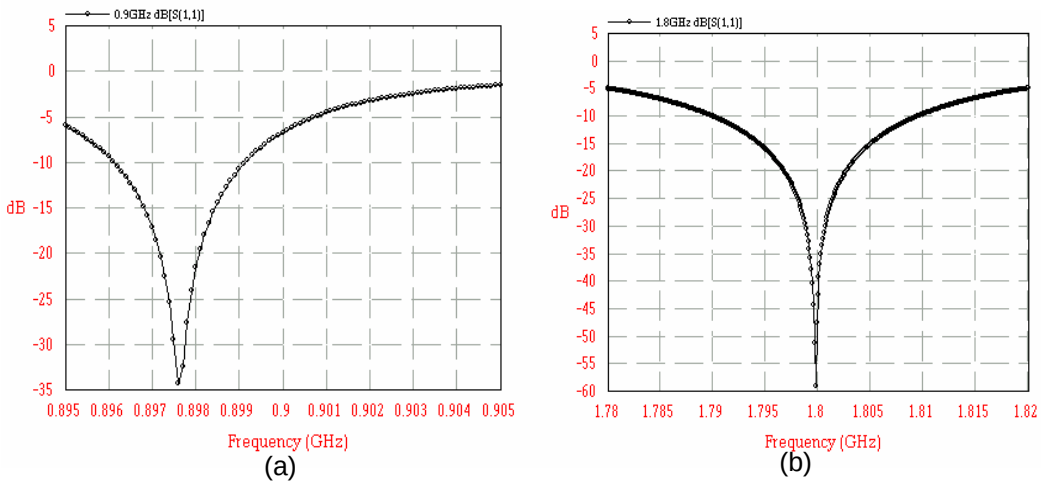

Figure 4.20: Plot of return loss against frequency for the range at (a)0.9GHz (b) 1.8GHz

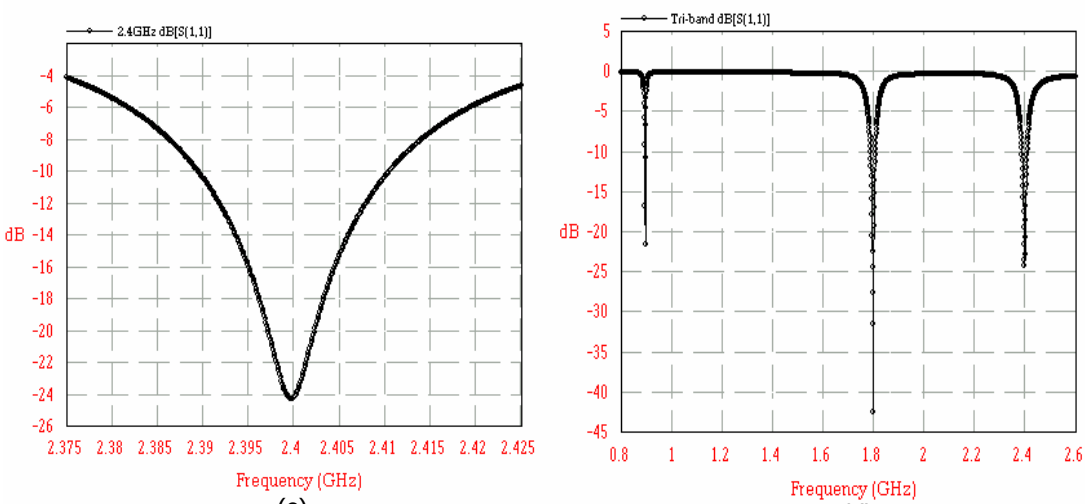

Figure 4.20: Plot of return loss against frequency for the range at (c)2.4GHz (d)tri-band

The bandwidth response of the above simulation result is not good. Therefore it is considered to change the dipole arrangement by putting the 2.4GHz dipole between the other two dipoles. The design consideration for this tri-band antenna is the same as the first tri-band antenna by changing the dipole positions longitudinally, transversely until the optimum simulation results are achieved.

Band	0.9GHz	1.8GHz	2.4GHz
Width of dipole (W_d)	4.6mm	4.6mm	4.6mm
Length of dipole (L_d)	78.4mm	36.55mm	26.15mm
Distance from the feedline port (L_y)	65.6mm	146.8mm	93.2mm
Transverse distance from dipole (d_x)	0.69mm	3.45mm	3.68mm
Resonant frequency (f_0)	0.898GHz	1.798GHz	2.397GHz
Bandwidth (BW)	0.334%	1.1%	2.17%
Return loss (S_{11})	-33dB	-44dB	-31dB

Table 4.11: The dimensions of tri-band antenna design with conventional feedline

The next step is to get the remarkably reduced the physical dimension the EMC dipole antenna design. As mentioned above, the PBG cell with one dimensional structure microstrip line give not only give the reduced physical dimension of the tri-band antenna also the improve bandwidth seen from the practical result. The width of the

PBG cell is the same as the conventional feedline width that is 2.3mm corresponding to 50Ω microstrip line. This PBG one dimensional PBG structure is perforated on the line itself which means some metallic parts are remove from the microstrip line itself. The design simulation results for this PBG feedline structure is tabulated in Table 4.12.

Band	0.9GHz	1.8GHz	2.4GHz
Width of dipole (W_d)	4.6mm	4.6mm	4.6mm
Length of dipole (L_d)	78.2mm	36.25mm	26mm
Distance from the feedline port (L_y)	10mm	72mm	35mm
Transverse distance from dipole (d_x)	1.15mm	2.53mm	1.84mm
Resonant frequency (f_0)	0.899GHz	1.793GHz	24GHz
Bandwidth (BW)	0.43%	0.7%	2.2%
Return loss (S_{11})	-24dB	-30dB	-25dB

Table 4.12: The dimensions of tri-band antenna design with PBG feedline

4.8.3 Measurement results of tri-band EMC dipole antenna

The FR4 substrate with the relative permittivity of 4.4 is used for this EMC dipole antenna design. After fabricating the tri-band EMC dipole antenna designs, the measurements of S-parameters were done using the Hewlett Packard Vector Network Analyzer which is given the input sweep for the antenna input and the coaxial cable of 50Ω used for measuring the return loss and the bandwidth of the antenna. The results obtained were notable on VSWR of 2:1 which correspond to a return loss of -10dB where the antenna bandwidth is calculated on this return loss. The comparison of measured results between the EMC dipole with the conventional feedline and with the PBG feedline is tabulated in Table 4.13.

	Conventional feedline	PBG feedline
Center frequency (f_0)	0.943GHz	0.96GHz
Bandwidth (BW)	1%	0.73%
Return loss (S_{11})	-17dB	-12dB
Center frequency (f_0)	1.91GHz	1.93GHz
Bandwidth (BW)	3.14%	2.7%
Return loss (S_{11})	-20dB	-22dB
Center frequency (f_0)	2.52GHz	2.6GHz
Bandwidth (BW)	3.6%	12.5%
Return loss (S_{11})	-15dB	-23dB

Table 4.13: The comparison measured results of EMC dipole antenna between the conventional feedline and the PBG feedline

The measured results obtained is not exactly the same as the simulation results due to a large variation of the dielectric constant of FR4 substrate, the variation of the loss tangent at different frequencies and the misalignments of the substrate layers. The followings results are the comparison of EMC dipole antenna design with the conventional feedline simulation results and the measurements results for S_{11} parameters at each resonant frequency range and the whole range.

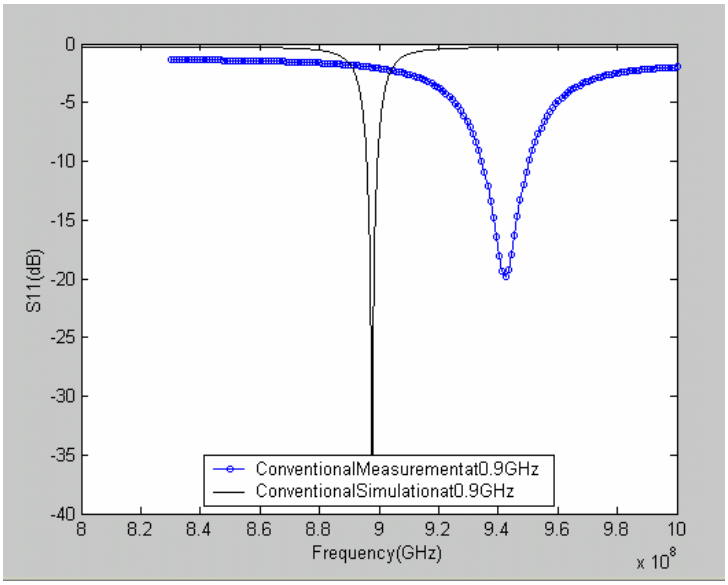

(a)

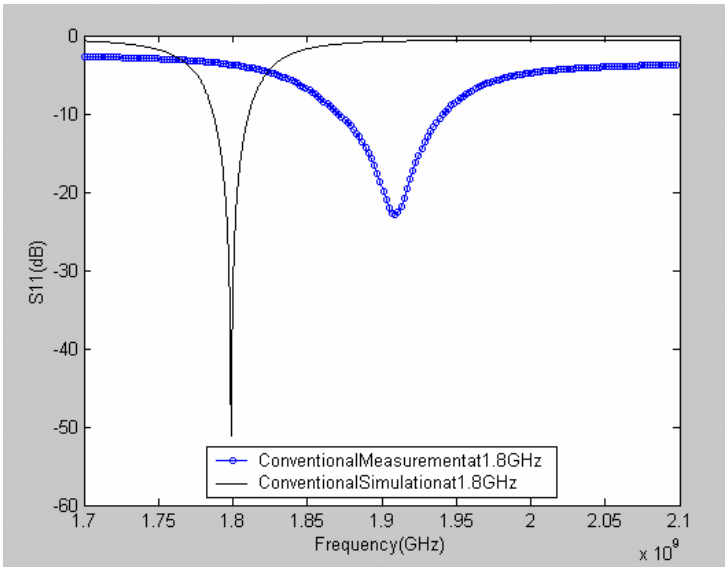

(b)

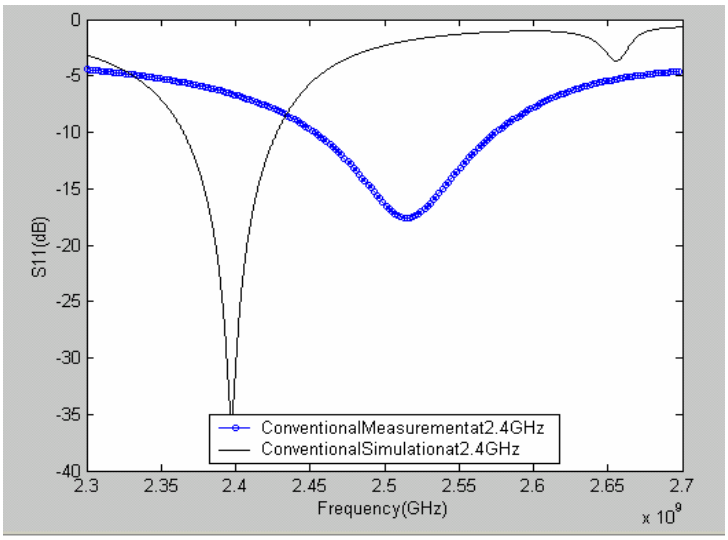

(c)

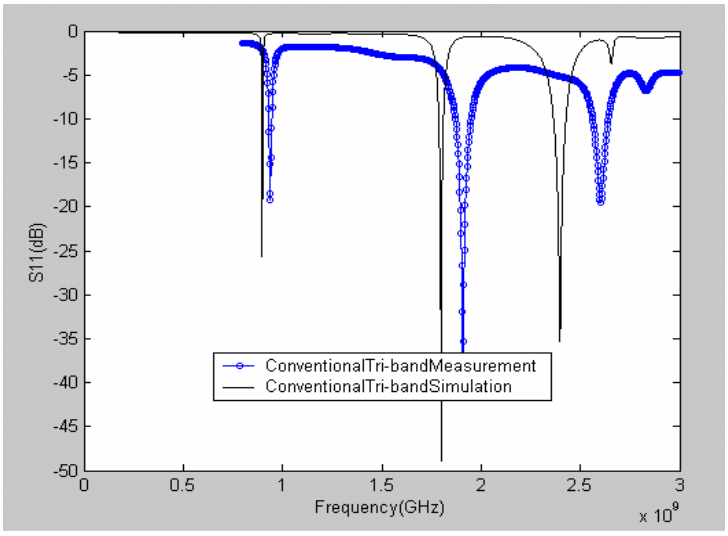

(d)

Figure 4.21: Compare the results between the measurement and simulation for the EMC dipole with the conventional feedline (a) at 0.9GHz resonance (b) at 1.8GHz resonance (c) at 2.4GHz resonance (d) the whole frequency range

All the three frequency resonances of the antenna designs are shifted towards higher frequencies resonance compared to the simulated results obtained. All the substrate layers for the antenna designs in this project are screwed together and therefore there may be presence of air gaps between each substrate which causes the permittivity value decreased, in turn, the bandwidth of the antenna design is also improved. The other effect of deviation in the effective permittivity may be affected a shift of the resonance frequency.

The impedance bandwidth of 0.9GHz band is 1% in measured result while the impedance bandwidth of 2.4GHz band is 3.6% in measured result for EMC dipole with the conventional feedline. It can be seen that all the bandwidth measured results are better than the simulation results due to introducing of the air gap between the substrate. The bandwidth improved due to the effect of the air gap is already explained in this chapter. It is also noticed that the higher the frequency, the wider the bandwidth achievable.

The next step is the comparison of the measurement results and the simulation results for EMC dipole antenna design with the PBG feedline S_{11} parameters at each resonant frequency range and the whole range are described as follows:

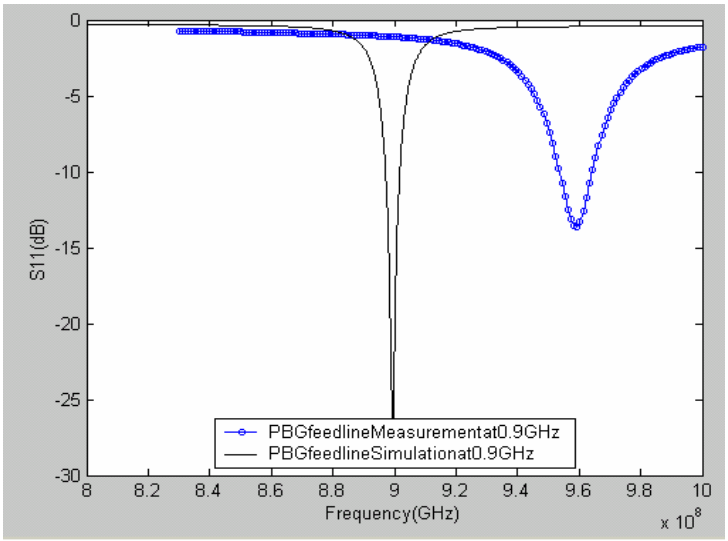

(a)

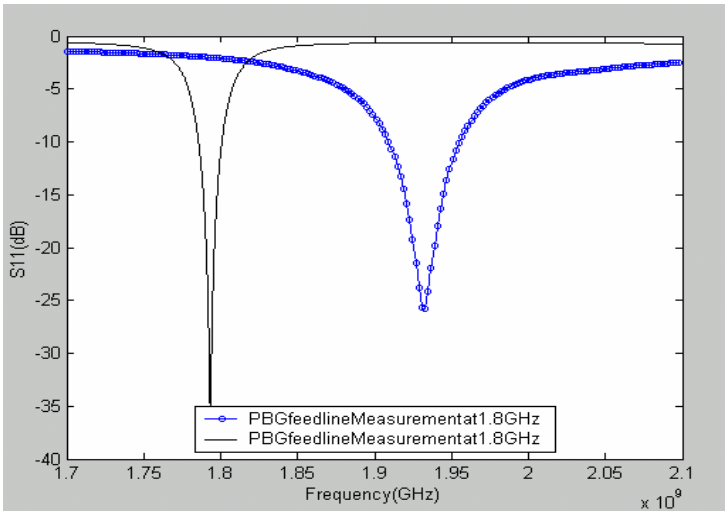

(b)

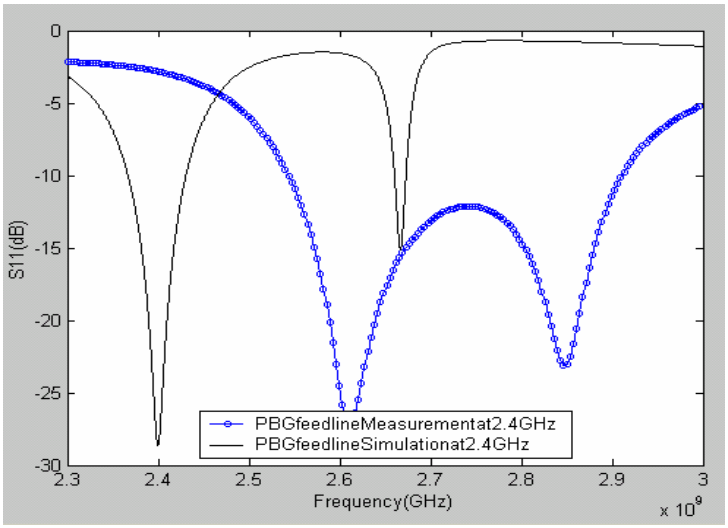

(c)

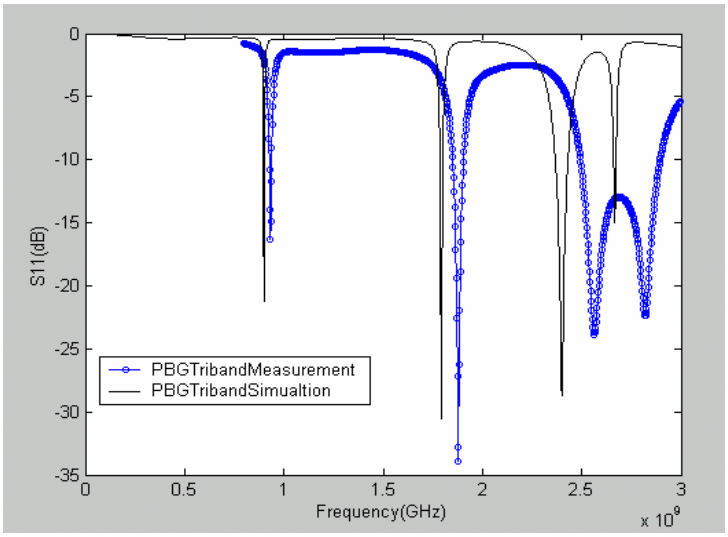

(d)

Figure 4.22: Compare the results between the measurement and simulation for the EMC dipole with the PBG feedline (a) at 0.9GHz resonance (b) at 1.8GHz resonance
(c) at 2.4GHz resonance (d) the whole frequency range

The return loss for the antenna design with the conventional feedline and with the PBG feedline both are significantly lower compared to the simulation results one while the bandwidth for both the antenna designs are larger than the simulation results. The bandwidth for the antenna design with the PBG feedline is remarkably larger for the higher frequency range as well as reduced the physical dimension of the antenna design.

4.8.4 The final EMC dipole antenna with tapered shape

The bandwidth measured results for both the antenna designs are not satisfied for the low frequency range and hence there is tried to improve bandwidth by changing the shape of the low frequency EMC dipoles with the tapered section. A tapered shape dipole is a tapered transition which has already shown in Figure 4.5 in which characteristic impedance is varied along the line continuously.

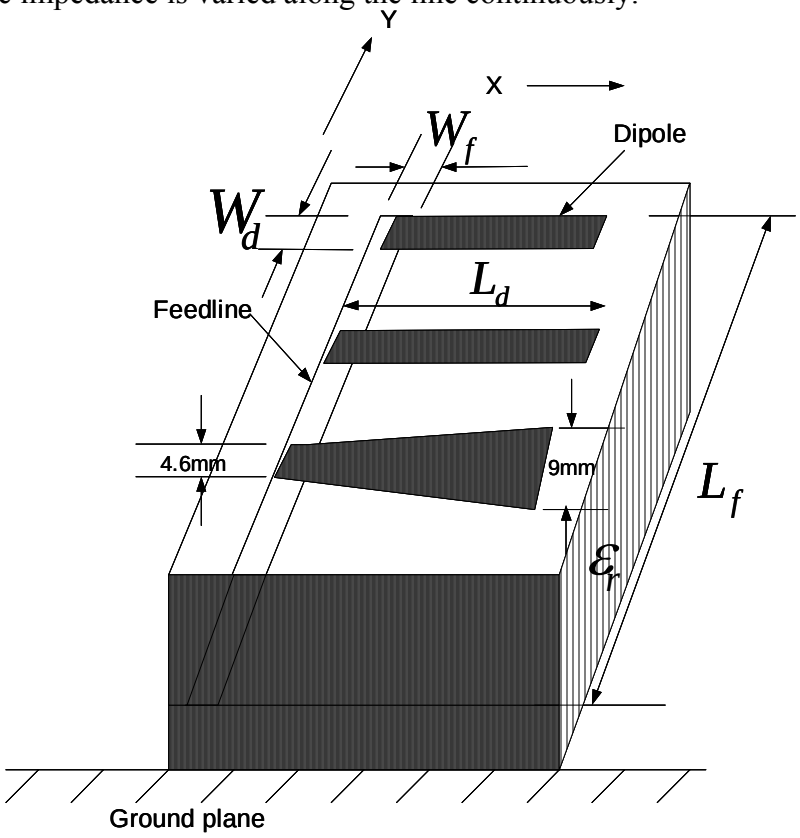

Figure 4.23: The final design of electromagnetically coupled tapered shaped microstrip dipole antennas

The design considerations for the tri-band antenna with the tapered shaped dipole are investigated by optimizing the dipole positions longitudinally (Yoffset) and transversely (Xoffset) and so on. After optimizing the antenna design with IE3D software using the FR4 substrate, the optimization simulation results are tabulated in Table 4.14.

Band	0.9GHz	1.8GHz	2.4GHz
Width of dipole (W_d)	4.6 to 9mm	4.6mm	4.6mm
Length of dipole (L_d)	77mm	37mm	25.9mm
Distance from the feedline port (L_y)	82mm	146mm	99mm
Transverse distance from dipole (d_x)	-3mm	-5mm	-4mm
Resonant frequency (f_0)	0.899GHz	1.775GHz	2.395GHz
Bandwidth (BW)	1.06%	1.97%	3.13%
Return loss (S_{11})	-29dB	-35dB	-49dB

Table 4.14: The dimensions of the final tapered shape EMCdipole antena diesign with the conventional feedline

Band	0.9GHz	1.8GHz	2.4GHz
Width of dipole (W_d)	4.6 to 9mm	4.6mm	4.6mm
Length of dipole (L_d)	77.1mm	36.5mm	25.9mm
Distance from the feedline port (L_y)	18mm	76mm	37mm
Transverse distance from dipole (d_x)	-3mm	-5mm	-4mm
Resonant frequency (f_0)	0.9GHz	1.785GHz	2.399GHz
Bandwidth (BW)	1.08%	1.43%	3%
Return loss (S_{11})	-36dB	-48dB	-39dB

Table 4.15: The dimensions of the final tapered shape EMCdipole antena diesign with the PBG feedline

The measured results for the final EMC tapered shape dipole antenna designs are fabricated using the FR4 substrate with the relative permittivity of 4.4 and the substrate thickness of 1.57mm. The final measurements results are as follows:

	Conventional feedline	PBG feedline
Center frequency (f_0)	0.934GHz	0.932GHz
Bandwidth (BW)	1.8%	2.12%
Return loss (S_{11})	-19dB	-19dB
Center frequency (f_0)	1.87GHz	1.88GHz
Bandwidth (BW)	2.6%	2.13%
Return loss (S_{11})	-22dB	-22dB
Center frequency (f_0)	2.53GHz	2.56GHz
Bandwidth (BW)	8.53%	14.54%
Return loss (S_{11})	-19dB	-34dB

Table 4.16: The comparison measured results of EMC tapered shape dipole antenna between the conventional feedline and the PBG feedline

It can be observed that the final tapered shape dipole antenna designs measured results are better than the first fabrication measurement results due to the 0.9GHz tapered dipole. All the three frequency resonances of both antenna designs are still shifted towards higher frequency due to the effects of deviation in the permittivity. As mentioned in the first fabrication measurements, all the substrate layers are screwed together and there may be a presence of air gap between each layer and this can be improved the bandwidth measurements results but deviated the permittivity due to this air gap effect.

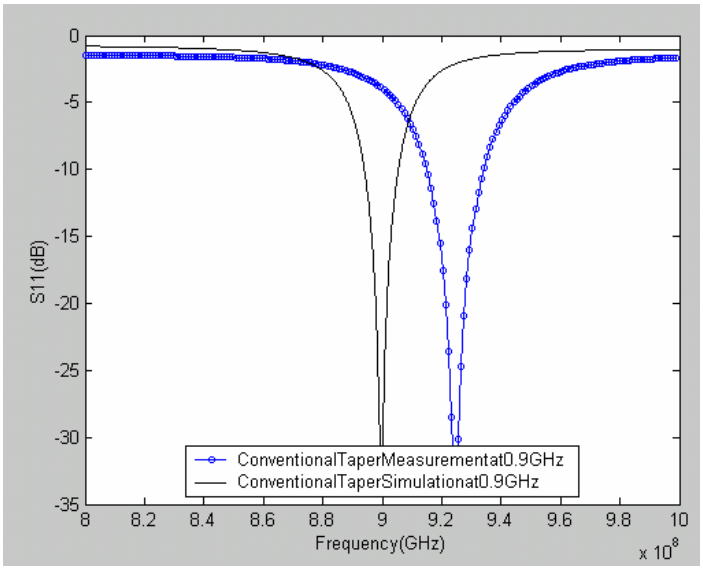

(a)

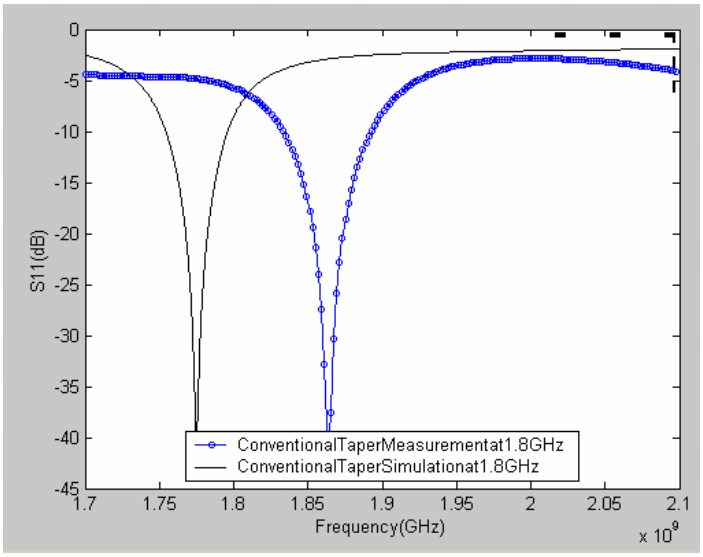

(b)

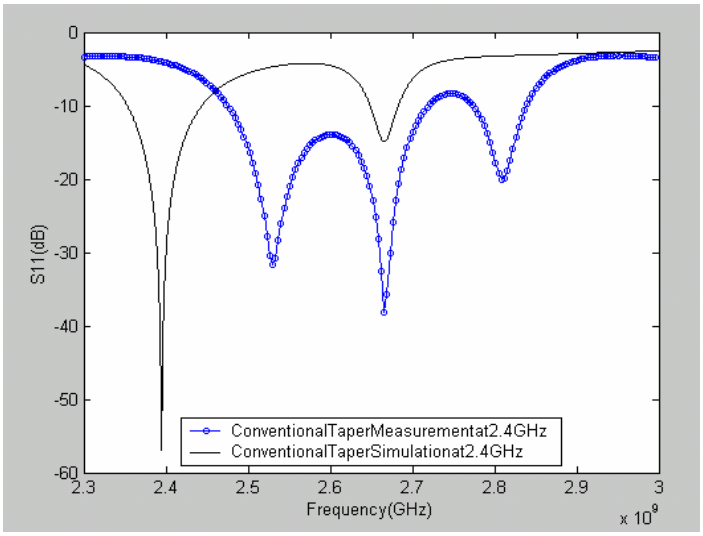

(c)

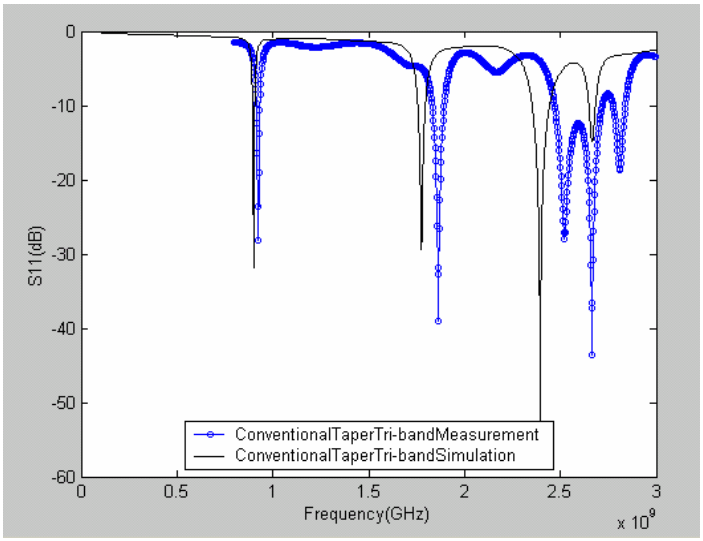

(d)

Figure 4.24: Compare the results between the measurement and simulation for the EMC tapered shape dipole with the conventional feedline (a) at 0.9GHz resonance (b) at 1.8GHz resonance (c) at 2.4GHz resonance (d) the whole frequency range

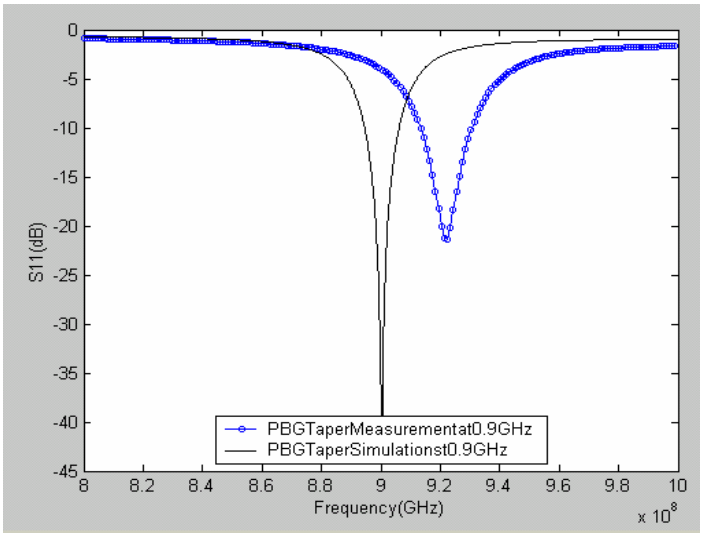
S11(dB)
Frequency(GHz)
x 10^8
PBGTaperMeasurementat0.9GHz
PBGTaperSimulationst0.9GHz

(a)

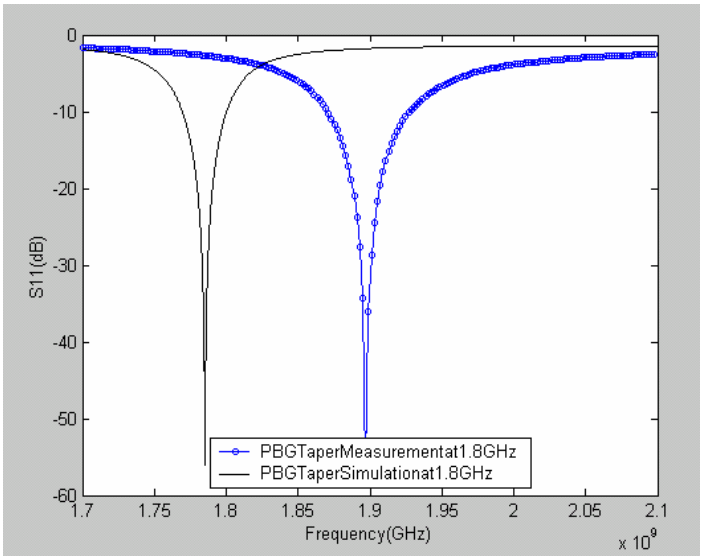
S11(dB)
Frequency(GHz)
x 10^9
PBGTaperMeasurementat1.8GHz
PBGTaperSimulationat1.8GHz

(b)

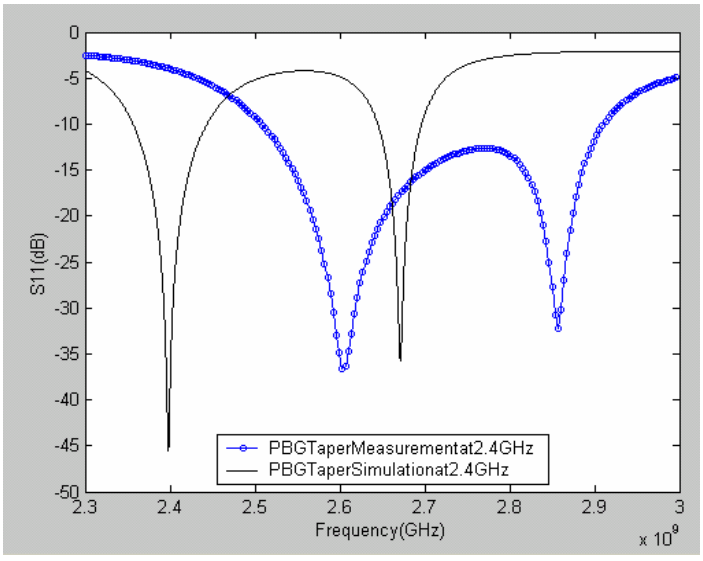
S11(dB)
Frequency(GHz)
x 10^9
PBGTaperMeasurementat2.4GHz
PBGTaperSimulationat2.4GHz

(c)

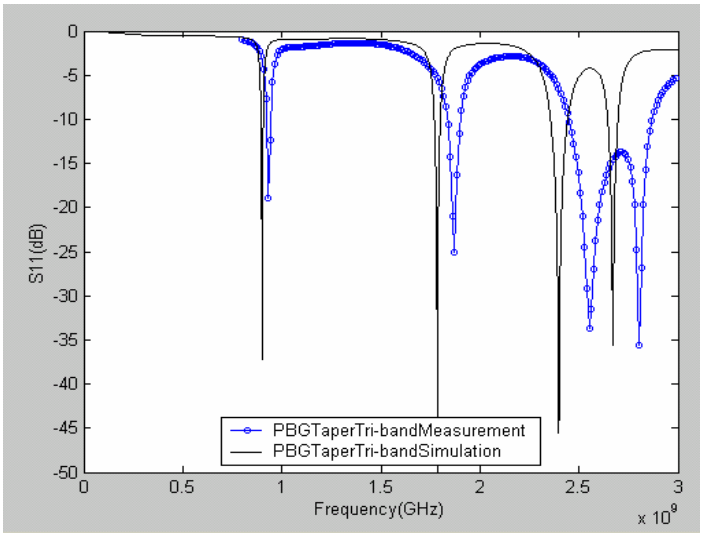

(d)

Figure 4.25: Compare the results between the measurement and simulation for the EMC tapered shape dipole with the PBG feedline (a) at 0.9GHz resonance (b) at 1.8GHz resonance (c) at 2.4GHz resonance (d) the whole frequency range

The radiation pattern for the simulation result of the 1.8GHz frequency range is not good due to the coupled effect of the tapered 0.9GHz dipole and so it is tried to slide the transverse parameter of the 1.8GHz dipole. The simulation result for this antenna design is tabulated in Table 4.17.

Band	0.9GHz	1.8GHz	2.4GHz
Width of dipole (W_d)	4.6 to 9mm	4.6mm	4.6mm
Length of dipole (L_d)	77.1mm	36.5mm	25.9mm
Distance from the feedline port (L_y)	18mm	76mm	37mm
Transverse distance from dipole (d_x)	-3mm	10mm	-4mm
Resonant frequency (f_0)	0.9GHz	1.786GHz	2.4GHz
Bandwidth (BW)	1.07%	1.2%	3.04%
Return loss (S_{11})	-38dB	-33dB	-33dB

Table 4.17: The dimensions of the final tapered shape EMC dipole antenna design with the PBG feedline (changing the transverse parmeter value of 1.8GHz dipole)

The modified measured results of the final tapered shape EMC dipole antenna design with the PBG feedline are compared with the measured results of the final tapered

shape EMC dipole antenna with the conventional feedline and the dates are tabulated in Table 4.18.

	Conventional feedline	PBG feedline
Center frequency (f_0)	0.934GHz	0.943GHz
Bandwidth (BW)	1.8%	2%
Return loss (S_{11})	-19dB	-22dB
Center frequency (f_0)	1.87GHz	1.878GHz
Bandwidth (BW)	2.6%	2.13%
Return loss (S_{11})	-22dB	-22dB
Center frequency (f_0)	2.53GHz	2.58GHz
Bandwidth (BW)	8.53%	16.2%
Return loss (S_{11})	-19dB	-32dB

Table 4.18: The final comparison measured results of EMC tapered shape dipole antenna between the conventional feedline and the PBG feedline

The poor alignment of the substrate layers could be caused due to cut using a manual cutter. Although the alignment of the layers is doing accurately, the poor alignment of a 0.5mm shift on one of the layers will affect a significant degradation in the impedance performance of the antenna and the resonance frequency shifts slightly and the value of the return loss decreases which can be also known from the simulation results.

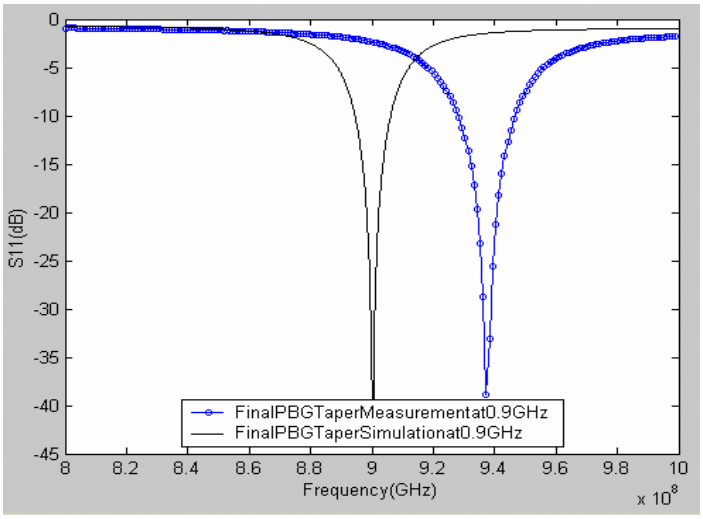

(a)

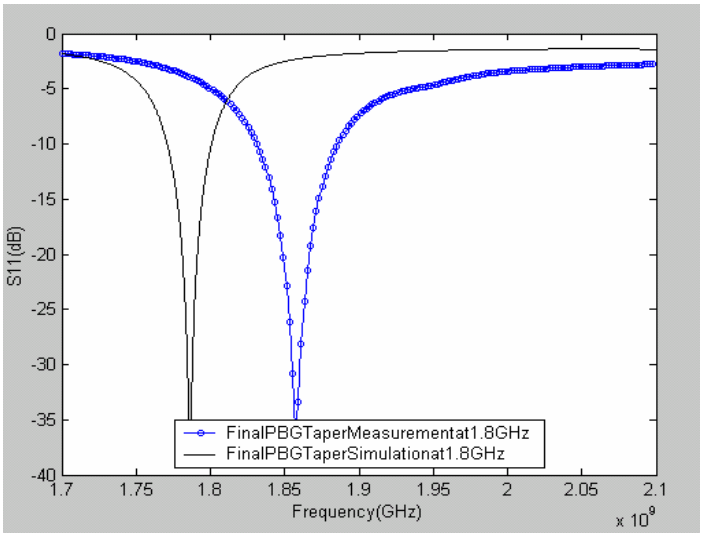

(b)

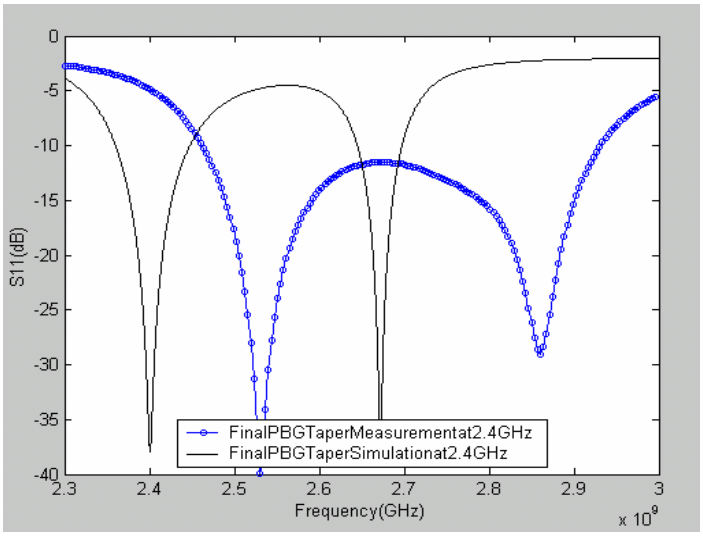

(c)

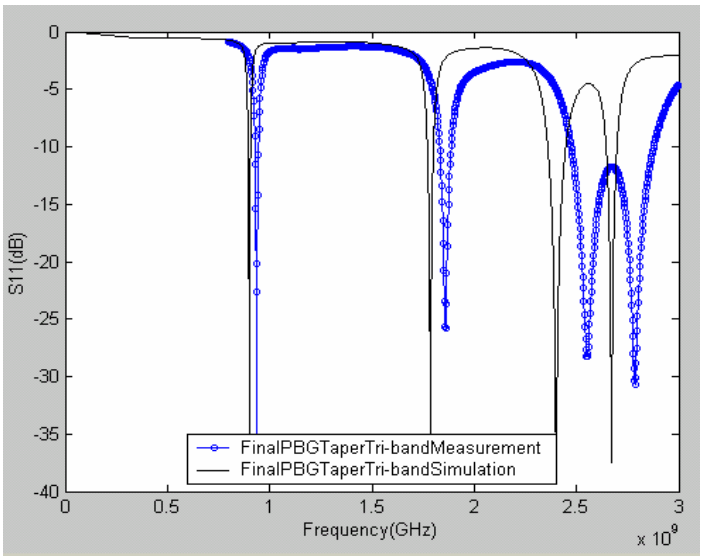

(d)

Figure 4.26: The final compare results between the measurement and simulation for the EMC tapered shape dipole with the PBG feedline (a) at 0.9GHz resonance (b) at 1.8GHz resoanance (c) at 2.4GHz resonance (d) the whole frequency range

4.9 The Measured Results for the Radiation Pattern

The following figures are the simulation results and the measurement results for the electromagnetically coupling dipole antenna designs.

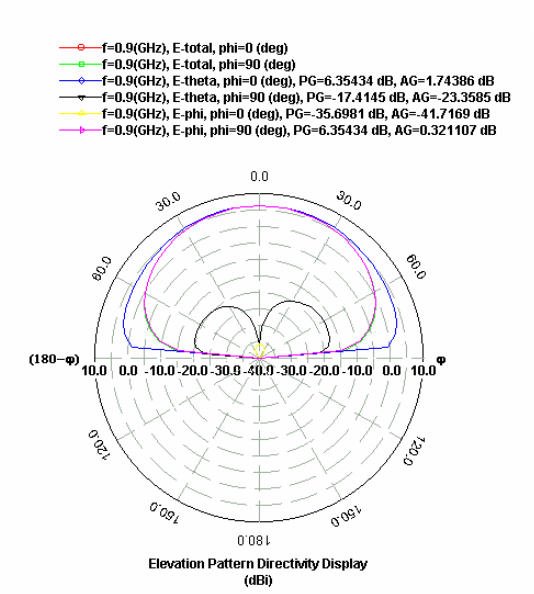

(a)

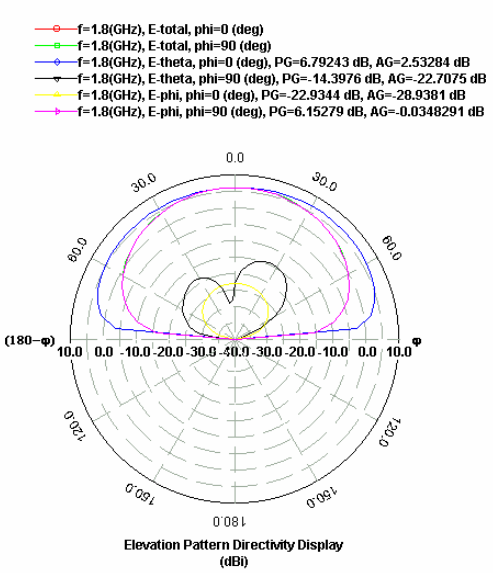

(b)

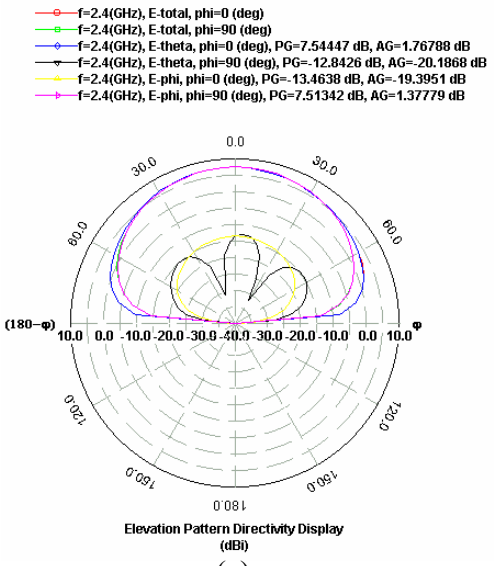

(c)

Figure 4.27: Simulated radiation pattern results for the EMC dipole antenna with the conventional feedline (a) at 0.9GHz (b) at 1.8GHz and (c) 2.4GHz

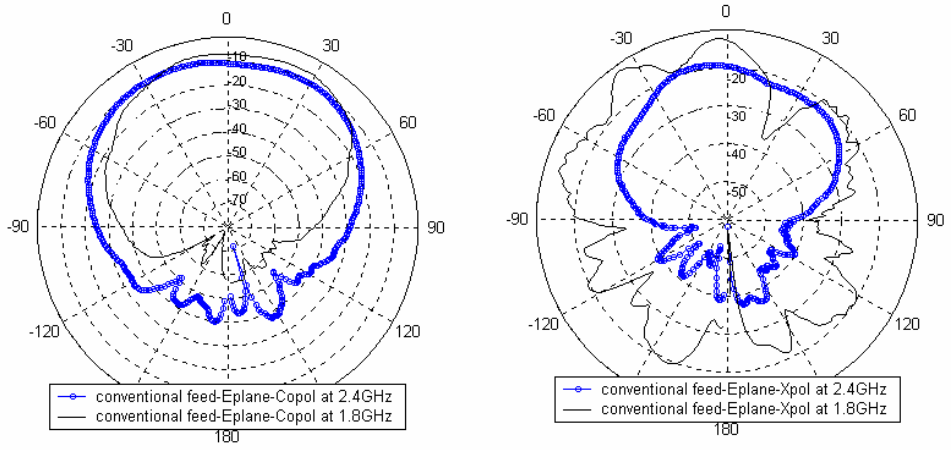

(a) (b)

Figure 4.28: Measured E-plane radiation pattern results of the EMC dipole antenna with the conventional feedline at 1.8GHz and 2.4GHz for (a) co-polarization (b) cross-polarization

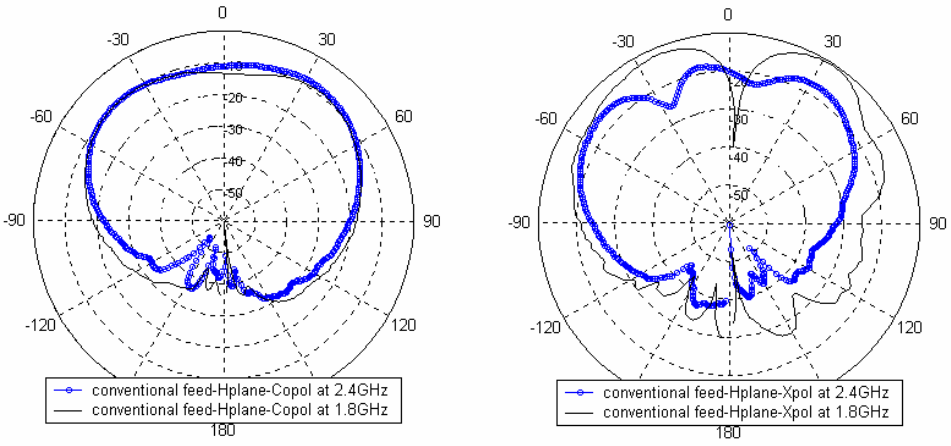

(a) (b)

Figure 4.29: Measured H-plane radiation pattern results of the EMC dipole antenna with the conventional feedline at 1.8GHz and 2.4GHz for (a) co-polarization (b) cross-polarization

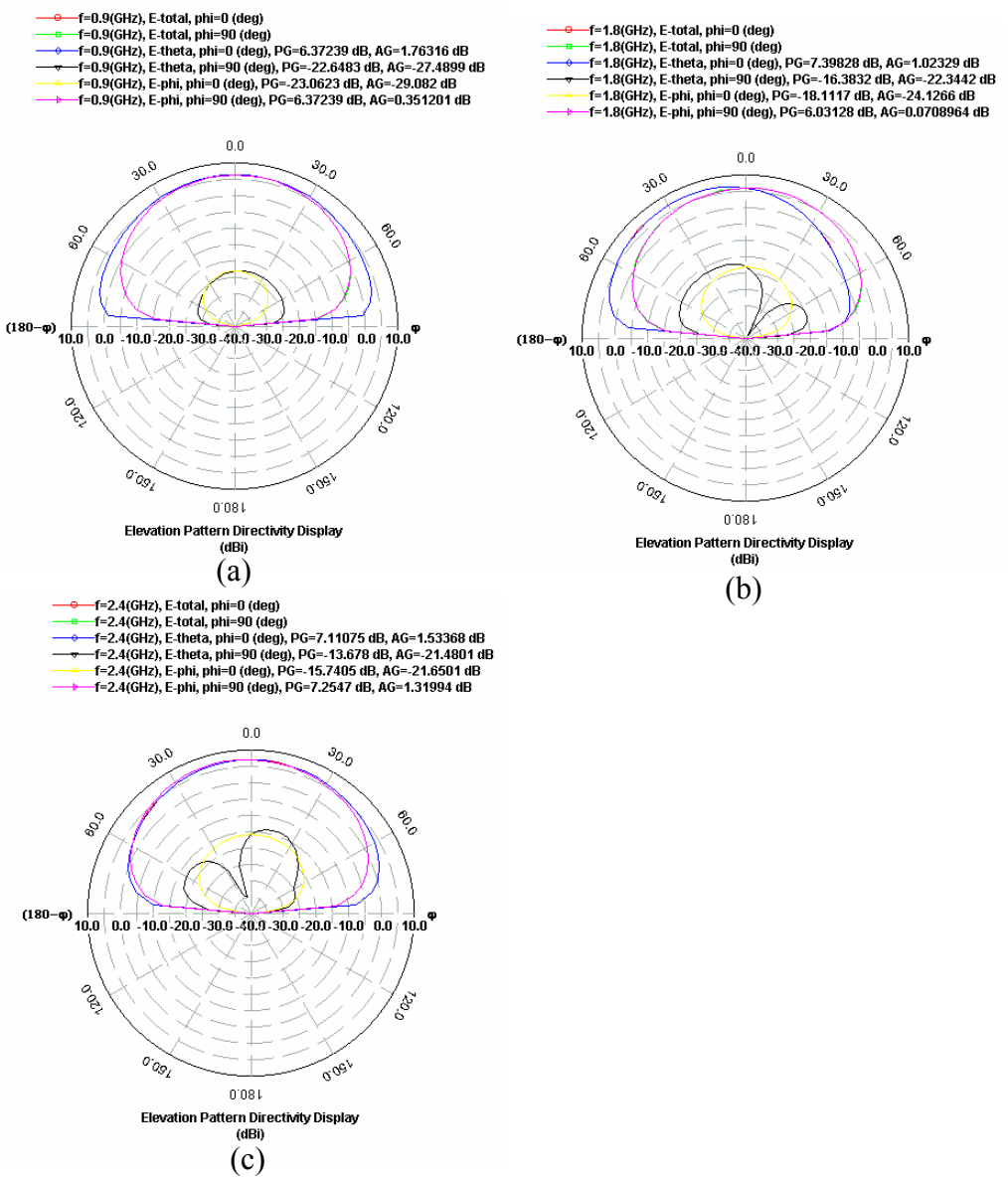

Figure 4.30: Simulated radiation pattern results for the EMC dipole antenna with the PBG feedline (a) at 0.9GHz (b) at 1.8GHz and (c) 2.4GHz

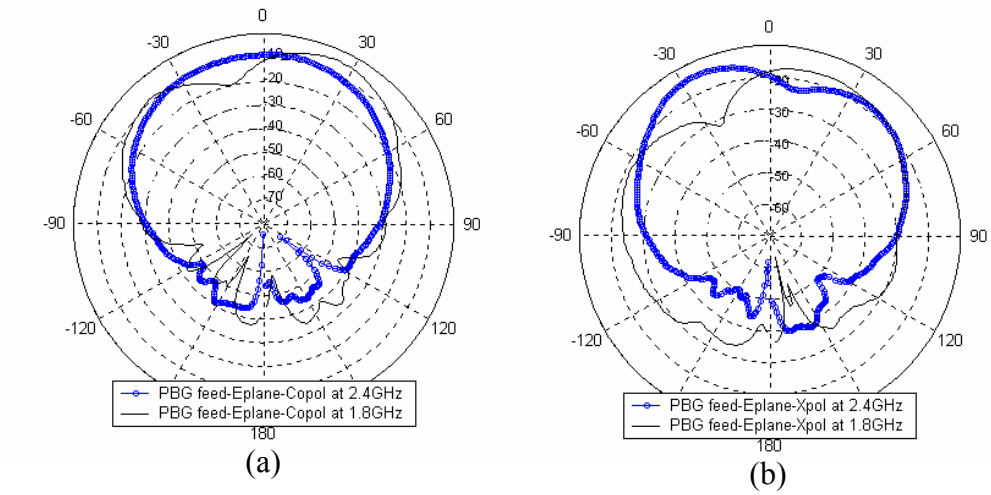

Figure 4.31: Measured E-plane radiation pattern results of the EMC dipole antenna with the PBG feedline at 1.8GHz and 2.4GHz for (a) co-polarization (b) cross-polarization

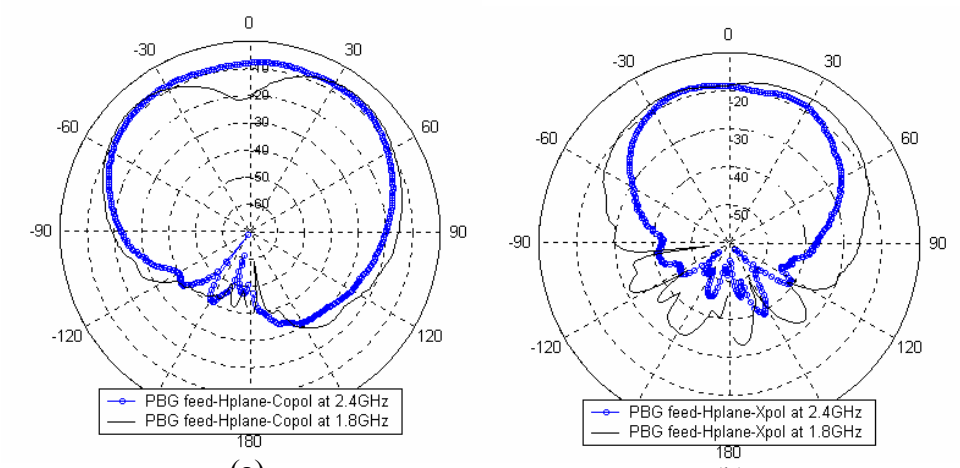

(a) (b)

Figure 4.32: Measured H-plane radiation pattern results of the EMC dipole antenna with the PBG feedline at 1.8GHz and 2.4GHz for (a) co-polarization (b) cross-polarization

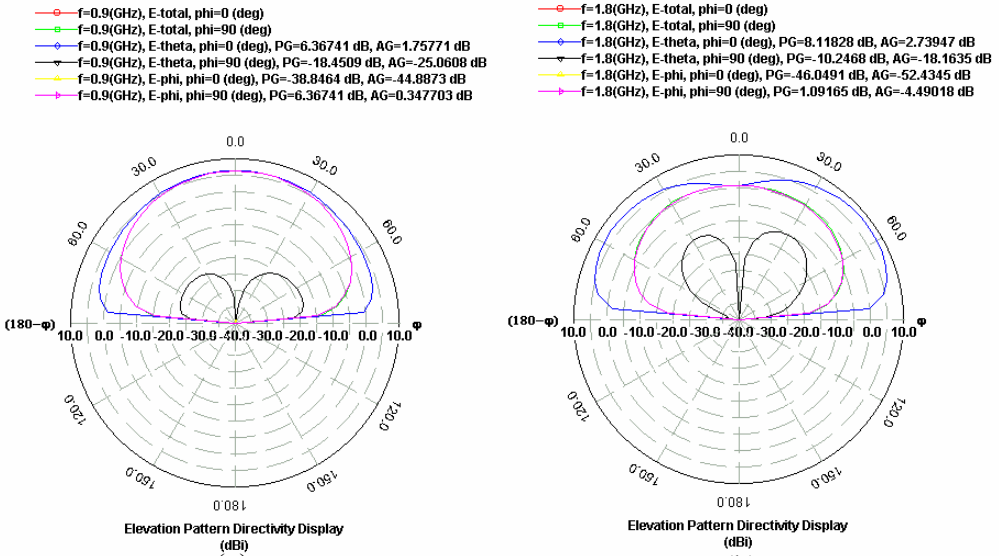

(a) (b)

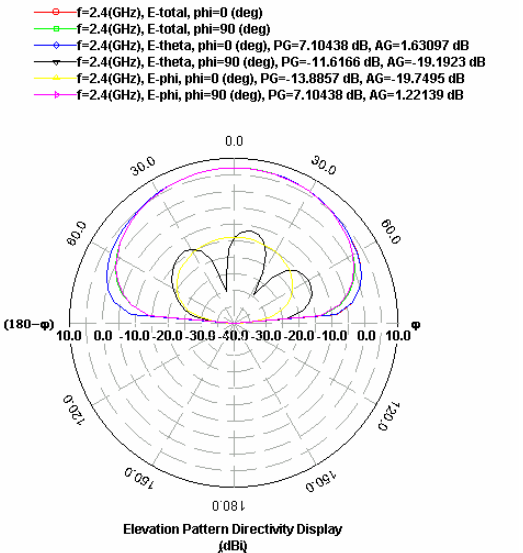

(c)

Figure 4.33: Simulated radiation pattern results for the EMC tapered-shape dipole antenna with the conventional feedline (a) at 0.9GHz (b) at 1.8GHz and (c) 2.4GHz

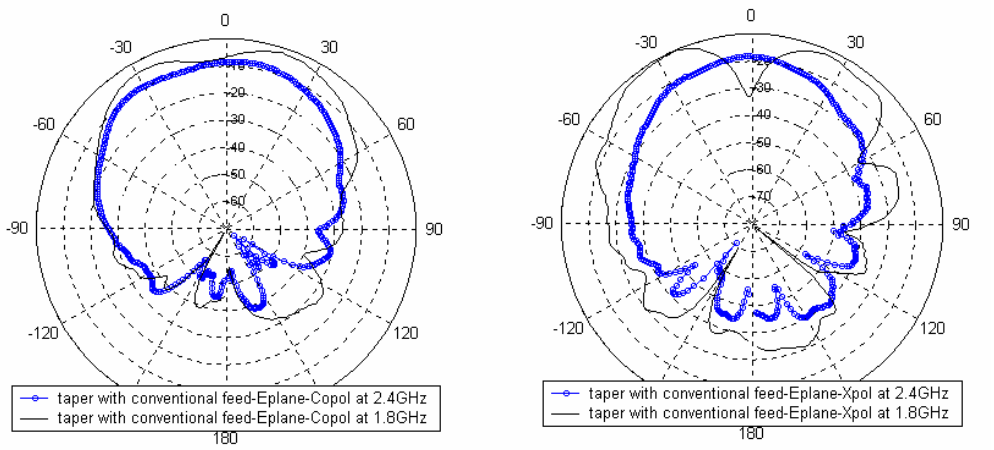

(a) (b)

Figure 4.34: Measured E-plane radiation pattern results of the EMC tapered-shape dipole antenna with the conventional feedline at 1.8GHz and 2.4GHz for (a) co-polarization (b) cross-polarization

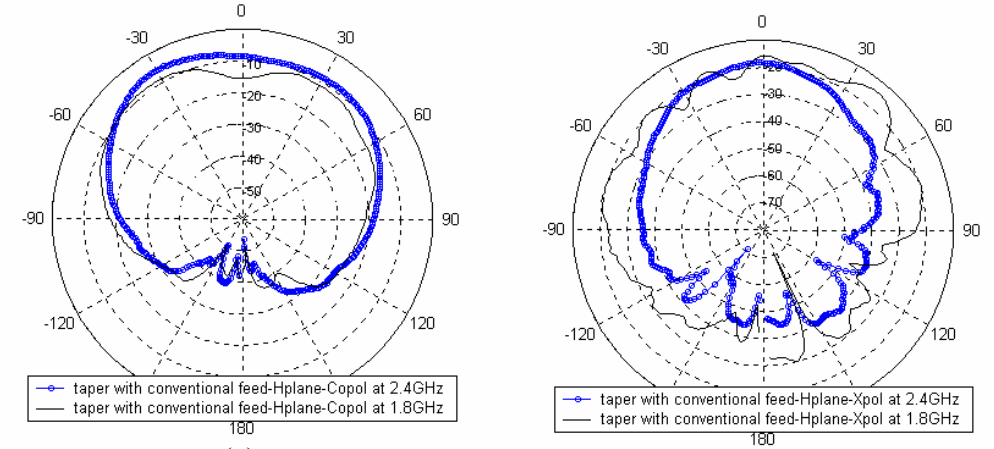

(a) (b)

Figure 4.35: Measured H-plane radiation pattern results of the EMC tapered-shape dipole antenna with the conventional feedline at 1.8GHz and 2.4GHz for (a) co-polarization (b) cross-polarization

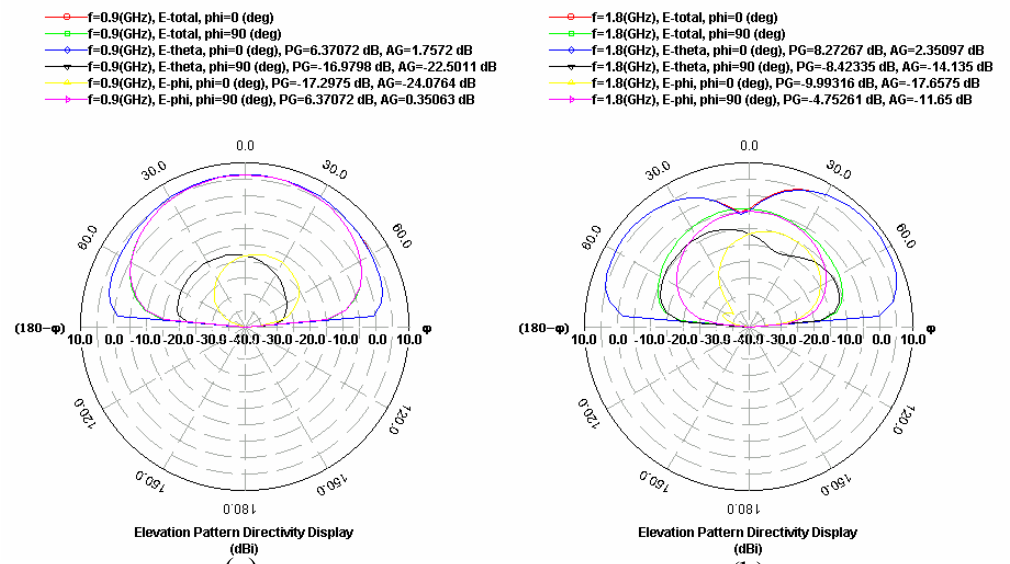

(a) (b)

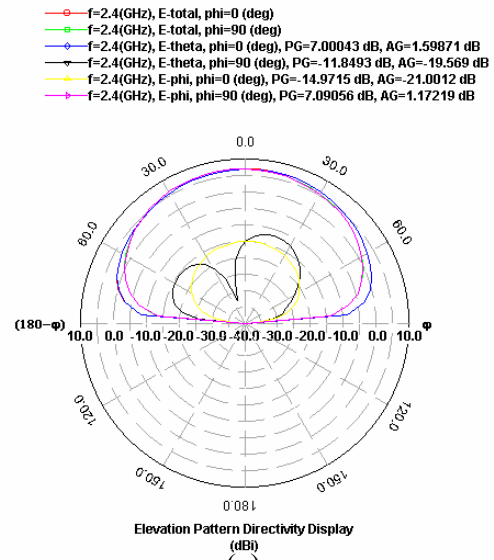

(c)

Figure 4.36: Simulated radiation pattern results for the EMC tapered-shape dipole antenna with the PBG feedline (a) at 0.9GHz (b) at 1.8GHz and (c) 2.4GHz

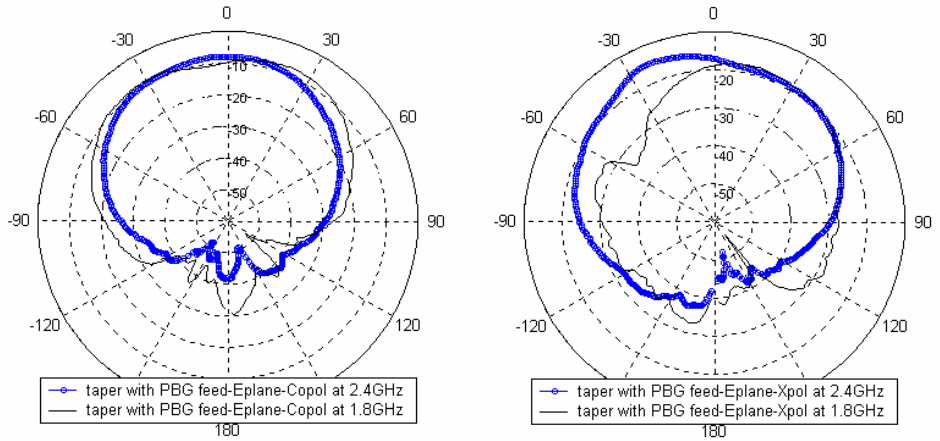

(a) (b)

Figure 4.37: Measured E-plane radiation pattern results of the EMC tapered-shape dipole antenna with the PBG feedline at 1.8GHz and 2.4GHz for (a) co-polarization (b) cross-polarization

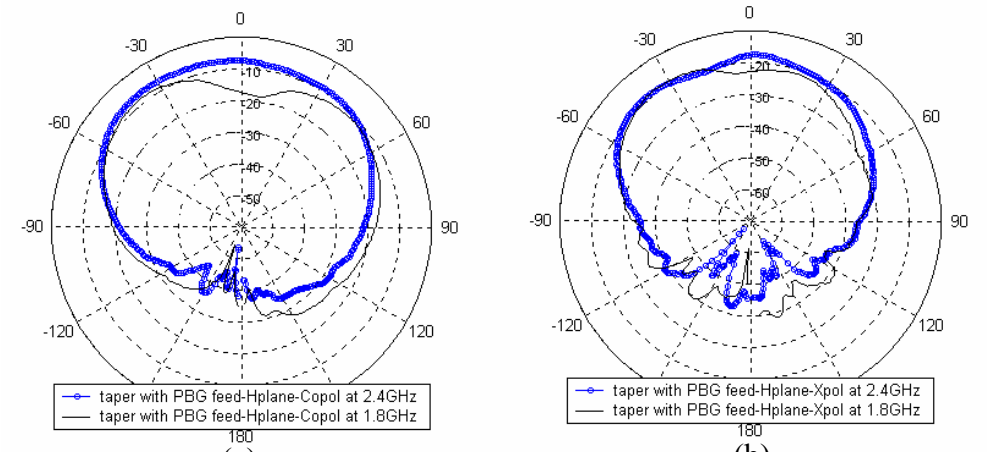

(a) (b)

Figure 4.38: Measured H-plane radiation pattern results of the EMC tapered-shape dipole antenna with the PBG feedline at 1.8GHz and 2.4GHz for (a) co-polarization (b) cross-polarization

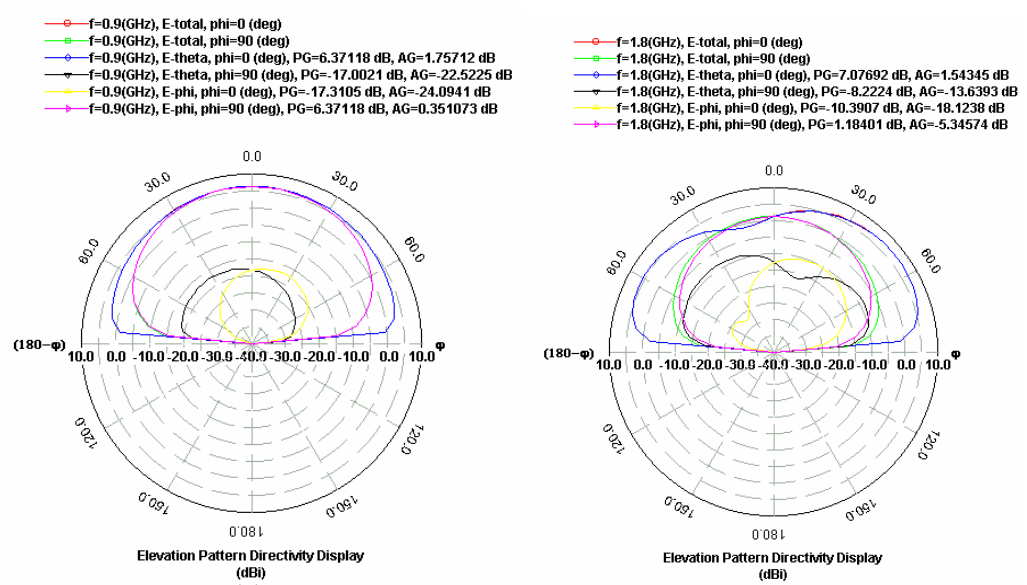

(a) (b)

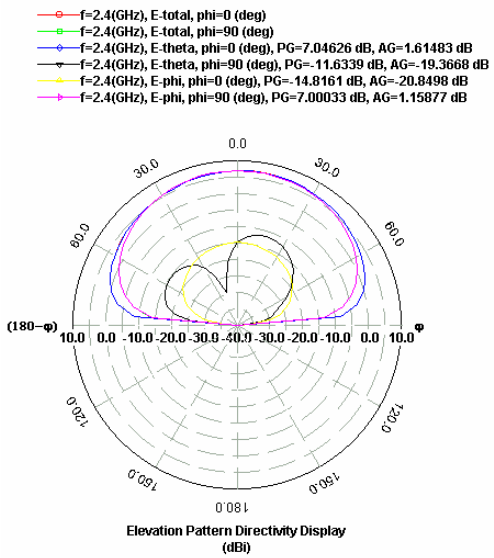

(c)

Figure 4.39: Simulated final results of radiation pattern for the EMC tapered-shape dipole antenna with the PBG feedline (a) at 0.9GHz (b) at 1.8GHz and (c) 2.4GHz

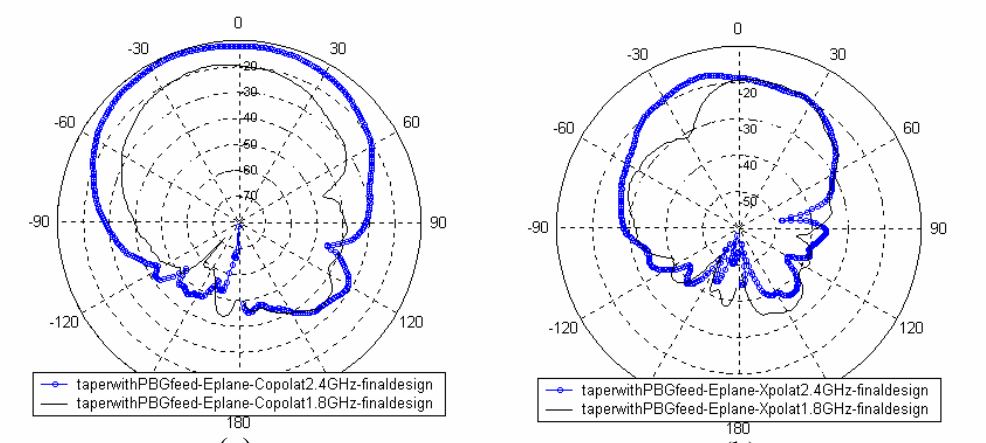

(a) (b)

Figure 4.40: Measured E-plane final radiation pattern results of the EMC tapered-shape dipole antenna with the PBG feedline at 1.8GHz and 2.4GHz for (a) co-polarization (b) cross-polarization

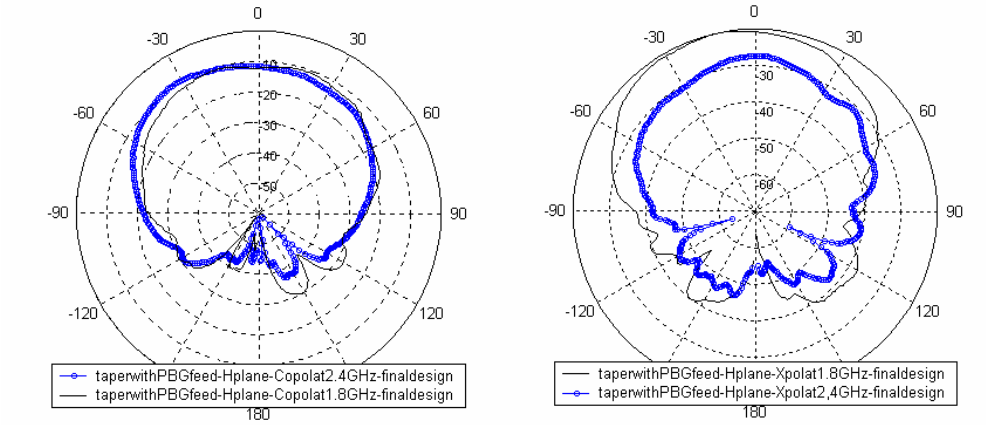

(a) (b)

Figure 4.41: Measured H-plane final radiation pattern results of the EMC tapered-shape dipole antenna with the PBG feedline at 1.8GHz and 2.4GHz for (a) co-polarization (b) cross-polarization

CHAPTER V
Conclusion

The artificial transmission line incorporating with lumped elements has displayed a reduction in physical length and still having the same characteristic as the transmission line at the desired frequency. At microwave frequencies, the artificial transmission line incorporating with the loaded capacitor is realized with an open-circuit stub. When the characteristic impedance of the artificial transmission line becomes smaller and smaller, it is found that the length of the open stub becomes larger and larger.

The proposed four-stub feed U-slot rectangular patch antenna is next investigated by varying certain characteristics of the physical dimensions while keeping others constant. The four-feed design based on differing lengths of stubs to achieve broadband characteristics. Increasing the feed's width is employed as it matches the feed to the patch more effective than tapering. The U-slot size and position is systematically determined so that maximum matching and bandwidth is achieved for the antenna. An attempt was made to increase the impedance bandwidth by using feed of different stub lengths.

The characteristic of an omni-directional tri-band EMC microstrip dipole, with return loss better than 10dB, in transverse configuration with the conventional feedline and the photonic bandgap (PBG) feedline have been investigated in this project. The EMC microstrip dipole with the PBG feedline has achieved the largest impedance bandwidth as well as a reduction in overall physical size.

Since the goal of the EMC proximity coupling microstrip dipole is to improve the impedance bandwidth for the desired bands, the design consideration was initially considered on a single band antenna. Based on the single band design, the tri-band antenna design considerations are improved.

It has been found that dipole placement farther away from the ground plane can help to improve the impedance bandwidth. The investigation shows that the length of the dipole can affect the resonance frequency of the tri-band antenna design. The change of the position of the dipole transversely (Xoffset) and longitudinally (Yoffset) can give the optimum matched to the feed. For optimum matching, it has been found by placing the lower resonant frequency band nearer to the feeding port.

An omni-directional tri-band EMC microstrip dipole antenna in transverse configuration of the final antenna design was designed and fabricated with the center frequencies at 0.9GHz, 1.8GHz and 2.4GHz respectively. The impedance bandwidths of 1%, 2% and 3% have been achieved respectively. The comparison between the measured and simulated results show that the return loss for actual antenna was lower but the impedance bandwidth is improved significantly due to the air gap between the substrate layers. The alignment of the substrate layers is an important fact. The measured results of the five fabricated antennas generally have impedance bandwidths exceeding that of the simulations.

CHAPTER VI

Future Work and Recommendations

One of the main disadvantages of the antenna in this thesis is its thickness. This could be remedied by using substrates of different permittivity. It has been concluded that thin substrate with high permittivity generally achieve lower impedance bandwidths. In this project, some of these options were not exercised for various reasons. The variation of the dipole's height and substrate thickness was restricted because of the type of substrate that was available and the budget reason. Permittivity of the substrate could not be varied either. Future investigation can be done on the effects of variation of substrate thickness and permittivity. An improved design might be achievable with better substrate options.

There exist other novel techniques for improvement in the impedance bandwidth. Some examples include by using irregular feedline configurations and tapered microstrip lines. The use of a slot-feed instead of an EMC feed may also provide enhancement to the impedance bandwidth.

REFERENCES

1. T. C. Edwards, M. B. Steer, " Foundation of Interconnect and Microstrip Design", John Wiley, 3rd Edition, New York 2000.
2. Jia-Sheng G. Hong and M.J. Lancaster, " Microstrip Filters for RF/Microwave Applications", John Wiley, New York 2001.
3. Kai Chang, Inder Bahl, and Vijay Nair, " RF and Microwave Circuit and Component Design for Wireless systems", John Wiley, New York 2001.
4. Inder Bahl, Prakash Bhartia, " Microwave Solid Stste Circuit Design John Wiley & Sons, 1988.
5. Robert E. Collin, " Foundations for Microwave Engineering", 2nd Edition, Mc Graw-Hill, New York 1992.
6. David M. Pozar, " Microwave engineering", John Wiley & Sons, Inc., Canada,1998.
7. C. A. Balanis, "Antenna Theory: Analysis and Design", John Wiley & Sons, Inc., 1997.
8. David M. Pozar and Daniel H. Schaubert, " Microstrip Antennas: The Analysis and Design of Microstrip Antennas and Arrays", IEEE Press, The Institute of electrical and Electronics Engineers, Inc., New York 1995.
9. Y. T. Lo, D. Solomon and W. F. Richards, "Theory and Experiment on microstrip antennas", IEEE Trans. Antennas Propagat., vol. AP-27, no.2, pp137-145.
10. H. George Oltman and Donald A. Huebner, " Electromagnetically coupled microstrip dipoles", IEEE Trans. Antennas Propagat., vol. AP-29, pp151-157, Jan 1981.
11. P. Lepeltier, J. M. Floc'h and J. Citerne, "Complete and rigorous analysis of electromagnetically coupled transverse microstrip dipole", Electron Lett., vol. 23, no. 16, pp.822-824, July 30, 1987.
12. J. M. Floc'h, L. Desclos and G. Poilasne, " Low-profile printed antennas using a surface-mounted component concept", Microwave and Optical Technology Lett., vol. 25, no.1, pp.58-65, April 5, 2000.
13. K. R. Carver and J. W. Mink, " Microstrip Antenna Technology", IEEE Trans. Antennas Propagat., vol. AP-29, pp2-24, 1981.
14. D. M. Pozar and B. Kaufman, " Increasing the Bandwidth of a Microstrip Antenna by proximity coupling", Electron Lett., vol. 23, no. 8, pp.368-369, July 30, 1987.

15. J. R. James & P. S. Hall, “ Handbook of Microstrip Antennas”, IEEE electromagneticwaves series; 28. London, UK. 1989.
16. David M. Pozar, “ Microwave and RF Design of Wireless Systems”, John Wiley & Sons, Inc., United State of America.
17. Ramesh Garg, Prakash, Inder Bahl and Apisak Ittipiboon, “ Microstrip Antenna Design Handbook”, Artech House, Inc., 2001.
18. James Sor, Yongxi Qian and Tatsuo Itoh, “Miniature Low-loss CPW Periodic Structures for Filter Applications”, IEEE Trans., on Microwave Theory and Techniques, vol. 49, no. 12, December 2001.
19. Quan Xue, Kam Man Shum and Chi Hou Cha, “Novel 1-D Microstrip PBG Cells”, IEEE Trans., Microwave and Guided Wave Letters, vol. 10, pp.403-405, October 2000.
20. F. R. Yong, Y. Qian, R. Coccioli and T. Itoh, “ A novel low-loss slow-wave microstrip structure”, IEEE Trans., Microwave and Guided Wave Letters, vol. 8, pp. 372-374, Nov. 1998.
21. A. Gorur, C. Kapuz, and M. ALkan “ Characteristic of periodically loaded CPW structure”, IEEE Trans., Microwave and Guided Wave Letters, vol. 8, pp. 278-280, Aug. 1998.
22. Fei-Ran Yang, Roberto Coccioli, Yongxi Qian and Tatsuo Itoh, “ Analysis and Application of coupled microstrip on periodically patterned ground plane”, IEEE MTT-S Digest, 2000.
23. Fei-Ran Yang, Roberto Coccioli, Yongxi Qian and Tatsuo Itoh, “ Planar PBG Structure: Basic Properties and Applications”, IEICE Trans, Electron, vol. E83-C, no. 5, May 2000.
24. Yongxi Qian and Tatsuo Itoh, “ Planar Periodic Structures for microwave and millimeter wave circuit applications”, IEEE MTT-S Digest, 1999.
25. Inder Bahl, Prakash Bhartia, “ Microstrip antennas”, Dedham, Mass: Artech House, 1980.
26. VesanRadisic, Yongxi Qian, Roberto Coccioli and Tatsuo Itoh, “ Novel 2-D Photonic Bandgap Structure for Microstrip Lines”, IEEE Trans., Microwave and Guided Wave Letters, vol. 8, pp. 69-71,Feb. 1998.
27. Yongxi Qian and Tatsuo Itoh, “ Planar Periodic Structures for Microwave and Millimeter Wave Circuit Applications”, IEEE, MTT-S Digest, pp. 1533-1536, 1999.

28. J. S. Dahele and Prof. K. F. Lee, " Theory and Experiment on Microstrip Antennas with airgaps", IEE Proceedings, vol. 132, Pt.H, no. 7, December 1985.
29. COMTEST datasheet, Rev. 3. 27-11-1996, Model 1420, Amstelveen, The Netherlands
30. HUYNH, T., and LEE K. F.: 'Single-layer single patch wideband microstrip antenna', Electron Lett., 1995, 31, (16), pp. 1310-1312
31. M. CLENET and L. SHAFAI: 'Multiple resonance and polarization pf U-slot patch antenna', Electron Lett., 1999, 35, (2), pp. 101-103
32. K. F. TONG, K. M. LUK and K. F. LEE: 'A Broadband U-Slot rectangular patch antenna on a microwave substrate', IEE Proc.-Microw. Antenna Propag., 2000, 48, (6), pp. 954-960
33. C. L. MAK, K. M. LUK and K. F. LEE: 'Proximity-coupled U-slot patch antenna', Electron Lett. 1998, 34, (8), pp. 715-716
34. LUK, K. M., GUO, Y. X., LEE, K. F., and CHOW, Y. L.: 'L-Probe proximity fed U-slot patch antenna', Electron. Lett., 1998, 34, (19), pp. 1806-1807
35. LAU, K. L., LUK, K. M., and LEE, K. F.: 'Wideband U-slot microstrip patch antenna array', IEE Proc.-Microw. Antenna Propag., 2001, 148, (1), pp 41-44
36. Hugo F. Pues and Antoine R. Van De Capelle, "An Impedance Matching Technique for increasing the bandwidth of microstrip antennas", IEEE Trans. Antennas and Propagation, vol. Ap-37, pp.1345-1354, Nov 1989.

APPENDIX A

COMPUTER PROGRAMS FOR ARTIFICIAL TRANSMISSON LINE

```
% 8Ω ATL design with 13Ω microstrip transmission line

E0=8.854187818e-12;              %permittivity if free space
f=1.8e9;                         %operating frequency
w=2*pi*f;                        %angular frequency
Er=2.2;                          %Duroid relative dielectric constant
c=3e8;                           %velocity of light
h=0.254e-3;                      %substrate thickness
Z0TL=13;                         %characteristic impedance of transmission line
% Microstrip Design equation
A=Z0TL/60*(sqrt((Er+1)/2))+((Er-1)/(Er+1)*(0.23+(0.11/Er)));
B=377*pi/(2*(sqrt(Er))*Z0TL);
WhA=8*exp(A)/(exp(2*A)-2)
WhB=2/pi*(B-1-log(2*B-1)+((Er-1)/2/Er)*(log(B-1)+0.39-(0.61/Er)))
if (abs(WhA)<1)
   Wh=WhA
elseif (abs(WhB)>1)
   Wh=WhB
end
Ere=((Er+1)/2)+((Er-1)/2)/(sqrt(1+12/Wh))          %effective dielectric constant
W=h*Wh                           %width of microstrip impedance transmission line
vp=c/(sqrt(Ere));                %phase velocity of TL
Z0TL=13;
C=sqrt(Ere)/(Z0TL*c);            %capacitance per unit length of TL
L=sqrt(Ere)*Z0TL/c;              %inductance per unit length of TL
Z0ATL=8;                         %characteristic impedance of ATL design
phiATL=pi/2;                     %phase of ATL
N=12;                            %number of stages
d=phiATL*Z0ATL*c/(w*N*sqrt(Ere)*Z0TL)        %one unit cell length
%the capacitance value of loaded capacitor
Cp=(sqrt(Ere)*Z0TL/(c*Z0ATL)-
(sqrt(Ere)*Z0ATL/(Z0TL*c)))*phiATL*c/(w*N*sqrt(Ere)*Z0TL)
%design of the open stub
wstub=d/2;                       %width of open stub
h1=0.254e-3;                     %substrate thickness
Wh1=wstub/h1;                    %open stub width to substrate height ratio
% to find effective dielectric constant of open stub
Ee=((Er+1)/2)+((Er-1)/2)/(sqrt(1+12/Wh1))
%calculation of open stub impedance
if(Wh1<1)
   Z0stub=60/(sqrt(Ee))*log(8/Wh1+(Wh1/4))
elseif(Wh1>1)
   Z0stub=120*pi/((sqrt(Ee))*(Wh1+1.393+0.667*log(Wh1+1.444)))
end
lstub=c/(w*sqrt(Ee))*atan(w*Cp*Z0stub/2)          %length of open stub
%claculation trapezian shape
b=d;                             %width of one side of the open stub
b1=(d-0.3e-3)                    %width of another side of the open stub
hactual=wstub*lstub*2/(b+b1)  %length of open stub
```

```
% ATL design

E0=8.854187818e-12;              %permittivity if free space
f=1.8e9;                         %operating frequency
w=2*pi*f;                        %angular frequency
Er=2.2;                          %Duroid relative dielectric constant
c=3e8;                           %velocity of light
h=0.254e-3;                      %substrate thickness
Z0TL=20;                         %characteristic impedance of transmission line
% Microstrip Design equation
A=Z0TL/60*(sqrt((Er+1)/2))+((Er-1)/(Er+1)*(0.23+(0.11/Er)));
B=377*pi/(2*(sqrt(Er))*Z0TL);
WhA=8*exp(A)/(exp(2*A)-2)
WhB=2/pi*(B-1-log(2*B-1)+((Er-1)/2/Er)*(log(B-1)+0.39-(0.61/Er)))
if (abs(WhA)<1)
   Wh=WhA
elseif (abs(WhB)>1)
   Wh=WhB
end
Ere=((Er+1)/2)+((Er-1)/2)/(sqrt(1+12/Wh))          %effective dielectric constant
W=h*Wh                           %width of microstrip impedance transmission line
vp=c/(sqrt(Ere));                %phase velocity of TL
Z0TL=20;
C=sqrt(Ere)/(Z0TL*c)             %capacitance per unit length of TL
L=sqrt(Ere)*Z0TL/c               %inductance per unit length of TL
Z0ATL=15;                        %characteristic impedance of ATL design
phiATL=pi/2;                     %phase of ATL
N=12;                            %number of stages
d=phiATL*Z0ATL*c/(w*N*sqrt(Ere)*Z0TL)          %one unit cell length
%the capacitance value of loaded capacitor
Cp=(sqrt(Ere)*Z0TL/(c*Z0ATL)-
(sqrt(Ere)*Z0ATL/(Z0TL*c)))*phiATL*c/(w*N*sqrt(Ere)*Z0TL)
%design of the open stub
wstub=(d-0.4e-3);                %width of open stub
h1=0.254e-3;                     %substrate thickness
Wh1=wstub/h1;                    %open stub width to substrate height ratio
% To find effective dielectric constant of open stub
Ee=((Er+1)/2)+((Er-1)/2)/(sqrt(1+12/Wh1))
%calculation of open stub impedance
if(Wh1<1)
   Z0stub=60/(sqrt(Ee))*log(8/Wh1+(Wh1/4))
elseif(Wh1>1)
   Z0stub=120*pi/((sqrt(Ee))*(Wh1+1.393+0.667*log(Wh1+1.444)))
end
lstub=c/(w*sqrt(Ee))*atan(w*Cp*Z0stub/2)          %length of open stub
```

```
% The relation between Z0ATL and the one unit cell length & the capacitive loading
    value

E0=8.854187818e-12;        %permittivity if free space
f=1.8e9;                   %operating frequency
w=2*pi*f;                  %angular frequency
Er=2.2;                    %Duroid relative dielectric constant
c=3e8;                     %velocity of light
h=0.254e-3;                %substrate thickness
Z0TL=10;                   %characteristic impedance of transmission line
% Microstrip Design equation
A=Z0TL./60.*(sqrt((Er+1)/2))+((Er-1)./(Er+1).*(0.23+(0.11/Er)));
B=377*pi./(2.*(sqrt(Er)).*Z0TL);
WhA=8*exp(A)./(exp(2.*A)-2)
WhB=2./pi.*(B-1-log(2.*B-1)+((Er-1)./2./Er).*(log(B-1)+0.39-(0.61./Er)))
if (abs(WhA)<1)
   Wh=WhA
elseif (abs(WhB)>1)
   Wh=WhB
end
Ere=((Er+1)/2)+((Er-1)/2)/(sqrt(1+12/Wh))          %effective dielectric constant
W=h.*Wh                    %width of microstrip impedance transmission line
vp=c./(sqrt(Ere));         %phase velocity of TL
Z0TL=10;
C=sqrt(Ere)./(Z0TL.*c);    %capacitance per unit length of TL
L=sqrt(Ere).*Z0TL./c;      %inductance per unit length of TL
Z0ATL=2:1:20;              %characteristic impedance of ATL design
phiATL=pi;                 %phase of ATL
N=12;                      %number of stages
d=phiATL*Z0ATL.*c./(w*N.*sqrt(Ere).*Z0TL)          %one unit cell length
%the capacitance value of loaded capacitor
Cp=(sqrt(Ere).*Z0TL./(c.*Z0ATL)-
(sqrt(Ere).*Z0ATL./(Z0TL.*c))).*phiATL.*c./(w.*N.*sqrt(Ere).*Z0TL)



Z0TL=11;                   %characteristic impedance of transmission line
% Microstrip Design equation
A=Z0TL./60.*(sqrt((Er+1)/2))+((Er-1)./(Er+1).*(0.23+(0.11/Er)));
B=377*pi./(2.*(sqrt(Er)).*Z0TL);
WhA=8*exp(A)./(exp(2.*A)-2)
WhB=2./pi.*(B-1-log(2.*B-1)+((Er-1)./2./Er).*(log(B-1)+0.39-(0.61./Er)))
if (abs(WhA)<1)
   Wh=WhA
elseif (abs(WhB)>1)
   Wh=WhB
end
Ere=((Er+1)/2)+((Er-1)/2)/(sqrt(1+12/Wh))          %effective dielectric constant
W=h.*Wh                    %width of microstrip impedance transmission line
```

```
vp=c./(sqrt(Ere));              %phase velocity of TL
Z0TL=11;
C=sqrt(Ere)./(Z0TL.*c);     %capacitance per unit length of TL
L=sqrt(Ere).*Z0TL./c;       %inductance per unit length of TL
Z0ATL=2:1:20;               %characteristic impedance of ATL design
phiATL=pi;                  %phase of ATL
N=12;                       %number of stages
d2=phiATL*Z0ATL.*c./(w*N.*sqrt(Ere).*Z0TL)              %one unit cell length
%the capacitance value of loaded capacitor
Cp2=(sqrt(Ere).*Z0TL./(c.*Z0ATL)-
(sqrt(Ere).*Z0ATL./(Z0TL.*c))).*phiATL.*c./(w.*N.*sqrt(Ere).*Z0TL)
```

```
Z0TL=12;                    %characteristic impedance of transmission line
% Microstrip Design equation
A=Z0TL./60.*(sqrt((Er+1)/2))+((Er-1)./(Er+1).*(0.23+(0.11/Er)));
B=377*pi./(2.*(sqrt(Er)).*Z0TL);
WhA=8*exp(A)./(exp(2.*A)-2)
WhB=2./pi.*(B-1-log(2.*B-1)+((Er-1)./2./Er).*(log(B-1)+0.39-(0.61./Er)))
if (abs(WhA)<1)
   Wh=WhA
elseif (abs(WhB)>1)
   Wh=WhB
end
Ere=((Er+1)/2)+((Er-1)/2)/(sqrt(1+12/Wh))              %effective dielectric constant
W=h.*Wh                     %width of microstrip impedance transmission line
vp=c./(sqrt(Ere));          %phase velocity of TL
Z0TL=12;
C=sqrt(Ere)./(Z0TL.*c);     %capacitance per unit length of TL
L=sqrt(Ere).*Z0TL./c;       %inductance per unit length of TL
Z0ATL=2:1:20;               %characteristic impedance of ATL design
phiATL=pi;                  %phase of ATL
N=12;                       %number of stages
d3=phiATL*Z0ATL.*c./(w*N.*sqrt(Ere).*Z0TL)              %one unit cell length
%the capacitance value of loaded capacitor
Cp3=(sqrt(Ere).*Z0TL./(c.*Z0ATL)-
(sqrt(Ere).*Z0ATL./(Z0TL.*c))).*phiATL.*c./(w.*N.*sqrt(Ere).*Z0TL)
```

```
Z0TL=13;                    %characteristic impedance of transmission line
% Microstrip Design equation
A=Z0TL./60.*(sqrt((Er+1)/2))+((Er-1)./(Er+1).*(0.23+(0.11/Er)));
B=377*pi./(2.*(sqrt(Er)).*Z0TL);
WhA=8*exp(A)./(exp(2.*A)-2)
WhB=2./pi.*(B-1-log(2.*B-1)+((Er-1)./2./Er).*(log(B-1)+0.39-(0.61./Er)))
if (abs(WhA)<1)
   Wh=WhA
elseif (abs(WhB)>1)
```

```
   Wh=WhB
end
Ere=((Er+1)/2)+((Er-1)/2)/(sqrt(1+12/Wh))          %effective dielectric constant
W=h.*Wh                    %width of microstrip impedance transmission line
vp=c./(sqrt(Ere));         %phase velocity of TL
Z0TL=13;
C=sqrt(Ere)./(Z0TL.*c);    %capacitance per unit length of TL
L=sqrt(Ere).*Z0TL./c;      %inductance per unit length of TL
Z0ATL=2:1:20;              %characteristic impedance of ATL design
phiATL=pi;                 %phase of ATL
N=12;                      %number of stages
d4=phiATL*Z0ATL.*c./(w*N.*sqrt(Ere).*Z0TL)          %one unit cell length
%the capacitance value of loaded capacitor
Cp4=(sqrt(Ere).*Z0TL./(c.*Z0ATL)-
(sqrt(Ere).*Z0ATL./(Z0TL.*c))).*phiATL.*c./(w.*N.*sqrt(Ere).*Z0TL)



Z0TL=14;                   %characteristic impedance of transmission line
% Microstrip Design equation
A=Z0TL./60.*(sqrt((Er+1)/2))+((Er-1)./(Er+1).*(0.23+(0.11/Er)));
B=377*pi./(2.*(sqrt(Er)).*Z0TL);
WhA=8*exp(A)./(exp(2.*A)-2)
WhB=2./pi.*(B-1-log(2.*B-1)+((Er-1)./2./Er).*(log(B-1)+0.39-(0.61./Er)))
if (abs(WhA)<1)
   Wh=WhA
elseif (abs(WhB)>1)
   Wh=WhB
end
Ere=((Er+1)/2)+((Er-1)/2)/(sqrt(1+12/Wh))          %effective dielectric constant
W=h.*Wh                    %width of microstrip impedance transmission line
vp=c./(sqrt(Ere));         %phase velocity of TL
Z0TL=14;
C=sqrt(Ere)./(Z0TL.*c);    %capacitance per unit length of TL
L=sqrt(Ere).*Z0TL./c;      %inductance per unit length of TL
Z0ATL=2:1:20;              %characteristic impedance of ATL design
phiATL=pi;                 %phase of ATL
N=12;                      %number of stages
d5=phiATL*Z0ATL.*c./(w*N.*sqrt(Ere).*Z0TL)          %one unit cell length
%the capacitance value of loaded capacitor
Cp5=(sqrt(Ere).*Z0TL./(c.*Z0ATL)-
(sqrt(Ere).*Z0ATL./(Z0TL.*c))).*phiATL.*c./(w.*N.*sqrt(Ere).*Z0TL)



Z0TL=15;                   %characteristic impedance of transmission line
% Microstrip Design equation
A=Z0TL./60.*(sqrt((Er+1)/2))+((Er-1)./(Er+1).*(0.23+(0.11/Er)));
B=377*pi./(2.*(sqrt(Er)).*Z0TL);
```

```
WhA=8*exp(A)./(exp(2.*A)-2)
WhB=2./pi.*(B-1-log(2.*B-1)+((Er-1)./2./Er).*(log(B-1)+0.39-(0.61./Er)))
if (abs(WhA)<1)
   Wh=WhA
elseif (abs(WhB)>1)
   Wh=WhB
end
Ere=((Er+1)/2)+((Er-1)/2)/(sqrt(1+12/Wh))          %effective dielectric constant
W=h.*Wh                  %width of microstrip impedance transmission line
vp=c./(sqrt(Ere));       %phase velocity of TL
Z0TL=15;
C=sqrt(Ere)./(Z0TL.*c);  %capacitance per unit length of TL
L=sqrt(Ere).*Z0TL./c;    %inductance per unit length of TL
Z0ATL=2:1:20;            %characteristic impedance of ATL design
phiATL=pi;               %phase of ATL
N=12;                    %number of stages
d6=phiATL*Z0ATL.*c./(w*N.*sqrt(Ere).*Z0TL)          %one unit cell length
%the capacitance value of loaded capacitor
Cp6=(sqrt(Ere).*Z0TL./(c.*Z0ATL)-
(sqrt(Ere).*Z0ATL./(Z0TL.*c))).*phiATL.*c./(w.*N.*sqrt(Ere).*Z0TL)
```

```
Z0TL=16;                 %characteristic impedance of transmission line
% Microstrip Design equation
A=Z0TL./60.*(sqrt((Er+1)/2))+((Er-1)./(Er+1).*(0.23+(0.11/Er)));
B=377*pi./(2.*(sqrt(Er)).*Z0TL);
WhA=8*exp(A)./(exp(2.*A)-2)
WhB=2./pi.*(B-1-log(2.*B-1)+((Er-1)./2./Er).*(log(B-1)+0.39-(0.61./Er)))
if (abs(WhA)<1)
   Wh=WhA
elseif (abs(WhB)>1)
   Wh=WhB
end
Ere=((Er+1)/2)+((Er-1)/2)/(sqrt(1+12/Wh))          %effective dielectric constant
W=h.*Wh                  %width of microstrip impedance transmission line
vp=c./(sqrt(Ere));       %phase velocity of TL
Z0TL=16;
C=sqrt(Ere)./(Z0TL.*c);  %capacitance per unit length of TL
L=sqrt(Ere).*Z0TL./c;    %inductance per unit length of TL
Z0ATL=2:1:20;            %characteristic impedance of ATL design
phiATL=pi;               %phase of ATL
N=12;                    %number of stages
d7=phiATL*Z0ATL.*c./(w*N.*sqrt(Ere).*Z0TL)   %one unit cell length
%the capacitance value of loaded capacitor
Cp7=(sqrt(Ere).*Z0TL./(c.*Z0ATL)-
(sqrt(Ere).*Z0ATL./(Z0TL.*c))).*phiATL.*c./(w.*N.*sqrt(Ere).*Z0TL)
```

```
Z0TL=17;                    %characteristic impedance of transmission line
% Microstrip Design equation
A=Z0TL./60.*(sqrt((Er+1)/2))+((Er-1)./(Er+1).*(0.23+(0.11/Er)));
B=377*pi./(2.*(sqrt(Er)).*Z0TL);
WhA=8*exp(A)./(exp(2.*A)-2)
WhB=2./pi.*(B-1-log(2.*B-1)+((Er-1)./2./Er).*(log(B-1)+0.39-(0.61./Er)))
if (abs(WhA)<1)
   Wh=WhA
elseif (abs(WhB)>1)
   Wh=WhB
end
Ere=((Er+1)/2)+((Er-1)/2)/(sqrt(1+12/Wh))          %effective dielectric constant
W=h.*Wh                     %width of microstrip impedance transmission line
vp=c./(sqrt(Ere));          %phase velocity of TL
Z0TL=17;
C=sqrt(Ere)./(Z0TL.*c);     %capacitance per unit length of TL
L=sqrt(Ere).*Z0TL./c;       %inductance per unit length of TL
Z0ATL=2:1:20;               %characteristic impedance of ATL design
phiATL=pi;                  %phase of ATL
N=12;                       %number of stages
d8=phiATL*Z0ATL.*c./(w*N.*sqrt(Ere).*Z0TL)          %one unit cell length
%the capacitance value of loaded capacitor
Cp8=(sqrt(Ere).*Z0TL./(c.*Z0ATL)-
(sqrt(Ere).*Z0ATL./(Z0TL.*c))).*phiATL.*c./(w.*N.*sqrt(Ere).*Z0TL)
```

```
Z0TL=18;                    %characteristic impedance of transmission line
% Microstrip Design equation
A=Z0TL./60.*(sqrt((Er+1)/2))+((Er-1)./(Er+1).*(0.23+(0.11/Er)));
B=377*pi./(2.*(sqrt(Er)).*Z0TL);
WhA=8*exp(A)./(exp(2.*A)-2)
WhB=2./pi.*(B-1-log(2.*B-1)+((Er-1)./2./Er).*(log(B-1)+0.39-(0.61./Er)))
if (abs(WhA)<1)
   Wh=WhA
elseif (abs(WhB)>1)
   Wh=WhB
end
Ere=((Er+1)/2)+((Er-1)/2)/(sqrt(1+12/Wh))          %effective dielectric constant
W=h.*Wh                     %width of microstrip impedance transmission line
vp=c./(sqrt(Ere));          %phase velocity of TL
Z0TL=18;
C=sqrt(Ere)./(Z0TL.*c);     %capacitance per unit length of TL
L=sqrt(Ere).*Z0TL./c;       %inductance per unit length of TL
Z0ATL=2:1:20;               %characteristic impedance of ATL design
phiATL=pi;                  %phase of ATL
N=12;                       %number of stages
```

```
d9=phiATL*Z0ATL.*c./(w*N.*sqrt(Ere).*Z0TL)                %one unit cell length
%the capacitance value of loaded capacitor
Cp9=(sqrt(Ere).*Z0TL./(c.*Z0ATL)-
(sqrt(Ere).*Z0ATL./(Z0TL.*c))).*phiATL.*c./(w.*N.*sqrt(Ere).*Z0TL)
```

```
Z0TL=19;                    %characteristic impedance of transmission line
% Microstrip Design equation
A=Z0TL./60.*(sqrt((Er+1)/2))+((Er-1)./(Er+1).*(0.23+(0.11/Er)));
B=377*pi./(2.*(sqrt(Er)).*Z0TL);
WhA=8*exp(A)./(exp(2.*A)-2)
WhB=2./pi.*(B-1-log(2.*B-1)+((Er-1)./2./Er).*(log(B-1)+0.39-(0.61./Er)))
if (abs(WhA)<1)
   Wh=WhA
elseif (abs(WhB)>1)
   Wh=WhB
end
Ere=((Er+1)/2)+((Er-1)/2)/(sqrt(1+12/Wh))          %effective dielectric constant
W=h.*Wh                     %width of microstrip impedance transmission line
vp=c./(sqrt(Ere));          %phase velocity of TL
Z0TL=19;
C=sqrt(Ere)./(Z0TL.*c);     %capacitance per unit length of TL
L=sqrt(Ere).*Z0TL./c;       %inductance per unit length of TL
Z0ATL=2:1:20;               %characteristic impedance of ATL design
phiATL=pi;                  %phase of ATL
N=12;                       %number of stages
d10=phiATL*Z0ATL.*c./(w*N.*sqrt(Ere).*Z0TL)               %one unit cell length
%the capacitance value of loaded capacitor
Cp10=(sqrt(Ere).*Z0TL./(c.*Z0ATL)-
(sqrt(Ere).*Z0ATL./(Z0TL.*c))).*phiATL.*c./(w.*N.*sqrt(Ere).*Z0TL)
```

```
Z0TL=20;                    %characteristic impedance of transmission line
% Microstrip Design equation
A=Z0TL./60.*(sqrt((Er+1)/2))+((Er-1)./(Er+1).*(0.23+(0.11/Er)));
B=377*pi./(2.*(sqrt(Er)).*Z0TL);
WhA=8*exp(A)./(exp(2.*A)-2)
WhB=2./pi.*(B-1-log(2.*B-1)+((Er-1)./2./Er).*(log(B-1)+0.39-(0.61./Er)))
if (abs(WhA)<1)
   Wh=WhA
elseif (abs(WhB)>1)
   Wh=WhB
end
Ere=((Er+1)/2)+((Er-1)/2)/(sqrt(1+12/Wh))          %effective dielectric constant
W=h.*Wh                     %width of microstrip impedance transmission line
vp=c./(sqrt(Ere));          %phase velocity of TL
```

```
Z0TL=20;
C=sqrt(Ere)./(Z0TL.*c);   %capacitance per unit length of TL
L=sqrt(Ere).*Z0TL./c;     %inductance per unit length of TL
Z0ATL=2:1:20;             %characteristic impedance of ATL design
phiATL=pi;                %phase of ATL
N=12;                     %number of stages
d11=phiATL*Z0ATL.*c./(w*N.*sqrt(Ere).*Z0TL)          %one unit cell length
%the capacitance value of loaded capacitor
Cp11=(sqrt(Ere).*Z0TL./(c.*Z0ATL)-
(sqrt(Ere).*Z0ATL./(Z0TL.*c))).*phiATL.*c./(w.*N.*sqrt(Ere).*Z0TL)
```

```
Z0TL=21;                  %characteristic impedance of transmission line
% Microstrip Design equation
A=Z0TL./60.*(sqrt((Er+1)/2))+((Er-1)./(Er+1).*(0.23+(0.11/Er)));
B=377*pi./(2.*(sqrt(Er)).*Z0TL);
WhA=8*exp(A)./(exp(2.*A)-2)
WhB=2./pi.*(B-1-log(2.*B-1)+((Er-1)./2./Er).*(log(B-1)+0.39-(0.61./Er)))
if (abs(WhA)<1)
   Wh=WhA
elseif (abs(WhB)>1)
   Wh=WhB
end
Ere=((Er+1)/2)+((Er-1)/2)/(sqrt(1+12/Wh))          %effective dielectric constant
W=h.*Wh                   %width of microstrip impedance transmission line
vp=c./(sqrt(Ere));        %phase velocity of TL
Z0TL=21;
C=sqrt(Ere)./(Z0TL.*c);   %capacitance per unit length of TL
L=sqrt(Ere).*Z0TL./c;     %inductance per unit length of TL
Z0ATL=2:1:20;             %characteristic impedance of ATL design
phiATL=pi;                %phase of ATL
N=12;                     %number of stages
d12=phiATL*Z0ATL.*c./(w*N.*sqrt(Ere).*Z0TL)          %one unit cell length
%the capacitance value of loaded capacitor
Cp12=(sqrt(Ere).*Z0TL./(c.*Z0ATL)-
(sqrt(Ere).*Z0ATL./(Z0TL.*c))).*phiATL.*c./(w.*N.*sqrt(Ere).*Z0TL)
```

```
Z0TL=22;                  %characteristic impedance of transmission line
% Microstrip Design equation
A=Z0TL./60.*(sqrt((Er+1)/2))+((Er-1)./(Er+1).*(0.23+(0.11/Er)));
B=377*pi./(2.*(sqrt(Er)).*Z0TL);
WhA=8*exp(A)./(exp(2.*A)-2)
WhB=2./pi.*(B-1-log(2.*B-1)+((Er-1)./2./Er).*(log(B-1)+0.39-(0.61./Er)))
if (abs(WhA)<1)
   Wh=WhA
```

```
elseif (abs(WhB)>1)
   Wh=WhB
end
Ere=((Er+1)/2)+((Er-1)/2)/(sqrt(1+12/Wh))          %effective dielectric constant
W=h.*Wh                    %width of microstrip impedance transmission line
vp=c./(sqrt(Ere));         %phase velocity of TL
Z0TL=22;
C=sqrt(Ere)./(Z0TL.*c);   %capacitance per unit length of TL
L=sqrt(Ere).*Z0TL./c;      %inductance per unit length of TL
Z0ATL=2:1:20;              %characteristic impedance of ATL design
phiATL=pi;                 %phase of ATL
N=12;                      %number of stages
d13=phiATL*Z0ATL.*c./(w*N.*sqrt(Ere).*Z0TL)                %one unit cell length
%the capacitance value of loaded capacitor
Cp13=(sqrt(Ere).*Z0TL./(c.*Z0ATL)-
(sqrt(Ere).*Z0ATL./(Z0TL.*c))).*phiATL.*c./(w.*N.*sqrt(Ere).*Z0TL)
```

```
Z0TL=23;                   %characteristic impedance of transmission line
% Microstrip Design equation
A=Z0TL./60.*(sqrt((Er+1)/2))+((Er-1)./(Er+1).*(0.23+(0.11/Er)));
B=377*pi./(2.*(sqrt(Er)).*Z0TL);
WhA=8*exp(A)./(exp(2.*A)-2)
WhB=2./pi.*(B-1-log(2.*B-1)+((Er-1)./2./Er).*(log(B-1)+0.39-(0.61./Er)))
if (abs(WhA)<1)
   Wh=WhA
elseif (abs(WhB)>1)
   Wh=WhB
end
Ere=((Er+1)/2)+((Er-1)/2)/(sqrt(1+12/Wh))          %effective dielectric constant
W=h.*Wh                    %width of microstrip impedance transmission line
vp=c./(sqrt(Ere));         %phase velocity of TL
Z0TL=23;
C=sqrt(Ere)./(Z0TL.*c);   %capacitance per unit length of TL
L=sqrt(Ere).*Z0TL./c;      %inductance per unit length of TL
Z0ATL=2:1:20;              %characteristic impedance of ATL design
phiATL=pi;                 %phase of ATL
N=12;                      %number of stages
d14=phiATL*Z0ATL.*c./(w*N.*sqrt(Ere).*Z0TL)                %one unit cell length
%the capacitance value of loaded capacitor
Cp14=(sqrt(Ere).*Z0TL./(c.*Z0ATL)-
(sqrt(Ere).*Z0ATL./(Z0TL.*c))).*phiATL.*c./(w.*N.*sqrt(Ere).*Z0TL)
```

```
Z0TL=24;                   %characteristic impedance of transmission line
% Microstrip Design equation
```

```
A=Z0TL./60.*(sqrt((Er+1)/2))+((Er-1)./(Er+1).*(0.23+(0.11/Er)));
B=377*pi./(2.*(sqrt(Er)).*Z0TL);
WhA=8*exp(A)./(exp(2.*A)-2)
WhB=2./pi.*(B-1-log(2.*B-1)+((Er-1)./2./Er).*(log(B-1)+0.39-(0.61./Er)))
if (abs(WhA)<1)
   Wh=WhA
elseif (abs(WhB)>1)
   Wh=WhB
end
Ere=((Er+1)/2)+((Er-1)/2)/(sqrt(1+12/Wh))          %effective dielectric constant
W=h.*Wh                    %width of microstrip impedance transmission line
vp=c./(sqrt(Ere));          %phase velocity of TL
Z0TL=24;
C=sqrt(Ere)./(Z0TL.*c);    %capacitance per unit length of TL
L=sqrt(Ere).*Z0TL./c;      %inductance per unit length of TL
Z0ATL=2:1:20;              %characteristic impedance of ATL design
phiATL=pi;                 %phase of ATL
N=12;                      %number of stages
d15=phiATL*Z0ATL.*c./(w*N.*sqrt(Ere).*Z0TL)          %one unit cell length
%the capacitance value of loaded capacitor
Cp15=(sqrt(Ere).*Z0TL./(c.*Z0ATL)-
(sqrt(Ere).*Z0ATL./(Z0TL.*c))).*phiATL.*c./(w.*N.*sqrt(Ere).*Z0TL)
```

```
Z0TL=25;                   %characteristic impedance of transmission line
% Microstrip Design equation
A=Z0TL./60.*(sqrt((Er+1)/2))+((Er-1)./(Er+1).*(0.23+(0.11/Er)));
B=377*pi./(2.*(sqrt(Er)).*Z0TL);
WhA=8*exp(A)./(exp(2.*A)-2)
WhB=2./pi.*(B-1-log(2.*B-1)+((Er-1)./2./Er).*(log(B-1)+0.39-(0.61./Er)))
if (abs(WhA)<1)
   Wh=WhA
elseif (abs(WhB)>1)
   Wh=WhB
end
Ere=((Er+1)/2)+((Er-1)/2)/(sqrt(1+12/Wh))          %effective dielectric constant
W=h.*Wh                    %width of microstrip impedance transmission line
vp=c./(sqrt(Ere));         %phase velocity of TL
Z0TL=25;
C=sqrt(Ere)./(Z0TL.*c);    %capacitance per unit length of TL
L=sqrt(Ere).*Z0TL./c;      %inductance per unit length of TL
Z0ATL=2:1:20;              %characteristic impedance of ATL design
phiATL=pi;                 %phase of ATL
N=12;                      %number of stages
d16=phiATL*Z0ATL.*c./(w*N.*sqrt(Ere).*Z0TL)          %one unit cell length
%the capacitance value of loaded capacitor
Cp16=(sqrt(Ere).*Z0TL./(c.*Z0ATL)-
(sqrt(Ere).*Z0ATL./(Z0TL.*c))).*phiATL.*c./(w.*N.*sqrt(Ere).*Z0TL)
```

```
figure (1);
plot
(Z0ATL,d,Z0ATL,d3,Z0ATL,d5,Z0ATL,d7,Z0ATL,d9,Z0ATL,d11,Z0ATL,d13,Z0A
TL,d15,Z0ATL,d16)
xlabel('Z0ATL(ohm)')
ylabel('d(m)')


figure(2);
plot(Z0ATL,Cp,Z0ATL,Cp3,Z0ATL,Cp5,Z0ATL,Cp7,Z0ATL,Cp9,Z0ATL,Cp11,Z0
ATL,Cp13,Z0ATL,Cp15,Z0ATL,Cp,Z0ATL,Cp16)
xlabel('Z0ATL(ohm)')
ylabel('Cp(F)')
```